SISSA - SCUOLA
INTERNAZIONALE
SUPERIORE
DI STUDI AVANZATI
TRIESTE
Strada Costiera 11

ISAS - INTERNATIONAL SCHOOL FOR ADVANCED STUDIES

Understanding the HR Diagram of massive stars

Submitted for the degree of
Doctor Philosophiæ

CANDIDATE
Licai Deng

SUPERVISOR
Prof. Dennis W. Sciama
Prof. Cesare Chiosi
Dr. Alessandro Bressan

Academic Year 1992-1993

Astrophysics Sector

TRIESTE

Understanding the HR Diagram of massive stars

Doctor Philosophiæ

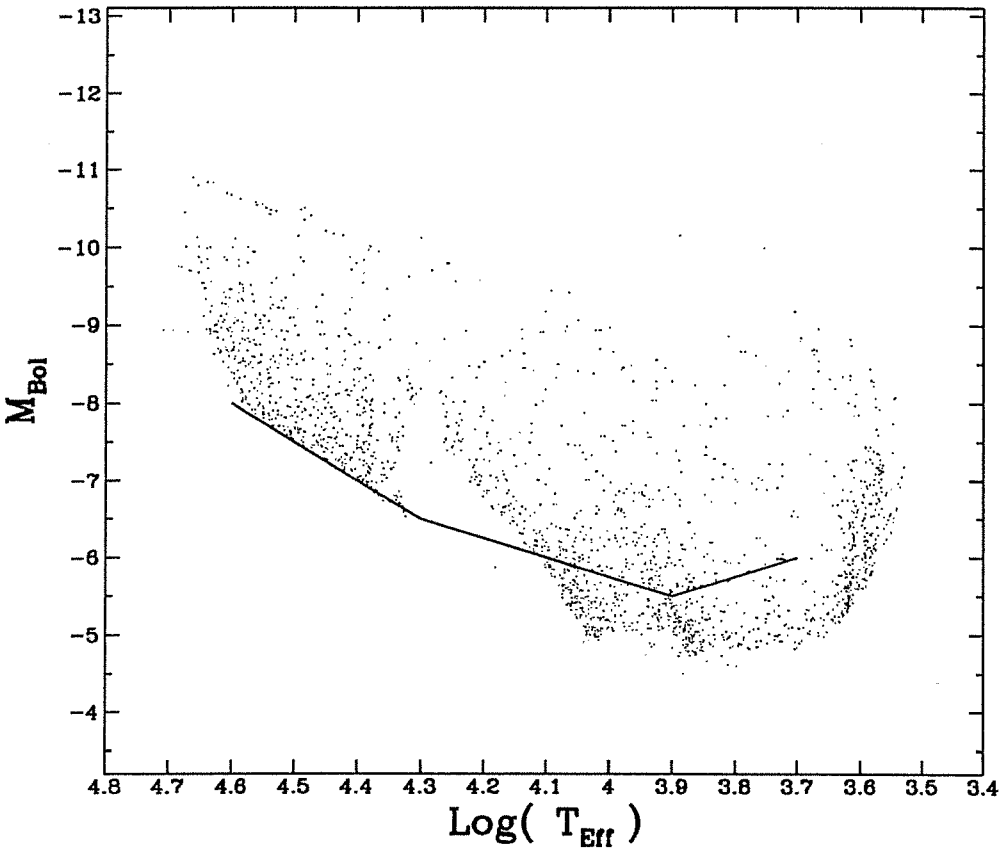

CANDIDATE
Licai Deng

SUPERVISOR
Prof. Dennis W. Sciama
Prof. Cesare Chiosi
Dr. Alessandro Bressan

Academic Year 1992-1993
Astrophysics Sector

To my wife,

and my little daugther

Table of Contents

List of Tables

List of Figures

1 Introduction

Mixing inside deep interior is one of the still scarcely known physical processes that bear very much upon the theory of stellar structure and evolution. Indeed, mixing redistributes over extended regions of a star or even brings to the surface the local products of nucleosynthesis. In stars more massive than the Sun the extension of the convective cores affects both the luminosity and the amount of nuclear fuel, and hence the lifetime of the evolutionary phases. Unfortunately at present, a fully sounded theory of the mixing processes is missing, so that one is forced to address the problem in an indirect fashion looking at the effects of simplified models of mixing on observable stellar quantities for instance the the position of a star in the Hertzsprung Russel Diagram (HRD).

In this thesis I will concentrate on a new model of mixing with particular attention to the evolution of the massive stars as they are known to possess very extended convective cores and envelopes. We remind the reader that convection is the dominant mechanism of energy transport of inside the cores of these stars.

In the standard theory of convection, the extension of the convective regions (either cores or envelopes) is determined by means of a local stability criterion (either Schwarzschild or Ledoux), and use of the so called Mixing Length Theory (MLT) to describe the motion of convective elements. Any uncertainty in the boundary of the unstable regions has straightforward consequences on the star structure. In particular, an uncertainty on the extension of the convective core makes uncertain the amount of available fuel and therefore the duration of the phase, so that the effects of assuming different criterions is soon evident. This was first

shown by the classical study of Chiosi and Summa (1970), who defined two distinct evolutionary scenarios for a typical model of $20M_{\odot}$. Since we will find that almost all assumptions about the convective instability criterion, nuclear cross-section, radiative opacities, etc... lead to results for the evolution of massive stars that can be classified according to the Chiosi and Summa (1970) scheme, it is worth recalling here the salient feature of their classification. In the scheme named case A, the star, after the main sequence phase, ignites central helium as a red supergiant (RSG), performs a loop into the region of the blue supergiants (BSG), and finally evolves toward the red supergiant regions as central helium gets exhausted. On the contrary, in the scheme named case B the star ignites the central helium near the main sequence as a blue object and slowly moves toward the region of the RSG stars. As pointed out by Fitzpatrick and Garmany (1990), these two evolutionary scenarios constitute the basis to understand the HRD of supergiant stars.

Tightly related with convection is overshoot, While this phenomenon is easily experienced in meteorology and laboratory experiments of hydrodynamics, its existence and efficiency in stellar conditions have been the subject of a vivid debate over the last two decades.

The problem of convective overshoot arises from an obvious weak point of the MLT, i.e. in the basic assumption that convectively unstable regions extend up to the layer where the acceleration imparted by the bouancy forces to the fluid elements gets zero. without taking into account the inertia of their motions. In metereology and laboratory fluid mechanics, convective overshoot is an observed fact extending over regions whose size is comparable to that of the unstable region itself. Unfortunately, because of the extreme difference between the physical conditions inside a star and those met in laboratory conditions on the Earth, we cannot simply extend to stellar interiors what we learn from ordinary fluid dynamics. In fact, the extension of laboratory convection (atmosphere, oceans) is often a small fraction of the pressure scale height, whereas within the stars the unstable regions usually extend over a large fraction or even up to several times the local pressure scale height.

Current stellar models are generally divided into two groups, depending on the credit given

to this phenomenon. However, owing to the lack of a fully sounded theory, oversimplified descriptions of convective overshoot have been adopted, which parameterize its extension by means of a suitable scale height (usually pressure scale height) and therefore introduce in the problem a certain degree of arbitrariness.

Avoiding this parameter seems impossible, as even in the very complicate theory of convection formulated by Xiong (1985) with the aid of the full hydrodynamics description of the the fluid there is trace of this scale factor. This is intrinsic to fluid dynamics because the basic equations (eg. **Fluid Mechanics**, by Landau & Lifchitz) do not provide constraints to length scale in the case of a free boundary problem, such as that of stellar convection. On the contrary, laboratory hydrodynamical problems are bounded by the natural borders of the container. In stellar interiors the problem is further complicated by the interplay between nuclear burning, convection, and mixing and their corresponding time scales. As the evolution goes on, nuclear reactions (usually concentrated into a small central region) modify the local chemical composition and convective mixing both carries out the energy from this region, brings away the products of nucleosynthesis, and refuels the central furnace. Because the MLT does not specifically deal with nuclear species, the usual assumption is that mixing is instantaneous and fully efficient Therefore, the complex physics inside a convective region is simply reduced to establishing its boundary, with obvious advantage as far as the numerical calculations of stellar models are concerned. However, there is a natural time scale associated to convective motion to consider, which actually drives the phenomenon. This time scale is the turn-over time scale of the largest convective element, which turns out to be much shorter than the characteristic nuclear time scale. Nevertheless, according to the MLT, mixing length theory, motions with this scale cannot induce any kind of mixing (both chemical and thermal) before motions have ended. Supposedly, the mixing takes place only at the end of the motion, and some unknown instantaneous process secures the exchange of thermal energy and chemical properties with the surrounding medium. If the assumption of instantaneous mixing is relaxed, the convective motions at this large scale could constitute a

sort of ordered circulation, mixing matter on a longer time scale via the effects of dissipation at smaller spatial scales. Similar consideration apply also to models with overshoot as mixing of chemical elements is once more supposed to occur instantaneously.

Further complications are related to the mechanism of penetration (overshoot) of convective elements into radiatively stable regions zone which is customarily treated as sort of parameter. However, several sophisticated studies (Xiong, ARIZONA group) have shown that overshoot is a more complicated process, in which different physical quantities have different distances of penetration. The numerical results of these detailed hydrodynamic theories show that the fluctuations of the physical quantities decrease exponentially above the classical border defined by the local criterion. Nevertheless, the thermodynamic structure of the overshoot region can be well reproduced even by a simple version of a non-local treatment. Indeed, the thermodynamic structure of the overshoot region has very little effect on the overall structure of the star. It has been demonstrated (Licai 1992, Magister Thesis) that assuming the overshoot region to be adiabatic, almost exactly reproduces the same results as from assuming it to be radiative, in agreement with the more sophisticated models by Xiong (1985). The main result of models with overshoot is that the size of 'core' size can be significantly increased. The main effect of overshoot manifest itself in the kind of chemical mixing that can occur with profound consequences on the evolutionary results. In Xiong's hydrodynamic studies, the mixing efficiency within the overshoot region exponentially decreases up to about two pressure scale heights above the unstable core.

Given these premises, the aim of this thesis is to investigate a model in which the efficiency of mixing instead of being treated as a parameter, directly results from the motions at the smallest scales.

Chapter 2 contains a short summary of the basic equations of stellar structure, the method of solution, and the main evolutionary results. *Chapter* 3 deals with the Mixing Length Theory of convection, its application to stars, and the mixing mechanisms used in stellar evolutionary calculations.

Chapter 4 shortly summarizes the current understanding of the HRD of supergiant stars and the evolution of stars that are the main subject of my study. In *Chapter* 5 we present a thorough description of the mixing mechanisms inside stars, with particular emphasis on our diffusive scheme. In *Chapter* 6, we briefly discuss the physical ingredients used to compute the stellar models. Models with chemical abundance typical of the solar vicinity and the Large Magellanic Cloud (LMC) are presented in *Chapter* 7 together with a complete description of the new results from the diffusive mixing and the comparison with other stellar models in literature. In *Chapter* 8, we discuss the observational HRD for the supergiant stars in the light of the new models. Finally some conclusions and hints of future work are given in *Chapter* 9.

2 Fundamentals of Stellar Structure and Evolution

The fundamentals of stellar structure and evolution were set by the classical studies of R. Emden (1907), A. S. Eddington (1926), S Chandrasekhar (1939), and Schwarzschild (1958) during the first decades of this century. However, the overall formulation of the problem was achieved much later, thanks to the numberless contributions of generations of scientists. Nowadays the status of the theory is far from being complete, because some of the basic physical ingredients are either still insufficiently understood, like in the case of the convective transport, or are continuously improved like in the case of the radiative opacities, nuclear reaction cross sections, and equation of state. Others like mass loss by stellar wind, rotation, and magnetic fields are either described by means of empirical formulations or neglected at all.

The basic mathematical formulation of the problem is however known from long time with little or no change from the early book by S. Chandrasekhar (1939) to the recent ones by Cox & Giuli(1968) and R. Kippenhahn and & A. Weigert (1990).

For sake of completeness, in the following I will briefly review the basic equations of stellar structure.

2.1 The basic equations

The basic equations of stellar structure stands on the law of mass, momentum, and energy conservation, and the law of energy transports in condition of local thermodynamical equilibrium. These equations uniquely define a stellar structure of a given mass and chemical

composition. Accordingly, the evolution of a non-rotating, non-magnetic, spherically symmetric star is described by the following system of partial differential equations,

$$\frac{\partial r}{\partial m_r} = \frac{1}{4\pi r^2 \rho} \tag{2.1}$$

$$\frac{\partial P}{\partial m_r} = -\frac{G m_r}{4\pi r^4} - \frac{1}{4\pi r^2}\frac{\partial^2 r}{\partial t^2} \tag{2.2}$$

$$\frac{\partial l}{\partial m_r} = \epsilon_n - \epsilon_\nu - c_P \frac{\partial T}{\partial t} + \frac{\delta}{\rho}\frac{\partial P}{\partial t} \tag{2.3}$$

$$\frac{\partial T}{\partial m_r} = -\frac{G m_r T}{4\pi r^4 P}\nabla \tag{2.4}$$

where the independent variables are the mass within a sphere of radius r, m_r (Lagrangian description) and time t. THe time dependence allows to follow the evolution of the structure and the behaviour of dynamical solutions (for instance stellar pulsation). In the case of quasi static configurations (which apply to most of the stellar history up to the very advanced phases), the time-dependent terms reduce to the sole local source or sink of energy,so that the above equations became ordinary differential equations in the independent variable m_r supplemented by suitable boundary conditions, whose solutions determines the structure of the star, namely the dependence of the radius r, pressure P, temperature t, and luminosity l as function of the mass m_r.

Generally the second term in equation (2.2) is neglected (hydrostatic equilibrium) as the hypothetical departure from this condition would imply for a star like the Sun the existence of acceleration terms leading to a change of the radius of the Sun over a time scale of the order of an hour (Cox & Giuli 1968) which contradicts the observations over very long periods of time. The dynamical time scale is indeed much shorter than the ordinary time scale of fast evolutionary phases, namely the Kelvin-Helmholtz time scale. Only in extreme cases, such as supernova explosions, the acceleration term is required.

All the thermodynamic quantities depend also upon the chemical abundance, which continuously varies under the action of nuclear burning according to

$$\frac{\partial X_i}{\partial t} = \frac{m_i}{\rho}\left(\Sigma_j r_{ij} - \Sigma_{kj}\right), \quad i = 1, ...N \tag{2.5}$$

where X_i is the abundance by mass of the element i, m_i is the atomic mass of the element; r_{ij} is the nuclear burning rates (see below); these are a series of N-equations for all the chemical elements involved in the nuclear network. In addition mixing processes like convection concur to the modification of the internal profile of the chemical elements. Usually the chemical equations are not solved simultaneously with the structure equations but they are solved separately once the equilibrium structure of the star is known, and the variations of chemical abundance by nuclear reactions and mixing are determined over a given time step.

2.2 Supplementary Relations

The other quantities appearing in the equations (2.1-2.4) are the density ρ, the specific heat at constant pressure c_P, the nuclear energy generation rate ϵ_n, the rate of neutrino energy loss ϵ_ν, the temperature gradient ∇ $(d\log T/d\log P)$. They are either related by suitable thermodynamics relations or are the result of detailed calculations of nuclear and atomic physics.

Equation of state: The density appearing in the basic equations is related temperature, pressure and chemical composition by the equation of state:

$$\rho = \rho(P, T, X_i)$$

where X_i is the chemical composition of the local material. In massive stars the equation of state is that of a non degenerate perfect gas plus radiation pressure with a high degree of accuracy during almost the entire life. On the contrary, low and intermediate mass stars soon or later enter the regime of electron degeneracy and the pressure is sustained basically by the degenerate electrons.

The thermodynamic relations of stellar matter:

$$c_P = c_P(P, T, X_i)$$

$$\delta = \delta(P, T, X_i)$$

$$\nabla_{ad} = \nabla_{ad}(P, T, X_i)$$

Nuclear physics inputs: The nuclear reaction rates, the energy output rates for certain reactions and the energy carried by neutrinos (which are supposed not to contribute to the radiative luminosity because in virtue of their extremely small cross section they actually escape from the star without interacting with the stellar matter) are obtained from nuclear and elementary particle physics:

$$r_{ij} = r_{ij}(P, T, X_i)$$

$$\epsilon_n = \epsilon_n(P, T, X_i)$$

$$\epsilon_\nu = \epsilon_\nu(P, T, X_i)$$

The temperature gradient: If radiation is the dominant heat transport mechanism the temperature gradient appearing in equation (2.4) is given by

$$\nabla = \nabla_{rad} = \frac{3}{16\pi acG}\frac{\kappa l P}{m_r T^4} \tag{2.6}$$

where

$$\kappa = \kappa(P, T, X_i)$$

is the Rosseland mean opacity. This is usually available in form of extended tabulations as function of chemical composition, density, and temperature of the stellar material. When conduction becomes important the total opacity is given by the harmonic mean between radiative and conductive opacities.

When convection dominates, the real temperature gradient has to be given by some theory of convection. In deep convective regions, due to the very high efficiency of convective energy transport, the temperature gradient can be approximated by the adiabatic gradient within an accuracy of 10^{-8} (Cox & Giuli 1968), therefore,

$$\nabla = \nabla_{ad}. \tag{2.7}$$

For the convective envelope, the MLT of convection (see below) must used to derive a temperature gradient which is intermediate between the radiative and the adiabatic ones (Cox & Giuli, 1968).

2.3 Mass loss

Equations (2.1-2.2) and (2.5) describe the evolution of stellar models at constant mass. However mass loss from the stellar surface is a important observational fact which, at least for massive stars, has profound consequences upon evolution and cannot be neglected (see Chiosi & Maeder 1986). Because a self-consistent theory allowing to derive the rate of mass loss from the overall structure of the stars is still missing, mass loss is included by simply decreasing the total mass in the course of evolution according to empirical mass loss rates. The most widely used parameterization of the mass loss rate is by de Jager et al. (1988) which extend over the whole HRD. The mass loss rate is expressed as

$$\begin{aligned} \log \dot{M} = -a_1 \quad & -a_2 \quad x - a_3 x^2 - a_4 x^3 \\ & -a_5 y \quad -a_6 y^2 - a_7^3 \\ & -a_8 xy \quad -a_9 x^2 y - a_{10} x y^2, \end{aligned} \tag{2.8}$$

where $x = \log T_{eff} a_2 = 0.1104$ $a_3 = -0.4311$ $a_4 = 3.579$

$y = \log L - 5 a_5 = -1.571 a_6 = -0.0109$ $a_7 = -0.2175$

$a_1 = 6.3168$ $a_8 = -0.838 a_9 = -1.2487$ $a_{10} = 1.5822$

The above relation is often modified to include a suitable dependence on the metal content as suggested by the theory of radiation driven mass loss (Kudritzki et al. 1987 and references therein). Accordingly the above law of mass loss is commonly multiplied by the factor $\sqrt{(Z/Z_\odot)}$ (see Maeder 1993; Bressan et al. 1993).

Finally because the above formula definitely underestimates the mass loss rates observed in case of the very bright Wolf Rayet stars (WR), when the stars enter the WR stage, the mass loss rate is expressed by

$$\dot{M}_{WR} = 0.6 \times 10^{-7} (M_{WR}/M_{\odot})^{2.5} \tag{2.9}$$

where the rate is in $M_{\odot}$/yr, M_{WR} is current mass of the star (see Langer 1989).

3 Theory of Convection and Mixing Processes

Convection is perhaps the most disputed topic of stellar physics. Even today, while the main the main features of the structure of stars and the evolutionary scenarios are well understood, we are still facing with the lack of a satisfactory theory of convection.

Historically, our understanding of convection, comes from laboratory experiments (a good review is by Spiegel 1971,1972), in which the Boussinesq approximation is always acceptable. This stands on the notion that the vertical extension of the fluid is much shorter than the density and pressure scale heights, allowing the state quantities to be treated as constants. Another approximation usually assumed in astrophysical convection is that the fluid is anelastic (Gough 1969, Xiong 1986). The main consequence of this is that high frequency phenomena such as sound waves are filtered out, in the assumption that they are e not relevant to the energy transport. The Boussinesq approximation is adequate for laboratory convection, but does not hold for stellar convection, where all the thermodynamical quantities are known to vary considerably inside convective zones. In spite of this, the MLT of stellar convection follows actually the Boussinesq approximation.

3.1 Theory of Stellar Convection

The MLT has bee originally proposed by Böhm-Vitense (1958). The basic idea is to model the complicated pattern of structure and motion of convective elements by a suitable mean element with suitable velocity. In reality, convective elements may have sizes as small as the molecules and as large as the dimension of the whole field. On the contrary, the ideal elements

of the MLT all possess the same physical properties if generated at a certain radial distance r from the center. Each of theses is supposed to travel, on the average, over the distance Λ (defined as the mixing length), and then dissolve into the surrounding medium losing its identity By assumption, the dimensions of the average elements are assumed equal to Λ, the mixing length, and the shape of the elements is not specified. The are two characteristic lengths: the mixing length and the dimension of the element (in the MLT both are assumed to be equally proportional to the local the pressure scale height, with the proportionality coefficient taken as a free parameter to be fixed by comparing model results with observations. It is worth noticing that this kind of parameters exist also in some sophisticated models of stellar convection (cf. Xiong 1985,1986). A ideal self-consistent theory of convection should derive those typical scales from first principles instead of assuming them as parameters.

Despite the above drawbacks of the MLT, stellar models constructed with the MLT are in good agreement with the observations. Over the years, several attempts have been made to improve upon the theory of convection (cf. Spiegel 1960), and non-mixing length theories in alternative to the MLT have been proposed (Faulkner et al 1965, Unno 1967, Xiong 1985). Whether they are better than the classical MLT is not very clear. The same arguments apply also to current descriptions of convective overshoot (Maeder 1978, Bressan et al. 1981), which contain the same type of parameters to be determined by comparing model results with observations (see Chiosi & Maeder 1986, Chiosi et al. 1991).

Key point of convection theories is the formulation of the flux of energy carried by convection. In the framework of the MLT, the expression turns out to be very simple (see Cox and Giuli 1968) to whom we refer to shortly summarize the topic. In a convective region we assume complete pressure equilibrium between the elements and the surrounding medium, and the condition of hydrostatic equilibrium at each layer. A convective element formed at a certain radial distance r from the center starts moving with an initial temperature $T'(r)$ which is assumed to be the same as the value of the field. After travelling a distance δr from the original position, the temperature of the element changes by $\delta T' = \frac{dT'}{dr}\delta r$, while the

temperature of the average field is varies by $\delta T = \frac{dT}{dr}\delta r$. At the new position $r + dr$, the difference between the element and the surroundings is

$$\Delta T(\delta r) = \delta T' - \delta T = \delta r(\frac{dT'}{dr} - \frac{dT}{dr}) \tag{3.1}$$

Using the Schwarzschild notation (Schwarzschild 1958), $\nabla\Delta T = [(-dT/dr) - (-dT'/dr)]$, we have

$$\Delta T(\delta r) = \delta r \nabla \Delta T \tag{3.2}$$

Supposing here that the temperature will not change drastically over δr, and setting $T' \approx T$ along the path of the element, we can write

$$\Delta T = \delta r T[(-dlnT/dr) - (-dlnT'/dr)] = -\frac{dlnP}{dr}\delta r T[(\frac{dlnT}{dlnP}) - (\frac{dlnT'}{dlnP})] \tag{3.3}$$

or, with the definition of local pressure scale height: $\lambda_p = -\frac{dr}{dlnP}$

$$\nabla\Delta T(\delta r) = \frac{T}{\lambda_p}(\nabla - \nabla') \tag{3.4}$$

where $\nabla = \frac{dlnT}{dlnP}$ is the logarithmic temperature gradient (with respect to pressure), and the prime indicates the same quantity for the rising element. This gives the excess in temperature after the element has traveled a distance δr.

The distance is assumed to be equal to the mixing length Λ, which implies that the Boussinesq approximation is adopted. Specifically, replacing the distance with the mixing length requires Λ to be small so that T, ρ, P, etc... are approximately constant. This is immediately at variance with the value of Λ obtained from comparing model results with observations, indicating that Λ is about one pressure scale height (Schwarzschild et al. 1957, Sears 1959, Demarque et al. 1964).

The motion of this ideal element with an excess of temperature implies the flux of energy

$$F_c = \frac{1}{2}\rho v c_p \delta r \nabla \Delta T \tag{3.5}$$

where, ρ is the density, v is the speed of the element which will be given later, and c_p is the specific heat at constant pressure because of the pressure equilibrium. The numerical factor

comes from considering that both rising and sinking elements are present. Equation (3.5) gives the total flux with the factor replaced by one.

To determine the flux, the MLT uses an average over all possible δr. To this aim, δr is replaced by Λ, and all other factors are considered as averaged both over the distance the the horizontal layers at radial distance r. Accordingly, the flux is written as

$$\mathrm{F}_c = \frac{1}{2}\rho\bar{v}c_p\Lambda\nabla\Delta T \tag{3.6}$$

where $\bar{v}$ is the averaged speed of convective elements. With the aid of equation (3.4) we may write the expression for convective flux in the more convenient

$$\mathrm{F}_c = \frac{1}{2}\rho\bar{v}c_pT\frac{\Lambda}{\lambda_p}(\nabla - \nabla') \tag{3.7}$$

In order to evaluate the average velocity $\bar{v}$ we proceed as follows. Because of the temperature excess of the convective element with respect to the medium and pressure equilibrium, the density of the element is different from from the surroundings, and the element experiences the buoyancy acceleration and obey the equation of motion

$$\ddot{r} = -g - \frac{1}{\rho}\frac{\partial P}{\partial r} \tag{3.8}$$

Writing $\rho = \rho_0(1 + \Delta\rho/\rho)$, where ρ_0 is the equilibrium value, we get

$$\ddot{r} = -g\Delta\rho/\rho \tag{3.9}$$

where the subscription for equilibrium values has been dropped

This expression corresponds to the net buoyancy force: $f = -g\Delta\rho$.

At the starting point, there is no excess both in temperature and density, so this force is virtually zero there. The above equation gives actually the force at some new position after a displacement of δr.

Supposing the gravitational acceleration to be constant over the small distance δr, the work done by the net force over a finite distance Δr is

$$W(\Delta r) = \int_0^{\Delta r} f(\delta r)\mathrm{d}(\delta r) = -g\int_0^{\Delta r}\Delta\rho(\delta r)\mathrm{d}(\delta r) = -\frac{1}{2}g\Delta\rho(\Delta r)\Delta r \tag{3.10}$$

where in the last equality, we have supposed that $\Delta\rho$ varies linearly with Δr. The work is finally averaged over all possible Δr. To this aim Δr is replaced by the mixing length Λ, and a suitable numerical factor is introduced. the averaged work is

$$\bar{W}(\Lambda) = \frac{1}{4}W(\Lambda) = -\frac{1}{8}g\Delta\rho(\Lambda)\Lambda \tag{3.11}$$

However, during the motion a certain amount of energy is exchanged with the surrounding medium (friction, heat losses etc...) and therefore not all available work is turned into kinetic energy of the rising elements. The correct evaluation of the actual amount of work converted into kinetic energy is uncertain and its estimate require a detailed examination of convection efficiency. Therefore, for the sake of simplicity, we assume that only half of the work goes into kinetic energy of convective motions

$$\overline{\frac{1}{2}\rho v^2} \approx \frac{1}{2}\rho\bar{v}^2 = -\frac{1}{16}g\Delta\rho(\Lambda)\Lambda$$

from which the velocity to be inserted in the convective flux is derived

$$\bar{v}^2 = -\frac{1}{8}\frac{g}{\rho}\Delta\rho(\Lambda)\Lambda \tag{3.12}$$

Using the equation of state, we can replace density with temperature, keeping in mind the assumption of pressure equilibrium,

$$\Delta ln\rho = -Q\Delta lnT$$

where

$$-Q \equiv (\frac{\partial ln\rho}{\partial ln\mu})_{P,T}(\frac{\partial ln\mu}{\partial lnT})_P + (\frac{\partial ln\rho}{\partial lnT})_{\mu,P} \tag{3.13}$$

For a perfect gas, $Q = 1 - (\partial ln\mu/\partial lnT)_P$, while in general for a gas made of particles and radiation $Q = \frac{4-3\beta}{\beta} - (\frac{\partial ln\mu}{\partial lnT})_P$

In general the mean squared velocity can be written as

$$\bar{v}^2 = \frac{1}{8}gQ\frac{\Lambda^2}{T}\Delta\nabla T \tag{3.14}$$

Finally, the following expression for the convective flux is derived

$$F_c = \frac{1}{4\sqrt{2}} g^{1/2} Q^{1/2} \frac{\rho}{T^{1/2}} c_p \Lambda^2 (\Delta\nabla T)^{3/2} \tag{3.15}$$

to be used in the energy conservation equation of stellar structure, when the medium is found to be unstable against convection.

Before concluding this section, we present the typical values assumed by various quantities in external and internal convective zones.

Because of the high efficiency of convection in the core, the temperature gradient is very close to the adiabatic value (see also Xiong 1985). With aid of equation 3.15, and limited to solar conditions we estimate the departure from adiabaticity. Adopting $\beta = 1$, $Q = 1$, $c_P = (5/2)(\mathcal{R}/\mu)$, $\mu = 0.5$, $r = (1/2)R_\odot = 3 \times 10^{1}0\text{cm}$, $\Lambda = (1/10)R_\odot$,$T = 10^{7^\circ}K$, $\rho = 100gm/cm^3$,$M_r = (1/2)M_\odot = 1 \times 10^{33}gm$, $\kappa = 100cm^2/gm$, and $L = 4^{33}erg/sec$, we get

$$\Delta\nabla T \sim< 5 \times 10^{-12^\circ} K/cm \tag{3.16}$$

Noticing that $\mid dT/dr \mid \sim 10^{-4^\circ} K/cm$, it follows

$$\Delta\nabla T/\mid dT/dr \mid \sim< 5 \times 10^{-8}. \tag{3.17}$$

This is an extremely small number which implies that the adiabatic gradient is a fairly good approximation of the real gradient in stellar interiors. THe above values are significantly different for the outermost convection which is not of interest here.

As far as mixing is concerned we notice that the convective eddies moves randomly with a speed $v \sim 400cm/sec$ (once more estimated for the solar conditions), which gives a characteristic time scale of motion and mixing of the order of $\tau_c = \Lambda/v \sim 1year$. This is orders of magnitude lower than the nuclear burning time scale, and therefore, the core can be assumed to be homogeneous. It will be seen that this constitutes one of the major points of uncertainty of current treatments of of core convection.

3.2 Convective Overshoot

Classically, the border of a convective region (either core or envelope) is defined by the so-called Schwarzschild criterion, which actually gives the point where the acceleration of the convective elements vanishes. In fact the condition of instability in a homogeneous medium reduces to the inequality $\nabla_R > \nabla_{ad}$, which implies a small acceleration at the point where $\nabla_R = \nabla_{ad}$ But the elements may still move, due to their inertia, further into the stable region outside the convective zones. This is the problem of overshooting. Although the extent of overshoot and even its existence have been the subject of vivid debate (see the review papers by Renzini 1987, and Zahn 1991), the problem has been tackled in an impressive number of studies, among which we recall Shaviv & Salpeter (1973), Meader (1975,1990), Cloutman & Whitaker (1980), Bressan et al. (1981), Stothers & Chin (1981,1990), Matraka et al. (1982), Xiong (1983,1985), Langer (1986), Baker & Kuhfuss (1987), Meader & Maynet (1987,1989,1991), and Alongi et al. (1991a,b).

There are different formulations for overshoot that vary from author to author sometime with contradictory results. Saslaw and Schwarzschild (1965) found a very small overshoot distance, while Shaviv and Salpeter (1973) argued that this amounts to a significant fraction of the pressure scale height. In most studies the overshoot region region is described by means of the MLT and therefore contains the scale of mixing as free parameter (e.g. Maeder 1975, Bressan et al. 1981). On the contrary, the criterion proposed by Roxburgh (1975), is claimed to be parameter free. However, this has been convincingly criticized by Bressan (1984), and Baker and Kuhfub (1986) for its consistency. Nowadays, it is considered to to provide the maximum allowed distance of penetration (Roxburg I.W. 1989) According to Renzini (1987), the overshooting zone is small if the temperature gradient is radiative there, large if adiabatic. On the contrary, in Xiong's (****) treatment, the overshoot regions at the border of the convective cores of massive stars can be very large and radiative at the same time (see below).

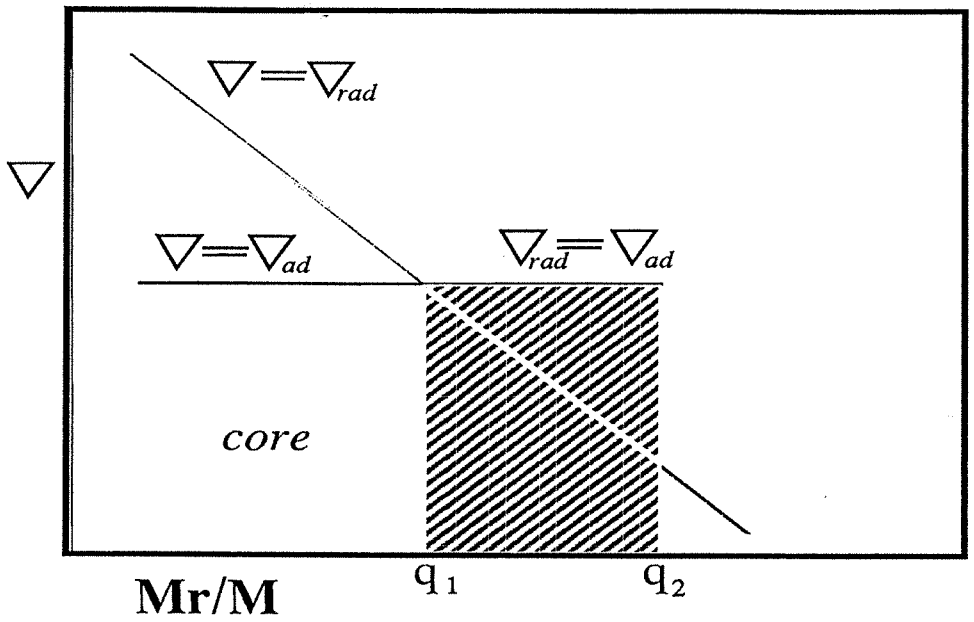

Figure 3.1: Temperature gradients in the stellar models. the dashed area indicates the region of overshooting. The fractional masses q_1 and q_2 correspond to the level at which acceleration and velocity of the convective elements become zero, respectively

Th local MLT is not adequate to study the problem of overshoot because the velocity is set to be zero at the border defined by Schwarzschild criterion. Therefore one hast to address to a non-local description of the motion. There are several ways in which this aim can be achieved (Maeder 1975, Cloutman & Whitaker 1980, Bressan et al. 1981). The one used in this thesis is by Bressan et al. (1981). This is shortly described here and extended to the general case in order to account for envelope and intermediate convective zones.

The Bressan et al (1981) treatment is based on the assumption that the temperature gradient is adiabatic

up to the point where the velocity becomes zero (*Figure* 3.1). and makes use of a non local version of the MLT. We start from the equation of motion (eq. 3.9) written as as

$$v\frac{\partial v}{\partial r} = -g\frac{\Delta\rho}{\rho}. \tag{3.18}$$

and instead of approximating $\Delta\rho$ as in in eq.(3.10), we integrate it from the original position r_1 to r,

$$\Delta\rho = \int_{r_1}^{r}[\frac{\partial\rho'}{\partial x} - \frac{\partial\rho}{\partial x}]\mathrm{d}x \tag{3.19}$$

The is not be the same as equation (3.15), because the excess of temperature of equation (3.2) is

$$\Delta T = \int_{r_1}^{r} [\frac{\partial T'}{\partial x} - \frac{\partial T}{\partial x}] \mathrm{d}x. \tag{3.20}$$

Correspondingly, the flux becomes

$$F_1 = k c_p \rho v \int_{r_1}^{r} [\frac{\partial T'}{\partial x} - \frac{\partial T}{\partial x}] \mathrm{d}x \tag{3.21}$$

where k is a numerical factor, which is set to 2 to take into account both rising and sinking elements. After some mathematical manipulations and ignoring the contribution of the gradient in molecular weight, one gets

$$\frac{1}{3} v^3 = \frac{1}{k} \int_{r_1}^{r} \frac{g}{T} \frac{X_T}{X_\rho} \frac{F_c}{c_P \rho} \mathrm{d}x \tag{3.22}$$

The convective flux is the difference between the radiative flux and the total flux, both of which are known throughout the whole star. The above equation is numerically integrated from the starting level r_1, up $r = r_1 + l$. where $l = \lambda H_p$ (H_p being the pressure scale height), and λ is mixing length parameter. The above integration is performed for all elements originated in the range r to $r - l$. Because the elements formed in this range may arrive at r with different velocities, the maximum velocity is used to characterize the velocity field at this position. Finally, the border of the convective core is defined where the velocity vanishes.

This condition refers to a chemically homogenous convective core. However, the term relative to the gradient in molecular weight cab be several orders of magnitude higher than the term relative to the gradient in temperature. This gives rise to the so-called barrier against the penetration of convection into stable radiative regions. Despite this, the barrier can be eroded by convective overshoot on a very short time scale and further extension of the convective zone is then possible (Castellani et al. 1971, Maeder 1975b, Renzini 1977).

3.3 The Xiong Model of Overshoot

Xiong's theory (Xiong 1985,1986) is perhaps the most sophisticated yet complicate treatment of convection by means of a non local MLT. His complex nature, does not allows to extend it

to all evolutionary phases, but only to the core H-burning phase where H and He dominate the chemical evolution in the core.

This theory stands on the basic dynamical equations of fluids with two components (cf. Landau and Lifchitz), and describe the turbulent convection in the classical manner. All quantities are written as the sum of the mean value plus their fluctuations. Furthermore, the equations for the fluctuations derived from subtracting the mean equations from the original ones. Finally, the equations for the correlation functions are obtained. The following assumptions are used

- In stellar interiors, the molecular diffusion flux and molecular viscosity are always small compared with turbulent diffusion and radiative conduction.
- Turbulent convection is supposed to be subsonic, therefore the fluctuations in temperature and density are negligible.
- High Reynolds numbers are characteristic of stellar convection, namely the dimension of the eddies for which viscous dissipation becomes important is much smaller than the dimension of the mean field.
- The inelastic approximation is used to filter out the sound waves.
- The fluctuation in gravitational potential is neglected.
- Turbulence is quasi-isotropic.
- Turbulent motion is quasi-steady, because the time scale of turbulent motion is much shorter than evolutionary time scales.
- The third order correlation functions are approximated by a gradient in those of the second order.

All the above assumptions but the last one seem to be appropriate. The effects of the last assumption have not yet fully explored. Furthermore, even in this theory there are

parameters measuring non-local effects and their relation with overshoot. This makes the theory somewhat uncertain.

3.3.1 An Application to Massive Stars

Xiong's theory has been used to calculate models of massive stars on the main sequence (Xiong 1986) and to study variable stars and helioseismology (Xiong 1980, 1982). In the case of massive stars, the total convective region (unstable core + overshoot) shrinks, leaving the convective region fully homogeneous because complete mixing is found. In the case of variable stars, since chemically homogeneous envelopes are considered, the complications arising from abundance gradients are removed, thus greatly simplifying the problem.

The main results for the models of massive stars can summarized as follows:

- Semiconvective instability does not occur.
- The evolutionary tracks run at higher luminosity than in classical models. The difference depends on the choice of the convection parameters c_1,c_2 (two numerical parameters in the Xiong theory which regulate the transport efficiency and mixing extension) and becomes larger for lower masses.
- The lifetime of the burning phase is much longer because the core is enlarged by a considerable amount. This however depends on the choice for the various parameters.
- The evolution occurs at much lower T_{eff}, which widens the main sequence band.
- A simple criterion for the onset of convection and overshoot does not exist. More precisely, neither the Schwarzschild nor the Ledoux criterion apply. The boundary of the convective core is set at the layer where the defined the convective flux changes sign. in any case, the structure of the stars is closer to that with the Schwarzschild criterion.
- The turbulent kinetic energy flux is less than 1% of the total, so it does never influence the star structure.

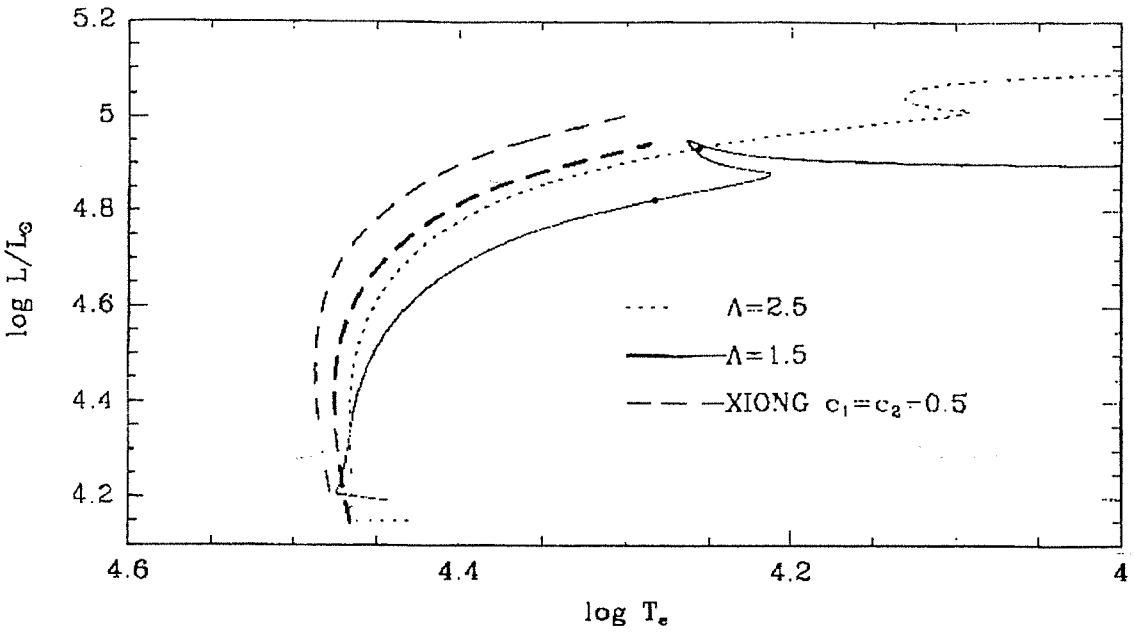

Figure 3.2: Evolutionary tracks of a. The thin dashed line is the Xiong model (1986). The solid and dotted lines indicate our models with $\Lambda = 1.5$ and $\Lambda = 2.5$, respectively. The heavy line show the Xiong model corrected for the different opacity in usage

- As a result of a negligible turbulent flux in overshoot region, the temperature gradient is very close to the radiative temperature gradient instead of the adiabatic one.
- The mass of the convective core is almost constant during the H-burning phase, but the overshoot region shrinks.

Many of the above results recover what already found with the overshoot model by Bressan et al. (1981) based on the MLT (see the recent review by Chiosi et al. 1991). To check the point I calculated models of massive stars using the PADOVA code and overshoot scheme. I recovered the results by Xiong (1986) adopting a large overshoot efficiency (Λ=2.5–1.5, where Λ is the overshoot parameter of Bressan et al. (1981). This is shown by the evolutionary sequences for a $15M_{\odot}$ star with different Λ

calculated for this purpose. As we can see from (*Figure* 3.2), the effective temperature in the hydrogen burning phase gets lower at increasing Λ. All the tracks run at higher luminosity

than the classical models. Concerning the positions of the ZAMS, we find some difference between Xiong's models and ours which is mainly due to the opacity. The opacity of our models is from Huebner et al. (1977) however modified to suitably enhance the opacity of the CNO ionization region (see Bertelli et al. 1984). Therefore, if we correct for the opacity and shift Xiong's track to the one with $\Lambda = 2.5$, we find a good fit. Table 1 gives $log(L/L_{\odot})$, $logT_{eff}$, the central composition, pressure and temperature, and the core mass of our models together with those by Xiong. Note that while the mass of the convective core in Xiong's models is defined approximately by the Schwarzschild criterion, the mixing region is larger than the value listed there. To conclude, it is clear that the main features of the Xiong models correspond to those of models calculated with the MLT and large overshoot.

However there are several systematic differences with respect to models from the MLT implying a different internal structure.

3.3.2 Difficulties with the Intermediate and Low Mass Stars

I have tried to apply the Xiong theory and numerical code to intermediate mass stars, namely stars more massive than 2 $M_{\odot}$ and with homogeneous chemical composition. As already pointed out by Maeder (1975), Bressan et al (1981) and Xiong (1985), models on the ZAMS are only marginally affected by overshoot. In the Xiong scheme, this is caused by the negligible energy transport by convection in the overshoot region. However, the size of the overshoot

region is larger than what found by other authors (Meader 1990, Bressan 1990), Fig. 3.3. This is mainly due to the choice made by Xiong for the convective parameters $c_1 = c_2 = 1/2$, which roughly corresponds to using $2H_p$ in the Bressan et al. (1981) formalism. However, we warn the reader that such extended overshoot regions lead to models whose properties disagree with the observations (see Chiosi et al. 1992 for a thorough discussion of this topic)

The application of the Xiong model for overshoot to evolutionary stages beyond the ZAMS is very difficult. Specifically, in evolved models the fluctuations of chemical abundances (here, the hydrogen content) are required, so that 17 equations (instead of 10 for homogeneous

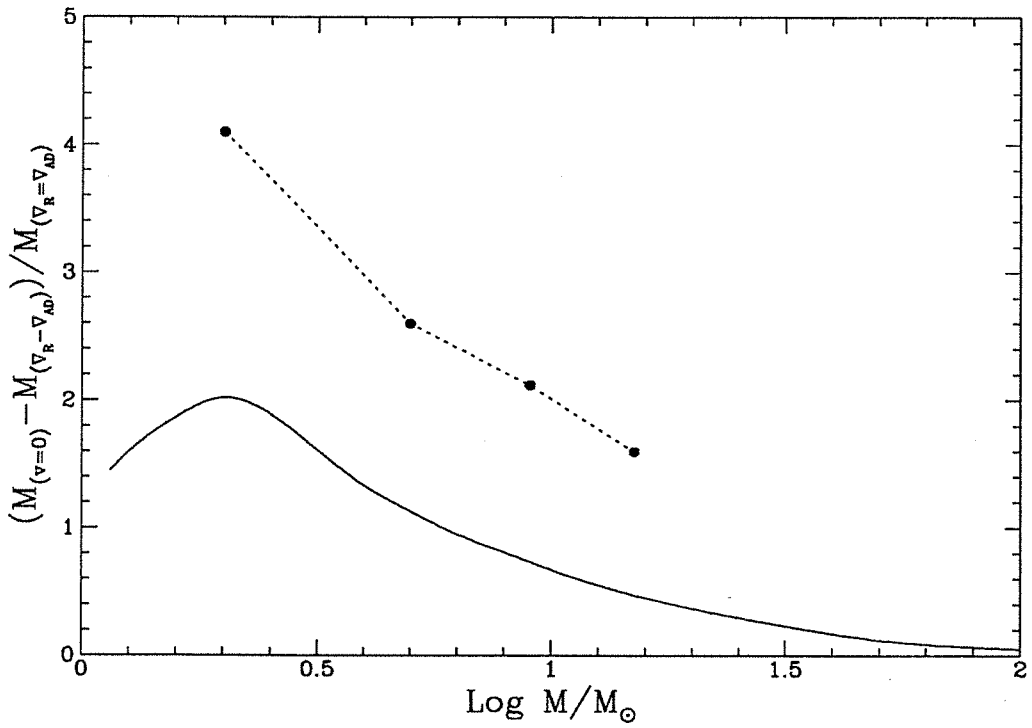

Figure 3.3: The ratios of the mass in overshooting region to the core mass (determined by Schwarzschild criterion). The solid line is from Bressan (1990), the dots are our results with Xiong's code

case) must be solved. As pointed out by Xiong (1986), these equations are of stiff-type, and the problem of spatial oscillations is met in the convective region. As a matter of facts, pressure and density in intermediate mass stars are larger than in the high mass ones, so that occurrence of the spatial oscillations renders difficult the convergency of the models to a solution. Very small time steps, which means small adjustments in chemical abundance and other quantities, are required to achieve a stable solution. Since the times steps get very small, the the numerical calculations become exceedingly time consuming.

In addition to this, there is another difficulty in Xiong's scheme, i.e. the increasing number of equations as more chemical elements are involved. If one more chemical element is included, four variables and four equations must be added, namely the cross-correlation functions with temperature, velocity and the other chemicals, and the auto-correlation functions. All this implies an enormous computational effort that is not paid by the final results, which look similar to those obtained from much simpler theories.

Furthermore, as the dependence on the pressure scale height used to determine the boundary of convective region, like in other overshoot models, the Xiong treatment suffers from the same problems met by other authors, i.e. the unbound growth of the core in low mass stars. Specifically, in the range of low mass stars (about $1.2M_{\odot}$), the core grows because the pressure scale height becomes large. This trend continues and tend to diverge. This is shown in Fig. 3.3, where the results from the Xiong method are illustrated. The overshoot region is very large (large core mass), whereas the ratio of the mass in the overshoot region to that in the Schwarzschild varies, with the stellar mass in the same way as in other simple methods.

To be used in stellar model calculations, ways out must be found to cope with the above difficulties. The key point are the chemical equations. One possible way out is to treat mixing of chemical abundances and all other processes involving the chemical abundances in a diffusion-like scheme, and and treat the structure and dynamic properties of turbulence in a separate manner. Although Xiong himself has argued against this possibility (Xiong 1986), in light of the problems mentioned above, I think it is worth looking back to diffusion. This

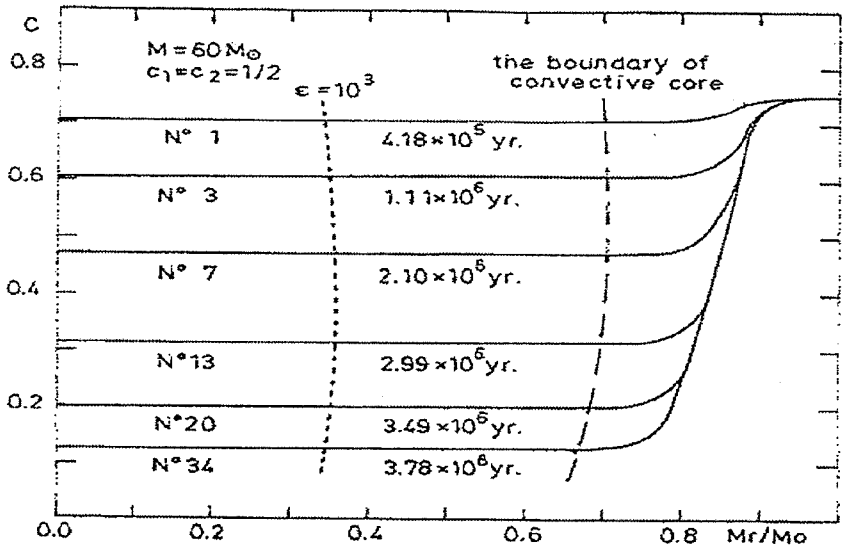

Figure 3.4: The hydrogen profiles in the model of the $60M_{\odot}$ star at various times at indicated. The dashed curve and the dotted curve demonstrate the location of the convective core and the nuclear energy generation rate $\epsilon = 1000 erg/cm\ s$, respectively. Reproduced from Xiong (1986). The region to the right of the dashed line is the overshoot region where the profiles of hydrogen are clear.

may not be so ad hoc as it may seem to be. In this context it is worth noticing that also in Xiong models, the composition profile of the overshoot region

smoothly varies across the structure (see Fig. 3.4). Although the Xiong treatment of the chemical composition is not a diffusive one, a diffusive-like profile results by suitably choosing the parameters of his model. All this will be discussed in a great detail in chapter 4.

3.4 Semiconvective Mixing

Semiconvective instability was first introduced by Schwarzschild (1958) studying the evolution of massive stars. The existence of semiconvection is due to the fact that radiation pressure and electron scattering dominate pressure and opacity respectively in massive stars. As a consequence of the high radiation pressure, the convective core tends to grow at increasing star mass and to expand as the star evolves, causing a chemical discontinuity to occur at the border of the core. Such a discontinuity would be less of a problem if the opacity were dominated by Kramers bound-free terms, but with dominant electron scattering, it soon becomes evident that radiative equilibrium outside the external border of the formal convective core cannot be maintained. The stability is restored if suitable mixing in that

region is allowed to occur. Theoretical models picture this region as undergoing sufficient mixing until the condition of neutrality is reached, but carrying very little energy flux. This type of mixing is conventionally called semiconvection (Chiosi & Summa 1970, Demarque & Mengel 1972). The neutrality condition is in turn affected by the presence of a gradient in molecular weight. Indeed, while for a homogeneous medium the neutrality condition is

$$\nabla_r = \nabla_{ad} \quad (Schwarzschild \quad criterion), \tag{3.23}$$

in the presence of a molecular weight gradient it becomes

$$\nabla_r = \nabla_{ad} + \frac{\beta}{4-3\beta}\frac{d\ln\mu}{d\ln P} \quad (Ledoux \quad criterion). \tag{3.24}$$

Theoretical models taking into account different conditions lead to different evolutionary scenarios. The Schwarzschild criterion tends to give smooth chemical profiles and some times leads to the onset of a fully intermediate convective layer. The Ledoux criterion is stronger than the Schwarzschild condition and tends to suppress the convective (semiconvective) instability.

The results from using the two conditions have been thoroughly described in Chiosi & Summa (1970), to whom the reader should refer.

There is another type of semiconvective instability that occurs during the core He-burning phase of stars of any mass. As He-burning proceeds in the convective core, the C-rich mixture inside the core becomes more opaque than the material outside; therefore the radiative temperature gradient increases within the core as the evolution proceeds. The resulting superadiabaticity at the edge of the core leads to a progressive increase (so called local convective overshoot) in the size of the convective core during the early phase of He-burning (Schwarzschild 1970, Paczynski 1971, Castellani et al. 1971a,b). Once the convective core exceeds a certain size, local overshoot is no longer able to restore the neutrality condition at the boundary. The core splits into an inner convective core and a outer convective shell. Engulfing a certain amount of helium, the shell becomes stable and leaves behind a region

of varying composition in which $\nabla_r = \nabla_{ad}$. This precess of mixing is named helium semi-convection, which is found to be important for low and intermediate masses up to, say $5M_\odot$, and negligible or missing at all for higher masses. Various algorithms have been devised to treat this kind of mixing (Castellani et al. 1971b, Demarque & Mengel 1972, Sweigart & Demarque 1972, Gingold 1976, Robertson & Faulkner 1972, Sweigart & Gross 1976, 1978, Castellani et al. 1985, Lattanzio 1986, 1987b, 1991, Fagotto 1990). This mixing is connected with another process taking place the end of the He-burning phase when $Y_c \leq 0.1$. It is otherwise named "Breathing Pulses of convection" (Castellani 1985). This type of convective instability alters the C-O core left over at the end of He-burning phase and the lifetime of the early asymptotic giant brunch (AGE) phase. The number ratio of AGB to horizontal branch (HB) stars suggest that the breathing pulses do not occur and that they are are an artifact of the particular algorithm in use (Renzini & Fusi-Pecci 1988, Chiosi 1986).

Semiconvective mixing can be also described by means of a diffusion process (Sreenivasan & Wilson 1977, Eggleton 1971, Cloutman & Whitaker 1980, Cloutman & Eoll 1976, Baglin et al. 1985) Indeed, the time-dependent mixing of diffusion generates a sort of smooth profile in the semiconvective region which mimics mixing imposed by the neutrality condition. The mixing efficiency is controlled by the diffusion coefficient which is usually taken as a parameter (see our discussion in *Chapter* 5) A clear advantage diffusion model of semiconvection resides in the fact that the time dependence of the mixing is automatically taken into account.

Including the effects of thermal dissipation in the analysis of the neutrality condition, Kato (1966) showed that the Schwarzschild criterion ought to be preferred to the Ledoux criterion in regions of varying molecular weight. However Langer (1983,1985) pointed out that this assumption was correct only for characteristic evolutionary times longer than the dissipation time scale and that the Ledoux criterion is recovered in the opposite case. Making use of a diffusive scheme, he adopted a fully convective diffusion coefficient when $\nabla > \nabla_L$

$$\mathcal{D}_L = \frac{1}{3} v l, \tag{3.25}$$

and a value suitable to semiconvective transport (with an efficiency parameter α) when $\nabla_S < \nabla < \nabla_L$,

$$\mathcal{D}_L = \frac{\alpha K_r}{6C_p\rho}\frac{\nabla - \nabla_S}{\nabla_L - \nabla}. \tag{3.26}$$

In this way, diffusion can account for the time dependence of the mixing process in different evolutionary phases. Furthermore, Langer (1983,1985) found that, for particular values of the efficiency parameter α, the Ledoux criterion was recovered inside the intermediate semiconvective regions which develop in massive stars after the central H-burning phase.

Finally, if semiconvective instability happens to occur in the region that could be interested by overshoot region, its mixing can be modelled by suitably choosing the diffusion coefficient. This point has originally been suggested by Caloi & Mazzitelli (1990), in the case of semiconvection for the core He-burning phase.

3.5 Global turbulent diffusion

The concept of turbulent diffusion was first introduced in stellar models by Schatzman (1977) to study the problem of the lithium abundance for the solar type stars. Solar type stars have a rather shallow convective envelope, which does not reach the layer where the lithium is burned, nevertheless they show continuous depletion of surface lithium with the age. This suggests that the material at the bottom of the convective envelope is transported in regions of higher temperature where lithium burning can occur. To this aim, Schatzman suggested the so-called mild turbulent mixing process, inducing slow mixing. The suggestion stands on the idea that mild turbulence exists throughout the star, which slowly carries material from the surface down to the regions where lithium is burned. The diffusion is regulated by the critical Reynolds number at which mild turbulence is supposed to develop. The diffusion coefficient is $D = \frac{1}{9}\nu R_e$.

Numerical models yield very promising results. WE like to point out that turbulent diffusion could also develop in massive and it could be the unknown mixing mechanism invoked by Bohannan & Fitzpatrick (1992) to account for the surface abundance anomalies

observed of several blue supergiants. These stars are found to be Helium and Nitrogen enriched as if they are exposing CNO processed material at the surface.

This possibility of turbulent diffusion in massive stars (thereinafter the *global mixing*) will be examined in *Chapter* 8.

4 Problem in the Interpretation of the HRD of Massive Stars

In recent years, the evolution of massive star has received much attention thanks to the flourishing of observational data for supergiant stars in the Milky Way and nearby galaxies, the discovery of high rates of mass loss, and the exceptional event of the the explosion of the supernova 19878A in the Large Magellanic Cloud (LMC) and the problem raised by its blue progenitor. These observations put very strong constraints on current theoretical models for massive stars. the theoretical models that have been proposed so far.

4.1 The HRD of supergiant stars

The most recent HRDs of the massive stars in the solar vicinity and in the LMC have been published by Blaha & Humphreys (1989) and Fitzpatrick & Garmany (1990), respectively. *Figure* 4.1 shows the HRD of all known luminous (massive) stars in clusters and associations within 3 Kpc of the sun together with the schematic position of the WR stars from Schmutz et al. (1989). *Figure* 4.2 gives the HRD for the supergiant stars of the LMC. Although these samples are based on different selection criteria (the spectral types for the galactic supergiants and the two colour photometry for the LMC supergiants), and suffer from a certain degree of incompleteness difficult to assess, in particular among the earliest and the latest spectral types, the above HRDs show common features that can be used to constrain theoretical models.

In particular, we notice the following features deserving a careful examination: (1)*The Upper Luminosity Boundary*, (2) *The Absence of the Blue Hertzsprung Gap*, (3) *The Ledge*

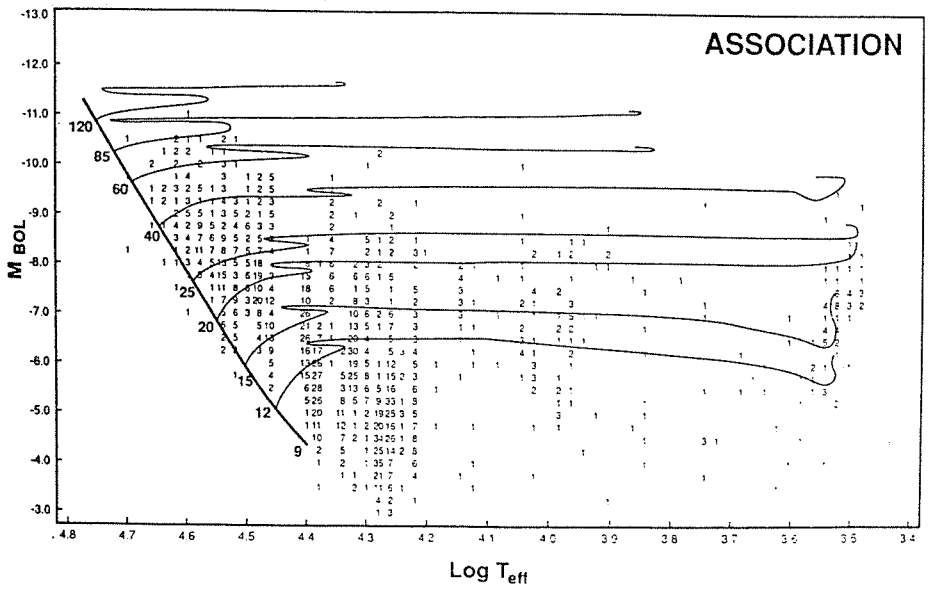

Figure 4.1: the HRD for luminous stars within 3 Kpc of the Sun. The tracks are from Maeder & Meynet (1987), a total number of 2002 stars are included. Reproduced from Blaha & Humphreys (1989)

of Blue Stars, (4) *The Population of Red Supergiants*, (5) *The red Hertzsprung Gap*, (6) *The Deficiency of Main Sequence Stars.* All they will discussed in detail below.

4.1.1 The Upper Luminosity Boundary

In both of the HRDs, the most luminous blue stars are about a factor of six brighter than the most luminous red stars, as first pointed out by Humphreys & Davidson (1979). The most luminous hot stars reveal an upper envelope of declining luminosity with decreasing temperature, whereas stars stars cooler than about 8000-10,000 K, show a limit at a roughly constant luminosity of $M_{bol} \sim$ -9.5. Humphreys & Davidson (1979) and Chiosi et al. (1978) first drew the attention to the physical significance of this empirical boundary and the lack of cool, evolved massive stars at highest luminosity. Since massive stars evolve from the main sequence towards cooler effective temperature at roughly constant luminosity (Chiosi & Maeder 1986), the observed absence of stars to the right of the boundary may mean that either

stellar evolution proceeds so fast that the probability of observing star with M$\geq$ 50M$_\odot$ is very low, or that the most luminous blue stars never become red supergiants but evolve directly to WR stages (bright stars located near the main sequence, with anomalous spectra, and the highest rates of mass loss).

Humphreys & Davidson (1979) suggested that this boundary is caused by a kind of instability related to mass loss, which encountered by the most massive stars as they evolve away from the main sequence. As a matter of fact, the highest mass loss rates are observed along the boundary (de Jager et al. 1988). The boundary itself is marked by the presence of some very luminous unstable stars, known as Luminous Blue Variables (BLV). The LBVs which mark the luminosity boundary are evolved, very luminous, hot and unstable stars which suffer irregular ejection of mass. Typical members of this group are η Car, P Cyg, and S Dor. These objects are characterized by: 1. An outburst or ejection phase at visual maximum with an enhanced mass outflow of 10^{-4} to 10^{-5}M$_\odot$/yr, a slowly expanding (100-200 km/sec), cool (8000-9000) and dense ($N \sim 10^{1}1cm^{-3}$) envelope or false photosphere; 2. At visual minimum or quiescent stage the star resembles a high temperature supergiant ($\geq 25,000\ K$) with emission lines of hydrogen, helium and permitted and forbidden life of Fe II and with lower mass loss rate; 3. During these variations in visual light, the bolometric luminosity remains the constant. The visual variations are caused by the shift in the stars' energy distribution; 4. Many of LBVs are surrounded by structures (observable in the visual and IR) including circumstellar nebulae, visible ring an shells; 5. The ejecta and atmospheres of the LBVs are hydrogen and helium rich showing that the LBVs are evolved, post-hydrogen stars.

The physical cause of the boundary is usually identified with the balance between the acceleration due to gravity and Eddington gradient of radiation pressure. However to explain the temperature dependence of the boundary for the hot stars, other effects must be considered. The work of several investigators (Humphreys & Davidson 1984, Appenzeller 1986, Lamers 1986, Lamers & Fitzpatrick 1988, Davidson 1987, de Jager 1984, Boer et al. 1988,

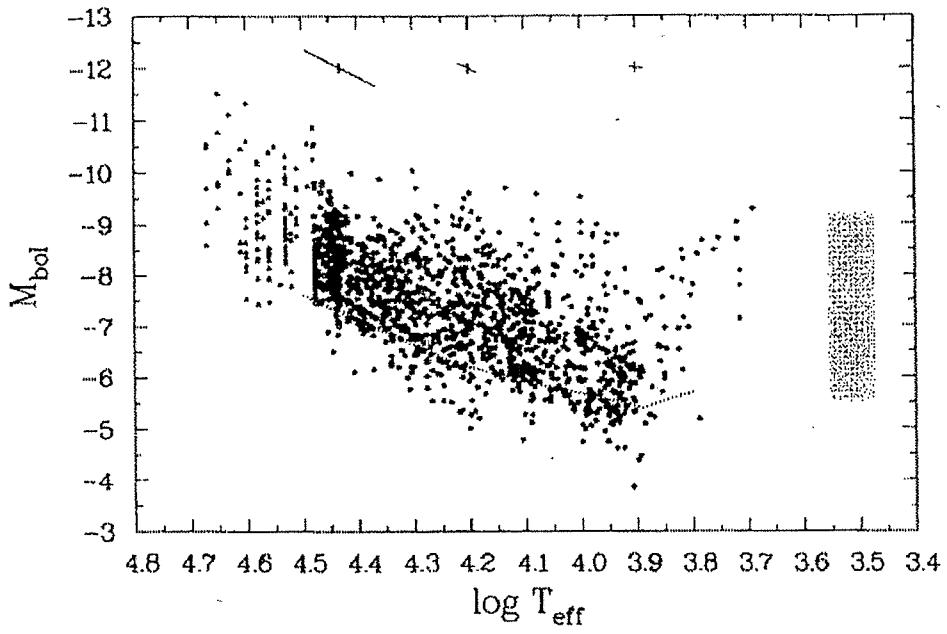

Figure 4.2: the HRD for luminous stars in the LMC. The tracks are from Maeder & Meynet (1988), The ledge is shown by the solid diagonal line. The dotted and dashed lines are the luminosity boundaries from Garmany et al. (1987) and Humphreys (1987). the shaded area is the population of red supergiants. Reproduced from Fitzpatrick & Garmany (1990).

Piters et al. 1988; de Koter et al. 1988, Carpay 1989) have shown that the boundary (stability limit) is the consequence of radiation pressure for the hot stars, and turbulent pressure gradient in the atmospheres for cool stars.

4.1.2 The Blue Hertzsprung Gap

The problem of the blue Hertzsprung gap comes from the comparison of the observed HRDs of the supergiants with the theoretical tracks, and refers to the region just to the right of the main sequence band. In this region, due to the very short evolutionary time scale (Kelvin–Helmholtz) there should be very few stars, whereas a large number of stars is observed.

The nature of these star is a matter of debate. The same area of the HRD, especially the upper left corner of the HRDs above, can be populated by stars from different evolutionary stages according to current understanding. A large fraction of the bright OB type stars can

be more evolved than the position of these objects in HRD may imply. This is substantiated by the observations of CNO processed an helium rich material at the surface of some of these stars. In fact, the group of OBN/OBC stars (Walborn 1988) and the helium rich objects near the main sequence (Kudritzki et al. 1983, 1989; Bohannan et al. 1986) are considered typical examples of stars, in addition to WR stars, whose interpretation is based on the exhibition at the surface of CNO and 3α processed material.

Spectral observational data for several B–type supergiants, like the stars in the blue Hertzsprung gap of the LMC-HRD (Fitzpatrick & Bohannan 1992), shows that the vast majority of LMC B-type supergiants has their surfaces contaminated by material from their original hydrogen-burning cores. The very high rate of contaminated (80%) objects cannot be attributed to peculiarities or anomalies affecting a few stars. Four possibilities were proposed by Fitzpatrick & Bohannan, namely: (1) accretion by blue supergiant secondaries of processed matter from initially more massive and more evolved companions; (2) stripping of the original H-rich envelope by mass loss; (3) rotationally induced mixing during the main sequence phase; and (4) convective mixing during the previous red supergiant phase.

The first possibility is excluded by the high rate of 80%; The second one would imply that, since the initial mass of the stars in the sample is about 20 $M_{\odot}$, the mass loss rates are roughly one order of magnitude greater than currently assumed. Indeed, the observations by Feast (1992) of the RSG variables, in the LMC, show on average mass loss rate about one order of magnitude higher than that derived by the empirical formulation of de Jager et al. (1988), thus making plausible this possibility. The third suggestion is advanced by Meader (1987). Specifically, below some critical rotational velocities the evolution is normal and the stars evolve toward the red regions of HRD, with some changes in the surface abundances when rotation is close enough to the critical value. The last possibility seems the most promising, as stellar models with the required type of evolution, namely blue-red-blue, have been proposed long ago (see for instance case A of Chiosi & Summa 1970). Models of case A can undergo surface enrichment in agreement with the observations. caused by the deep

convective mixing in the red phase (Langer 1989, Bressan et al. 1993, Fagotto et al. 1993). The crucial point with this scheme is the extension of the blue loop. More precisely, models with the desired abundaces at the surface tend to possess rather short blue loops thus failing to account for the position in the HRD of the type of stars on consideration. When the blue loops develop, the surface abundances are not in the right pattern.

4.1.3 The Blue Ledge

The density of stars in the HRD of the LMC supergiants (see *Figure* 4.2) shows a distinct decrease redwards of $3.9 \leq \log T_{eff} \leq 4.2$, with the density drop-off following a diagonal line, otherwise called the "ledge" that goes to lower luminosities at decreasing T_{eff}. Similar ledge is marginally visible in the HRD of galactic supergiants (*Figure* 4.1) but somehow washed out by the uncertainties in the distance and hence the absolute magnitudes of galactic stars. The plausible explanation of the ledge is that stars of initial mass up to about 40–50$M_{\odot}$either perform an extended blue loop in the HRD during helium burning phase (Chiosi & Summa 1970, Langer 1990, Bressan et al. 1993), or slowly move redwards in the HRD (Brunish & Truran 1982a,b). However, it is not yet possible to discriminate the real evolutionary scheme without additional information such as data on surface abundances.

4.1.4 The Population of Red Supergiants

The population of red supergiants is distinctly separated from all remaining stars in the HRDs. The maximum luminosity attended by the stars in this group in about $M_{bol} = -9.5$. There are a few differences between the Galactic and LMC M-type supergiants that can be ascribed to different chemical compositions. The ratio of red to blue supergiants in the luminosity range $-9.5 \leq M_{bol} \leq -6.5$ is about 1:10 (Humphreys & McElroy 1984). Since the generally accepted idea is that the vast majority of red supergiants are genetically connected with the massive blue stars, rather than AGB stars coming from the lower range of mass (Brunish et al. 1986), the obvious implications is that in the above luminosity range the evolutionary models must account for the existence of blue and red supergiants at the same time. How

this can be achieved is not very clear. The most popular view is that red supergiants are in some early stages of core He-burning, therefore following the scenario of case A, even if the alternative of late stage of the same phase as in Case B cannot be excluded. From the data on surface abundances the former is more likely, because the deep mixing during the red phase may explain the existence of the processed matter at the surface. There are however several points of uncertainty: first current models with loop do not extend it enough, second the efficiency of mixing during the red supergiant stages is not fully understood.

4.1.5 The Red Hertzsprung Gap

Very few stars occupy the region just to the blue side of the M-supergiants, or in other wards the so-called red gap. This is clearly shown by the HRDs of *Figure* 4.2 and *Figure* 4.1. The interpretation of this gap does not give rise to particular difficulties as almost all evolutionary models, no matter whether they evolve during the core He-burning phase according to Case A or the Case B scheme, are known to cross this region on a very short time scale.

4.1.6 The Deficiency of Main Sequence Stars

The inspection of *Figure* 4.2 reveals a deficiency of stars with $M \geq 40$ $M_{\odot}$near the theoretical ZAMS. This was first noticed by Garmany et al. (1982) using a different sample of stars. The comparison with theoretical isochrones indicates that the youngest known H-burning O-type stars have already an age of about $1-2\times\ 10^6$ years so that about 20% of thee core H-burning life time is not observed. This agrees with the empirical estimate by Wood & Churchwell (1989) that about 10–20% of all O stars in the solar vicinity are embedded in molecular clouds, and therefore only indirectly detectable by their interaction with the surrounding medium. Only about 10^6 yèars after the start of central H-burning, the star becomes visible. Since the fraction of 10–20% is comparable to or even larger than the total fraction of stars in post main sequence stages, this point together with that of the photometric incompleteness of the data sets are crucial when comparing the theoretical predictions with the observed star frequencies.

4.2 The Peculiar Class of Wolf-Rayet Stars

Massive stars lose a large fraction of their mass by stellar wind. Mass loss gets more and more important as the initial mass increases, and finally dominates the whole structure and evolution of a massive star (Chiosi & Maeder 1986). Starting from certain initial mass, the strong stellar wind may strip off all the envelope, and gradually expose the processed material, otherwise buried in the deep interiors in absence of mass loss. This has a direct observational counterpart, namely the group of Wolf-Rayet stars (WR).

The WR stars are commonly understood as central He-burning objects that have lost the main part of their hydrogen-rich envelope, and in consequence show products of different burning stages. The surface composition is used to assign the evolutionary stage of these objects and to classify these stars.

The situation is as follows. For initial masses higher than $60M_{\odot}$, the winds are strong enough to remove all stellar outer layers, leaving almost a bare He core during the core H-burning phase. This prevents further evolution towards the red supergiant stage, and therefore the stars always remain at the blue side of the HRD. They are located in a region of so called Luminous Blue Variables (LBV). Such an identification is confirmed by spectroscopic observations (Conti et al. 1983, Smith & Willis 1982, Hamann et al. 1993). As a result of the very high mass loss rates ($10^{-3}M_{\odot}$/yr or more), remaining part of of the envelope is ejected and the star evolves directly as a bare core, becoming a good candidate to the WR phenomenon

On the contrary, for initial masses between $25M_{\odot}$, and $60M_{\odot}$, because the mass loss is not strong enough to peel off the outer layers, the stars move rapidly to the red side of the HRD and spend part of their He-burning life time as red supergiants. The evolution toward the red is facilitated by the absence or very small size of the intermediate convective zone above the H-burning shell.

The red supergiant phase of these stars is expected to be longer than in the case of

constant mass models. Because the strong winds in this stage progressively remove the outer envelope, the outward shifting of the H-burning shell increases size of the He-core, and the fractionary mass of the core gets larger and larger, these models will evolve toward the blue areas of the HRD (Chiosi et al. 1978, Maeder 1981a,b). The occurrence of the blue loop depends on weather or not the wind is strong enough to remove the envelope within the lifetime of core He-burning. The lower mass limit for this to happen is estimated about $40M_{\odot}$ (Chiosi & Maeder 1986).

WR stars, whose spectra are dominated by strong emission lines, are generally grouped into 3 sequences according to their spectra: WN, WC and WO. The spectra of the WN stars exhibit transition lines of He and N ions with little evidence of C; those of the WC stars predominantly show lines of He and C with little evidence of N; finally the spectra of rarer WO stars are dominated by lines of O. In general, WN stars show little or no evidence of hydrogen, and no hydrogen is seen in the other two sequences: WC & WO stars. However, WN stars are commonly separated into two further groups according to whether or not they show evidence of some significant H. Broadly speaking, separation corresponds to that between early (WNE–little or no H) and late (WNL–some significant H) WN stars.

The formation of the WR stars are generally understood as result of the evolution of massive stars under the effect of mass loss, and the various groups are associated to different stages of evolution and different type of processed material being exposed at the surface: WN stars should exhibit CNO processed material, while WC and WO should exhibit He-burning products. Depending on the mass loss rate and initial mass of the star (and hence size of the core), CNO material can be exposed either in late stages of core H-burning or during the core He-burning. In this context the formation of WC and WO stars is always associated to some advanced stage of central He-burning, and high rates of mass loss. The lower mass limit for the WR phenomenon to develop is estimated at about $20\text{-}30M_{\odot}$. (Chiosi 1982, Bertelli et al. 1984, Chiosi & Maeder 1986).

4.3 The Progenitor of the SN1987A in LMC

The blue progenitor of the SN1987A in LMC has spurred many questions about the evolution of massive stars. In particular it has called the attention on the various physical causes that may determine the final explosion of a massive star as a blue supergiant. The various possibilities have been presented by Meader (1992):

- **Constant Mass Models with low Z:** These models (cf. Hillebrandt et al. (1987) may terminate their evolution as blue supergiants, but they cannot produce red supergiants and N/C-enhanced abundances at the surface, in contradiction with the observation.

- **Models with low Z and Mass Loss:** these models may terminate their life in the blue as a result of mass loss (cf. Wood & Faulkner 1987, Maeder 1987) only if the envelope mass is smaller than $1M_{\odot}$, which is not supported by the interpretation of the light curve of SN1987A itself.

- **Constant Mass Models with the Ledoux Criterion:** Constant mass models with this condition for intermediate convective shell have been proposed by Woosley (1988). However, when a moderate amount of mass loss is taken into account, these models get the blue supergiant configuration too early in their life, i.e. during the core He-burning phase. This does not agree with the observational evidence that the precursor of SN1987A was a red supergiant a few thousand years before the explosion.

- **Models with late Mixing:** The possibility of extra mixing of the external layers of a red supergiant at the end of the He-burning phase has been investigated by Saio et al. (1988). Although the physical cause of the mixing is not clear there is the remote possibility that the external and intermediate convective zone get very close each other, so that a small efficiency of overshoot could cause the merge of the two regions, If this occurs, the resulting mixing would simultaneously produce He- and N/C-enhancement at the surface and the desired blue supergiant configuration In this

context, the evolution during the core H- and He-burning phases occurs normally, and the extra mixing intervenes only during the very late stages.

- **Models with semiconvection:** Semiconvection produces mild mixing in zones with a μ gradient. Models including this effect have been proposed by Langer (1991) and Arnett (1991). These models are able to explain the blue progenitor. The physical cause responsible for the blue final location has been described by (Langer 1991). Semiconvective mixing reduces the He-content in the He-shell, which is therefore less efficient. Thus at the time of CO core contraction, i.e. at the end of He-burning, the He-burning produces only a weak expansion of the layers between the He- and H-burning shells. Thus the H-burning shell does not extinguish, and according to the "mirror principle" (see Chiosi & Maeder 1986 for details) induces a a strong contraction of the external envelope. The blue progenitor can form. However, these models require very fine tuning of the various physical parameters of model structure (initial composition, opacities, nuclear reactions, etc....) in addition to those driving mixing so that the general applicability of these models is weakened.

In general, the most successful models of the progenitor of SN1987A are those with semiconvection (eg. Langer 1989). However, since these models should also account for the overall properties of supergiant stars and not be specific to the supernova event the application to the whole family of supergiants is hampered by their limited validity.

5 A New Model for Diffusive Mixing by Convection

In almost all stellar model calculations, mixing of chemical elements inside the convective zones is assumed to be instantaneous, i.e. on much shorter time scales compared with any other time scale in which the chemical abundances can change (eg. nuclear reactions). The velocities predicted by the MLT are high enough to secure a time scale for mixing much shorter than that of the nuclear burning, so that homogenization of the convective region is achieved.

However, the MLT does not specify the detailed structure structure of the velocity field, but consider only the mean properties convective elements, i.e. the large scale motions. It goes without saying that fine mixing cannot be the result of considering only large scales. Specifically, contrary to what happens with other physical quantities the homogenization of chemical elements requires motions all over the possible scales down to very small eddies.

This requires a good theory of convection which unfortunately is not yet available. In fluid mechanics, the mixing process is viewed as a sort of stretching of the material in the turbulent field (see Ottino 1990). What we learn from laboratory experiments is that the speed of mixing is not high enough to wipe out inhomogeneities over large periods of the large scale motions. Actually, fine mixing can be reached only asymptotically, which means that mixing is rather slow, at least much slower than the turnover time scale of the largest element of fluid. If the mixing of chemical elements in a convective zones is directly related to the motions on the smallest scales, the smaller velocity and length scale of motion the

slowest the speed of mixing

There is another phenomenon to be considered, namely intermittence. This has been observed in laboratory experiments and meterological studies, and also found in numerical simulations. Intermittence tends to slow down the mixing process for small scales.

The plan of this section is first demonstrate that MLT cannot give the desired type of mixing, second to formulate the problem of the mixing time scale by means of a phenomenological description of of turbulence.

5.0.1 What Does MLT Tell Us About Mixing ?

The basic assumptions of the MLT, namely the mixing length scale, the average eddy dimensions, and the mean free path over which elements keep their identity, lead to inconsistent results as far as mixing is concerned. The motion of the largest elements of fluid does not generate mixing. Rather this has to be assumed to suddenly occur at the end of an eddy lifetime. This can be easily proved by the following arguments.

The time required by a convective element to travel the largest distance scale, i.e. the core radius, is

$$\tau = L/v \tag{5.1}$$

where v is the mean velocity predicted by MLT for an eddy of dimension L. This time scale is also a measure of the rate at which mixing can occur if pictured as a diffusion process with the coefficient

$$D = \frac{1}{3} vL, \tag{5.2}$$

(see eg. Malagoli et al, 1990). However this is exactly the lifetime of an eddy given by the MLT, during which there should be no mixing at all. Instantaneous mixing is likely not to exist.

Let us now examine what kind of mixing can be generated by the eddies with the largest dimensions. The large dimensions of the bubbles also mean that only few of them can be present at the same time. Should all the bubbles keep their identity, very little mixing would

result. Furthermore, if the hypothesis of final sudden mixing is dropped, in order to keep the convective region active and conserve the net flux of mass at each layer equal to zero, the matter contained in the ascending flow has to return back to the original position maintaining unchanged the composition as any other times scale for mixing should be equal to or longer than the motion and thermal diffusion time scales. In such a case a sort of circulation at constant chemistry would result.

However, the above arguments do not mean that convective motions at large scales cannot homogenize the central regions. In fact, even with a low mixing rate, the largest scale motion in the nuclear burning region may keep the region homogeneous, because the nuclear burning time scale is much longer than the crossing time of a convective element, and all the material contained within one mean free path from the center has the same probability of entering the central regions where nuclear burning is vigorous. No matter how slow the actual mixing process is at the small scales, the convective motions at the scale of the one free path homogenize this region. The mixing speed is given by equation (5.1)

5.0.2 A Phenomenological Picture of the Velocity Field

By velocity field we mean the velocity distribution as function of the scales. Since we are re not dealing with the convective energy transport, we adopt the the formulation by Bressan et al. (1981) which makes use of the MLT and can also describe velocity of the largest elements of fluid in the overshoot region.

The high Reynold number of stellar convection shows that the convective regions inside the stars are turbulent. All the spatial scales are present from the largest ones (which are of the order of the dimension of the field) down to tiny bubbles (which may have the dimension of molecules).

5.0.3 Intermittence of the Turbulence

Intermittence has been observed in the laboratory turbulence (see Fernando 1990, and references therein), and in astrophysics it has been applied to study turbulent convective motions

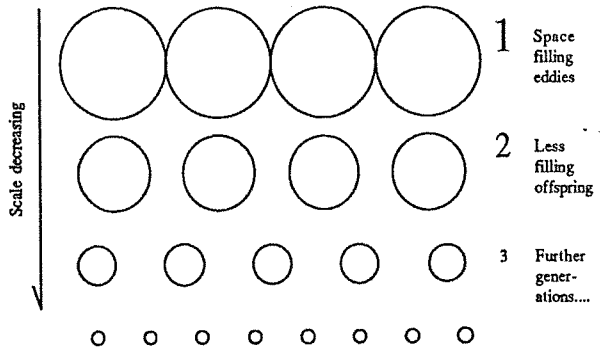

Figure 5.1: A schematic plot of the intermittent turbulent field. The off-springs of any given generation can be embedded in their parental eddy, which is not shown for the sake clarity

by Malagoli et al. (1990). In short, when we look at the small structures in a turbulent field, the eddies are seen to acquire smaller spatial fractions as their dimension decreases as sketched in *Figure* 5.1; a 3D simulation of convection showing this phenomenon can be found in Malagoli et al. (1990). Small fraction means that in order the turbulent motion be able to cover all the field, the eddies requires much longer times (many more periods) to statistically fill the available space. This incomplete space filling affects the transfer of momentum in the turbulent field, and in turn the transport of chemical elements, because mixing is preferentially produced by the small scales. The main effect would be a slower speed of mixing.

There are many ways in which intermittence can be taken into account. In this study, we prefer to adopt the simple description based on a dimensional analysis by Fisch (1977), i.e. the so-called β-model which provides useful expressions for both the kinetic energy transfer and intermittence.

5.0.4 Effects of a Steep Gradient in Molecular Weight

To complete our discussion of convective mixing we need to consider the distortion of the velocity field caused by a gradient in molecular weight. This situation could happen inside real stars either at the border of a growing convective core or at the base of a penetrating envelope. In massive stars ($M > M_{\odot}$) and low mass stars ($1.1\ M_{\odot} < M < 1.6\ M_{\odot}$) during the

central H-burning phase, and in all stars during the central He-burning phase the convective core tend to increase giving rise to a barrier of molecular weight. The second alternative may be present when the star approaches the Hayashi limit and a depth convective envelope develops. There are many speculations about how this barrier of molecular weight could affect the efficiency of mixing (see Renzini 1977). It turns out that it could even stop the convective motions if we limit the analysis to those along the direction of the strong restoring force. However, if we consider that in a real situation elements may undergo stretching or deformation (Ottino 1990), motions in other directions may be produced when the convective elements meet the barrier. It will be shown that the barrier of the one dimensional case can be source of other instabilities, the effect of which may disrupt the boundary and therefore provide some extra mixing.

First of all, we need to discuss whether or not penetration (mixing) through a molecular gradient is possible. To estimate the overshoot distance, one usually takes a test element with the average properties given by the MLT (e.g. Renzini 1977) and seeks the point were the restoring force overwhelms inertia. Therefore, the penetration distance of a cylindrical element is

$$d_p^2 = \frac{\lambda v_0^2}{g(1-\mu^o/\mu^i)} \tag{5.3}$$

where λ is the mixing length, g is the local gravity, μ^o and μ^i are the mean molecular weight for matter outside and inside of the discontinuity respectively.

The penetration distance is $\sim$ 3 orders of magnitude smaller than λ, so that overshoot through the molecular barrier is virtually zero.

However as the element is not a rigid body, it is hard to conceive that it would immediately stop. Similarly, it is difficult to accept the that an element moving with the large speed of the bulk motion, keeps its shape when it matches the barrier. WE can picture the real situation imagining that the element will change shape and move toward another direction. Since the total mass of the element must be conserved, the only possible motion is along the tangential direction, along which no buoyancy force, and negligible viscous force are experienced. If the

tangential motion turns out to be turbulent, mixing along this direction would be easier than along the vertical direction (e.g. Zahn 1991, Charbonnel & Vauclair 1989).

The tangential velocity can be estimated using the mass conservation condition. Writing

$$\frac{1}{4}\pi l^2 v_0 \approx 2\pi(\frac{l}{2})d_p v_t \tag{5.4}$$

we get the tangential velocity v_t

$$v_t \approx \frac{1}{4}\frac{l}{d_p}v_0 \tag{5.5}$$

where v_0 and l are the velocity and dimension of the element, respectively. It is clear from this equation that larger v_t is to be expected for larger values of l and v_0, and for smaller d_p. To derive the above estimate, we have assumed the density to be constant. It follows that in presence of a discontinuity in molecular weight, the tangential velocity is greatly amplified (e.g. Renzini 1977).

Because the matter above the transition level is basically at rest, the tangential motion will surely create shears at the interface. The question arises whether these shears are strong enough to trigger an instability. To this aim we consider the Richardson number for a stratified fluid (Chandrasehkar 1958 Chap.103), in our case that of the gradient in molecular weight (Zahn 1983),

$$J_r = \frac{g}{H_p}\frac{d\ln\mu/d\ln P}{(dv_0/dz)^2} \tag{5.6}$$

The Richardson condition says that the interface is stable if $J_r > \frac{1}{4}$ everywhere. Rewriting equation 5.6 in our formalism we obtain,

$$J_r = g d_p \frac{\mu^i - \mu^o}{\bar{\mu}v_0^2}. \tag{5.7}$$

With the aid of typical estimates of the various quantities at the border of the convective core of a He-burning star, namely $g \sim 7 \times 10^6$, $v_0 \sim 5 \times 10^3$, $\mu^i \sim 1.36$, $\mu^o \sim 1.33$, we have $J_r \sim 3.14\ 10^{-3}$, which is smaller than the critical value by 2 orders of magnitude! Therefore the region is highly unstable

It is worth noticing that even the border of a growing convective core fixed by MLT theory, this condition is always violated. For instance, for a main sequence model of a $20M_{\odot}$ star $J_r \approx 7 \times 10^{-2}$, while during the He-burning phase $J_r \approx 5 \times 10^{-2}$.

Owing to the crudeness of our analysis and the complications introduced by the continuous shooting of many elements against the barrier, we cannot go further than this.Nevertheless, the above considerations suggest that the shear instability sets in very easily.

5.0.5 Remarks on the Basic Assumptions for our Diffusion Scheme

Diffusion plays an important role in our understanding of convective mixing. As already discussed, when the mixing rate is faster than a threshold value, there is no chemical profile in the convective region and fully mixing scheme will be used. On the contrary, if the mixing rate is small, there will be no transport of chemical elements by turbulence.

Our formulation of the diffusion phenomenon will stand on the following general considerations;

- Turbulence can propagate through the interface between the convective zone and the stable region independently of the presence of a discontinuous or smooth chemical profile at this interface. We have seen in the previous crude analysis that the stronger the molecular barrier, the thinner the interface layer, but also the stronger the shear. So, while the barrier can stops the convective motion in one direction (vertical), it can induce turbulence in others (tangential).

- This type of turbulence is caused by the convective motions at the boundary of the fully mixed core, but it cannot be accounted for by the standard MLT. Similarly to all convection theories, we assign to this type of turbulence a typical length scale assumed to be proportional to pressure scale height. This means that we are introducing a free parameter.

- Since there is no good theory of turbulence to be applied to stellar conditions, we introduce another free parameter controlling the mixing efficiency. By varying this

parameter, we can generate stellar models going from the case with potential overshoot but no mixing (roughly speaking the radiative case) to those with overshoot and full mixing.

The basic equation governing the time variation of any elemental species is

$$\left(\frac{dC}{dt}\right) = \left(\frac{\partial C}{\partial t}\right)_{nucl} + \frac{\partial}{\partial m_r}\left[(4\pi r^2\rho)^2 D_{dif}\frac{\partial C}{\partial m_r}\right], \tag{5.8}$$

where C is the abundance of the chemical element under consideration and m_r is the independent mass coordinate. The first term on the right hand side describes the variation due to nuclear burning, while the second term accounts for mixing induced by diffusion with coefficient D_{dif}.

The general expression for the diffusion coefficient takes the form

$$D_{dif} = \frac{1}{3}vl \tag{5.9}$$

where v and l are the characteristic velocity of the chemical mixing and the dimension of the velocity field, respectively.

The velocity field conveying the chemical elements from one region to another follows the phenomenological description of turbulence by Frisch (1977). Finally, the transport of energy is according to the formulation by Bressan et al. (1981).

5.1 Prescriptions for the Diffusion Coefficient

In general two distinct mixing processes can be envisaged. The first one refers to the core and leads to complete mixing. As already specified, it originates from the fact that all the matter within one mean free path from the center has the same probability of being exposed to vigorous nuclear burning (centre). No matter of how slow the actual mixing process is, the convective motion at the element scale given by the MLT smooths out this region. This gives an effective diffusion coefficient

$$D_{fm} \approx v_0 L_0 \tag{5.10}$$

which corresponds to a mixing time scale approximately equal to the crossing time scale.

The other process is related to the effective scale of mixing by turbulence in any convective region (either the core or the overshoot zone). In order to clarify the point we premise the following considerations aimed to determine the dependence of the diffusion coefficient on the characteristic velocity v_d and scale l_d of mixing, respectively. As the scale decreases from the largest to the smallest ones, there are two factors that decrease the diffusion coefficient: the smaller characteristic velocity and intermittence.

First of all, we need to determine the scale to which mixing of chemical elements is mostly related. In a turbulent region all scales are possible going from maximum scale equal to dimension the unstable zone itself down to a minimum scale set by dissipative processes, which otherwise known as the Kolmogorov micro-scale,

$$l_K = (\nu^3/\bar{\epsilon})^{1/4} \tag{5.11}$$

where ν is the kinematic viscosity, and $\bar{\epsilon}$ is the kinetic energy flux injected to the turbulence. This is given by v_0^3/l_0. The quantities v_0, l_0 are the velocity and scale length of the largest element in the field under consideration. All these are to be determined from the convection theory in usage.

The relation between velocity and linear dimensions at any given scale is derived from the conservation of kinetic energy flux

$$\frac{v_0^3}{l_0} = \beta_{int}\frac{v_d^3}{l_d} \tag{5.12}$$

where β_{int} takes intermittence into account according to Frisch (1977). Generalizing β_{int}

to a continuous scale, we get [1] we find

$$\beta_{int} = (l_d/l_0)^{\frac{1}{2}}. \tag{5.13}$$

Inserting the velocity v_d and the dimension of the mixing field (L_0) into the general form of the equation (5.9) for the diffusion coefficient, we obtain

$$D^*_{dif} = \frac{1}{3} v_d L_0 = \frac{1}{3} v_0 \left(\frac{l_d}{L_0}\right)^{\frac{1}{6}} L_0. \tag{5.14}$$

This is not yet the final equation to use, because the intermittence not only affects the characteristic velocity, but also the amount of volume interested by mixing.

Indeed, the intermittence tells us that the space originally filled by the largest scales is only partially occupied by the small scales. Therefore, within the time scale $\tau \sim L_0^2/D^*_{dif}$, only a fraction $\beta_{int} = (l_d/L_0)^{\frac{1}{2}}$ of the volume is mixed. To have the whole volume statistically filled, a much longer time is required, or equivalently the diffusion coefficient must be decreased by the factor β^n_{int}. Here we assume $n = 3$, to get enough overlap to render mixing complete. Finally, we can write

$$D_{dif} = \frac{1}{3} v_0 L_0 \left(\frac{l_d}{l_0}\right)^{\frac{5}{3}}. \tag{5.15}$$

This corresponding characteristic time scale of mixing is

$$\tau_m = L_0^2/D_{dif} \tag{5.16}$$

In order to determine l_d we argue as follows. Within the fully unstable core, l_d is the typical scale set by the MLT (the maximum allowed value). This secures full mixing in the unstable region.

[1] For a scale changing by a factor of two between two successive generations, the intermittence factor is

$$\beta = N/\mathbf{2}^3$$

where N is the number of off-springs from each parental element It is assumed to be $N = \mathbf{2}^{2.5}$. Substituting in equation (5.12) for the nth generation,

$$\beta_n = (\sqrt{\mathbf{2}})^{-n}$$

In the case of continuously decreasing scales, in the above equations the factor "2" is replaced by $(\frac{l_i}{l_{i+1}})$. The derivation of equation 5.13 for the scale l_d is straightforward.

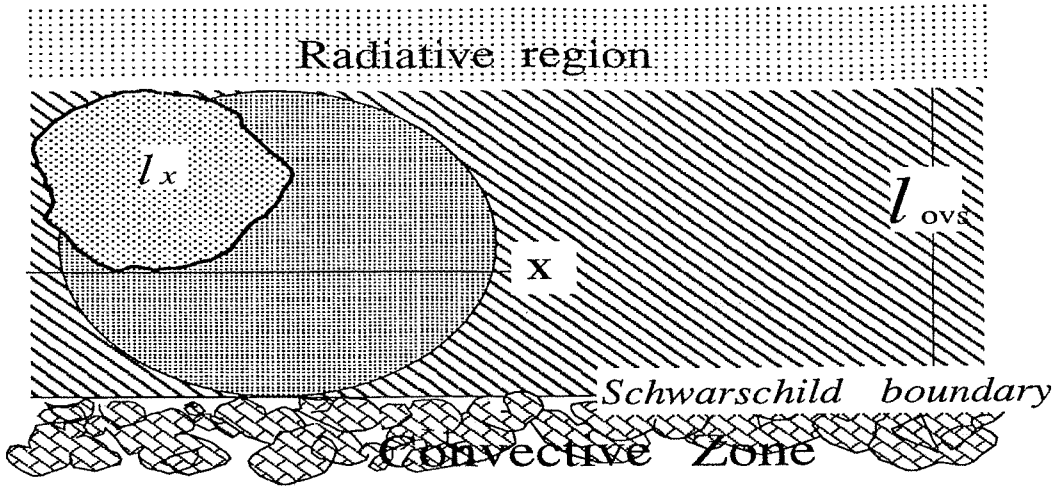

Figure 5.1 A sketch of the mixing regions. The l_{ovs} is the linear dimension of the overshoot region, l_x is the size of the largest bubble at the level **X** from the *Schwarzschild* boundary.

In the overshoot region, the velocity distribution is estimated in the following way. As sketched in *Figure* 5.1, the largest element at level X has its maximum dimension l_x. We consider this element as is the offspring of the element generated at a point closer to the Schwarzschild border, for which equation 5.12 should be used. Therefore, the velocity distribution can be expressed with L_{ovs}, U_0, l_x by

$$v_x = U_0 \left(\frac{l_x}{L_{ovs}}\right)^{\frac{1}{6}}. \tag{5.17}$$

where $U_0 = v_0(\nabla=\nabla_{ad})$

Because of the effect by intermittence, we introduce an additional factor $\left(\frac{l_x}{L_{ovs}}\right)^{\frac{3}{2}}$ in above equation. Therefore, the typical velocity at this layer is supposed to equal to the velocity corresponding to of the largest scale at this same layer of the overshoot region. Thus the diffusion coefficient is still given by equation 5.15, in which L_{ovs} replaces L_0, and v_x replaces v_0. The equation for the diffusion coefficient becomes

$$D_{dif}^{ovs} = \frac{1}{3} U_0 L_{ovs} \left(\frac{l_d}{l_{ovs}}\right)^{\frac{5}{3}} \left(\frac{l_x}{l_{ovs}}\right)^{\frac{5}{3}}. \tag{5.18}$$

As indicated in equation 5.16, the time scale for mixing is expressed by means of the linear dimension of the turbulence field. The largest element is assumed have the size of the pressure scale height.

Noteworthy, the ratio between the radius of the unstable core and the dimension of the largest element varies with stellar masses.

ThIn certain circumstances the dimension of one pressure scale height can be much larger than the size of the convective region (e.g. the case of low mass stars possessing convective cores). This fact may have profound implications as far as the efficiency of mixing is concerned. Specifically, the motion of too a large element can stir the surrounding medium at much less efficiency than in the case of a small element. In order to take this into account, we introduce a linear factor, namely the ratio between the volume of the whole region to that of the bubble. This factor is expressed by $(\mathcal{L}/L_0)^3$. It turns out not be important for the central convective zone, but only for the envelope, because this latter extends over several pressure scale heights.

Now we have all the ingredients to calculate the diffusion coefficient in the overshoot region, once the effective length l_d for mixing of chemicals is given. Adopting the mixing length l_0 one recovers full mixing as in the case of the unstable central core. On the contrary, adopting the Kolmogorov micro scale l_K as the effective mixing scale, essentially no mixing is obtained because $l_K \sim 10^2$cm.

Because for all other scales in between l_0 and l_K no theory can be invoked to make a choice of a particular scale, we have used it as a parameter. We find that for a $20M_\odot$ star, $l_d = 10^{-3.6}H_P$ gives a mixing rate which is approximately the same as the time scale for changing the central fuel $dt/d\ln C$ by nuclear burning. In general the scale in use is

$$l_d = 10^{-4}P_{dif}H_P. \tag{5.19}$$

Where P_{dif} is our parameter controlling the efficiency of turbulent diffusion.

The diffusion equation 5.8 can be solved by specifying the diffusion coefficient. The

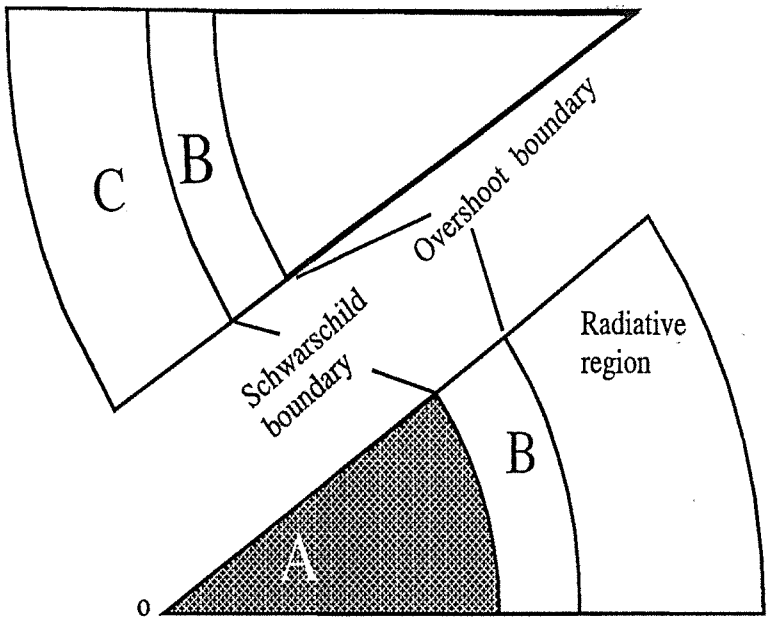

Figure 5.2: A schematic plot of a star slice showing the mixing regions. **A** is the convective core while **C** is the convective envelope when present. Both are defined by Schwarzschild criterion. **B** denotes the overshoot regions surrounding the unstable zones.

prescription we have adopted for $\mathcal{D}$ are sketched *Figure* 5.2 and the following relations

$$\textit{Radiative}: \mathcal{D} = 0 \tag{5.20}$$

$$\textit{Region } A: \mathcal{D} = \frac{1}{3}v_0(r)\mathcal{L} \tag{5.21}$$

$$\textit{Region } C: \mathcal{D} = \frac{1}{3}(\mathcal{L}/L_0 - 1)^3(\frac{l_d}{L_0})^{\frac{5}{3}}v_0(r)\mathcal{L} \tag{5.22}$$

$$\textit{Region } B: \mathcal{D} = \frac{1}{3}(\mathcal{L}/L_0 - 1)^3(\frac{l_d}{L_0})^{\frac{5}{3}}(\frac{l_z}{L_{ov}})^{\frac{5}{3}}v_0^S\mathcal{L} \tag{5.23}$$

5.1.1 Intermediate convective zones

Whenever intermediate convection occurs, we extend it by allowing some 'overshoot' over a distance parameterized in the same way as in the case of the convective cores. We find that all the intermediate zones are very thin, the radial thickness of these being only a small fraction of local pressure scale height. Their thinness engender physical difficulties even in the context of the MLT. In the models presented here, we adopt a diffusion coefficient large enough to secure mixing of the unstable zone. Furthermore, we allow for extra mixing extending both sides

over half of the zone thickness. This prescription does give rise to serious problem, because in our models intermediate convective zones are found only during the core He-burning phase in a region which has been already smoothed by the deep convective envelope.

5.1.2 Envelope convection

In general, envelope convection is not fully understood. We find that mixing of the region is complete even with equations (5.22) and (5.23) which on the contrary when applied to the central core led to the formation of marked gradient in chemical abundances at the border of the fully mixed central part of it. The reason for it resides in the fact that the velocity from Bressan's et al. (1981) formula is almost subsonic, thus implying a huge diffusion coefficient and in turn full mixing.

5.2 Mathematics of Diffusion

The mathematics of diffusion can simply be described as follows. Suppose we have a medium with some chemical profile. As time goes on, diffusion homogenizes the medium. According to Jost (1960), Fick's first law gives,

$$\vec{\mathbf{J}} = -\mathbf{D}\vec{\nabla}C \tag{5.24}$$

where C is the chemical concentration with dimension $[g\ cm^{-3}]$, and $\vec{\mathbf{J}}$ is the flux (corresponding to concentration diffusion Chapman & Cowling [1970]) of this chemical with dimension of $[g\ cm^{-2}\ sec^{-1}]$. $\mathbf{D}$ is defined as the diffusion coefficient. The diffusion, in this case, happens because of the gradient in concentration, and the effect of diffusion is to reduce this gradient. In general, any gradient of physical parameters in a mixture will lead to transportation of species. A more precise definition of diffusion flux for a two component mixture is found in Landau & Lifchitz's book on **Fluid Mechanics** (1987), which is the following,

$$\vec{\mathbf{J}} = -\rho\mathbf{D}_{12}(\vec{\nabla}C + k_T\vec{\nabla}lnT + k_P\vec{\nabla}lnP) \tag{5.25}$$

The meaning of the symbols are: $\mathbf{D}_{12}$ is the mutual diffusion coefficient, k_T the dimensionless thermal diffusion ratio with its product with $\mathbf{D}_{12}$ giving the thermal diffusion coefficient, and

$k_P \mathbf{D}_{12}$ the so-called barodiffusion. If we have convection in our medium, the turbulent mixing is dominant. A simple picture of turbulent mixing is that the large eddies get energy from the average field and start the motion with the composition of their original positions, they distribute the kinetic energy to smaller eddies and so on. As this energy is being turned to thermal energy at the level of smallest eddies, the composition will be mixed there with the surrounding. As we can find from the literature, mixing due to convection in a stellar interior, despite being very complicated, could nevertheless be treated as a diffusion process. There were some discussions in the literature about the equation to be used for the problem of diffusion (Sreenivasan et al 1977, Cloutman et al 1976). Cloutman et al used a one point correlation function of fluctuations of turbulent velocity and chemical concentration to treat the problem of turbulent mixing. Actually, we can arrive at the final equation as the one used by Weaver et al (1978), and Langer (1985), by making some assumptions to the flux of the diffusion. We assume that the diffusion flux due to turbulence can be formally written as, being proportional to the gradient of the fractional abundance of the diffused chemical, with all physical details contained in the coefficient. This is actually the Boussenisq approximation. So the total flux inside a convective region is

$$\vec{\mathbf{J}} = -\rho \mathbf{D}(\vec{\nabla} C + k_T \vec{\nabla} ln T + k_P \vec{\nabla} ln P) - \rho \mathbf{D}_c \vec{\nabla} C \tag{5.26}$$

where $\mathbf{D}_c$ is the coefficient due to convection.

All the terms except the last one in the above equation describe the contribution of molecular diffusion as the results of gradients of chemical concentration, temperature and pressure respectively. Molecular diffusion can be neglected in astrophysical contexts because of its low efficiency or long time scale compared with that of turbulence (Cloutman et al 1976, Xiong 1985, Kippenhanh & Weigert 1991). With this definition, we can derive the equation for diffusion as follows. The mass conservation is always fulfilled

$$\frac{\partial \rho}{\partial t} + \vec{\nabla} \cdot (\rho \vec{\mathbf{v}}) = 0 \tag{5.27}$$

and the equation of *conservation* for species i can be written as

$$\frac{\partial \rho U_i}{\partial t} + \vec{\nabla} \cdot (\rho U_i \vec{\mathbf{v}}) = -\vec{\nabla} \cdot \vec{\mathbf{J}}_i - q_i \tag{5.28}$$

Using equation (4.4), we can write equation (4.5) as

$$\rho \frac{dU_i}{dt} = -\vec{\nabla} \cdot \vec{\mathbf{J}}_i - q_i \tag{5.29}$$

where, $d/dt = \partial/\partial t + \vec{\mathbf{v}} \cdot \vec{\nabla}$ is the Lagrangian time derivative and q_i is the burning rate of the species under consideration.

Putting the flux into the above equation, and taking into account the spherical symmetry of our problem, yields,

$$\frac{dU_i}{dt} = -\frac{q_i}{\rho} + \frac{1}{\rho}\frac{\partial}{\partial r}(r^2 \rho \mathcal{D} \frac{\partial U_i}{\partial r})$$

and writing the spatial derivatives into Lagrangian coordinate, using,

$$\frac{\partial}{\partial m_r} = \frac{1}{4\pi r^2 \rho}\frac{\partial}{\partial r}$$

m_r (mass inside the sphere with radius r), as we use for structures, at last we have,

$$\frac{dU_i}{dt} = -\frac{q_i}{\rho} + \frac{\partial}{\partial m_r}[(4\pi r^2)^2 \rho^2 \mathcal{D} \frac{\partial U_i}{\partial m_r}] \tag{5.30}$$

Equation (5.30) gives the usual diffusion equation to be solved for chemical distributions in stars.

Some authors obtain a simultaneous solutions of the equation of diffusion with those of the normal stellar structure equation (Simpson 1971), which means introducing a second order differential equation to the general problem. Doing this might improve the accuracy of the problem (Cloutman & Eoll 1976) as the diffusion coefficient becomes very large, but this can also be quite time consuming, the extreme case was found in Xiong's method. Others solved this equation independently (Weaver et al 1978; Langer et al 1985, 1990). There are not any significant differences besides the different ways of solving the above equations. Here we will adopt the latter method, normally, we will first solve the structure equations and then compute the chemical profile.

In the following I will describe the adopted numerical scheme for solving the diffusion equation. The first term in equation (5.30) can be written as the rate of change of the abundance of the chemical element i, then we have,

$$\frac{d\mathbf{U}}{dt} = (\frac{\partial \mathbf{U}}{\partial t})_{nucl} + \frac{\partial}{\partial m_r}[(4\pi r^2)^2 \mathcal{D}\rho^2 \frac{\partial \mathbf{U}}{\partial m_r}] \tag{5.31}$$

The term $(\frac{\partial \mathbf{U}}{\partial t})_{nucl}$ times the time step is the variation of fractional abundance at each mesh point before and after a time step, given as numbers on each mesh through a nuclear reaction routine. Now the equation is ready for discretization.

5.3 Numerical Methods

Our grid is the same as the one used for stellar structure models, with the center being mesh M, going down to mesh 1 at the fitting point with atmospheric solution. The left hand side of the equation is discreticized with forward difference,

$$dU_i/dt = (U_i^{n+1} - U_i^n)/\Delta t$$

where Δt is the step-width in time, the superscript give the chemical concentration at time t^{n+1}, and time t^n. The subscripts stand for the mesh m_i.

To discreticize the right hand side, we have to consider the stability of our scheme. There are many schemes for this kind of parabolic equation (e.g. Crank 1986). In our case, as the mesh is not a equal-spaced one, the scheme turns out to be slightly different from others usually found in numerical books. For a general discussion, we use a weighted mean scheme as follows. For simplicity, we first make the following substitution,

$$D_i = [\mathcal{D}_i(4\pi r^2)^2\rho^2]_i \tag{5.32}$$

So the second term on the right hand side of our equation is discreticized in the following way. The first step is to make a centre space difference of the second derivative with respect to mass, at two intermediate points, $P_{+\frac{1}{2}}$:$\frac{1}{2}(m_{i-1} - m_i)$, and $P_{-\frac{1}{2}}$:$\frac{1}{2}(m_i - m_{i+1})$ with half

step-width in mass which gives,

$$\frac{2}{(m_{i-1}-m_{i+1})}[(D\partial U/\partial m)_{P_{+\frac{1}{2}}}-(D\partial U/\partial m)_{P_{-\frac{1}{2}}}]$$

The second step is to make the difference for the first derivative, again with center space difference, which yields,

$$\frac{2}{(m_{i-1}-m_{i+1})}\{(1-\alpha)[\frac{1}{(m_{i-1}-m_i)}\frac{(D_{i-1}+D_i)}{2}(U_{i-1}-U_i)] -[\frac{1}{(m_i-m_{i+1})}\frac{(D_i+D_{i+1})}{2}(U_i-U_{i+1})]\}^{n+1} \tag{5.33}$$

where $0 \leq \alpha \leq 1$ is the weight constant, which takes into account contributions from different epochs. $\alpha = 1$ gives a complete explicit scheme, $\alpha = 0$ complete a implicit scheme, and $\alpha = 1/2$ the well known Crank-Nicolson scheme which has second order accuracy both in time and space. The superscript in the above equation defines quantities at different times.

Some comments should be made here about the above scheme. For any problem of this kind, with α different from 1, the above discreet form for our diffusion equation are unconditionally stable. Of course some specific value of α will be chosen; we will come to this point later. Now to simplify the above difference equation, we make some substitutions:

$$A_i = \frac{(D_{i+1}+D_i)}{(m_{i-1}-m_{i+1})(m_i-m_{i+1})} \tag{5.34}$$

$$C_i = \frac{(D_i+D_{i-1})}{(m_{i-1}-m_{i+1})(m_{i-1}-m_i)} \tag{5.35}$$

$$\begin{aligned} B_i &= A_i + C_i \\ &= \frac{(D_{i-1}+D_i)}{(m_{i-1}-m_{i+1})(m_i-m_{i+1})} + \frac{(D_i+D_{i+1})}{(m_{i-1}-m_{i+1})(m_i-m_{i+1})} \end{aligned} \tag{5.36}$$

And take δU_i to represent the term due to nuclear burning in our equation:

$$\frac{\delta U_i}{\Delta t} = (\partial U_i/\partial t)_{nucl} \tag{5.37}$$

Then we have the following difference equation for our problem:

$$\begin{aligned} &\frac{U_i^{n+1}-U_i^n}{\Delta t} = \delta U_i/\Delta t + \\ &(1-\alpha)\{A_{i+1}U_{i+1} - B_iU_i + C_{i-1}U_{i-1}\}^{n+1} \\ &+\alpha\{A_{i+1}U_{i+1} - B_iU_i + C_{i+1}U_{i+1}\}^n \end{aligned} \tag{5.38}$$

Suppose there is convection between mesh points N_1 and N_2, equation (5.38) valid for i goes from $N_1 - 1$, to $N_2 + 1$ and give us a set of $(N_1 - N_2 - 2)$ linear equations. Fortunately, as can be seen from the above equation, this set turns out to be *tridiagonal*, which can be solved with a very efficient method. At both boundary points, however, we have to provide other two equations given by the boundary conditions of our problem.

5.4 Boundary Conditions

We will assume that the boundary of the turbulent region is will be wall-like, which means no net mass flows across the boundary. This will have the advantage of keeping easily the conservation of matter. So, we have,

$$J_{N_1} = J_{N_2} = 0 \tag{5.39}$$

To discreticize the boundary conditions, we also have to write the original equation for the boundary points. To do this, we imagine that there is an extra point outside each end of the region $[N_1, N_2]$, and each point set at a distance from the boundary which is the same as the first point inside the zone from the border. Each fictitious point outside the boundary has the same D (defined by [5.32]) as the corresponding inner point. This is just to guarantee eqs (5.39). Then we have:

$$J_k = (U_k - \tilde{U}_k)/2\Delta m = 0$$

which gives:

$$U_k = \tilde{U}_k$$

where subscript k denotes boundary meshes. $\tilde{U}_k$ means imaginary points.

The equations for boundary points are, for the inner boundary N_1,

$$\begin{aligned} \frac{U_{N_1}^{n+1} - U_{N_1}^n}{\Delta t} &= \delta U_{N_1}/\Delta t \\ &+(1-\alpha)\{\tilde{A}_{N_1}\tilde{U}_{N_1} - B_{N_1}U_{N_1} + C_{N_1-1}U_{N_1-1}\}^{n+1} \\ &+\alpha\{\tilde{A}_{N_1}\tilde{U}_{N_1+1} - B_{N_1}U_{N_1} + C_{N_1-1}U_{N_1-1}\}^{n} \end{aligned} \tag{5.40}$$

and for the upper boundary N_2,

$$\begin{aligned}\frac{U_{N_2}^{n+1}-U_{N_2}^{n}}{\Delta t} &= \delta U_{N_2}/\Delta t \\ &+(1-\alpha)\{A_{N_2+1}U_{N_2+1}-B_{N_2}U_{N_2}+\tilde{C}_{N_2}\tilde{U}_{N_2}\}^{n+1} \\ &+\alpha\{A_{N_2+1}U_{N_2+1}-B_{N_2}U_{N_2}+\tilde{C}_{N_2}\tilde{U}_{N_2}\}^{n} \qquad (5.41)\end{aligned}$$

where the tilde variables mean the quantities of fictitious points.

The above equation also holds if the boundary becomes the center or the surface of the star as in the cases of core convection and envelope convection respectively. Using the above equations, we arrive at

$$\begin{aligned}\frac{U_{N_1}^{n+1}-U_{N_1}^{n}}{\Delta t} &= \delta U_{N_1}/\Delta t + \\ &(1-\alpha)\{C_{N_1-1}U_{N_1-1}-B_{N_1}U_{N_1}\}^{n+1} \\ &+\alpha\{C_{N_1-1}U_{N_1-1}-B_{N_1}U_{N_1}\}^{n} \qquad (5.42)\end{aligned}$$

$$\begin{aligned}\frac{U_{N_2}^{n+1}-U_{N_2}^{n}}{\Delta t} &= \delta U_{N_2}/\Delta t + \\ &(1-\alpha)\{A_{N_2+1}U_{N_2+1}-B_{N_2}U_{N_2}\}^{n+1} \\ &+\alpha\{A_{N_2+1}U_{N_2+1}-B_{N_2}U_{N_2}\}^{n} \qquad (5.43)\end{aligned}$$

The Fictitious points are cancelled out, and B_{N_1},C_{N_1}, A_{N_2},B_{N_2}, are given below:

$$B_{N_1}=\frac{1}{(m_{N_1-1}-m_{N_1})^2}\frac{(D_{N_1-1}+D_{N_1})}{2}=-C_{N_1}$$

$$B_{N_2}=\frac{1}{(m_{N_2+1}-m_{N_2})^2}\frac{(D_{N_2+1}+D_{N_2})}{2}=-A_{N_2}$$

The above boundary equations, plus the set of equations for interior points form a complete set of tridiagonal system.

We will show below that our numerical scheme together with the accepted boundary conditions gives a conservative finite difference formalism. The variation of chemical U in a mesh labeled i is,

$$\frac{(U_i^{n+1}-U_i^{n})}{\Delta t}=(\frac{\Delta U_i}{\Delta t})_i+\frac{2}{m_{i-1}-m_{i+1}}(\mathbf{F}_{i-1/2}-\mathbf{F}_{i+1/2})$$

where,

$$\mathbf{F}_{i\pm1/2} = \frac{1}{2}(D_i + D_{i\pm1})\frac{\pm U_i \mp U_{i\pm1}}{\pm m_{i\mp1} \mp m_i}$$

Summing up $\frac{(U_i^{n+1} - U_i^n)}{\Delta t}$ over the whole range $[N_1, N_2]$ gives the total variation in this zone, i.e.,

$$\sum_{N_1}^{N_2}\frac{(U_i^{n+1} - U_i^n)}{\Delta t} = \sum_{N_1}^{N_2}\frac{\Delta U_i}{\Delta t} + \frac{2}{m_{N_1-1} - m_{N_1+1}}\mathbf{F}_{N_1+1/2} + \frac{2}{m_{N_2+1} - m_{N_2-1}}\mathbf{F}_{N_2-1/2} \quad (5.44)$$

So the total variation in this region will be the total change due to nuclear reaction, and marginal terms which are flux of matter flowing across the boundary. As our boundary conditions set those terms to zero, this formula give strict conservation of species, i.e. any change of species inside a zone will be completely due to reactions, *if we are free of numerical errors.* As found in the numerical calculations, rounding errors may be important in some circumstances, and we have to find a way to correct them

Some assumptions are to be made here. The coefficients in our difference equations, A_i, B_i, A_i all have superscript, i.e. they are values taken at different times. This means that in order to solve this tridiagonal system, two models of structure should be stored. In practice, we couldn't know a priori the structure quantities for the next epoch, because the structure is to be decided upon our solutions for the chemical abundances. A possible assumption is that the chemical elements diffuse at a given structure, i.e. diffusion will not affect our structure. This of course is not a physical picture, because the thermodynamic quantities depend up on the chemical abundance. However, solving the chemical distributions independently will be more convenient, and the results of new chemical profiles will have the consequences on structure. In practice, every time we have a new chemical distribution, just like nuclear burning for each step, we will adjust the structure to fit the changes in the chemical composition. This adjustment is automatically done by the routines that solve the structure equations. In this case, we will have

$$A_i^n = A_i^{n+1}$$

$$B_i^n = B_i^{n+1}$$

$$C_i^n = C_i^{n+1}$$

This assumption is shown to be acceptable by our numerical experiment, if the time step is well tuned.

5.5 Conservation of chemical abundances during diffusion

In solving the linear equation in the above section, we have to keep the chemical contents inside our diffusion regions, so as to be conserved. Although the numerical scheme and the boundary conditions of the problem are conservative ones, numerical errors in our system act as a source of leakage. This will surely affect the age estimate, and possibly affect evolution on later phases. To control this problem, we integrate the abundances in diffusion zones, and check this integral before and after the solution of our linear equations. The integration is done with the following method.

As the mesh is non-equally spaced, we fit two sets of three successive points,

$$(m_{i+1}, m_i, m_{i-1}) \quad (m_i, m_{i-1}, m_{i-2})$$

with two second order parabola, and take simple averages of the two fitted functions to approximate the value of the abundance U in the interval $[m_i, m_{i-1}]$, i.e.

$$U \approx \mathbf{P}_i = \frac{1}{2}[\mathbf{P}_1 + \mathbf{P}_2] \tag{5.45}$$

where

$$\mathbf{P}_1 = a_i x^2 + b_i x + c_i$$

$$\mathbf{P}_2 = a_{i-1} x^2 + b_{i-1} x + c_{i-1}$$

The integral of U is then approximated by the integration of the fitted function $\mathbf{P}$;

$$\int_{m_i}^{m_{i-1}} U\,dm \approx \int_{m_i}^{m_{i-1}} \mathbf{P}\,dm = \frac{1}{2}\int_{m_i}^{m_{i-1}} (\mathbf{P}_1 + \mathbf{P_2})\,dm \tag{5.46}$$

The final formula of this approximation is

$$\int_{m_i}^{m_{i-1}} \mathbf{P}_i\,dm = \frac{h_i}{6}(3\,U_i + 3\,U_{i-1} - \frac{L_i + R_i}{2}) \;(i = M-1, M-2, ...3, 2) \tag{5.47}$$

Then, the total integration over the diffusion region, $[N_1, N_2]$ is given by,

$$\int_{m_{N_1}}^{m_{N_2}} U\,dm = \frac{1}{6}\sum_{i=m}^{2}(3\,U_i + 3\,U_{i-1} - \frac{L_i + R_i}{2}) \tag{5.48}$$

where

$$L_i = \frac{\delta_i^2}{1+\delta_i}U_{i+1} - \delta_i U_i + \frac{\delta_i}{1+\delta_i}U_{i-1}$$

$$R_i = \frac{\lambda_i}{1+\lambda_i}U_i - \lambda_i U_{i-1} - \frac{\lambda_i^2}{1+\lambda_i}U_{i-2}$$

$$h_i = m_{i-1} - m_i$$

$$\delta_i = h_i/h_{i+1}$$

$$\lambda_i = h_i/h_{i-1}$$

$$L_M = R_2 = 0$$

and m_i is the mass inside the sphere of mesh i.

We make the integration with equation (5.48) for every diffusion zone at each time step to check for conservation. If the relative error is greater than some given value (say, 10^{-4}, as I used for this work), then, the difference between the integrations of the two epochs will be attributed to the profile before nuclear burning, and the whole diffusion equation is solved again until the condition is fulfilled.

5.6 The Diffusion Coefficient used by others

In the literature, the diffusion description has been used for the treatment of incomplete mixing such as semiconvection. I will simply go over of the expressions the diffusion coefficient used by others, for the purpose of comparison.

Numerically calculation of the coefficient: Simpson (1971), Sreenivasan & Wilson (1977) accepted a direct calculation of the coefficient by checking the run of hydrogen content to keep the convective neutrality fulfilled. Then it is assumed that the other chemical elements will be dispersed with the same diffusion coefficient. This is carried out in practice by the

following. The diffusion coefficient is written in to two first order equations (using Simpson's notation), for the diffusion flux,

$$\phi^s = -\lambda \frac{\partial x^s}{\partial m} \tag{5.49}$$

and for the time variation of the abundance x^s,

$$\frac{\partial x^s}{\partial t} - \theta^s = \frac{\partial \phi^s}{\partial m} \tag{5.50}$$

And the neutrality condition is also specified,

$$(\frac{\partial T}{\partial P})_{ad} - \frac{3\kappa L}{64\sigma G T^3 m} = 0 \tag{5.51}$$

where x^s is the chemical abundance of chemical s, λ is Simpson's diffusion coefficient (corresponding to $4\pi r^2 \rho^2 D$ in our notation), θ^s is the burning rate of chemical s, the other symbols have the usual meaning. Now the equations (5.49), (5.49) and (5.49) are solved simultaneously. And here x^s is only the hydrogen content which determines the almost purely electron scattering opacity in interior of massive stars. Because the runs of luminosity, temperature, and adiabatic temperature gradient are all known, the diffusion coefficient can be determined, and the same coefficient is then used for solving other chemical elements.

Prescriptions of the Diffusion Coefficient:

This is more general way to get the coefficient. The prescription is usually given by dependence with the local thermodynamical quantities. Eggleton (1972) used, for semiconvection,

$$D_{sc} \propto (\nabla_{rad} - \nabla_{ad})^2 \tag{5.52}$$

and Weaver et al (1978) gave

$$D_{sc} \propto \frac{D_c D_r}{D_c + D_r} \tag{5.53}$$

where D_r is the radiative diffusion coefficient. These choices of diffusion coefficient give very convenient numerical treatment, but contain some arbitrariness.

The physical arguments underlying the choice of the diffusion coefficient are connected with our understanding of the nature of convection. As we have no clear judgement on

the convection theories, probably we will have no judgement on diffusion process used for chemical distribution.

6 Stellar Models with Convective Diffusion; Input Physics

6.1 Mixing time scale

Under our treatment of mixing, the life time for each burning stage is critical depending on the time scale given by the diffusion coefficient (5.16) so that a lot can be learned from the analysis of time scales.

Anticipating the results from model calculation, we compare in *Figure* 6.1 the scale of diffusion with of nuclear burning. The data refer to the first 10 models of stars with different mass near the ZAMS with the chemical composition Y=0.25 Z=0.008 and the value of $P_{dif} = 0.04$.

Remarkably, for the adopted value of P_{dif} the two time scale are almost identical independently of the stellar mass. This means that in the region of overshoot a partial mixing exists.

In order to check the effect of different P_{dif} we show in *Figure* 6.2 the H-profile in the overshoot region of a $20M_{\odot}$model. Depending on P_{dif} the profile goes from the case of no mixing ($P_{dif} = 0.01$) thus recovers the radiative structure, to an intermediate situation ($P_{dif} = 0.05$, to the case of almost full mixing ($P_{dif} = 0.1$), which recovers standard treatment of overshoot.

We like to point out that our diffusion mechanism also improves upon a well known difficulty encountered by the standard treatment of overshoot, namely that the linear dimensions and the mass stored in the overshoot region tend to increase at decreasing star mass. This is

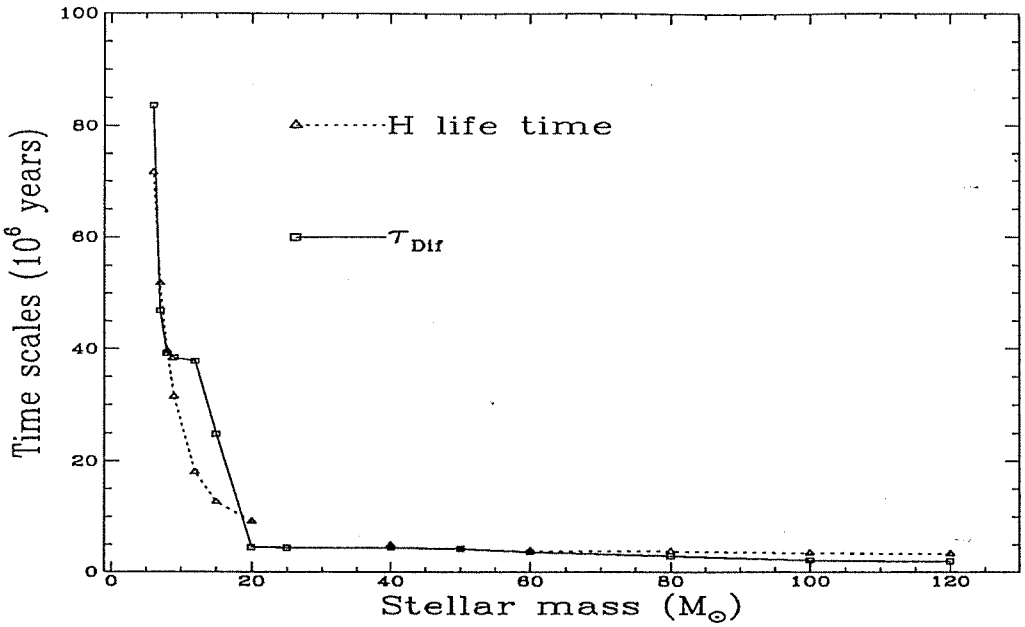

Figure 6.1: The diffusion time scale near the ZAMS (the dotted line and squares), and the H-burning life time (the solid line and triangles) versus the initial mass

shown in *Figure* 6.3, where we plot the linear size and the relative mass content of the overshoot region. Our models show that the increase of the diffusion time scale at decreasing star mass balances the effect of the increasing relative dimensions of the overshoot region, so that the actual size of the mixed zone gets smaller at decreasing mass. The above inconsistency does no longer occur.

Preliminary model calculations not described here for the sake of brevity suggest the

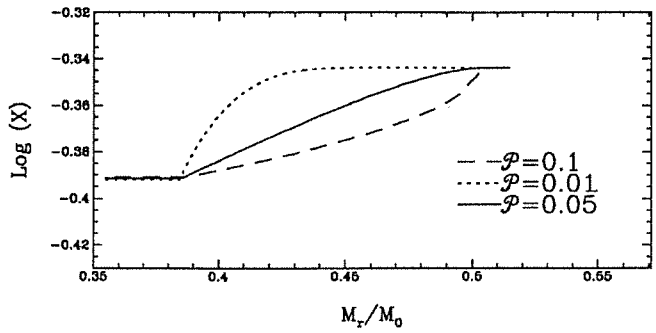

Figure 6.2: The chemical profile of a $20M_\odot$star near evolving on the main sequence, at an age of 6.462 10^6 years. 3 values of mixing efficiency parameter P_{dif} are used for comparison.

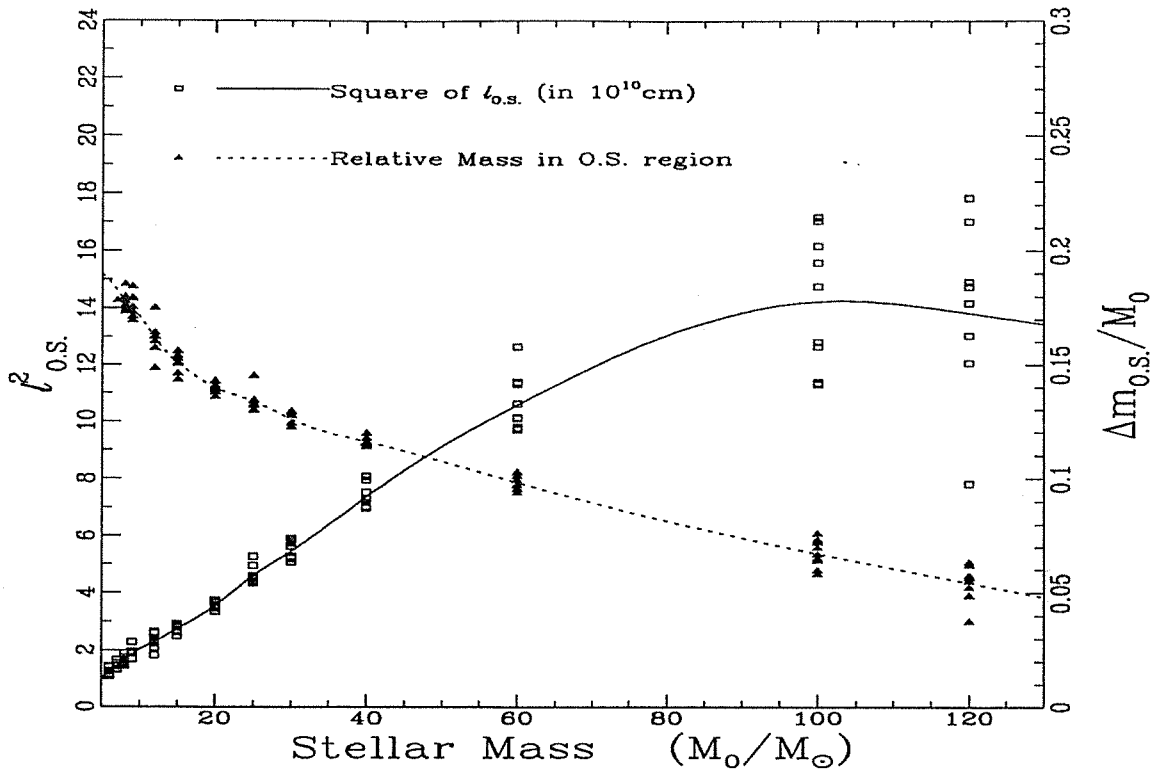

Figure 6.3: The linear scale and the fractionary mass content of the overshoot region for intermediate and massive stars near the ZAMS. Dots and triangles refer to the first 10 models for each mass, the lines are the mean values of these quantities. The linear distance for the diffusive overshoot is measured in 10^{10} cm. M_0 is the initial mass, which is slightly affected by mass loss for higher masses in the plot.

following precept for the diffusion coefficient P_{dif}

$$\begin{aligned} P_{dif} &= 0.08 \qquad when\ M_i \geq 20M_\odot \\ &= 0.04 \qquad When\ M_i < 20M_\odot, \end{aligned} \tag{6.1}$$

The use of an higher value of P_{dif} above $20M_\odot$ is needed in order to have the same degree of mixing also in this mass range where the effects of mass loss dominate the evolution and have some side effects that cannot be easily foreseen. It will be shown that an high efficiency of mixing is also required to get models in agreement with the observational properties of supergiant stars.

As far as the the dimensions of the overshoot region we stand on the analyses by Bressan

et al. (1981) and Alongi et al. (1992). These dimensions are expressed as a fraction Λ of the local pressure scale height with $\Lambda_c = 1.0$ for the core overshoot, and $\Lambda_{env} = 0.7$ for the envelope overshoot.

Finally, the stellar models have been calculated for the chemical abundances

1. Z= 0.008 Y = 0.250
2. Z= 0.020 Y = 0.280

which are typical of composition of the stars the abundances of the stars in the LMC and in the solar's vicinity.

6.2 Chemical Network, Nuclear Reaction Rates, Neutrino Losses

The temporal evolution of the chemical abundances were computed in detail by solving a network of nuclear reactions involving sixteen elements following the method described in Alongi et al. (1992). These elements are ^{1}H, ^{2}H, ^{3}He, ^{4}He, ^{7}Be, ^{7}Li ^{12}C, ^{13}C, ^{14}N, ^{16}O, ^{17}O, ^{18}O, ^{20}Ne, ^{22}Ne, ^{25}Mg, and ^{26}Mg.

We considered, for the H-burning reactions, the three pp chains and he CNO tri-cycle considered (cf. Maeder 1983). For the He-burning we toke into account the following reactions:

$$^{4}He(\alpha,\gamma)^{8}Be(\alpha,\gamma)^{12}C(\alpha,\gamma)^{16}O(\alpha,\gamma)^{20}Ne$$

$$(\alpha,\gamma)^{26}Mg$$

$$^{14}N(\alpha,\gamma)^{18}F(e+\nu)^{18}O(\alpha,\gamma)^{22}Ne$$

$$(\alpha,n)^{25}Mg$$

The reaction rates were taken from Caughlan and Fowler (1988). The rate for the $^{12}C(\alpha,\gamma)^{16}O$ reaction is lower than the value estimated by Kettner et al (1982), Langanke & Koonin (1982), and Caughlan et al (1985) and it is similar to the value given by Fowler et

al (1975). The β-decay processes and the $^8Be(\alpha,\gamma)^{12}C$ reaction were considered as instantaneous. Finally, the screening factors were computed from Graboske et al (1973).

Abundances of light elements such as ^{2}H, ^{7}Be and ^{7}Li were considered at their equilibrium value while those of the remaining elements ^{1}H, ^{3}He, ^{4}He, ^{12}C, ^{13}C, ^{14}N, ^{16}O, ^{17}O, ^{18}O, ^{20}Ne, ^{22}Ne, ^{25}Mg, ^{26}Mg) were followed in detail using an explicit scheme of integration according to the formulation by Arnett & Truran (1969)

Letting Y_i the abundance by mass of the elemental species i , $Y_i = X_i/A_i$, where X_i is the mass fraction of the species i and A_i its atomic mass number, the time variations of the abundances are governed by the following system of equations,

$$dY_i/dt = -[ij]Y_iY_j + [rs]Y_rY_s \tag{6.2}$$

where [ij] is the rate of the generic reaction converting the element i into another element because of the interaction with the element j, whereas [rs] is the rate of the generic reaction transforming elements r and s into the element i.

The system of differential equations 6.2is integrated over the evolutionary time interval (Δt), determined on the basis of the structural variations of the stellar models, by means of sub-time steps (δt), whose number depends on the temperature in the given mesh point. The variations of the abundance of a species i is determined by

$$\Delta Y_i = (dY_i/dt) \cdot (\Delta t) \tag{6.3}$$

where the derivatives are computed evaluating the reaction rates at t+(Δt)/2, by means of extrapolation from the two preceeding models. During H-burning, special care has been paid to avoid oscillations in the abundances once equilibrium between supplying and depleting reactions is achieved by any element: the results of the numerical integration are compared to the appropriate equilibrium abundances at each time step, and the equilibrium value is adopted if necessary. The conservation of the total number of CNO nuclei and of the total number of nucleons are secured in the computation of the abundances of ^{14}N and ^{3}He, respectively, once equilibrium of these two elements is achieved.

Finally, the rates of neutrino emissions are from Munakata et al (1985).

6.3 Radiative and Molecular Opacities

We have adopted the most recent opacity tables of the Livermore group (Iglesias et al. 1992). These include the spin-orbit interaction in the treatment of Fe atomic data and adopt the recent measurement of the solar photospheric Fe abundance by Grevesse (1991) and Hannaford et al. (1992). With respect to previous opacity tables (Huebner et al 1977) the new one show two significant enhancements. The first enhancement occurs at temperatures of a few hundred thousand degrees and, for densities typical of the envelope of a red giant star with solar composition, it amounts to a factor of 3. This increase strongly depends on the metallicity, being higher at higher metal contents. The second enhancement occurs at temperatures of about one million degrees, but it is of much smaller amplitude (about 20% only).

Because the OPAL tables do not extend below 6000 K and above 10^8 K, the opacities at lower and higher temperatures, respectively, are taken from the LAOL tabulations by Huebner et al. (1977) and Cox and Stewart (1970a,b).

We also included the contribution by the CN, CO, H_2O and TiO molecules by means of the analytical relationships by Bessel et al. (1989, 1991), which are based on the tabulations of molecular opacities by Alexander (1975) and Alexander et al. (1983).

6.4 Calibration of Outer Convection

Convection in the outermost envelope was treated with the mixing length theory to derive the temperature gradient. The mixing length parameter was assumed to be $1.63H_p$ after calibration with the solar model.

6.5 Mass loss for $M \geq 12M_{\odot}$

The evolution of massive stars is dominated by mass loss by stellar wind (see Chiosi & Maeder 1986; Chiosi et al 1992a,b). To account for this phenomenon we adopted in stars more massive than M=12M$_{\odot}$the empirical formulation of the mass loss rate given by de Jager et al (1988, equation 2.3 in page 11) for all evolutionary stages from the main sequence up to the so-called de Jager limit in the CMD. Beyond this limit, the mass loss rate was increased to 10^{-3} M$_{\odot}$ yr^{-1} as indicated by the observational data for the Luminous Blue Variables (LBV). For the WR stages, which we suppose to begin when the surface abundance of hydrogen falls below X=0.300 (WNL stage), we applied the mass-loss rate suggested by Langer (1989, equation 2.9, in page12). Finally we included the dependence from the metal content ($\propto \sqrt{Z}$) suggested by the theoretical models of stellar wind (Kudritzki et al1989).

6.6 Density Inversion

It is well known that in the outermost layers of stars with $T_{eff} \leq 10^4 K$ a convective zone appears due to the incomplete ionization of hydrogen. If convection is treated according to the mixing-length theory with the mixing-length proportional to the pressure scale height, $l=\alpha \times H_P$, and the parameter α in the range (1-2), when $T_{eff} \leq 10^4 K$ a density inversion occurs, i.e. the density reaches a minimum and then starts to increase at increasing radius. The consequences of this phenomena have been recently reviewed by Maeder (1992) where it is discussed whether it can cause a sudden increase of the mass loss rate, or lead to the Rayleigh-Taylor instability, etc. In our calculations, we have imposed that the density inversion cannot develop by assuming that the temperature gradient ∇_T is such that the density gradient obeys the condition $\nabla_\rho \geq 0$. The required temperature gradient is given by $\nabla_{T_{Max}} = \frac{1-\chi_\mu \nabla_\mu}{\chi_T}$, where ∇_μ is the gradient in molecular weight, and χ_μ and χ_T have the usual meaning.

7 New Stellar Models with Turbulent Diffusion

In this section we present the results of stellar models calculations including the new scheme of mixing that we have amply discussed in the previous sections. The results are compared with those of Bressan et al. (1993), Fagotto et al. (1993 a,b), and Meader et al. (1992), which are obtained from the standard treatment of convective overshoot, and the major novelties given by our diffusion mechanism are highlighted. In particular we discuss the occurrence of the blue loops during the core He-burning phase that bear very much on the interpretation of the HRD of intermediate and high mass stars.

7.1 Evolutionary Sequences

The two grids of stellar evolutionary models are computed. The initial masses range from 6 to 120 $M_{\odot}$, Since our main goal it the interpretation of massive star, the discussion of the intermediate mass stars is limited to the main results, namely the effect of mixing.

The main physical properties of each evolutionary sequence are summarized in *table* 7.1 for $Z = 0.008$ and *table* 7.2 for $Z = 0.020$ respectively. The entries of the tables are as follows:

AGE :age of the model in years

$L/L_{\odot}$:logrithmic (base 10) of the total luminosity in solar units

T_{eff} :logarithmic (base 10) of the effective temperature

G :logrithmic (base 10) of the surface gravity

T_c :logrithmic (base 10) of the central temperature

ρ_c :logrithmic (base 10) of the central density

COMP :central abundance by mass of hydrogen or helium

X_C :central abundances of ^{12}C

X_O :central abundances of ^{16}O

Conv :fractional mass of the convective core (inclusive of Diffusion)

Q_{disk} :fractional mass of the first mesh point where the chemical composition differs from the surface value

L_H : logrithmic (base 10) of the hydrogen luminosity in solar unit

$Q1_H$:fractionary mass of the inner border of the hydrogen rich region

$Q2_H$:fractionary mass of the outer border of H-burning region. the boundary is taken where the nuclear energy generation rate becomes greater than a suitable value

L_{He} : logrithmic (base 10) of the helium luminosity in solar units

$Q1_{He}$:fractionary mass of the inner border of the He-burning region (when greater than zero He-burning is in shell). The boundary is taken where the nuclear energy generation rate becomes greater than a suitable value

$Q2_{He}$: fractional mass of the upper border of the He-burning region. the boundary is take as above.

L_C :logrithmic (base 10) of the neutrinos luminosity (absolute value) in solar units

Q_{Tmas} :fractionary mass of the point where the temperature attains the maximum

M_{dot} : logrithmic (base 10) of the absolute value of the mass-loss rate in $M_\odot$ per year

X_{sur} : surface abundance (by mass) of ^{1}H

Y_{sur} : surface abundance (by mass) of ^{4}He

XC_{sur} : surface abundance (by mass) of ^{12}C

XN_{sur} : surface abundance (by mass) of ^{14}N

XO_{sur} : surface abundance (by mass) of ^{16}O

For stars more massive than $M \geq 12M_{\odot}$, the tables also display the surface abundance of several important elements. The numbers appearing in the second column of each table indicate mark several characteristic points along the evolution tracks in the HRD. The numbers have the following meaning: 1) ZAMS stage; (2) red edge of the main sequence band, otherwise called terminal main sequence (TAMS); (3) stage of maximum T_{eff} reached by the track after TAMS; (4) point where the luminosity of the track reaches the peak value while crossing the HRD towards the Hayashi track; (5) first arrival of the track on the Hayashi track; (6) first peak luminosity along the Hayashi track, called the tip of red giant branch (RGB) in case of mass star; (7) first departure from the Hayashi track; (8) tip of the blue loop (if present) during the core He-burning phase; (9) end of the loop phase and return of the track to the Hayashi line; (10) the final point along the sequence.

Table 7.1: (Page 80-88) Evolutionary sequences for Z=0.008 and Y=0.250. The dimensions of the overshoot regions are fixed by $\Lambda_c = 1.0$ for the core (Bressan et al. 1981) and $\Lambda_{env} = 0.7$ for the envelope (Alongi et al. 1992). The corresponding tracks are given in *Figure* (7.1), the life-times and life-time ratios are listed in *table* (7.3)

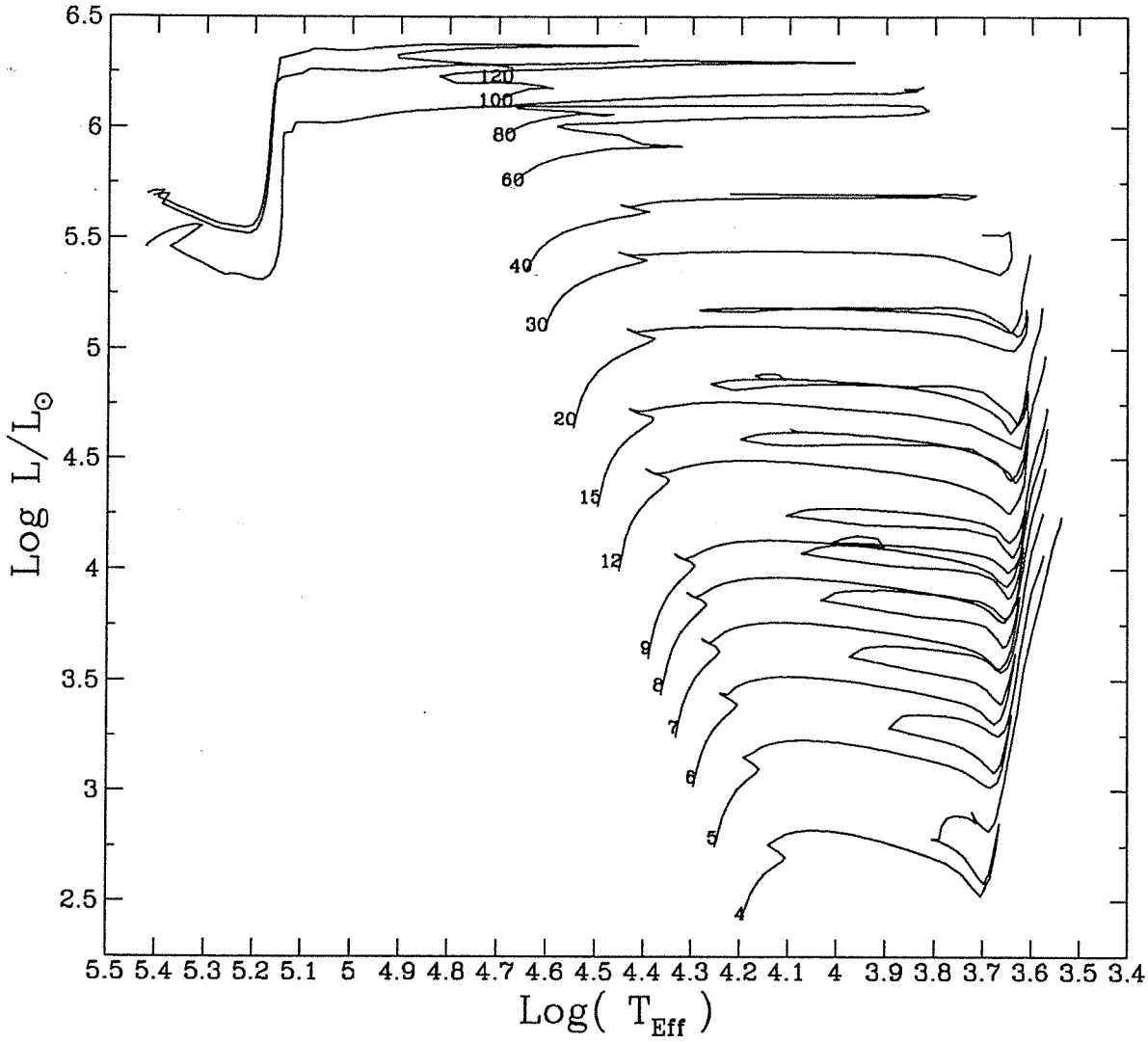

Figure 7.1: Theoretical HRD for the evolutionary tracks with initial masses M_i=4, 5, 6, 7, 8, 9, 12, 15, 20, 25, 60, 100, 120 $M_\odot$and composition $Z = 0.008Y = 0.250$.

Table 7.1 M = 20.00 $M_\odot$ Z=0.008 Y=0.250 Diffusion

		AGE	M	$L/L_\odot$	T_{eff}	G	T_c	ρ_c	COMP	XC	XO	CONV	Q_{disc}	L_H	$Q1_H$	L_{He}	$\dot{M}$	X_{sup}	Y_{sup}	XC_{sup}	XN_{sup}	XO_{sup}
H	1	0.00000E+00	20.00	4.618	4.551	4.272	7.564	0.720	0.730	4.61E-5	3.74E-3	0.5885	0.5808	4.612	0.000	0.000	-8.111	7.42E-1	2.50E-1	1.98E-3	4.97E-4	4.23E-3
		6.41069E+05	19.99	4.638	4.547	4.237	7.561	0.704	0.700	4.54E-5	1.90E-3	0.5848	0.5887	4.640	0.000	0.000	-8.033	7.42E-1	2.50E-1	1.98E-3	4.97E-4	4.23E-3
B		2.74313E+06	19.96	4.710	4.540	4.134	7.565	0.686	0.600	6.36E-5	5.46E-4	0.5615	0.5952	4.711	0.000	0.000	-7.784	7.42E-1	2.50E-1	1.98E-3	4.97E-4	4.23E-3
U		4.42733E+06	19.92	4.779	4.531	4.029	7.575	0.688	0.500	6.89E-5	2.73E-4	0.5335	0.5963	4.780	0.000	0.000	-7.559	7.42E-1	2.50E-1	1.98E-3	4.97E-4	4.23E-3
R		5.76097E+06	19.87	4.842	4.517	3.909	7.586	0.699	0.400	7.36E-5	1.94E-4	0.5035	0.5978	4.843	0.000	0.000	-7.342	7.42E-1	2.50E-1	1.98E-3	4.97E-4	4.23E-3
N		6.84450E+06	19.81	4.900	4.496	3.765	7.599	0.719	0.300	7.77E-5	1.65E-4	0.4700	0.5997	4.902	0.000	0.000	-7.133	7.42E-1	2.50E-1	1.98E-3	4.97E-4	4.23E-3
I		7.72323E+06	19.73	4.954	4.465	3.587	7.615	0.754	0.200	8.29E-5	1.51E-4	0.4339	0.6022	4.956	0.000	0.000	-6.931	7.42E-1	2.50E-1	1.98E-3	4.97E-4	4.23E-3
N		8.44314E+06	19.62	5.004	4.421	3.357	7.638	0.816	0.100	9.08E-5	1.39E-4	0.3988	0.6055	5.006	0.000	0.000	-6.734	7.42E-1	2.50E-1	1.98E-3	4.97E-4	4.23E-3
G		8.79643E+06	19.55	5.029	4.393	3.219	7.659	0.878	0.050	9.38E-5	1.33E-4	0.3802	0.6077	5.031	0.000	0.000	-6.642	7.42E-1	2.50E-1	1.98E-3	4.97E-4	4.23E-3
	2	8.99348E+06	19.50	5.045	4.379	3.145	7.684	0.953	0.020	1.04E-4	1.27E-4	0.3669	0.6092	5.046	0.000	0.000	-6.589	7.42E-1	2.50E-1	1.98E-3	4.97E-4	4.23E-3
		9.05957E+06	19.48	5.052	4.381	3.145	7.704	1.012	0.010	1.06E-4	1.25E-4	0.3638	0.6098	5.050	0.000	0.000	-6.577	7.42E-1	2.50E-1	1.98E-3	4.97E-4	4.23E-3
		9.13534E+06	19.46	5.066	4.406	3.233	7.765	1.197	0.001	1.35E-4	1.29E-4	0.3428	0.6104	5.043	0.000	0.000	-6.585	7.42E-1	2.50E-1	1.98E-3	4.97E-4	4.23E-3
	3	9.14120E+06	19.46	5.073	4.417	3.268	7.792	1.282	0.000	1.43E-4	1.29E-4	0.3318	0.6104	5.030	0.000	0.000	-6.588	7.42E-1	2.50E-1	1.98E-3	4.97E-4	4.23E-3
		9.14319E+06	19.46	5.077	4.422	3.285	7.808	1.332	0.000	1.49E-4	1.29E-4	0.3201	0.6104	5.012	0.000	0.000	-6.588	7.42E-1	2.50E-1	1.98E-3	4.97E-4	4.23E-3
	4	9.14636E+06	19.46	5.094	4.435	3.322	7.891	1.624	0.000	1.72E-4	1.28E-4	0.1028	0.6105	4.818	0.207	0.000	-6.572	7.42E-1	2.50E-1	1.98E-3	4.97E-4	4.23E-3
		9.15333E+06	19.46	5.099	4.322	2.861	8.057	2.308	0.000	1.72E-4	1.28E-4	0.0000	0.6258	5.100	0.268	0.000	-6.425	7.42E-1	2.50E-1	1.98E-3	4.97E-4	4.23E-3
He	5	9.15608E+06	19.46	5.103	4.224	2.466	8.126	2.557	0.992	1.76E-4	1.28E-4	0.0000	0.6259	5.088	0.284	1.404	-6.363	7.42E-1	2.50E-1	1.98E-3	4.97E-4	4.23E-3
		9.15618E+06	19.46	5.103	4.220	2.449	8.128	2.565	0.992	1.76E-4	1.28E-4	0.0000	0.6259	5.088	0.284	1.405	-6.362	7.42E-1	2.50E-1	1.98E-3	4.97E-4	4.23E-3
B		9.15803E+06	19.46	5.102	4.120	2.050	8.179	2.723	0.992	3.05E-4	1.28E-4	0.0059	0.6259	5.072	0.294	3.222	-6.347	7.42E-1	2.50E-1	1.98E-3	4.97E-4	4.23E-3
U		9.15934E+06	19.46	5.097	4.012	1.623	8.211	2.808	0.991	5.93E-4	1.28E-4	0.0462	0.6259	5.047	0.302	4.244	-6.350	7.42E-1	2.50E-1	1.98E-3	4.97E-4	4.23E-3
R		9.16030E+06	19.46	5.090	3.885	1.125	8.226	2.835	0.990	1.09E-3	1.29E-4	0.0886	0.6259	5.009	0.305	4.630	-6.341	7.42E-1	2.50E-1	1.98E-3	4.97E-4	4.23E-3
N		9.16136E+06	19.46	5.062	3.746	0.594	8.232	2.838	0.990	1.78E-3	1.29E-4	0.1156	0.6260	4.969	0.308	4.751	-6.272	7.42E-1	2.50E-1	1.98E-3	4.97E-4	4.23E-3
I		9.16222E+06	19.46	4.997	3.636	0.221	8.234	2.836	0.989	2.28E-3	1.29E-4	0.1369	0.6260	4.927	0.312	4.792	-6.180	7.42E-1	2.50E-1	1.98E-3	4.97E-4	4.23E-3
N	6	9.16222E+06	19.46	4.997	3.636	0.221	8.234	2.836	0.989	2.28E-3	1.29E-4	0.1369	0.6260	5.689	0.312	5.677	-6.180	7.42E-1	2.50E-1	1.98E-3	4.97E-4	4.23E-3
G	7	9.16359E+06	19.46	5.076	3.612	0.045	8.239	2.839	0.988	3.32E-3	1.30E-4	0.1532	0.6260	4.913	0.315	4.766	-6.088	7.42E-1	2.50E-1	1.88E-3	5.46E-4	4.23E-3
	8	9.16553E+06	19.45	5.180	3.610	-0.066	8.243	2.845	0.985	5.31E-3	1.32E-4	0.1664	0.4085	4.930	0.319	4.771	-5.905	6.56E-1	3.36E-1	1.23E-3	2.27E-3	3.12E-3
		9.18888E+06	19.43	5.100	3.615	0.033	8.253	2.844	0.950	4.01E-2	3.18E-4	0.1952	0.3955	4.762	0.340	4.827	-6.039	6.53E-1	3.40E-1	1.21E-3	2.34E-3	3.07E-3
		9.23310E+06	19.39	5.066	3.634	0.142	8.258	2.837	0.900	8.89E-2	1.07E-3	0.2447	0.3965	4.635	0.354	4.853	-6.136	6.53E-1	3.40E-1	1.21E-3	2.34E-3	3.07E-3
		9.24619E+06	19.38	5.190	3.757	0.510	8.259	2.837	0.882	1.06E-1	1.45E-3	0.2435	0.3971	4.747	0.357	4.856	-6.117	6.53E-1	3.40E-1	1.21E-3	2.34E-3	3.07E-3
		9.24761E+06	19.38	5.187	3.882	1.014	8.259	2.838	0.880	1.08E-1	1.50E-3	0.2480	0.3971	4.780	0.357	4.854	-6.194	6.53E-1	3.40E-1	1.21E-3	2.34E-3	3.07E-3
		9.24919E+06	19.38	5.188	3.991	1.450	8.259	2.838	0.878	1.10E-1	1.55E-3	0.2436	0.3971	4.803	0.358	4.857	-6.208	6.53E-1	3.40E-1	1.21E-3	2.34E-3	3.07E-3
		9.25245E+06	19.38	5.180	4.119	1.966	8.260	2.838	0.873	1.15E-1	1.67E-3	0.2480	0.3972	4.835	0.358	4.858	-6.213	6.53E-1	3.40E-1	1.21E-3	2.34E-3	3.07E-3
		9.26453E+06	19.37	5.170	4.221	2.385	8.261	2.840	0.855	1.32E-1	2.16E-3	0.2481	0.5994	4.864	0.361	4.865	-6.245	6.53E-1	3.40E-1	1.21E-3	2.34E-3	3.07E-3
		9.30110E+06	19.35	5.173	4.267	2.567	8.265	2.845	0.800	1.85E-1	4.17E-3	0.2492	0.6331	4.863	0.366	4.882	-6.257	6.53E-1	3.40E-1	1.21E-3	2.34E-3	3.07E-3
	9	9.36356E+06	19.32	5.177	4.285	2.632	8.271	2.852	0.711	2.68E-1	9.71E-3	0.2580	0.6342	4.850	0.373	4.904	-6.259	6.53E-1	3.40E-1	1.21E-3	2.34E-3	3.07E-3
		9.37152E+06	19.31	5.177	4.283	2.627	8.272	2.854	0.700	2.78E-1	1.06E-2	0.2580	0.6344	4.847	0.374	4.907	-6.258	6.53E-1	3.40E-1	1.21E-3	2.34E-3	3.07E-3
		9.43019E+06	19.27	5.179	4.273	2.584	8.281	2.869	0.600	3.68E-1	2.10E-2	0.2622	0.6356	4.828	0.378	4.930	-6.248	6.53E-1	3.40E-1	1.21E-3	2.34E-3	3.07E-3
		9.50745E+06	19.24	5.181	4.256	2.510	8.291	2.891	0.500	4.52E-1	3.71E-2	0.2649	0.6369	4.802	0.381	4.954	-6.237	6.53E-1	3.40E-1	1.21E-3	2.34E-3	3.07E-3
		9.58740E+06	19.19	5.184	4.235	2.424	8.302	2.912	0.400	5.25E-1	6.39E-2	0.2745	0.6384	4.768	0.384	4.979	-6.226	6.53E-1	3.40E-1	1.21E-3	2.34E-3	3.07E-3
		9.66839E+06	19.14	5.186	4.210	2.321	8.316	2.945	0.300	5.83E-1	1.06E-1	0.2813	0.6401	4.727	0.386	5.006	-6.217	6.53E-1	3.40E-1	1.21E-3	2.34E-3	3.07E-3
		9.76025E+06	19.08	5.186	4.170	2.160	8.335	2.988	0.200	6.11E-1	1.78E-1	0.2889	0.6420	4.669	0.390	5.031	-6.210	6.53E-1	3.40E-1	1.21E-3	2.34E-3	3.07E-3
		9.87105E+06	19.02	5.185	4.092	1.845	8.364	3.063	0.100	5.71E-1	3.17E-1	0.2949	0.6443	4.577	0.395	5.062	-6.209	6.53E-1	3.40E-1	1.21E-3	2.34E-3	3.07E-3
		9.92221E+06	18.99	5.181	3.991	1.446	8.392	3.144	0.050	5.12E-1	4.25E-1	0.2954	0.6453	4.495	0.397	5.084	-6.218	6.53E-1	3.40E-1	1.21E-3	2.34E-3	3.07E-3
		9.92258E+06	18.98	5.181	3.990	1.441	8.392	3.145	0.050	5.12E-1	4.26E-1	0.2954	0.6453	4.494	0.397	5.084	-6.218	6.53E-1	3.40E-1	1.21E-3	2.34E-3	3.07E-3
		9.95017E+06	18.97	5.174	3.888	1.040	8.411	3.199	0.028	4.65E-1	4.95E-1	0.2956	0.6459	4.430	0.399	5.090	-6.214	6.53E-1	3.40E-1	1.21E-3	2.34E-3	3.07E-3
		9.96425E+06	18.96	5.162	3.786	0.644	8.424	3.239	0.017	4.39E-1	5.31E-1	0.2958	0.6462	4.366	0.399	5.093	-6.179	6.53E-1	3.40E-1	1.21E-3	2.34E-3	3.07E-3
		9.97029E+06	18.96	5.115	3.682	0.275	8.432	3.263	0.013	4.26E-1	5.48E-1	0.2958	0.6464	4.260	0.400	5.092	-6.125	6.53E-1	3.40E-1	1.21E-3	2.34E-3	3.07E-3
		9.97407E+06	18.95	5.092	3.632	0.097	8.438	3.282	0.010	4.19E-1	5.58E-1	0.2922	0.6465	4.013	0.400	5.086	-6.098	6.53E-1	3.40E-1	1.21E-3	2.34E-3	3.07E-3
		9.98607E+06	18.94	5.139	3.626	0.026	8.488	3.435	0.001	3.93E-1	5.91E-1	0.2751	0.4998	3.989	0.401	4.981	-6.004	6.40E-1	3.52E-1	8.63E-4	3.18E-3	2.57E-3
	10	9.98836E+06	18.94	5.148	3.623	0.008	8.525	3.550	0.000	3.91E-1	5.94E-1	0.2575	0.5626	4.060	0.401	4.841	-5.991	6.40E-1	3.52E-1	8.62E-4	3.18E-3	2.56E-3
		9.98871E+06	18.94	5.151	3.623	0.003	8.531	3.568	0.000	3.91E-1	5.94E-1	0.2548	0.5809	4.062	0.401	4.842	-5.986	6.40E-1	3.52E-1	8.62E-4	3.18E-3	2.56E-3
	11	1.00259E+07	18.80	5.429	3.603	-0.358	8.911	4.792	0.000	3.90E-1	5.94E-1	0.1886	0.3939	0.000	0.394	5.090	-5.186	6.19E-1	3.73E-1	7.27E-4	3.57E-3	2.31E-3
		1.00456E+07	18.71	5.410	3.605	-0.333	8.913	4.783	0.000	3.90E-1	5.94E-1	0.1994	0.3826	0.000	0.383	5.010	-5.466	6.07E-1	3.85E-1	7.24E-4	3.62E-3	2.26E-3

Table 7.1 (continued) - M = 15.00 $M_\odot$ Z=0.008 Y=0.250 Diffusion

		AGE	M	$L/L_\odot$	T_{eff}	G	T_c	ρ_c	COMP	XC	XO	CONV	Q_{disc}	L_H	$Q1_H$	L_{He}	$\dot{M}$	X_{sup}	Y_{sup}	XC_{sup}	XN_{sup}	XO_{sup}
H	1	0.00000E+00	15.00	4.265	4.501	4.299	7.546	0.837	0.730	3.18E-5	3.59E-3	0.5481	0.5444	4.265	0.000	0.000	-9.146	7.42E-1	2.50E-1	1.98E-3	4.97E-4	4.23E-3
		9.38485E+05	15.00	4.286	4.496	4.260	7.542	0.816	0.700	4.09E-5	1.93E-3	0.5402	0.5460	4.287	0.000	0.000	-9.020	7.42E-1	2.50E-1	1.98E-3	4.97E-4	4.23E-3
B		3.97238E+06	14.99	4.358	4.489	4.157	7.544	0.795	0.600	5.99E-5	5.79E-4	0.5178	0.5482	4.359	0.000	0.000	-8.726	7.42E-1	2.50E-1	1.98E-3	4.97E-4	4.23E-3
U		6.36510E+06	14.99	4.426	4.481	4.058	7.554	0.796	0.500	6.53E-5	2.98E-4	0.4922	0.5485	4.427	0.000	0.000	-8.459	7.42E-1	2.50E-1	1.98E-3	4.97E-4	4.23E-3
R		8.23312E+06	14.98	4.489	4.469	3.947	7.565	0.806	0.400	6.98E-5	2.11E-4	0.4607	0.5488	4.490	0.000	0.000	-8.206	7.42E-1	2.50E-1	1.98E-3	4.97E-4	4.23E-3
N		9.71017E+06	14.97	4.547	4.452	3.822	7.578	0.825	0.300	7.40E-5	1.78E-4	0.4269	0.5492	4.548	0.000	0.000	-7.970	7.42E-1	2.50E-1	1.98E-3	4.97E-4	4.23E-3
I		1.08723E+07	14.95	4.599	4.429	3.677	7.594	0.859	0.200	7.88E-5	1.62E-4	0.3884	0.5498	4.600	0.000	0.000	-7.748	7.42E-1	2.50E-1	1.98E-3	4.97E-4	4.23E-3
N		1.18117E+07	14.93	4.647	4.399	3.508	7.617	0.920	0.100	8.61E-5	1.50E-4	0.3474	0.5506	4.648	0.000	0.000	-7.540	7.42E-1	2.50E-1	1.98E-3	4.97E-4	4.23E-3
G		1.22544E+07	14.91	4.670	4.384	3.422	7.638	0.980	0.050	9.00E-5	1.43E-4	0.3244	0.5512	4.671	0.000	0.000	-7.448	7.42E-1	2.50E-1	1.98E-3	4.97E-4	4.23E-3
	2	1.24348E+07	14.91	4.681	4.380	3.395	7.655	1.029	0.028	9.53E-5	1.38E-4	0.3100	0.5514	4.682	0.000	0.000	-7.410	7.42E-1	2.50E-1	1.98E-3	4.97E-4	4.23E-3
		1.25683E+07	14.90	4.691	4.385	3.406	7.682	1.110	0.010	1.06E-4	1.37E-4	0.2988	0.5516	4.689	0.000	0.000	-7.393	7.42E-1	2.50E-1	1.98E-3	4.97E-4	4.23E-3
		1.26470E+07	14.90	4.709	4.412	3.498	7.741	1.292	0.001	1.29E-4	1.40E-4	0.2657	0.5517	4.674	0.000	0.000	-7.412	7.42E-1	2.50E-1	1.98E-3	4.97E-4	4.23E-3
	3	1.26502E+07	14.90	4.712	4.416	3.511	7.751	1.324	0.001	1.32E-4	1.39E-4	0.2565	0.5517	4.671	0.000	0.000	-7.416	7.42E-1	2.50E-1	1.98E-3	4.97E-4	4.23E-3
		1.26556E+07	14.90	4.721	4.425	3.538	7.779	1.421	0.000	1.43E-4	1.39E-4	0.2251	0.5517	4.639	0.000	0.000	-7.414	7.42E-1	2.50E-1	1.98E-3	4.97E-4	4.23E-3
	4	1.26587E+07	14.90	4.729	4.431	3.552	7.825	1.627	0.000	1.60E-4	1.38E-4	0.0000	0.5517	4.610	0.111	0.000	-7.398	7.42E-1	2.50E-1	1.98E-3	4.97E-4	4.23E-3
		1.26708E+07	14.90	4.749	4.324	3.103	7.969	2.403	0.000	1.60E-4	1.38E-4	0.0000	0.5518	4.790	0.182	0.000	-7.156	7.42E-1	2.50E-1	1.98E-3	4.97E-4	4.23E-3
He	5	1.26769E+07	14.90	4.761	4.233	2.729	8.053	2.724	0.992	1.60E-4	1.38E-4	0.0000	0.5518	4.791	0.205	0.000	-7.015	7.42E-1	2.50E-1	1.98E-3	4.97E-4	4.23E-3
		1.26775E+07	14.90	4.761	4.223	2.688	8.061	2.754	0.992	1.60E-4	1.38E-4	0.0000	0.5518	4.791	0.205	0.000	-7.005	7.42E-1	2.50E-1	1.98E-3	4.97E-4	4.23E-3
B		1.26820E+07	14.90	4.752	4.120	2.287	8.132	2.983	0.992	2.20E-4	1.38E-4	0.0000	0.5518	4.779	0.220	1.832	-6.950	7.42E-1	2.50E-1	1.98E-3	4.97E-4	4.23E-3
U		1.26850E+07	14.90	4.735	4.016	1.885	8.184	3.097	0.991	1.01E-3	1.39E-4	0.0157	0.5518	4.764	0.227	3.539	-6.929	7.42E-1	2.50E-1	1.98E-3	4.97E-4	4.23E-3
R		1.26872E+07	14.90	4.713	3.888	1.396	8.206	3.107	0.989	2.22E-3	1.39E-4	0.0542	0.5518	4.728	0.231	4.173	-6.893	7.42E-1	2.50E-1	1.98E-3	4.97E-4	4.23E-3
N		1.26889E+07	14.90	4.658	3.727	0.808	8.210	3.091	0.988	3.51E-3	1.40E-4	0.0752	0.5518	4.698	0.234	4.250	-6.805	7.42E-1	2.50E-1	1.98E-3	4.97E-4	4.23E-3
I		1.26900E+07	14.90	4.548	3.622	0.498	8.211	3.082	0.987	4.03E-3	1.41E-4	0.0856	0.5519	4.630	0.235	4.267	-6.619	7.42E-1	2.50E-1	1.98E-3	4.97E-4	4.23E-3
N	6	1.26900E+07	14.90	4.548	3.622	0.498	8.211	3.082	0.987	4.03E-3	1.41E-4	0.0856	0.5519	5.213	0.235	5.178	-6.619	7.42E-1	2.50E-1	1.98E-3	4.97E-4	4.23E-3
G	7	1.26914E+07	14.90	4.798	3.608	0.190	8.212	3.072	0.987	4.38E-3	1.41E-4	0.0943	0.3376	4.656	0.236	4.256	-6.464	6.78E-1	3.14E-1	1.24E-3	2.05E-3	3.35E-3
	8	1.26927E+07	14.90	4.813	3.608	0.175	8.213	3.067	0.986	5.30E-3	1.42E-4	0.0980	0.3155	4.671	0.238	4.224	-6.426	6.72E-1	3.20E-1	1.20E-3	2.16E-3	3.28E-3
		1.27321E+07	14.88	4.738	3.612	0.268	8.224	3.049	0.950	4.03E-2	3.14E-4	0.1168	0.3114	4.555	0.257	4.262	-6.520	6.71E-1	3.21E-1	1.20E-3	2.18E-3	3.26E-3
		1.28062E+07	14.86	4.655	3.627	0.411	8.229	3.028	0.900	8.95E-2	1.03E-3	0.1586	0.3120	4.384	0.270	4.309	-6.650	6.71E-1	3.21E-1	1.20E-3	2.18E-3	3.26E-3
		1.28382E+07	14.86	4.836	3.758	0.753	8.231	3.026	0.873	1.15E-1	1.59E-3	0.1606	0.3122	4.479	0.274	4.320	-6.626	6.71E-1	3.21E-1	1.20E-3	2.18E-3	3.26E-3
		1.28399E+07	14.86	4.837	3.869	1.198	8.231	3.026	0.872	1.17E-1	1.62E-3	0.1606	0.3122	4.514	0.275	4.317	-6.716	6.71E-1	3.21E-1	1.20E-3	2.18E-3	3.26E-3
		1.28434E+07	14.85	4.843	4.016	1.776	8.232	3.027	0.869	1.20E-1	1.70E-3	0.1606	0.3133	4.565	0.275	4.317	-6.763	6.71E-1	3.21E-1	1.20E-3	2.18E-3	3.26E-3
		1.28490E+07	14.85	4.835	4.133	2.252	8.232	3.027	0.864	1.25E-1	1.83E-3	0.1606	0.3133	4.611	0.276	4.320	-6.805	6.71E-1	3.21E-1	1.20E-3	2.18E-3	3.26E-3
		1.29232E+07	14.84	4.820	4.221	2.622	8.237	3.025	0.800	1.86E-1	3.98E-3	0.1663	0.3135	4.640	0.284	4.355	-6.886	6.71E-1	3.21E-1	1.20E-3	2.18E-3	3.26E-3
		1.30422E+07	14.83	4.829	4.237	2.674	8.245	3.027	0.700	2.80E-1	9.92E-3	0.1718	0.3194	4.626	0.292	4.402	-6.880	6.71E-1	3.21E-1	1.20E-3	2.18E-3	3.26E-3
		1.31609E+07	14.81	4.838	4.256	2.743	8.255	3.033	0.600	3.69E-1	1.97E-2	0.1781	0.3281	4.612	0.299	4.449	-6.879	6.71E-1	3.21E-1	1.20E-3	2.18E-3	3.26E-3
	9	1.32275E+07	14.80	4.842	4.262	2.761	8.260	3.036	0.546	4.16E-1	2.74E-2	0.1843	0.3340	4.604	0.303	4.471	-6.876	6.71E-1	3.21E-1	1.20E-3	2.18E-3	3.26E-3
		1.32810E+07	14.80	4.844	4.259	2.748	8.265	3.044	0.500	4.54E-1	3.52E-2	0.1844	0.3373	4.595	0.306	4.491	-6.869	6.71E-1	3.21E-1	1.20E-3	2.18E-3	3.26E-3
		1.34031E+07	14.78	4.850	4.248	2.695	8.277	3.060	0.400	5.29E-1	5.94E-2	0.1923	0.3418	4.572	0.311	4.529	-6.848	6.71E-1	3.21E-1	1.20E-3	2.18E-3	3.26E-3
		1.35219E+07	14.76	4.855	4.236	2.643	8.291	3.086	0.300	5.92E-1	9.66E-2	0.1998	0.3479	4.545	0.316	4.568	-6.829	6.71E-1	3.21E-1	1.20E-3	2.18E-3	3.26E-3
		1.36493E+07	14.74	4.860	4.217	2.561	8.311	3.130	0.200	6.30E-1	1.58E-1	0.2042	0.3512	4.510	0.321	4.608	-6.806	6.71E-1	3.21E-1	1.20E-3	2.18E-3	3.26E-3
		1.38413E+07	14.71	4.866	4.190	2.446	8.334	3.177	0.100	5.90E-1	2.98E-1	0.2126	0.3570	4.457	0.329	4.652	-6.777	6.71E-1	3.21E-1	1.20E-3	2.18E-3	3.26E-3
		1.39272E+07	14.70	4.865	4.139	2.241	8.368	3.272	0.050	5.34E-1	4.04E-1	0.2128	0.3585	4.413	0.332	4.678	-6.756	6.71E-1	3.21E-1	1.20E-3	2.18E-3	3.26E-3
		1.41127E+07	14.66	4.861	4.037	1.837	8.400	3.353	0.021	3.52E-1	6.14E-1	0.2235	0.3628	4.317	0.339	4.731	-6.732	6.71E-1	3.21E-1	1.20E-3	2.18E-3	3.26E-3
		1.41386E+07	14.66	4.851	3.972	1.589	8.424	3.424	0.010	3.21E-1	6.57E-1	0.2199	0.3630	4.284	0.340	4.712	-6.730	6.71E-1	3.21E-1	1.20E-3	2.18E-3	3.26E-3
		1.41508E+07	14.66	4.832	3.872	1.207	8.449	3.501	0.003	3.02E-1	6.81E-1	0.2172	0.3624	4.237	0.340	4.685	-6.720	6.71E-1	3.21E-1	1.20E-3	2.18E-3	3.26E-3
		1.41556E+07	14.66	4.800	3.782	0.877	8.474	3.578	0.001	2.95E-1	6.90E-1	0.2048	0.3625	4.202	0.340	4.598	-6.698	6.71E-1	3.21E-1	1.20E-3	2.18E-3	3.26E-3
	10	1.41577E+07	14.66	4.745	3.706	0.628	8.499	3.656	0.000	2.93E-1	6.92E-1	0.1837	0.3625	4.181	0.341	4.318	-6.671	6.71E-1	3.21E-1	1.20E-3	2.18E-3	3.26E-3
		1.41582E+07	14.66	4.702	3.675	0.547	8.508	3.686	0.000	2.93E-1	6.92E-1	0.1743	0.3625	4.154	0.341	4.276	-6.646	6.71E-1	3.21E-1	1.20E-3	2.18E-3	3.26E-3
	11	1.42466E+07	14.55	5.189	3.577	-0.332	8.904	4.951	0.000	2.93E-1	6.92E-1	0.1542	0.3411	0.000	0.341	4.947	-5.814	6.63E-1	3.29E-1	1.00E-3	2.44E-3	3.20E-3
		1.44759E+07	14.32	5.039	3.590	-0.138	8.913	4.903	0.000	2.93E-1	6.92E-1	0.2006	0.3454	4.270	0.345	3.667	-6.084	6.60E-1	3.32E-1	1.00E-3	2.46E-3	3.19E-3

Table 7.1 (continued) - M = 12.00 $M_\odot$ Z=0.008 Y=0.250 Diffusion

		AGE	M	$L/L_\odot$	T_{eff}	G	T_c	ρ_c	COMP	XC	XO	CONV	Q_{disc}	L_H	$Q1_H$	L_{He}	$\dot{M}$	X_{sup}	Y_{sup}	XC_{sup}	XN_{sup}	XO_{sup}
H	1	0.00000E+00	12.00	3.972	4.457	4.318	7.528	0.931	0.732	3.03E-5	3.53E-3	0.5184	0.5167	3.973	0.000	0.000	-10.080	7.42E-1	2.50E-1	1.98E-3	4.97E-4	4.23E-3
		1.48366E+06	12.00	3.994	4.452	4.276	7.523	0.908	0.700	3.86E-5	1.92E-3	0.5103	0.5194	3.996	0.000	0.000	-9.964	7.42E-1	2.50E-1	1.98E-3	4.97E-4	4.23E-3
B		5.95203E+06	12.00	4.069	4.445	4.174	7.527	0.886	0.600	5.64E-5	6.25E-4	0.4847	0.5201	4.070	0.000	0.000	-9.622	7.42E-1	2.50E-1	1.98E-3	4.97E-4	4.23E-3
U		9.42661E+06	12.00	4.139	4.438	4.075	7.537	0.886	0.500	6.21E-5	3.28E-4	0.4572	0.5201	4.140	0.000	0.000	-9.307	7.42E-1	2.50E-1	1.98E-3	4.97E-4	4.23E-3
R		1.20743E+07	12.00	4.204	4.427	3.966	7.548	0.894	0.400	6.64E-5	2.32E-4	0.4279	0.5202	4.205	0.000	0.000	-9.012	7.42E-1	2.50E-1	1.98E-3	4.97E-4	4.23E-3
N		1.41303E+07	11.99	4.264	4.411	3.843	7.561	0.913	0.300	7.07E-5	1.91E-4	0.3907	0.5203	4.266	0.000	0.000	-8.732	7.42E-1	2.50E-1	1.98E-3	4.97E-4	4.23E-3
I		1.57270E+07	11.99	4.319	4.390	3.705	7.577	0.945	0.200	7.54E-5	1.72E-4	0.3561	0.5205	4.320	0.000	0.000	-8.473	7.42E-1	2.50E-1	1.98E-3	4.97E-4	4.23E-3
N		1.70011E+07	11.98	4.360	4.363	3.547	7.601	1.004	0.100	8.21E-5	1.59E-4	0.3114	0.5208	4.370	0.000	0.000	-8.229	7.42E-1	2.50E-1	1.98E-3	4.97E-4	4.23E-3
G		1.75825E+07	11.98	4.393	4.350	3.470	7.622	1.063	0.050	8.65E-5	1.58E-4	0.2900	0.5209	4.394	0.000	0.000	-8.124	7.42E-1	2.50E-1	1.98E-3	4.97E-4	4.23E-3
	2	1.77763E+07	11.98	4.402	4.348	3.453	7.635	1.101	0.032	9.04E-5	1.53E-4	0.2826	0.5210	4.402	0.000	0.000	-8.090	7.42E-1	2.50E-1	1.98E-3	4.97E-4	4.23E-3
		1.79882E+07	11.98	4.415	4.354	3.465	7.665	1.191	0.010	1.02E-4	1.47E-4	0.2644	0.5211	4.412	0.000	0.000	-8.066	7.42E-1	2.50E-1	1.98E-3	4.97E-4	4.23E-3
		1.80830E+07	11.98	4.435	4.381	3.553	7.723	1.370	0.001	1.24E-4	1.49E-4	0.2280	0.5211	4.395	0.000	0.000	-8.088	7.42E-1	2.50E-1	1.98E-3	4.97E-4	4.23E-3
	3	1.80869E+07	11.98	4.439	4.385	3.566	7.733	1.404	0.001	1.27E-4	1.48E-4	0.2193	0.5211	4.390	0.000	0.000	-8.091	7.42E-1	2.50E-1	1.98E-3	4.97E-4	4.23E-3
		1.80927E+07	11.98	4.448	4.392	3.584	7.757	1.494	0.000	1.38E-4	1.48E-4	0.1848	0.5211	4.362	0.000	0.000	-8.085	7.42E-1	2.50E-1	1.98E-3	4.97E-4	4.23E-3
	4	1.80957E+07	11.98	4.453	4.396	3.593	7.784	1.646	0.000	1.53E-4	1.47E-4	0.0000	0.5211	4.333	0.070	0.000	-8.071	7.42E-1	2.50E-1	1.98E-3	4.97E-4	4.23E-3
		1.81132E+07	11.97	4.475	4.289	3.143	7.883	2.408	0.000	1.53E-4	1.47E-4	0.0000	0.5211	4.531	0.138	0.000	-7.760	7.42E-1	2.50E-1	1.98E-3	4.97E-4	4.23E-3
		1.81240E+07	11.97	4.493	4.187	2.719	7.969	2.760	0.000	1.53E-4	1.47E-4	0.0000	0.5211	4.543	0.167	0.000	-7.535	7.42E-1	2.50E-1	1.98E-3	4.97E-4	4.23E-3
	5	1.81244E+07	11.97	4.493	4.183	2.704	7.971	2.771	0.000	1.53E-4	1.47E-4	0.0000	0.5211	4.543	0.167	0.000	-7.529	7.42E-1	2.50E-1	1.98E-3	4.97E-4	4.23E-3
He		1.81312E+07	11.97	4.483	4.085	2.318	8.035	2.984	0.992	1.53E-4	1.47E-4	0.0000	0.5212	4.541	0.181	0.000	-7.428	7.42E-1	2.50E-1	1.98E-3	4.97E-4	4.23E-3
		1.81356E+07	11.97	4.464	3.981	1.922	8.079	3.120	0.992	1.56E-4	1.47E-4	0.0000	0.5212	4.535	0.187	0.000	-7.356	7.42E-1	2.50E-1	1.98E-3	4.97E-4	4.23E-3
B		1.81386E+07	11.97	4.437	3.872	1.516	8.110	3.209	0.992	2.08E-4	1.47E-4	0.0000	0.5212	4.529	0.192	1.282	-7.280	7.42E-1	2.50E-1	1.98E-3	4.97E-4	4.23E-3
U		1.81406E+07	11.97	4.390	3.760	1.115	8.133	3.265	0.992	5.12E-4	1.47E-4	0.0000	0.5212	4.519	0.196	2.138	-7.180	7.42E-1	2.50E-1	1.98E-3	4.97E-4	4.23E-3
R		1.81422E+07	11.97	4.278	3.658	0.819	8.155	3.300	0.991	9.96E-4	1.48E-4	0.0043	0.5212	4.504	0.198	2.816	-7.084	7.42E-1	2.50E-1	1.98E-3	4.97E-4	4.23E-3
N	6	1.81428E+07	11.97	4.255	3.644	0.785	8.163	3.309	0.991	1.28E-3	1.48E-4	0.0082	0.5212	4.494	0.199	3.068	-7.083	7.42E-1	2.50E-1	1.98E-3	4.97E-4	4.23E-3
I	7	1.81464E+07	11.97	4.581	3.607	0.310	8.189	3.298	0.989	2.88E-3	1.48E-4	0.0457	0.3275	4.487	0.204	3.845	-6.696	6.99E-1	2.93E-1	1.28E-3	1.84E-3	3.54E-3
N	8	1.81608E+07	11.97	4.614	3.606	0.272	8.194	3.225	0.982	9.37E-3	1.59E-4	0.0810	0.2909	4.531	0.213	3.816	-6.646	6.86E-1	3.06E-1	1.22E-3	2.04E-3	3.39E-3
G		1.82134E+07	11.96	4.573	3.608	0.323	8.203	3.197	0.950	4.04E-2	3.17E-4	0.0914	0.2912	4.471	0.230	3.879	-6.692	6.86E-1	3.06E-1	1.22E-3	2.04E-3	3.39E-3
		1.83332E+07	11.94	4.463	3.617	0.466	8.211	3.157	0.900	8.96E-2	1.04E-3	0.1355	0.2919	4.296	0.248	3.961	-6.821	6.86E-1	3.06E-1	1.22E-3	2.04E-3	3.39E-3
		1.85152E+07	11.91	4.457	3.650	0.604	8.220	3.144	0.800	1.86E-1	3.95E-3	0.1448	0.2930	4.183	0.261	4.038	-6.922	6.86E-1	3.06E-1	1.22E-3	2.04E-3	3.39E-3
		1.85236E+07	11.91	4.564	3.801	1.101	8.220	3.143	0.796	1.90E-1	4.10E-3	0.1448	0.2930	4.275	0.262	4.029	-6.994	6.86E-1	3.06E-1	1.22E-3	2.04E-3	3.39E-3
		1.85320E+07	11.91	4.567	3.971	1.777	8.221	3.144	0.791	1.95E-1	4.33E-3	0.1448	0.2935	4.340	0.262	4.033	-7.208	6.86E-1	3.06E-1	1.22E-3	2.04E-3	3.39E-3
		1.85481E+07	11.91	4.561	4.073	2.190	8.222	3.145	0.782	2.04E-1	4.77E-3	0.1448	0.2935	4.382	0.264	4.041	-7.276	6.86E-1	3.06E-1	1.22E-3	2.04E-3	3.39E-3
		1.86940E+07	11.90	4.573	4.158	2.519	8.229	3.139	0.700	2.80E-1	9.80E-3	0.1510	0.2981	4.398	0.273	4.092	-7.327	6.86E-1	3.06E-1	1.22E-3	2.04E-3	3.39E-3
		1.88637E+07	11.90	4.587	4.197	2.662	8.238	3.139	0.600	3.70E-1	1.93E-2	0.1589	0.3084	4.393	0.281	4.145	-7.341	6.86E-1	3.06E-1	1.22E-3	2.04E-3	3.39E-3
	9	1.88892E+07	11.90	4.589	4.200	2.670	8.239	3.140	0.587	3.82E-1	2.10E-2	0.1597	0.3110	4.392	0.282	4.152	-7.340	6.86E-1	3.06E-1	1.22E-3	2.04E-3	3.39E-3
		1.90237E+07	11.89	4.595	4.193	2.637	8.249	3.150	0.500	4.56E-1	3.35E-2	0.1614	0.3163	4.380	0.288	4.191	-7.320	6.86E-1	3.06E-1	1.22E-3	2.04E-3	3.39E-3
		1.91830E+07	11.88	4.601	4.183	2.592	8.261	3.166	0.400	5.33E-1	5.53E-2	0.1656	0.3219	4.362	0.293	4.233	-7.295	6.86E-1	3.06E-1	1.22E-3	2.04E-3	3.39E-3
		1.93367E+07	11.87	4.607	4.174	2.547	8.275	3.189	0.300	5.99E-1	8.93E-2	0.1695	0.3269	4.341	0.297	4.273	-7.272	6.86E-1	3.06E-1	1.22E-3	2.04E-3	3.39E-3
		1.95100E+07	11.86	4.614	4.154	2.462	8.295	3.230	0.200	6.40E-1	1.48E-1	0.1741	0.3310	4.312	0.302	4.316	-7.241	6.86E-1	3.06E-1	1.22E-3	2.04E-3	3.39E-3
		1.97264E+07	11.85	4.620	4.127	2.345	8.320	3.283	0.100	6.14E-1	2.74E-1	0.1802	0.3366	4.272	0.309	4.360	-7.202	6.86E-1	3.06E-1	1.22E-3	2.04E-3	3.39E-3
		1.98380E+07	11.84	4.619	4.074	2.135	8.351	3.368	0.050	5.62E-1	3.76E-1	0.1803	0.3377	4.235	0.312	4.389	-7.164	6.86E-1	3.06E-1	1.22E-3	2.04E-3	3.39E-3
		2.00348E+07	11.83	4.611	3.969	1.723	8.390	3.470	0.016	4.15E-1	5.58E-1	0.1910	0.3400	4.168	0.317	4.414	-7.104	6.86E-1	3.06E-1	1.22E-3	2.04E-3	3.39E-3
		2.00498E+07	11.83	4.604	3.918	1.527	8.402	3.508	0.010	3.99E-1	5.79E-1	0.1916	0.3400	4.146	0.318	4.418	-7.080	6.86E-1	3.06E-1	1.22E-3	2.04E-3	3.39E-3
		2.00658E+07	11.83	4.578	3.817	1.149	8.427	3.584	0.003	3.81E-1	6.03E-1	0.1892	0.3401	4.106	0.318	4.389	-7.026	6.86E-1	3.06E-1	1.22E-3	2.04E-3	3.39E-3
		2.00720E+07	11.83	4.529	3.716	0.793	8.450	3.656	0.001	3.74E-1	6.12E-1	0.1764	0.3401	4.069	0.319	4.300	-6.951	6.86E-1	3.06E-1	1.22E-3	2.04E-3	3.39E-3
		2.00723E+07	11.83	4.524	3.709	0.771	8.452	3.660	0.001	3.74E-1	6.13E-1	0.1764	0.3401	4.067	0.319	4.289	-6.945	6.86E-1	3.06E-1	1.22E-3	2.04E-3	3.39E-3
		2.00752E+07	11.83	4.437	3.653	0.635	8.479	3.748	0.000	3.71E-1	6.16E-1	0.1321	0.3401	4.026	0.319	3.822	-6.929	6.86E-1	3.06E-1	1.22E-3	2.04E-3	3.39E-3
	10	2.00752E+07	11.83	4.437	3.653	0.635	8.479	3.748	0.000	3.71E-1	6.16E-1	0.1321	0.3401	5.042	0.319	5.019	-6.929	6.86E-1	3.06E-1	1.22E-3	2.04E-3	3.39E-3
	11	2.02087E+07	11.75	4.973	3.571	-0.235	8.874	5.030	0.000	3.71E-1	6.16E-1	0.1298	0.3107	0.000	0.311	4.799	-6.144	6.70E-1	3.22E-1	1.13E-3	2.22E-3	3.30E-3
		2.03770E+07	11.66	4.837	3.585	-0.047	8.883	4.966	0.000	3.71E-1	6.16E-1	0.1657	0.3132	4.314	0.312	3.780	-6.346	6.69E-1	3.23E-1	1.13E-3	2.24E-3	3.29E-3

Table 7.1 (continued) - M = 9.00 $M_\odot$ Z=0.008 Y=0.250 Diffusion

		AGE	$L/L_\odot$	T_{eff}	G	T_c	ρ_c	COMP	XC	XO	CONV	Q_{disc}	L_H	$Q1_H$	$Q2_H$	L_{He}	$Q1_{He}$	$Q2_{He}$	L_C	$-L_\mu$	Q_{Tmax}
H	1	0.00000E+00	3.577	4.396	4.347	7.504	1.068	0.735	2.57E-5	3.78E-3	0.4802	0.4712	3.576	0.0000	0.4227	0.000	0.0000	0.0000	0.000	0.000	0.0000
		3.07083E+06	3.601	4.390	4.299	7.499	1.039	0.700	3.74E-5	1.98E-3	0.4747	0.4784	3.602	0.0000	0.3144	0.000	0.0000	0.0000	0.000	0.000	0.0000
B		1.11824E+07	3.677	4.383	4.195	7.503	1.016	0.600	5.15E-5	7.03E-3	0.4476	0.4784	3.678	0.0000	0.2986	0.000	0.0000	0.0000	0.000	0.000	0.0000
U		1.72963E+07	3.750	4.376	4.094	7.513	1.012	0.500	5.77E-5	3.72E-4	0.4181	0.4784	3.751	0.0000	0.2819	0.000	0.0000	0.0000	0.000	0.000	0.0000
R		2.18170E+07	3.817	4.366	3.984	7.525	1.018	0.400	6.24E-5	2.59E-4	0.3872	0.4784	3.818	0.0000	0.2638	0.000	0.0000	0.0000	0.000	0.000	0.0000
N		2.52662E+07	3.880	4.351	3.863	7.538	1.034	0.300	6.60E-5	2.18E-4	0.3525	0.4784	3.881	0.0000	0.2441	0.000	0.0000	0.0000	0.000	0.000	0.0000
I		2.78904E+07	3.936	4.331	3.726	7.554	1.065	0.200	7.08E-5	1.92E-4	0.3167	0.4784	3.937	0.0000	0.2213	0.000	0.0000	0.0000	0.000	0.000	0.0000
N		2.98948E+07	3.987	4.306	3.577	7.578	1.122	0.100	7.72E-5	1.74E-4	0.2770	0.4784	3.988	0.0000	0.2031	0.000	0.0000	0.0000	0.000	0.000	0.0000
G		3.07844E+07	4.011	4.295	3.508	7.598	1.180	0.050	8.14E-5	1.70E-4	0.2537	0.4784	4.012	0.0000	0.2031	0.000	0.0000	0.0000	0.000	0.000	0.0000
	2	3.10058E+07	4.018	4.294	3.496	7.607	1.205	0.036	8.50E-5	1.67E-4	0.2501	0.4784	4.018	0.0000	0.2092	0.000	0.0000	0.0000	0.000	0.000	0.0000
a		3.13784E+07	4.034	4.302	3.511	7.641	1.305	0.010	9.62E-5	1.64E-4	0.2269	0.4784	4.031	0.0000	0.2441	0.000	0.0000	0.0000	0.000	0.000	0.0000
n		3.15057E+07	4.057	4.328	3.592	7.695	1.479	0.001	1.18E-4	1.60E-4	0.1816	0.4784	4.013	0.0000	0.3088	0.000	0.0000	0.0000	0.000	0.000	0.0000
d		3.15172E+07	4.069	4.335	3.610	7.721	1.594	0.000	1.31E-4	1.59E-4	0.1296	0.4784	3.994	0.0000	0.3471	0.000	0.0000	0.0000	0.000	0.000	0.0000
	3	3.15215E+07	4.067	4.335	3.611	7.729	1.737	0.000	1.43E-4	1.59E-4	0.0000	0.4784	4.057	0.0310	0.3729	0.000	0.0000	0.0000	0.000	0.000	0.0000
R		3.15462E+07	4.095	4.265	3.302	7.739	2.288	0.000	1.43E-4	1.59E-4	0.0000	0.4784	4.145	0.0779	0.3041	0.000	0.0000	0.0000	0.000	0.000	0.0000
G		3.15751E+07	4.129	4.183	2.944	7.803	2.677	0.000	1.43E-4	1.59E-4	0.0000	0.4784	4.167	0.1100	0.2708	0.000	0.0000	0.0000	0.000	0.000	0.0000
B	4	3.15868E+07	4.132	4.140	2.767	7.841	2.828	0.000	1.43E-4	1.59E-4	0.0000	0.4784	4.172	0.1217	0.2538	0.000	0.0000	0.0000	0.000	0.000	0.0000
		3.15945E+07	4.131	4.104	2.623	7.870	2.929	0.000	1.43E-4	1.59E-4	0.0000	0.4784	4.174	0.1306	0.2441	0.000	0.0000	0.0000	0.000	0.000	0.0000
		3.16058E+07	4.122	4.030	2.336	7.918	3.080	0.000	1.43E-4	1.59E-4	0.0000	0.4784	4.173	0.1381	0.2313	0.000	0.0000	0.0000	0.000	0.000	0.0000
		3.16136E+07	4.108	3.955	2.051	7.955	3.187	0.000	1.43E-4	1.59E-4	0.0000	0.4784	4.171	0.1464	0.2251	0.000	0.0000	0.0000	0.000	0.000	0.0000
		3.16193E+07	4.087	3.881	1.775	7.983	3.266	0.000	1.43E-4	1.59E-4	0.0000	0.4784	4.167	0.1498	0.2189	0.000	0.0000	0.0000	0.000	0.000	0.0000
		3.16233E+07	4.064	3.809	1.509	8.003	3.321	0.000	1.43E-4	1.59E-4	0.0000	0.4784	4.161	0.1533	0.2155	0.000	0.0000	0.0000	0.000	0.000	0.0000
He	5	3.16312E+07	3.928	3.649	1.009	8.045	3.434	0.992	1.44E-4	1.59E-4	0.0000	0.4784	4.128	0.1602	0.2089	0.000	0.0000	0.0082	0.000	0.000	0.0000
	6	3.16961E+07	4.276	3.611	0.506	8.167	3.459	0.976	1.52E-2	1.85E-4	0.0625	0.2780	4.227	0.1859	0.2104	3.252	0.0000	0.0310	0.000	0.000	0.0000
B		3.18319E+07	4.264	3.612	0.522	8.176	3.392	0.950	4.06E-2	3.51E-4	0.1017	0.2780	4.203	0.2064	0.2302	3.360	0.0000	0.0374	0.000	0.000	0.0000
U		3.20331E+07	4.217	3.615	0.582	8.186	3.347	0.900	8.97E-2	1.03E-3	0.1143	0.2780	4.128	0.2245	0.2478	3.479	0.0000	0.0374	0.000	0.000	0.0000
R		3.23786E+07	4.102	3.626	0.739	8.197	3.309	0.800	1.86E-1	3.99E-3	0.1262	0.2782	3.934	0.2424	0.2652	3.607	0.0000	0.0438	0.000	0.000	0.0000
N	7	3.26285E+07	4.057	3.638	0.836	8.205	3.297	0.720	2.62E-1	8.38E-3	0.1309	0.2784	3.825	0.2501	0.2730	3.669	0.0000	0.0505	0.000	0.000	0.0000
I		3.26905E+07	4.059	3.643	0.853	8.207	3.296	0.700	2.81E-1	9.79E-3	0.1328	0.2784	3.818	0.2520	0.2783	3.680	0.0000	0.0505	0.000	0.000	0.0000
N		3.29630E+07	4.227	4.037	2.261	8.216	3.295	0.600	3.71E-1	1.87E-2	0.1347	0.2829	4.051	0.2606	0.2977	3.736	0.0000	0.0505	0.000	0.000	0.0000
G	8	3.31745E+07	4.245	4.104	2.510	8.224	3.289	0.531	4.30E-1	2.83E-2	0.1425	0.2933	4.064	0.2679	0.2983	3.780	0.0000	0.0573	0.000	0.000	0.0000
		3.32543E+07	4.248	4.102	2.499	8.227	3.293	0.500	4.56E-1	3.31E-2	0.1427	0.2965	4.061	0.2703	0.2998	3.796	0.0000	0.0573	0.000	0.000	0.0000
		3.35096E+07	4.256	4.088	2.437	8.239	3.303	0.400	5.35E-1	5.40E-2	0.1467	0.3030	4.046	0.2759	0.3041	3.842	0.0000	0.0573	0.000	0.000	0.0000
		3.37378E+07	4.263	4.079	2.391	8.254	3.327	0.300	6.05E-1	8.37E-2	0.1472	0.3063	4.029	0.2797	0.3089	3.886	0.0000	0.0643	0.000	0.000	0.0000
		3.40497E+07	4.271	4.058	2.298	8.273	3.359	0.200	6.46E-1	1.42E-1	0.1554	0.3110	4.004	0.2850	0.3129	3.937	0.0000	0.0720	0.000	0.000	0.0000
		3.43825E+07	4.277	4.015	2.122	8.303	3.424	0.100	6.27E-1	2.61E-1	0.1588	0.3158	3.964	0.2909	0.3172	3.990	0.0000	0.0797	0.000	0.000	0.0000
		3.45519E+07	4.275	3.959	1.900	8.329	3.490	0.050	5.82E-1	3.56E-1	0.1614	0.3172	3.930	0.2937	0.3172	4.016	0.0000	0.0890	0.000	0.000	0.0000
		3.47074E+07	4.242	3.781	1.219	8.376	3.624	0.010	4.98E-1	4.80E-1	0.1614	0.3181	3.843	0.2965	0.3151	4.030	0.0000	0.0982	0.000	0.000	0.0000
	9	3.47355E+07	4.123	3.645	0.795	8.404	3.713	0.003	4.77E-1	5.08E-1	0.1553	0.3177	3.682	0.2971	0.3119	3.990	0.0000	0.1688	0.000	0.000	0.0000
		3.47427E+07	4.172	3.626	0.672	8.423	3.773	0.001	4.72E-1	5.15E-1	0.1431	0.3177	3.627	0.2974	0.3110	3.895	0.0000	0.1743	0.000	0.000	0.0000
		3.47468E+07	4.191	3.623	0.638	8.447	3.856	0.000	4.69E-1	5.18E-1	0.0981	0.3177	3.668	0.2974	0.3105	3.402	0.0000	0.1935	0.000	0.000	0.0000
		3.47729E+07	4.305	3.611	0.476	8.543	4.457	0.000	4.69E-1	5.19E-1	0.0000	0.3174	0.782	0.2978	0.3065	4.290	0.0906	0.2014	0.000	2.402	0.0000
E		3.47871E+07	4.407	3.603	0.345	8.592	4.704	0.000	4.69E-1	5.19E-1	0.0000	0.3173	0.000	0.2978	0.3023	4.375	0.1084	0.2014	0.000	2.746	0.0000
A		3.48054E+07	4.499	3.594	0.216	8.667	5.058	0.000	4.69E-1	5.19E-1	0.0000	0.3134	0.000	0.2978	0.0000	4.461	0.1319	0.1989	0.000	3.322	0.0000
G		3.48246E+07	4.583	3.582	0.083	8.831	5.555	0.000	4.69E-1	5.19E-1	0.0245	0.3051	0.000	0.2978	0.0000	4.463	0.1589	0.1930	4.689	4.367	0.0000
B		3.48632E+07	4.672	3.571	-0.050	8.835	5.279	0.000	4.69E-1	5.19E-1	0.0906	0.3002	0.000	0.2978	0.0000	4.595	0.1754	0.2071	4.653	4.583	0.0000
	10	3.49635E+07	4.737	3.568	-0.127	8.846	5.156	0.000	4.69E-1	5.19E-1	0.1133	0.2938	0.000	0.2937	0.0000	4.620	0.2152	0.2514	4.936	4.872	0.0000
		3.50561E+07	4.566	3.585	0.114	8.854	5.080	0.000	4.69E-1	5.19E-1	0.1389	0.2940	2.575	0.2937	0.2947	4.269	0.2479	0.2809	5.151	5.094	0.0000
		3.51188E+07	4.608	3.579	0.047	8.855	5.064	0.000	4.69E-1	5.19E-1	0.1437	0.2954	4.236	0.2946	0.2955	3.725	0.2568	0.2852	5.197	5.144	0.0000

Table 7.1 (continued) - M = 8.00 $M_\odot$ Z=0.008 Y=0.250 Diffusion

		AGE	$L/L_\odot$	T_{eff}	G	T_c	ρ_c	COMP	XC	XO	CONV	Q_{disc}	L_H	$Q1_H$	$Q2_H$	L_{He}	$Q1_{He}$	$Q2_{He}$	L_C	$-L_\mu$	Q_{Tmax}
H	1	0.00000E+00	3.411	4.370	4.257	7.494	1.126	0.736	2.55E-5	3.86E-3	0.4656	0.4582	3.410	0.0000	0.4254	0.000	0.0000	0.0000	0.000	0.000	0.0000
		3.99157E+06	3.435	4.364	4.309	7.489	1.097	0.700	3.52E-5	2.02E-3	0.4601	0.4638	3.436	0.0000	0.3095	0.000	0.0000	0.0000	0.000	0.000	0.0000
B		1.42660E+07	3.510	4.357	4.205	7.493	1.072	0.600	4.79E-5	7.25E-4	0.4332	0.4712	3.511	0.0000	0.2928	0.000	0.0000	0.0000	0.000	0.000	0.0000
U		2.19698E+07	3.582	4.349	4.102	7.503	1.068	0.500	5.57E-5	3.92E-4	0.4058	0.4712	3.583	0.0000	0.2750	0.000	0.0000	0.0000	0.000	0.000	0.0000
R		2.76849E+07	3.649	4.339	3.994	7.514	1.074	0.400	5.96E-5	2.73E-4	0.3736	0.4712	3.649	0.0000	0.2555	0.000	0.0000	0.0000	0.000	0.000	0.0000
N		3.19983E+07	3.710	4.324	3.874	7.528	1.089	0.300	6.37E-5	2.27E-4	0.3408	0.4712	3.711	0.0000	0.2357	0.000	0.0000	0.0000	0.000	0.000	0.0000
I		3.52454E+07	3.765	4.304	3.741	7.544	1.119	0.200	6.88E-5	2.11E-4	0.3051	0.4712	3.766	0.0000	0.2148	0.000	0.0000	0.0000	0.000	0.000	0.0000
N		3.76964E+07	3.814	4.281	3.597	7.567	1.176	0.100	7.51E-5	1.82E-4	0.2648	0.4712	3.815	0.0000	0.1872	0.000	0.0000	0.0000	0.000	0.000	0.0000
G		3.87812E+07	3.837	4.271	3.533	7.588	1.232	0.050	8.02E-5	1.73E-4	0.2444	0.4712	3.838	0.0000	0.1972	0.000	0.0000	0.0000	0.000	0.000	0.0000
	2	3.90421E+07	3.844	4.269	3.521	7.596	1.258	0.036	8.27E-5	1.71E-4	0.2331	0.4712	3.845	0.0000	0.2005	0.000	0.0000	0.0000	0.000	0.000	0.0000
a		3.94953E+07	3.861	4.278	3.539	7.630	1.357	0.010	9.38E-5	1.75E-4	0.2148	0.4712	3.857	0.0000	0.2314	0.000	0.0000	0.0000	0.000	0.000	0.0000
n		3.96420E+07	3.886	4.303	3.616	7.682	1.529	0.001	1.15E-4	1.70E-4	0.1634	0.4712	3.840	0.0000	0.2963	0.000	0.0000	0.0000	0.000	0.000	0.0000
d		3.96549E+07	3.896	4.310	3.631	7.703	1.642	0.000	1.27E-4	1.69E-4	0.1047	0.4712	3.831	0.0000	0.3357	0.000	0.0000	0.0000	0.000	0.000	0.0000
	3	3.96566E+07	3.896	4.310	3.631	7.706	1.678	0.000	1.31E-4	1.69E-4	0.0715	0.4712	3.840	0.0000	0.3582	0.000	0.0000	0.0000	0.000	0.000	0.0000
R		3.97021E+07	3.937	4.235	3.289	7.696	2.374	0.000	1.37E-4	1.68E-4	0.0000	0.4712	3.971	0.0640	0.2913	0.000	0.0000	0.0000	0.000	0.000	0.0000
G		3.97506E+07	3.962	4.160	2.964	7.762	2.768	0.000	1.37E-4	1.68E-4	0.0000	0.4712	3.992	0.1000	0.2505	0.000	0.0000	0.0000	0.000	0.000	0.0000
B	4	3.97629E+07	3.965	4.134	2.857	7.789	2.869	0.000	1.37E-4	1.68E-4	0.0000	0.4712	3.997	0.1073	0.2444	0.000	0.0000	0.0000	0.000	0.000	0.0000
		3.97809E+07	3.963	4.083	2.659	7.834	3.022	0.000	1.37E-4	1.68E-4	0.0000	0.4712	4.000	0.1177	0.2314	0.000	0.0000	0.0000	0.000	0.000	0.0000
		3.97978E+07	3.952	4.012	2.382	7.886	3.175	0.000	1.37E-4	1.68E-4	0.0000	0.4712	4.000	0.1284	0.2173	0.000	0.0000	0.0000	0.000	0.000	0.0000
		3.98086E+07	3.936	3.941	2.115	7.922	3.277	0.000	1.37E-4	1.68E-4	0.0000	0.4712	3.995	0.1341	0.2112	0.000	0.0000	0.0000	0.000	0.000	0.0000
		3.98170E+07	3.914	3.868	1.844	7.952	3.357	0.000	1.37E-4	1.68E-4	0.0000	0.4712	3.990	0.1398	0.2057	0.000	0.0000	0.0000	0.000	0.000	0.0000
		3.98230E+07	3.887	3.794	1.576	7.975	3.416	0.000	1.37E-4	1.68E-4	0.0000	0.4712	3.983	0.1420	0.2005	0.000	0.0000	0.0000	0.000	0.000	0.0000
		3.98272E+07	3.852	3.723	1.329	7.990	3.457	0.000	1.37E-4	1.68E-4	0.0000	0.4712	3.975	0.1442	0.1984	0.000	0.0000	0.0000	0.000	0.000	0.0000
He	5	3.98341E+07	3.761	3.656	1.150	8.017	3.526	0.992	1.38E-4	1.68E-4	0.0000	0.4675	3.947	0.1485	0.1942	0.000	0.0000	0.0015	0.000	0.000	0.0000
	6	4.00173E+07	4.100	3.616	0.651	8.159	3.520	0.963	2.81E-2	2.65E-4	0.0867	0.2635	4.055	0.1854	0.2074	3.060	0.0000	0.0281	0.000	0.000	0.0000
B		4.01015E+07	4.093	3.616	0.660	8.162	3.497	0.950	4.07E-2	3.65E-4	0.0904	0.2635	4.042	0.1934	0.2150	3.118	0.0000	0.0297	0.000	0.000	0.0000
U		4.03769E+07	4.047	3.620	0.721	8.173	3.443	0.900	8.96E-2	1.07E-3	0.1018	0.2635	3.969	0.2121	0.2336	3.252	0.0000	0.0336	0.000	0.000	0.0000
R		4.08440E+07	3.919	3.633	0.902	8.186	3.396	0.800	1.86E-1	4.12E-3	0.1154	0.2638	3.764	0.2301	0.2513	3.392	0.0000	0.0387	0.000	0.000	0.0000
N	7	4.11693E+07	3.872	3.647	1.004	8.193	3.383	0.721	2.61E-1	8.45E-3	0.1261	0.2640	3.658	0.2378	0.2591	3.455	0.0000	0.0441	0.000	0.000	0.0000
I		4.12569E+07	3.885	3.654	1.019	8.195	3.380	0.700	2.80E-1	9.97E-3	0.1227	0.2640	3.663	0.2393	0.2649	3.468	0.0000	0.0441	0.000	0.000	0.0000
N		4.16248E+07	4.059	4.028	2.342	8.205	3.375	0.600	3.71E-1	1.90E-2	0.1249	0.2707	3.900	0.2488	0.2848	3.520	0.0000	0.0441	0.000	0.000	0.0000
G	8	4.18202E+07	4.073	4.073	2.506	8.211	3.372	0.544	4.20E-1	2.59E-2	0.1281	0.2782	3.916	0.2540	0.2827	3.564	0.0000	0.0499	0.000	0.000	0.0000
		4.19863E+07	4.077	4.064	2.469	8.216	3.372	0.500	4.57E-1	3.31E-2	0.1317	0.2827	3.909	0.2575	0.2853	3.588	0.0000	0.0499	0.000	0.000	0.0000
		4.23093E+07	4.086	4.056	2.425	8.228	3.383	0.400	5.36E-1	5.29E-2	0.1229	0.2874	3.897	0.2629	0.2900	3.638	0.0000	0.0577	0.000	0.000	0.0000
		4.26549E+07	4.096	4.047	2.379	8.242	3.397	0.300	6.03E-1	8.55E-2	0.1288	0.2926	3.884	0.2674	0.2954	3.687	0.0000	0.0577	0.000	0.000	0.0000
		4.29670E+07	4.103	4.029	2.299	8.261	3.432	0.200	6.54E-1	1.34E-1	0.1292	0.2965	3.862	0.2719	0.2992	3.735	0.0000	0.0656	0.000	0.000	0.0000
		4.34053E+07	4.110	3.986	2.122	8.291	3.492	0.100	6.41E-1	2.47E-1	0.1452	0.3017	3.828	0.2779	0.3027	3.792	0.0000	0.0739	0.000	0.000	0.0000
		4.36063E+07	4.107	3.931	1.904	8.317	3.559	0.050	6.01E-1	3.38E-1	0.1452	0.3027	3.796	0.2807	0.3027	3.818	0.0000	0.0816	0.000	0.000	0.0000
		4.42231E+07	4.066	3.658	0.915	8.371	3.688	0.010	4.01E-1	5.77E-1	0.1526	0.3086	3.549	0.2886	0.3045	3.875	0.0000	0.0899	0.000	0.000	0.0000
	9	4.42405E+07	3.988	3.648	0.892	8.376	3.701	0.008	3.97E-1	5.83E-1	0.1515	0.3086	3.487	0.2886	0.3039	3.872	0.0000	0.0899	0.000	0.000	0.0000
		4.42748E+07	4.032	3.628	0.765	8.419	3.837	0.001	3.75E-1	6.11E-1	0.1355	0.3082	3.485	0.2891	0.3022	3.728	0.0000	0.0899	0.000	0.000	0.0000
		4.42796E+07	4.044	3.625	0.744	8.443	3.921	0.000	3.73E-1	6.15E-1	0.0853	0.3082	3.535	0.2893	0.3014	3.198	0.0000	0.1875	0.000	0.000	0.0000
		4.43061E+07	4.145	3.615	0.603	8.540	4.498	0.000	3.73E-1	6.15E-1	0.0000	0.3080	1.677	0.2898	0.2986	4.134	0.0912	0.2042	0.000	2.341	0.0000
E		4.43194E+07	4.251	3.607	0.465	8.574	4.694	0.000	3.73E-1	6.15E-1	0.0000	0.3079	0.000	0.2898	0.2955	4.227	0.1050	0.2042	0.000	2.576	0.0000
A		4.43402E+07	4.354	3.598	0.328	8.632	4.998	0.000	3.73E-1	6.15E-1	0.0000	0.3080	0.000	0.2898	0.0000	4.324	0.1262	0.2022	0.000	3.010	0.0000
G		4.43614E+07	4.444	3.586	0.188	8.706	5.427	0.000	3.73E-1	6.15E-1	0.0000	0.3001	0.000	0.2898	0.0000	4.406	0.1499	0.1990	0.746	3.666	0.0000
B		4.43754E+07	4.529	3.574	0.054	8.834	5.515	0.000	3.73E-1	6.15E-1	0.0590	0.2949	0.000	0.2898	0.0000	4.403	0.1653	0.1958	4.554	4.365	0.0000
		4.44537E+07	4.622	3.567	-0.066	8.843	5.310	0.000	3.73E-1	6.15E-1	0.1005	0.2852	0.000	0.2852	0.0000	4.541	0.1947	0.2265	4.705	4.648	0.0000
	10	4.44986E+07	4.629	3.566	-0.087	8.847	5.257	0.000	3.73E-1	6.15E-1	0.1092	0.2843	0.000	0.2843	0.0000	4.540	0.2119	0.2452	4.825	4.769	0.0000
		4.45706E+07	4.524	3.575	0.064	8.854	5.190	0.000	3.73E-1	6.15E-1	0.1289	0.2843	0.524	0.2843	0.2847	4.339	0.2371	0.2695	4.999	4.948	0.0000
		4.46378E+07	4.513	3.576	0.080	8.856	5.163	0.000	3.73E-1	6.15E-1	0.1377	0.2857	4.200	0.2850	0.2858	3.694	0.2489	0.2762	5.072	5.027	0.0000

Table 7.1 (continued) - M = 7.00 $M_\odot$ Z=0.008 Y=0.250 Diffusion

		AGE	$L/L_\odot$	T_{eff}	G	T_c	ρ_c	COMP	XC	XO	CONV	Q_{disc}	L_H	$Q1_H$	$Q2_H$	L_{He}	$Q1_{He}$	$Q2_{He}$	L_C	$-L_\mu$	Q_{Tmax}
H	1	0.00000E+00	3.220	4.339	4.366	7.481	1.191	0.736	2.31E-5	3.76E-3	0.4525	0.4066	3.220	0.0000	0.4201	0.000	0.0000	0.0000	0.000	0.000	0.0000
		5.26578E+06	3.242	4.333	4.319	7.477	1.165	0.700	2.16E-5	2.05E-3	0.4442	0.4487	3.244	0.0000	0.3075	0.000	0.0000	0.0000	0.000	0.000	0.0000
B		1.87070E+07	3.317	4.226	4.215	7.481	1.140	0.600	4.64E-5	7.68E-4	0.4172	0.4563	3.318	0.0000	0.2861	0.000	0.0000	0.0000	0.000	0.000	0.0000
U		2.88442E+07	3.388	4.318	4.113	7.491	1.135	0.500	5.26E-5	4.15E-4	0.3872	0.4563	3.388	0.0000	0.2668	0.000	0.0000	0.0000	0.000	0.000	0.0000
R		3.63096E+07	3.452	4.307	4.005	7.502	1.140	0.400	5.80E-5	2.89E-4	0.3569	0.4563	3.453	0.0000	0.2457	0.000	0.0000	0.0000	0.000	0.000	0.0000
N		4.18868E+07	3.512	4.292	3.886	7.515	1.155	0.300	6.15E-5	2.49E-4	0.3214	0.4563	3.513	0.0000	0.2254	0.000	0.0000	0.0000	0.000	0.000	0.0000
I		4.60320E+07	3.564	4.273	3.758	7.532	1.185	0.200	6.64E-5	2.19E-4	0.2861	0.4563	3.565	0.0000	0.2053	0.000	0.0000	0.0000	0.000	0.000	0.0000
N		4.91557E+07	3.609	4.250	3.622	7.554	1.242	0.100	7.27E-5	1.91E-4	0.2467	0.4563	3.611	0.0000	0.1867	0.000	0.0000	0.0000	0.000	0.000	0.0000
G	2	5.05281E+07	3.632	4.241	3.563	7.575	1.299	0.049	7.80E-5	1.80E-4	0.2225	0.4563	3.633	0.0000	0.1694	0.000	0.0000	0.0000	0.000	0.000	0.0000
		5.13685E+07	3.655	4.250	3.576	7.617	1.422	0.010	9.12E-5	1.80E-4	0.1956	0.4563	3.649	0.0000	0.2203	0.000	0.0000	0.0000	0.000	0.000	0.0000
a		5.15467E+07	3.681	4.275	3.648	7.666	1.589	0.001	1.12E-4	1.74E-4	0.1416	0.4563	3.634	0.0000	0.2836	0.000	0.0000	0.0000	0.000	0.000	0.0000
n	3	5.15592E+07	3.688	4.279	3.658	7.679	1.669	0.000	1.19E-4	1.73E-4	0.0991	0.4563	3.634	0.0000	0.3144	0.000	0.0000	0.0000	0.000	0.000	0.0000
d		5.15622E+07	3.688	4.279	3.659	7.680	1.709	0.000	1.23E-4	1.73E-4	0.0678	0.4563	3.647	0.0000	0.3286	0.000	0.0000	0.0000	0.000	0.000	0.0000
		5.16522E+07	3.740	4.207	3.320	7.642	2.452	0.000	1.30E-4	1.72E-4	0.0000	0.4563	3.759	0.0533	0.2764	0.000	0.0000	0.0000	0.000	0.000	0.0000
R		5.17590E+07	3.761	4.129	2.987	7.727	2.905	0.000	1.30E-4	1.72E-4	0.0000	0.4563	3.784	0.0931	0.2342	0.000	0.0000	0.0000	0.000	0.000	0.0000
G	4	5.17699E+07	3.761	4.117	2.936	7.742	2.957	0.000	1.30E-4	1.72E-4	0.0000	0.4563	3.786	0.0961	0.2282	0.000	0.0000	0.0000	0.000	0.000	0.0000
B		5.18098E+07	3.757	4.052	2.682	7.808	3.164	0.000	1.30E-4	1.72E-4	0.0000	0.4563	3.791	0.1100	0.2136	0.000	0.0000	0.0000	0.000	0.000	0.0000
		5.18367E+07	3.741	3.978	2.399	7.863	3.318	0.000	1.30E-4	1.72E-4	0.0000	0.4563	3.788	0.1190	0.2003	0.000	0.0000	0.0000	0.000	0.000	0.0000
		5.18535E+07	3.719	3.904	2.127	7.903	3.420	0.000	1.30E-4	1.72E-4	0.0000	0.4563	3.779	0.1253	0.1929	0.000	0.0000	0.0000	0.000	0.000	0.0000
		5.18655E+07	3.692	3.828	1.850	7.932	3.495	0.000	1.30E-4	1.72E-4	0.0000	0.4563	3.769	0.1288	0.1883	0.000	0.0000	0.0000	0.000	0.000	0.0000
		5.18745E+07	3.657	3.752	1.581	7.955	3.553	0.000	1.30E-4	1.72E-4	0.0000	0.4563	3.760	0.1324	0.1852	0.000	0.0000	0.0000	0.000	0.000	0.0000
		5.18839E+07	3.581	3.682	1.378	7.980	3.614	0.000	1.30E-4	1.72E-4	0.0000	0.4563	3.739	0.1359	0.1807	0.000	0.0000	0.0000	0.000	0.000	0.0000
	5	5.18890E+07	3.552	3.663	1.331	7.993	3.647	0.000	1.30E-4	1.72E-4	0.0000	0.4525	3.723	0.1376	0.1790	0.000	0.0000	0.0000	0.000	0.000	0.0000
He	6	5.22197E+07	3.880	3.624	0.844	8.146	3.633	0.959	3.16E-2	3.00E-4	0.0799	0.2475	3.840	0.1760	0.1952	2.797	0.0000	0.0252	0.000	0.000	0.0000
		5.23097E+07	3.876	3.624	0.850	8.149	3.615	0.950	4.07E-2	3.79E-4	0.0832	0.2475	3.832	0.1811	0.2002	2.839	0.0000	0.0252	0.000	0.000	0.0000
B		5.27326E+07	3.830	3.627	0.910	8.160	3.554	0.900	8.96E-2	1.11E-3	0.0931	0.2475	3.761	0.1992	0.2192	2.989	0.0000	0.0313	0.000	0.000	0.0000
U		5.34079E+07	3.693	3.643	1.109	8.172	3.502	0.800	1.86E-1	4.22E-3	0.1050	0.2475	3.549	0.2167	0.2364	3.139	0.0000	0.0360	0.000	0.000	0.0000
R	7	5.38517E+07	3.650	3.657	1.207	8.180	3.486	0.727	2.55E-1	8.28E-3	0.1099	0.2475	3.453	0.2237	0.2436	3.202	0.0000	0.0360	0.000	0.000	0.0000
N		5.39892E+07	3.691	3.671	1.222	8.182	3.484	0.700	2.80E-1	1.00E-2	0.1099	0.2475	3.488	0.2256	0.2494	3.218	0.0000	0.0413	0.000	0.000	0.0000
I		5.45439E+07	3.856	4.014	2.431	8.192	3.470	0.600	3.71E-1	1.95E-2	0.1187	0.2570	3.715	0.2357	0.2710	3.285	0.0000	0.0413	0.000	0.000	0.0000
N	8	5.47201E+07	3.864	4.032	2.496	8.195	3.467	0.568	3.98E-1	2.35E-2	0.1190	0.2612	3.726	0.2390	0.2651	3.308	0.0000	0.0413	0.000	0.000	0.0000
G		5.50241E+07	3.869	4.020	2.442	8.202	3.469	0.500	4.57E-1	3.29E-2	0.1207	0.2666	3.718	0.2432	0.2688	3.343	0.0000	0.0474	0.000	0.000	0.0000
		5.55358E+07	3.882	4.015	2.406	8.214	3.472	0.400	5.36E-1	5.41E-2	0.1253	0.2719	3.710	0.2486	0.2749	3.400	0.0000	0.0474	0.000	0.000	0.0000
		5.60042E+07	3.893	4.006	2.359	8.229	3.485	0.300	6.04E-1	8.52E-2	0.1288	0.2782	3.699	0.2535	0.2800	3.454	0.0000	0.0533	0.000	0.000	0.0000
		5.64657E+07	3.902	3.988	2.281	8.248	3.513	0.200	6.53E-1	1.36E-1	0.1328	0.2816	3.681	0.2585	0.2836	3.506	0.0000	0.0576	0.000	0.000	0.0000
		5.69698E+07	3.906	3.944	2.102	8.278	3.575	0.100	6.59E-1	2.30E-1	0.1350	0.2865	3.647	0.2638	0.2877	3.561	0.0000	0.0645	0.000	0.000	0.0000
		5.74733E+07	3.905	3.886	1.868	8.304	3.633	0.050	5.72E-1	3.66E-1	0.1398	0.2895	3.610	0.2688	0.2903	3.602	0.0000	0.0724	0.000	0.000	0.0000
		5.77469E+07	3.823	3.677	1.113	8.352	3.766	0.010	4.92E-1	4.86E-1	0.1414	0.2901	3.454	0.2717	0.2877	3.619	0.0000	0.0799	0.000	0.000	0.0000
	9	5.77722E+07	3.779	3.654	1.067	8.363	3.801	0.006	4.81E-1	5.01E-1	0.1360	0.2907	3.348	0.2719	0.2871	3.611	0.0000	0.0799	0.000	0.000	0.0000
		5.78059E+07	3.811	3.639	0.974	8.398	3.913	0.001	4.66E-1	5.21E-1	0.1211	0.2907	3.356	0.2722	0.2852	3.472	0.0000	0.1517	0.000	0.000	0.0000
		5.78124E+07	3.822	3.636	0.951	8.420	3.993	0.000	4.64E-1	5.24E-1	0.0764	0.2904	3.400	0.2724	0.2844	2.943	0.0000	0.1665	0.000	0.000	0.0000
		5.78549E+07	3.915	3.624	0.809	8.480	4.545	0.000	4.63E-1	5.25E-1	0.0000	0.2904	1.029	0.2727	0.2821	3.918	0.0671	0.1785	0.000	1.785	0.0000
E		5.78782E+07	4.018	3.615	0.674	8.511	4.739	0.000	4.63E-1	5.25E-1	0.0000	0.2903	0.000	0.2727	0.2784	4.003	0.0814	0.1785	0.000	1.991	0.0000
A		5.79102E+07	4.114	3.609	0.549	8.559	4.988	0.000	4.62E-1	5.25E-1	0.0000	0.2901	0.000	0.2727	0.0000	4.093	0.0994	0.1785	0.000	2.250	0.0000
G		5.79461E+07	4.208	3.600	0.423	8.620	5.299	0.000	4.63E-1	5.25E-1	0.0000	0.2888	0.000	0.2727	0.0000	4.182	0.1218	0.1785	0.000	2.852	0.0000
B		5.79750E+07	4.295	3.589	0.293	8.677	5.671	0.000	4.63E-1	5.25E-1	0.0000	0.2820	0.000	0.2727	0.0000	4.260	0.1414	0.1785	0.295	3.437	0.0000
		5.79963E+07	4.388	3.577	0.150	8.822	5.664	0.000	4.63E-1	5.25E-1	0.0728	0.2668	0.000	0.2667	0.0000	4.241	0.1581	0.1776	4.480	4.125	0.0000
	10	5.81092E+07	4.459	3.570	0.052	8.826	5.408	0.000	4.63E-1	5.25E-1	0.0936	0.2564	0.000	0.2564	0.0000	4.392	0.1868	0.2157	4.412	4.348	0.0000
		5.82087E+07	4.296	3.591	0.298	8.834	5.301	0.000	4.62E-1	5.25E-1	0.1119	0.2564	1.338	0.2564	0.2572	4.146	0.2145	0.2440	4.602	4.539	0.0000
		5.82496E+07	4.332	3.586	0.241	8.836	5.276	0.000	4.62E-1	5.25E-1	0.1168	0.2573	4.036	0.2566	0.2574	3.695	0.2210	0.2479	4.645	4.587	0.0000

Table 7.1 (continued) - M = 6.00 $M_\odot$ Z=0.008 Y=0.250 Diffusion

		AGE	$L/L_\odot$	T_{eff}	G	T_c	ρ_c	COMP	XC	XO	CONV	Q_{disc}	L_H	$Q1_H$	$Q2_H$	L_{He}	$Q1_{He}$	$Q2_{He}$	L_C	$-L_\mu$	Q_{Tmax}
H	1	0.00000E+00	2.997	4.303	4.379	7.467	1.272	0.737	2.22E-5	3.86E-3	0.4331	0.3234	2.997	0.0000	0.4228	0.000	0.0000	0.0000	0.000	0.000	0.0000
		7.45193E+06	3.018	4.296	4.330	7.462	1.244	0.700	3.32E-5	2.11E-3	0.4297	0.4331	3.019	0.0000	0.3096	0.000	0.0000	0.0000	0.000	0.000	0.0000
B		2.66249E+07	3.091	4.289	4.227	7.467	1.221	0.600	4.29E-5	8.15E-4	0.4029	0.4439	3.091	0.0000	0.2842	0.000	0.0000	0.0000	0.000	0.000	0.0000
U		4.07161E+07	3.159	4.280	4.124	7.476	1.215	0.500	5.08E-5	4.47E-4	0.3732	0.4439	3.160	0.0000	0.2613	0.000	0.0000	0.0000	0.000	0.000	0.0000
R		5.11505E+07	3.222	4.269	4.017	7.488	1.219	0.400	5.46E-5	3.10E-4	0.3413	0.4439	3.223	0.0000	0.2393	0.000	0.0000	0.0000	0.000	0.000	0.0000
N		5.87894E+07	3.278	4.254	3.900	7.501	1.235	0.300	5.92E-5	2.69E-4	0.3053	0.4439	3.279	0.0000	0.2162	0.000	0.0000	0.0000	0.000	0.000	0.0000
I		6.44214E+07	3.327	4.235	3.775	7.516	1.265	0.200	6.38E-5	2.29E-4	0.2678	0.4439	3.328	0.0000	0.1952	0.000	0.0000	0.0000	0.000	0.000	0.0000
N		6.85522E+07	3.368	4.213	3.648	7.539	1.322	0.100	6.99E-5	2.04E-4	0.2285	0.4439	3.369	0.0000	0.1770	0.000	0.0000	0.0000	0.000	0.000	0.0000
G		7.02922E+07	3.388	4.205	3.597	7.559	1.377	0.050	7.49E-5	1.91E-4	0.2082	0.4439	3.388	0.0000	0.1784	0.000	0.0000	0.0000	0.000	0.000	0.0000
	2	7.05295E+07	3.391	4.205	3.592	7.563	1.390	0.043	7.60E-5	1.89E-4	0.2019	0.4439	3.392	0.0000	0.1787	0.000	0.0000	0.0000	0.000	0.000	0.0000
a		7.14055E+07	3.411	4.216	3.615	7.600	1.499	0.010	8.79E-5	1.93E-4	0.1830	0.4439	3.405	0.0000	0.2084	0.000	0.0000	0.0000	0.000	0.000	0.0000
n		7.16244E+07	3.438	4.239	3.681	7.645	1.662	0.001	1.08E-4	1.85E-4	0.1201	0.4439	3.393	0.0000	0.2722	0.000	0.0000	0.0000	0.000	0.000	0.0000
d	3	7.16401E+07	3.442	4.241	3.686	7.652	1.750	0.000	1.14E-4	1.84E-4	0.0636	0.4439	3.406	0.0000	0.3053	0.000	0.0000	0.0000	0.000	0.000	0.0000
		7.16451E+07	3.440	4.241	3.685	7.650	1.800	0.000	1.17E-4	1.84E-4	0.0335	0.4439	3.428	0.0000	0.3269	0.000	0.0000	0.0000	0.000	0.000	0.0000
R		7.19157E+07	3.505	4.168	3.329	7.597	2.609	0.000	1.18E-4	1.83E-4	0.0000	0.4439	3.515	0.0518	0.2532	0.000	0.0000	0.0000	0.000	0.000	0.0000
G	4	7.21181E+07	3.519	4.098	3.035	7.690	3.030	0.000	1.18E-4	1.83E-4	0.0000	0.4439	3.538	0.0866	0.2224	0.000	0.0000	0.0000	0.000	0.000	0.0000
B		7.21377E+07	3.518	4.085	2.985	7.706	3.082	0.000	1.18E-4	1.83E-4	0.0000	0.4439	3.540	0.0890	0.2162	0.000	0.0000	0.0000	0.000	0.000	0.0000
		7.22226E+07	3.505	3.999	2.654	7.797	3.344	0.000	1.18E-4	1.83E-4	0.0000	0.4439	3.541	0.1056	0.1958	0.000	0.0000	0.0000	0.000	0.000	0.0000
		7.22658E+07	3.477	3.912	2.336	7.856	3.499	0.000	1.18E-4	1.83E-4	0.0000	0.4439	3.530	0.1136	0.1823	0.000	0.0000	0.0000	0.000	0.000	0.0000
		7.22925E+07	3.439	3.822	2.011	7.897	3.601	0.000	1.18E-4	1.83E-4	0.0000	0.4439	3.512	0.1191	0.1753	0.000	0.0000	0.0000	0.000	0.000	0.0000
		7.23090E+07	3.397	3.737	1.713	7.924	3.666	0.000	1.18E-4	1.83E-4	0.0000	0.4439	3.493	0.1227	0.1718	0.000	0.0000	0.0000	0.000	0.000	0.0000
	5	7.23318E+07	3.302	3.676	1.563	7.962	3.757	0.000	1.18E-4	1.83E-4	0.0000	0.4439	3.455	0.1281	0.1664	0.000	0.0000	0.0000	0.000	0.000	0.0000
		7.23352E+07	3.304	3.670	1.538	7.967	3.771	0.000	1.18E-4	1.83E-4	0.0000	0.4439	3.448	0.1281	0.1654	0.000	0.0000	0.0000	0.000	0.000	0.0000
He	6	7.27020E+07	3.622	3.632	1.070	8.126	3.802	0.970	2.15E-2	2.51E-4	0.0711	0.2336	3.593	0.1575	0.1740	2.410	0.0000	0.0207	0.000	0.000	0.0000
		7.30524E+07	3.619	3.633	1.075	8.133	3.749	0.950	4.09E-2	4.08E-4	0.0756	0.2336	3.581	0.1702	0.1872	2.524	0.0000	0.0252	0.000	0.000	0.0000
B		7.37308E+07	3.581	3.636	1.127	8.144	3.682	0.900	8.56E-2	1.18E-3	0.0866	0.2336	3.521	0.1879	0.2056	2.685	0.0000	0.0298	0.000	0.000	0.0000
U		7.48102E+07	3.437	3.653	1.337	8.157	3.622	0.800	1.86E-1	4.47E-3	0.0990	0.2336	3.306	0.2051	0.2231	2.850	0.0000	0.0298	0.000	0.000	0.0000
R	7	7.53168E+07	3.394	3.662	1.417	8.162	3.606	0.750	2.33E-1	7.27E-3	0.1030	0.2339	3.222	0.2101	0.2285	2.901	0.0000	0.0361	0.000	0.000	0.0000
N		7.57174E+07	3.421	3.678	1.453	8.167	3.600	0.700	2.80E-1	1.05E-2	0.1039	0.2339	3.232	0.2136	0.2360	2.935	0.0000	0.0361	0.000	0.000	0.0000
I		7.65802E+07	3.604	3.962	2.407	8.177	3.583	0.600	3.70E-1	2.03E-2	0.1095	0.2427	3.472	0.2235	0.2562	3.008	0.0000	0.0361	0.000	0.000	0.0000
N	8	7.67548E+07	3.610	3.974	2.449	8.179	3.581	0.577	3.90E-1	2.31E-2	0.1109	0.2458	3.480	0.2257	0.2500	3.024	0.0000	0.0361	0.000	0.000	0.0000
G		7.73242E+07	3.618	3.962	2.394	8.187	3.578	0.500	4.56E-1	3.42E-2	0.1130	0.2520	3.475	0.2306	0.2540	3.069	0.0000	0.0424	0.000	0.000	0.0000
		7.80126E+07	3.631	3.958	2.366	8.199	3.582	0.400	5.36E-1	5.40E-2	0.1150	0.2570	3.469	0.2352	0.2600	3.126	0.0000	0.0424	0.000	0.000	0.0000
		7.87858E+07	3.644	3.949	2.314	8.214	3.587	0.300	6.02E-1	8.71E-2	0.1218	0.2630	3.460	0.2407	0.2644	3.186	0.0000	0.0488	0.000	0.000	0.0000
		7.94414E+07	3.653	3.933	2.241	8.232	3.612	0.200	6.54E-1	1.35E-1	0.1245	0.2668	3.442	0.2452	0.2688	3.241	0.0000	0.0548	0.000	0.000	0.0000
		8.03245E+07	3.657	3.885	2.045	8.263	3.666	0.100	6.47E-1	2.41E-1	0.1300	0.2726	3.404	0.2513	0.2735	3.305	0.0000	0.0629	0.000	0.000	0.0000
		8.06954E+07	3.647	3.823	1.808	8.287	3.728	0.050	6.16E-1	3.22E-1	0.1301	0.2735	3.360	0.2539	0.2735	3.333	0.0000	0.0629	0.000	0.000	0.0000
		8.11348E+07	3.539	3.665	1.284	8.333	3.856	0.010	5.29E-1	4.49E-1	0.1301	0.2745	3.124	0.2568	0.2716	3.352	0.0000	0.0711	0.000	0.000	0.0000
	9	8.11438E+07	3.528	3.662	1.275	8.336	3.864	0.009	5.26E-1	4.53E-1	0.1301	0.2745	3.113	0.2568	0.2716	3.346	0.0000	0.0711	0.000	0.000	0.0000
		8.12241E+07	3.560	3.648	1.195	8.379	4.004	0.001	5.02E-1	4.85E-1	0.1102	0.2745	3.149	0.2575	0.2697	3.200	0.0000	0.1353	0.000	0.000	0.0000
		8.12328E+07	3.572	3.645	1.172	8.399	4.079	0.000	5.00E-1	4.88E-1	0.0689	0.2745	3.197	0.2575	0.2692	2.641	0.0000	0.1503	0.000	0.000	0.0000
		8.12953E+07	3.660	3.634	1.038	8.444	4.621	0.000	5.00E-1	4.89E-1	0.0000	0.2743	1.091	0.2580	0.2671	3.668	0.0586	0.1662	0.000	1.430	0.0000
E		8.13348E+07	3.771	3.624	0.886	8.468	4.812	0.000	5.00E-1	4.89E-1	0.0000	0.2741	0.000	0.2580	0.2637	3.762	0.0711	0.1662	0.000	1.591	0.0000
A		8.13922E+07	3.882	3.615	0.743	8.512	5.059	0.000	5.00E-1	4.89E-1	0.0000	0.2741	0.000	0.2580	0.0000	3.866	0.0897	0.1678	0.000	1.915	0.0000
G		8.14496E+07	3.982	3.608	0.614	8.561	5.315	0.000	5.00E-1	4.89E-1	0.0000	0.2741	0.000	0.2580	0.0000	3.962	0.1115	0.1710	0.000	2.321	0.0000
B		8.14934E+07	4.073	3.599	0.488	8.600	5.567	0.000	5.00E-1	4.89E-1	0.0000	0.2694	0.000	0.2580	0.0000	4.046	0.1295	0.1719	0.000	2.751	0.0000
		8.15254E+07	4.160	3.588	0.354	8.631	5.850	0.000	5.00E-1	4.89E-1	0.0000	0.2659	0.000	0.2580	0.0000	4.128	0.1440	0.1736	0.000	3.208	0.0014
		8.15501E+07	4.247	3.576	0.218	8.653	6.207	0.000	5.00E-1	4.89E-1	0.0000	0.2616	0.000	0.2580	0.0000	4.207	0.1569	0.1740	1.548	3.694	0.0282
	10	8.15524E+07	4.256	3.575	0.206	8.653	6.251	0.000	5.00E-1	4.89E-1	0.0000	0.2609	0.000	0.2580	0.0000	4.214	0.1583	0.1740	1.774	3.748	0.0429
		8.15671E+07	4.341	3.569	0.099	8.598	6.594	0.000	5.00E-1	4.89E-1	0.0000	0.1912	0.000	0.1912	0.0000	4.265	0.1665	0.1746	3.471	4.132	0.0801
		8.28861E+07	4.361	3.568	0.072	8.559	6.638	0.000	5.00E-1	4.89E-1	0.0000	0.1876	0.000	0.1876	0.0000	4.256	0.1679	0.1751	4.870	4.221	0.0429

Table 7.1 (continued) - M = 5.00 $M_\odot$ Z=0.008 Y=0.250 Diffusion

		AGE	$L/L_\odot$	T_{eff}	G	T_c	ρ_c	COMP	XC	XO	CONV	Q_{disc}	L_H	$Q1_H$	$Q2_H$	L_{He}	$Q1_{He}$	$Q2_{He}$	L_C	$-L_\mu$	Q_{Tmax}
H	1	0.00000E+00	2.727	4.259	4.392	7.448	1.369	0.739	2.29E-5	4.63E-3	0.4133	0.2608	2.728	0.0000	0.4287	0.000	0.0000	0.0000	0.000	0.000	0.0000
		1.19018E+07	2.748	4.252	4.344	7.444	1.343	0.700	3.08E-5	2.03E-3	0.4109	0.4123	2.749	0.0000	0.3245	0.000	0.0000	0.0000	0.000	0.000	0.0000
B		3.94386E+07	2.817	4.243	4.240	7.449	1.320	0.600	4.15E-5	8.11E-4	0.3838	0.4168	2.817	0.0000	0.2858	0.000	0.0000	0.0000	0.000	0.000	0.0000
U		6.03969E+07	2.885	4.234	4.136	7.459	1.315	0.500	4.78E-5	4.60E-4	0.3473	0.4462	2.886	0.0000	0.2574	0.000	0.0000	0.0000	0.000	0.000	0.0000
R		7.55334E+07	2.943	4.222	4.030	7.470	1.319	0.400	5.27E-5	3.24E-4	0.3222	0.4598	2.944	0.0000	0.2322	0.000	0.0000	0.0000	0.000	0.000	0.0000
N		8.69156E+07	2.997	4.207	3.913	7.483	1.335	0.300	5.62E-5	2.70E-4	0.2832	0.4685	2.998	0.0000	0.2067	0.000	0.0000	0.0000	0.000	0.000	0.0000
I		9.52289E+07	3.042	4.187	3.791	7.499	1.366	0.200	6.02E-5	2.36E-4	0.2457	0.4685	3.043	0.0000	0.1844	0.000	0.0000	0.0000	0.000	0.000	0.0000
N		1.01488E+08	3.079	4.166	3.669	7.521	1.421	0.100	6.60E-5	2.15E-4	0.2117	0.4747	3.080	0.0000	0.1666	0.000	0.0000	0.0000	0.000	0.000	0.0000
G	2	1.04025E+08	3.098	4.159	3.621	7.542	1.480	0.048	7.17E-5	2.03E-4	0.1927	0.4747	3.098	0.0000	0.1671	0.000	0.0000	0.0000	0.000	0.000	0.0000
		1.05491E+08	3.121	4.170	3.642	7.580	1.597	0.010	8.37E-5	1.99E-4	0.1658	0.4747	3.114	0.0000	0.1957	0.000	0.0000	0.0000	0.000	0.000	0.0000
a		1.05793E+08	3.150	4.191	3.699	7.620	1.761	0.001	1.03E-4	1.92E-4	0.0875	0.4747	3.116	0.0000	0.2617	0.000	0.0000	0.0000	0.000	0.000	0.0000
n	3	1.05806E+08	3.151	4.192	3.701	7.621	1.805	0.001	1.05E-4	1.92E-4	0.0604	0.4747	3.119	0.0000	0.2819	0.000	0.0000	0.0000	0.000	0.000	0.0000
d		1.05827E+08	3.147	4.190	3.695	7.605	1.927	0.000	1.08E-4	1.91E-4	0.0030	0.4747	3.162	0.0000	0.3132	0.000	0.0000	0.0000	0.000	0.000	0.0000
		1.06699E+08	3.220	4.120	3.542	7.563	2.740	0.000	9.85E-5	1.91E-4	0.0000	0.4747	3.227	0.0519	0.2435	0.000	0.0000	0.0000	0.000	0.000	0.0000
R	4	1.06978E+08	3.228	4.075	3.156	7.622	3.023	0.000	9.85E-5	1.91E-4	0.0000	0.4747	3.242	0.0725	0.2191	0.000	0.0000	0.0000	0.000	0.000	0.0000
G		1.07070E+08	3.227	4.049	3.050	7.658	3.148	0.000	9.85E-5	1.91E-4	0.0000	0.4747	3.246	0.0804	0.2127	0.000	0.0000	0.0000	0.000	0.000	0.0000
B		1.07219E+08	3.211	3.972	2.761	7.743	3.296	0.000	9.85E-5	1.91E-4	0.0000	0.4747	3.244	0.0962	0.1894	0.000	0.0000	0.0000	0.000	0.000	0.0000
		1.07296E+08	3.182	3.896	2.486	7.801	3.549	0.000	9.85E-5	1.91E-4	0.0000	0.4747	3.232	0.1048	0.1769	0.000	0.0000	0.0000	0.000	0.000	0.0000
		1.07352E+08	3.134	3.801	2.153	7.850	3.672	0.000	9.85E-5	1.91E-4	0.0000	0.4747	3.208	0.1114	0.1682	0.000	0.0000	0.0000	0.000	0.000	0.0000
		1.07391E+08	3.068	3.723	1.907	7.887	3.763	0.000	9.85E-5	1.91E-4	0.0000	0.4747	3.175	0.1163	0.1628	0.000	0.0000	0.0000	0.000	0.000	0.0000
	5	1.07423E+08	3.015	3.683	1.802	7.918	3.838	0.000	9.85E-5	1.91E-4	0.0000	0.4747	3.138	0.1203	0.1583	0.000	0.0000	0.0000	0.000	0.000	0.0000
		1.07477E+08	3.147	3.655	1.557	7.969	3.962	0.000	9.86E-5	1.91E-4	0.0000	0.4534	3.143	0.1252	0.1536	0.000	0.0000	0.0000	0.000	0.000	0.0000
He	6	1.07704E+08	3.346	3.639	1.295	8.104	4.029	0.985	7.13E-3	2.01E-4	0.0450	0.2183	3.322	0.1407	0.1547	2.051	0.0000	0.0166	0.000	0.000	0.0000
		1.08773E+08	3.336	3.641	1.311	8.116	3.885	0.950	4.12E-2	4.61E-4	0.0745	0.2183	3.301	0.1657	0.1806	2.196	0.0000	0.0208	0.000	0.000	0.0000
B		1.09950E+08	3.266	3.647	1.407	8.128	3.813	0.900	8.96E-2	1.32E-3	0.0845	0.2183	3.206	0.1826	0.1985	2.371	0.0000	0.0241	0.000	0.000	0.0000
U		1.11765E+08	3.091	3.669	1.667	8.141	3.754	0.800	1.86E-1	4.84E-3	0.0956	0.2183	2.947	0.1974	0.2137	2.533	0.0000	0.0276	0.000	0.000	0.0000
R	7	1.12222E+08	3.080	3.676	1.706	8.143	3.745	0.772	2.12E-1	6.39E-3	0.0972	0.2185	2.919	0.1998	0.2193	2.559	0.0000	0.0282	0.000	0.000	0.0000
N		1.13277E+08	3.225	3.783	1.989	8.150	3.732	0.700	2.79E-1	1.13E-2	0.1006	0.2208	3.092	0.2057	0.2298	2.610	0.0000	0.0300	0.000	0.000	0.0000
I	8	1.13983E+08	3.285	3.891	2.363	8.155	3.721	0.651	3.23E-1	1.58E-2	0.1035	0.2287	3.170	0.2107	0.2318	2.651	0.0000	0.0312	0.000	0.000	0.0000
N		1.14686E+08	3.290	3.881	2.317	8.160	3.715	0.600	3.69E-1	2.14E-2	0.1055	0.2329	3.167	0.2146	0.2348	2.685	0.0000	0.0318	0.000	0.000	0.0000
G		1.15989E+08	3.308	3.879	2.292	8.170	3.705	0.500	4.54E-1	3.62E-2	0.1101	0.2390	3.167	0.2200	0.2411	2.751	0.0000	0.0342	0.000	0.000	0.0000
		1.17220E+08	3.324	3.875	2.260	8.182	3.701	0.400	5.32E-1	5.77E-2	0.1146	0.2443	3.164	0.2251	0.2468	2.815	0.0000	0.0371	0.000	0.000	0.0000
		1.18380E+08	3.337	3.867	2.215	8.197	3.706	0.300	6.00E-1	8.92E-2	0.1187	0.2501	3.154	0.2298	0.2517	2.877	0.0000	0.0406	0.000	0.000	0.0000
		1.19548E+08	3.346	3.848	2.131	8.215	3.725	0.200	6.50E-1	1.40E-1	0.1228	0.2549	3.132	0.2346	0.2565	2.938	0.0000	0.0450	0.000	0.000	0.0000
		1.20862E+08	3.344	3.796	1.923	8.244	3.773	0.100	6.51E-1	2.37E-1	0.1272	0.2597	3.082	0.2399	0.2597	3.003	0.0000	0.0519	0.000	0.000	0.0000
		1.21498E+08	3.317	3.727	1.675	8.270	3.837	0.050	6.20E-1	3.18E-1	0.1278	0.2603	3.007	0.2422	0.2603	3.031	0.0000	0.0578	0.000	0.000	0.0000
	9	1.22142E+08	3.246	3.668	1.509	8.309	3.947	0.012	5.46E-1	4.20E-1	0.1279	0.2609	2.817	0.2444	0.2585	3.049	0.0000	0.0636	0.000	0.000	0.0000
		1.22192E+08	3.247	3.665	1.499	8.315	3.962	0.010	5.39E-1	4.39E-1	0.1279	0.2609	2.808	0.2447	0.2585	3.049	0.0000	0.0641	0.000	0.000	0.0000
		1.22254E+08	3.279	3.653	1.417	8.361	4.110	0.001	5.13E-1	4.74E-1	0.1047	0.2606	2.906	0.2454	0.2565	2.916	0.0000	0.0682	0.000	0.000	0.0000
		1.22368E+08	3.293	3.650	1.392	8.379	4.184	0.000	5.10E-1	4.78E-1	0.0573	0.2606	2.957	0.2455	0.2561	2.345	0.0000	0.1395	0.000	0.000	0.0000
		1.22393E+08	3.386	3.640	1.258	8.420	4.454	0.000	5.10E-1	4.78E-1	0.0000	0.2606	3.040	0.2458	0.2545	2.825	0.0383	0.1593	0.000	1.199	0.0000
E		1.22509E+08	3.477	3.632	1.134	8.431	4.868	0.000	5.10E-1	4.78E-1	0.0000	0.2606	-0.222	0.2461	0.2523	3.473	0.0671	0.1617	0.000	1.233	0.0000
A		1.22580E+08	3.576	3.625	1.007	8.454	5.044	0.000	5.10E-1	4.78E-1	0.0000	0.2606	0.000	0.2461	0.2499	3.565	0.0784	0.1637	0.000	1.409	0.0000
G		1.22670E+08	3.682	3.618	0.874	8.486	5.255	0.000	5.10E-1	4.78E-1	0.0000	0.2606	0.000	0.2461	0.0000	3.668	0.0968	0.1673	0.000	1.783	0.0000
B		1.22753E+08	3.789	3.610	0.734	8.519	5.470	0.000	5.10E-1	4.78E-1	0.0000	0.2606	0.000	0.2461	0.0000	3.771	0.1180	0.1695	0.000	2.121	0.0000
		1.22808E+08	3.884	3.601	0.604	8.547	5.655	0.000	5.10E-1	4.78E-1	0.0000	0.2562	0.000	0.2461	0.0000	3.860	0.1321	0.1727	0.000	2.428	0.0000
		1.22851E+08	3.974	3.587	0.459	8.567	5.844	0.000	5.10E-1	4.78E-1	0.0000	0.2533	0.000	0.2461	0.0000	3.946	0.1447	0.1755	0.000	2.730	0.0006
		1.22881E+08	4.055	3.573	0.322	8.578	6.024	0.000	5.10E-1	4.78E-1	0.0000	0.2508	0.000	0.2461	0.0000	4.020	0.1552	0.1787	0.000	2.999	0.0177
	10	1.22885E+08	4.067	3.573	0.309	8.579	6.051	0.000	5.10E-1	4.78E-1	0.0000	0.2504	0.000	0.2461	0.0000	4.030	0.1568	0.1791	0.000	3.037	0.0202

Table 7.1 (continued) - M = 4.00 $M_\odot$ Z=0.008 Y=0.250 Diffusion

		AGE	$L/L_\odot$	T_{eff}	G	T_c	ρ_c	COMP	XC	XO	CONV	Q_{disc}	L_H	$Q1_H$	$Q2_H$	L_{He}	$Q1_{He}$	$Q2_{He}$	L_C	$-L_\mu$	Q_{Tmax}
H	1	0.00000E+00	2.397	4.203	4.402	7.425	1.491	0.738	1.99E-5	3.92E-3	0.3895	0.2532	2.398	0.0000	0.4523	0.000	0.0000	0.0000	0.000	0.000	0.0000
		1.77833E+07	2.416	4.196	4.356	7.422	1.469	0.700	2.56E-5	2.27E-3	0.3827	0.3863	2.417	0.0000	0.3746	0.000	0.0000	0.0000	0.000	0.000	0.0000
B		6.30012E+07	2.473	4.186	4.257	7.426	1.448	0.600	3.82E-5	9.39E-4	0.3588	0.4667	2.474	0.0000	0.3116	0.000	0.0000	0.0000	0.000	0.000	0.0000
U		9.73339E+07	2.531	4.176	4.161	7.436	1.446	0.500	4.25E-5	5.42E-4	0.3284	0.4944	2.521	0.0000	0.2696	0.000	0.0000	0.0000	0.000	0.000	0.0000
R		1.21746E+08	2.580	4.163	4.059	7.446	1.453	0.400	4.76E-5	3.71E-4	0.2955	0.5077	2.581	0.0000	0.2328	0.000	0.0000	0.0000	0.000	0.000	0.0000
N		1.39373E+08	2.621	4.148	3.956	7.458	1.472	0.300	5.19E-5	3.00E-4	0.2638	0.5077	2.623	0.0000	0.2036	0.000	0.0000	0.0000	0.000	0.000	0.0000
I		1.52287E+08	2.654	4.129	3.850	7.473	1.504	0.200	5.57E-5	2.64E-4	0.2289	0.5077	2.655	0.0000	0.1772	0.000	0.0000	0.0000	0.000	0.000	0.0000
N		1.61907E+08	2.681	4.110	3.747	7.495	1.563	0.100	6.06E-5	2.35E-4	0.1892	0.5077	2.682	0.0000	0.1568	0.000	0.0000	0.0000	0.000	0.000	0.0000
G		1.65972E+08	2.695	4.105	3.710	7.514	1.617	0.050	6.52E-5	2.25E-4	0.1717	0.5077	2.695	0.0000	0.1565	0.000	0.0000	0.0000	0.000	0.000	0.0000
	2	1.66266E+08	2.697	4.104	3.708	7.516	1.624	0.046	6.57E-5	2.24E-4	0.1677	0.5077	2.697	0.0000	0.1565	0.000	0.0000	0.0000	0.000	0.000	0.0000
a		1.68654E+08	2.721	4.117	3.733	7.553	1.727	0.010	7.64E-5	2.23E-4	0.1411	0.5077	2.712	0.0000	0.1890	0.000	0.0000	0.0000	0.000	0.000	0.0000
n		1.69194E+08	2.754	4.140	3.793	7.591	1.913	0.001	9.38E-5	2.15E-4	0.0702	0.5077	2.710	0.0000	0.2593	0.000	0.0000	0.0000	0.000	0.000	0.0000
d	3	1.69217E+08	2.756	4.141	3.795	7.590	1.967	0.001	9.45E-5	2.14E-4	0.0457	0.5077	2.723	0.0000	0.2896	0.000	0.0000	0.0000	0.000	0.000	0.0000
		1.69258E+08	2.751	4.138	3.789	7.567	2.106	0.000	9.78E-5	2.13E-4	0.0002	0.5077	2.770	0.0000	0.3527	0.000	0.0000	0.0000	0.000	0.000	0.0000
R		1.71781E+08	2.819	4.064	3.424	7.542	3.016	0.000	8.59E-5	2.13E-4	0.0000	0.5077	2.826	0.0595	0.2236	0.000	0.0000	0.0000	0.000	0.000	0.0000
G	4	1.72019E+08	2.820	4.049	3.361	7.567	3.125	0.000	8.59E-5	2.13E-4	0.0000	0.5077	2.830	0.0663	0.2171	0.000	0.0000	0.0000	0.000	0.000	0.0000
B		1.72544E+08	2.807	3.982	3.110	7.664	3.446	0.000	8.59E-5	2.13E-4	0.0000	0.5077	2.829	0.0820	0.1825	0.000	0.0000	0.0000	0.000	0.000	0.0000
		1.72801E+08	2.772	3.909	2.850	7.740	3.656	0.000	8.59E-5	2.13E-4	0.0000	0.5077	2.810	0.0926	0.1677	0.000	0.0000	0.0000	0.000	0.000	0.0000
		1.72967E+08	2.709	3.817	2.547	7.801	3.811	0.000	8.59E-5	2.13E-4	0.0000	0.5077	2.773	0.1000	0.1536	0.000	0.0000	0.0000	0.000	0.000	0.0000
		1.73070E+08	2.624	3.742	2.332	7.841	3.913	0.000	8.59E-5	2.13E-4	0.0000	0.5077	2.724	0.1054	0.1473	0.000	0.0000	0.0000	0.000	0.000	0.0000
	5	1.73169E+08	2.524	3.703	2.275	7.882	4.014	0.000	8.59E-5	2.13E-4	0.0000	0.5077	2.650	0.1101	0.1411	0.000	0.0000	0.0000	0.000	0.000	0.0000
		1.73371E+08	2.705	3.675	1.982	7.954	4.203	0.000	8.61E-5	2.13E-4	0.0000	0.3912	2.697	0.1173	0.1371	0.000	0.0000	0.0000	0.000	0.000	0.0000
He		1.76606E+08	2.815	3.669	1.846	8.090	4.116	0.950	4.15E-2	5.43E-4	0.0643	0.1825	2.783	0.1491	0.1606	1.636	0.0000	0.0171	0.000	0.000	0.0000
		1.79513E+08	2.675	3.681	2.034	8.160	4.046	0.900	8.98E-2	1.62E-3	0.0724	0.1825	2.609	0.1614	0.1735	1.804	0.0000	0.0201	0.000	0.000	0.0000
B	6	1.82365E+08	2.578	3.697	2.196	8.107	4.008	0.840	1.47E-1	3.88E-3	0.0760	0.1825	2.469	0.1685	0.1833	1.905	0.0000	0.0248	0.000	0.000	0.0000
U		1.84023E+08	2.629	3.717	2.215	8.111	3.994	0.800	1.85E-1	5.93E-3	0.0797	0.1831	2.525	0.1719	0.1886	1.945	0.0000	0.0248	0.000	0.000	0.0000
R	7	1.85822E+08	2.781	3.803	2.418	8.115	3.980	0.756	2.26E-1	8.99E-3	0.0820	0.1898	2.705	0.1766	0.1922	1.990	0.0000	0.0248	0.000	0.000	0.0000
N		1.88192E+08	2.788	3.789	2.353	8.121	3.961	0.700	2.76E-1	1.41E-2	0.0865	0.1954	2.702	0.1817	0.1968	2.046	0.0000	0.0248	0.000	0.000	0.0000
I		1.91938E+08	2.817	3.787	2.318	8.131	3.935	0.600	3.64E-1	2.62E-2	0.0922	0.2032	2.714	0.1881	0.2041	2.139	0.0000	0.0298	0.000	0.000	0.0000
N		1.95525E+08	2.843	3.784	2.281	8.143	3.912	0.500	4.46E-1	4.38E-2	0.0989	0.2105	2.721	0.1946	0.2122	2.229	0.0000	0.0298	0.000	0.000	0.0000
G		1.98770E+08	2.865	3.779	2.239	8.155	3.896	0.400	5.21E-1	6.87E-2	0.1044	0.2171	2.723	0.2006	0.2187	2.312	0.0000	0.0345	0.000	0.000	0.0000
		2.01774E+08	2.881	3.769	2.183	8.170	3.891	0.300	5.85E-1	1.04E-1	0.1101	0.2236	2.712	0.2062	0.2246	2.391	0.0000	0.0407	0.000	0.000	0.0000
		2.04543E+08	2.889	3.752	2.107	8.189	3.902	0.200	6.32E-1	1.57E-1	0.1151	0.2286	2.685	0.2111	0.2296	2.465	0.0000	0.0407	0.000	0.000	0.0000
		2.07650E+08	2.872	3.724	2.010	8.217	3.940	0.100	6.29E-1	2.60E-1	0.1162	0.2334	2.607	0.2165	0.2334	2.539	0.0000	0.0457	0.000	0.000	0.0000
		2.10838E+08	2.827	3.694	1.937	8.245	3.982	0.050	5.36E-1	4.03E-1	0.1016	0.2364	2.461	0.2210	0.2359	2.590	0.0000	0.0560	0.000	0.000	0.0000
	8	2.11442E+08	2.817	3.687	1.918	8.262	4.030	0.029	5.07E-1	4.53E-1	0.1038	0.2368	2.417	0.2219	0.2355	2.598	0.0000	0.0560	0.000	0.000	0.0000
		2.12011E+08	2.828	3.680	1.878	8.290	4.112	0.010	4.67E-1	5.12E-1	0.1016	0.2368	2.434	0.2228	0.2346	2.596	0.0000	0.0587	0.000	0.000	0.0000
		2.12281E+08	2.876	3.672	1.799	8.334	4.260	0.001	4.41E-1	5.46E-1	0.0896	0.2368	2.563	0.2234	0.2334	2.448	0.0000	0.0615	0.000	0.000	0.0000
		2.12304E+08	2.892	3.670	1.775	8.350	4.328	0.000	4.39E-1	5.49E-1	0.0432	0.2366	2.614	0.2236	0.2327	1.865	0.0000	0.1234	0.000	0.000	0.0000
	9	2.12319E+08	2.915	3.667	1.739	8.358	4.426	0.000	4.38E-1	5.50E-1	0.0000	0.2366	2.650	0.2236	0.2323	1.538	0.0112	0.1387	0.000	0.578	0.0000
E		2.12349E+08	2.998	3.659	1.624	8.383	4.591	0.000	4.38E-1	5.50E-1	0.0000	0.2366	2.743	0.2236	0.2314	1.941	0.0301	0.1477	0.000	0.804	0.0000
A		2.12676E+08	3.128	3.648	1.449	8.403	5.140	0.000	4.38E-1	5.50E-1	0.0000	0.2366	0.267	0.2247	0.2302	3.126	0.0814	0.1604	0.000	1.181	0.0000
G		2.12824E+08	3.250	3.638	1.287	8.414	5.285	0.000	4.38E-1	5.50E-1	0.0000	0.2366	0.000	0.2247	0.2282	3.243	0.0941	0.1639	0.000	1.291	0.0000
B		2.12957E+08	3.357	3.628	1.142	8.429	5.419	0.000	4.38E-1	5.50E-1	0.0000	0.2366	0.000	0.2247	0.0000	3.345	0.1042	0.1672	0.000	1.457	0.0000
		2.13077E+08	3.467	3.621	1.003	8.447	5.557	0.000	4.38E-1	5.50E-1	0.0000	0.2367	0.000	0.2247	0.0000	3.451	0.1177	0.1706	0.000	1.668	0.0000
		2.13160E+08	3.560	3.614	0.884	8.462	5.673	0.000	4.38E-1	5.50E-1	0.0000	0.2350	0.000	0.2247	0.0000	3.540	0.1289	0.1745	0.000	1.865	0.0000
		2.13229E+08	3.655	3.605	0.753	8.472	5.792	0.000	4.38E-1	5.50E-1	0.0000	0.2322	0.000	0.2247	0.0000	3.632	0.1427	0.1792	0.000	2.072	0.0024
		2.13285E+08	3.747	3.594	0.617	8.475	5.911	0.000	4.38E-1	5.50E-1	0.0000	0.2302	0.000	0.2247	0.0000	3.719	0.1541	0.1839	0.000	2.279	0.0142
		2.13330E+08	3.824	3.583	0.484	8.472	6.027	0.000	4.38E-1	5.50E-1	0.0000	0.2290	0.000	0.2247	0.0000	3.803	0.1635	0.1887	0.000	2.475	0.0301
		2.13369E+08	3.924	3.573	0.355	8.459	6.151	0.000	4.38E-1	5.50E-1	0.0000	0.2280	0.000	0.2247	0.0000	3.887	0.1734	0.1936	0.000	2.670	0.0478
		2.13403E+08	4.015	3.564	0.228	8.432	6.284	0.000	4.38E-1	5.50E-1	0.0000	0.2269	0.000	0.2248	0.0000	3.973	0.1830	0.1993	0.000	2.865	0.0658
		2.13432E+08	4.103	3.555	0.102	8.387	6.422	0.000	4.38E-1	5.50E-1	0.0000	0.2252	0.000	0.2248	0.0000	4.055	0.1927	0.2053	0.000	3.049	0.0898
		2.13456E+08	4.186	3.541	-0.035	8.332	6.561	0.000	4.38E-1	5.50E-1	0.0000	0.2236	0.000	0.2236	0.0000	4.131	0.2022	0.2115	0.000	3.213	0.1118
	10	2.13477E+08	4.238	3.536	-0.107	8.276	6.701	0.000	4.38E-1	5.50E-1	0.0000	0.2225	0.000	0.2225	0.0000	4.174	0.2111	0.2178	0.000	3.348	0.1348
		2.13490E+08	4.100	3.555	0.109	8.242	6.795	0.000	4.38E-1	5.50E-1	0.0000	0.2224	1.003	0.2224	0.2225	4.006	0.2163	0.2212	0.100	3.415	0.1470
		2.13495E+08	4.143	3.549	0.040	8.230	6.829	0.000	4.38E-1	5.50E-1	0.0000	0.2225	3.870	0.2225	0.2225	3.667	0.2176	0.2218	0.143	3.426	0.1521

The theoretical tracks for the initial masses M_i=4, 5, 6, 7, 8, 9, 12, 15, 20, 25, 30, 40, 60, 100, 120$M_\odot$, with metallicity Z=0.008, and those for the initial masses M_i=5, 6, 7, 8, 9, 12, 15, 20, 25, 30, 40, 60, 100$M_\odot$with metallicity Z=0.02 are shown in *Figure* 7.1 and *Figure* 7.2, respectively. Table 7.3 contains the life-times (in units of 10^6 years) τ_H of the core H-burning phase and τ_{He} of the core He-burning phase; the lifetime ratios τ_{He}/τ_H, and the ratios of the current surface abundances of ^4He, ^{12}C, ^{14}N, ^{16}O after the first dredge-up to their initial value The cases in which only the core H-burning life time is given correspond to tracks in which numerical problem have been met at the stage when mass loss reaches the molecular weight discontinuity made by previous envelope convection. The lifetimes of the WR stages of the most massive stars are given in table 7.4.

Figures 7.3, 7.4, and 7.5 compare our current diffusion models with those in which instantaneous mixing caused by overshoot occurs (metallicities $Z = 0.008$ and $Z = 0.020$) and those calculated with semi-convective mixing according to the Schwarzschild criterion ($Z = 0.020$), respectively. It is worth pointing out that, a part from the different mixing scheme, all the above models contain the same input physics and are computed with the same code and the same accuracy.

In the HRD, models with diffusion run much closer to the overshoot models than to those with the classical scheme. The same holds for the lifetimes and the lifetime ratios (see the data of in *table* 7.5. This is even more remarkable considering that models with standard overshoot are calculated with adopted $\lambda_c = 0.5$ (Fagotto et al. 1993), while the diffusion models are obtained for $\lambda_c = 1.0$. The inspection of path in the HRD and H-burning lifetimes shows that diffusive mixing in the region outside the classical border does not mix the region as fast as the case of instantaneous overshoot. However, diffusion brings extra fuel into the core on a time scale comparable to that of the nuclear burning. As a result of it, in spite of the bigger penetration distance, the diffusive models develop smaller cores at the the end of H-burning phase. This effect is clearly evident near the red edge of the MS, where our models possess a slightly higher effective temperature and a lower luminosity.

7.2 Models for Intermediate Mass Stars

By intermediate mass stars we name all stars whose mass is high enough to ignite core He-burning non degenerately, but small enough to develop a degenerate C-O core following central helium exhaustion (see Chiosi et al. 1991). The Padova models with standard overshoot set the upper mass limit for this class of stars mass, M_{up}, at about $5M_{\odot}$. The HRDs for globular clusters of intermediate age in the Large Magellanic Cloud are the ideal laboratory to calibrate the efficiency of the core overshoot for the stars of this mass range. In the following, we compare the existing models with the aim of casting light on the effects of the new mixing scheme on stars of this mass range, where mass loss is less of a problem.

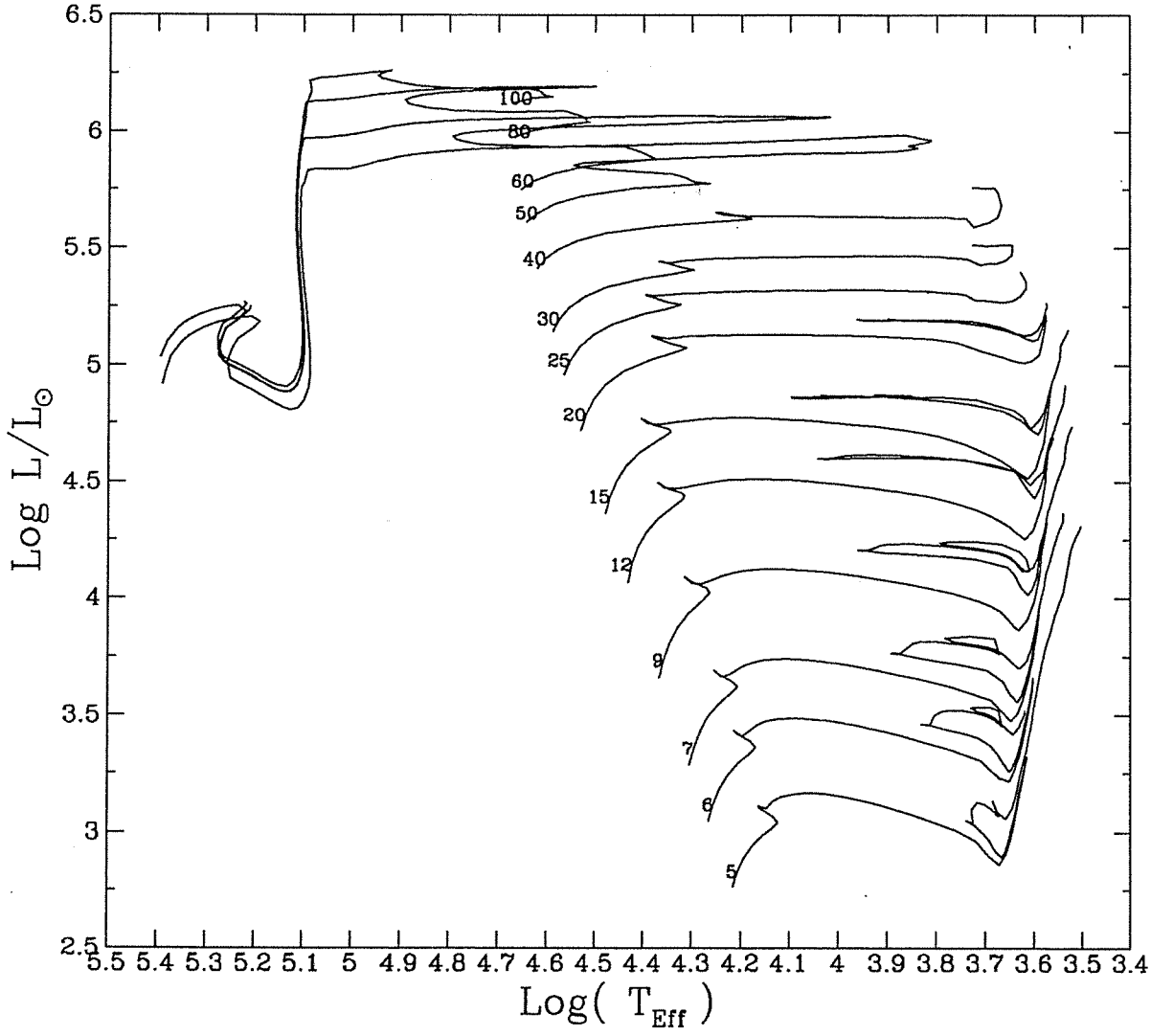

Figure 7.2: The theoretical HRD showing the evolutionary tracks for initial masses as indicated at the ZAMS in solar mass unit, for the chemical composition of $Z = 0.020, Y = 0.280$.

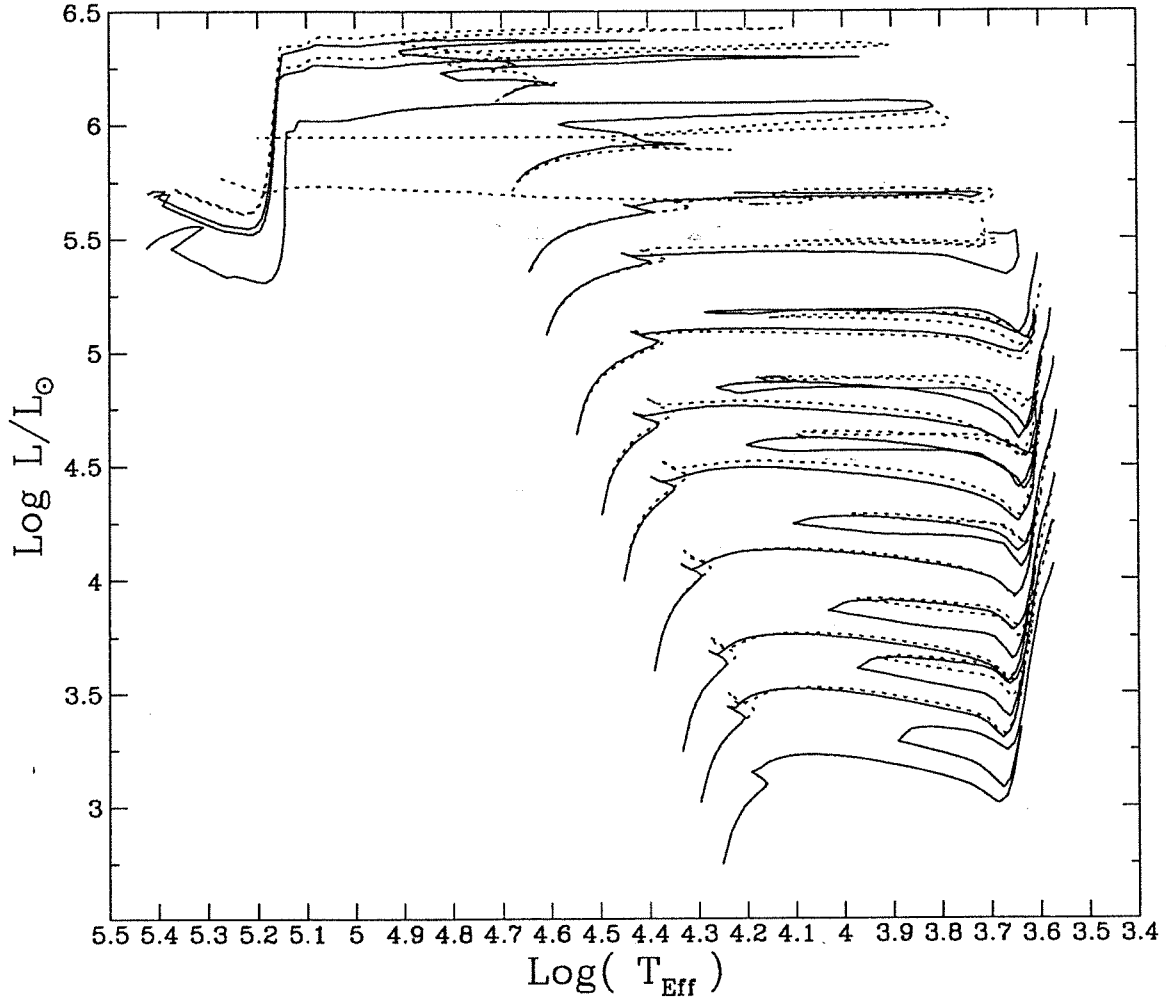

Figure 7.3: The theoretical evolutionary tracks of the current diffusion models, solid lines, and overshoot models from Fagotto et al. (1993), dashed lines, both for the metallicity $Z = 0.008$. The distance for core overshoot adopted for the later case is $0.5H_p$.

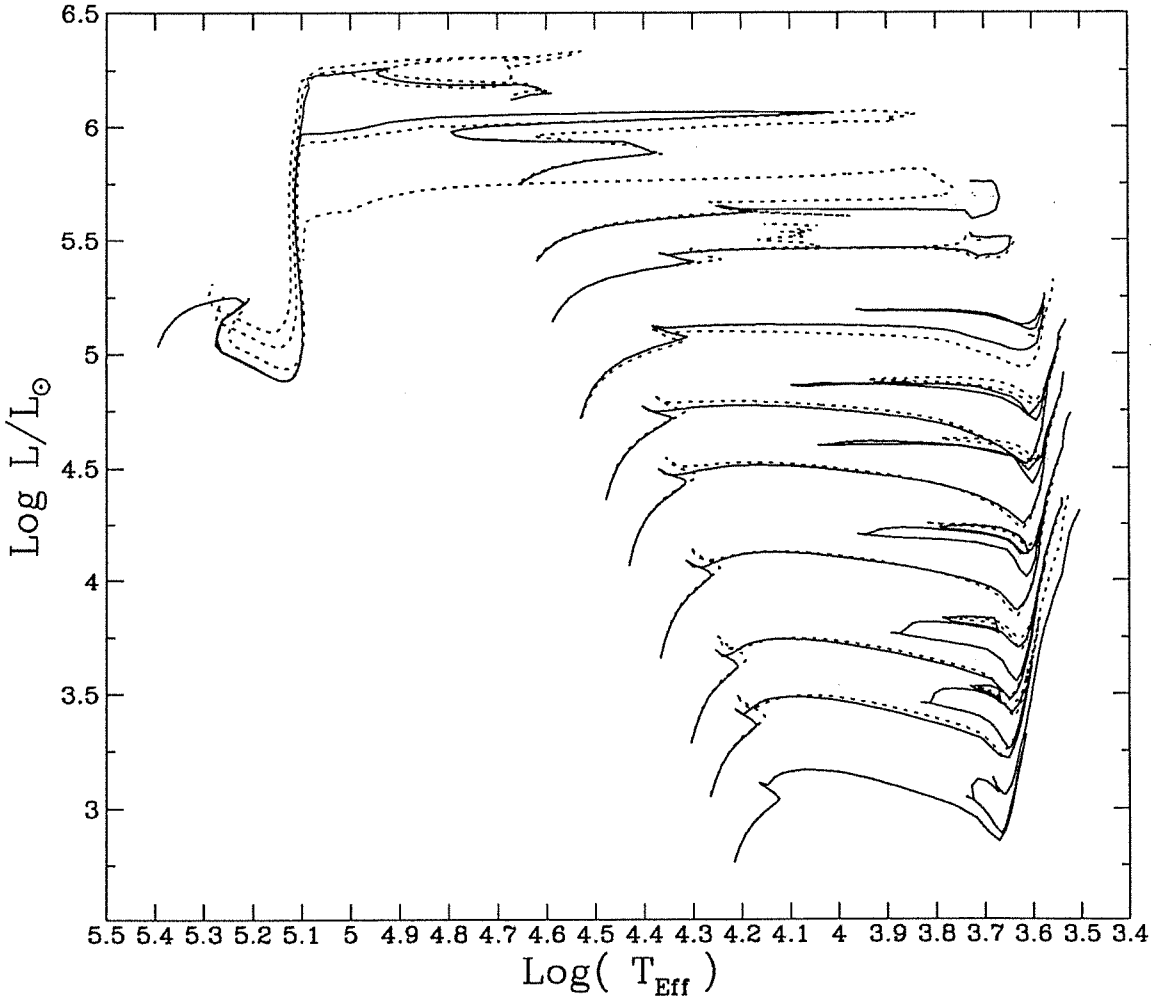

Figure 7.4: The same as *Figure* 7.3, but for $Z = 0.020$. The solid lines indicate the present models

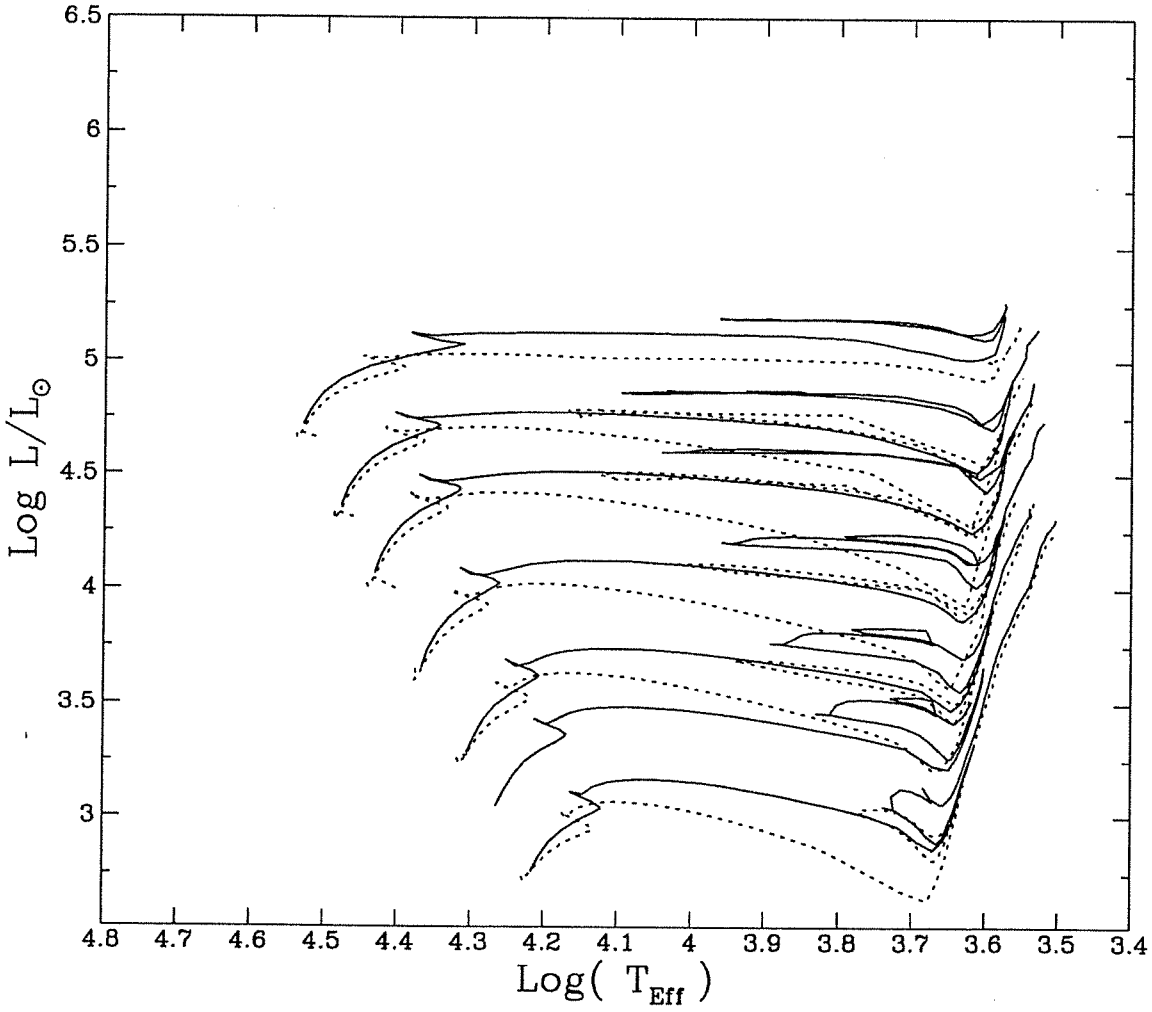

Figure 7.5: The same as *Figure* 7.4, but for of classical mixing scheme.

Indeed the whole evolution up to the very late stages virtually occurs at constant mass.

Figure 7.6 plots two tracks for $6M_{\odot}$star with $Z = 0.008$ and two schemes of mixing: the diffusive and instantaneous overshoot. The diffusive mixing model (solid line) has the overshoot distance outside the core given by $\Lambda = 1.0$, while the fully mixed overshoot model has this distance fixed by $\Lambda = 0.5$. All remaining physical ingredients of model structure are identical. During the core H-burning phase the two tracks are almost identical, but for the bluer and less luminous TAMS stage of the diffusive model with with respect to that with full overshoot. The lifetimes for each track are given in *table* 7.5. We see that the two tracks have almost identical core the H-burning lifetimes. THis can be explained as follows. Although the diffusive model has a larger overshoot distance, the efficiency of the mixing is significantly lower so that a much shallower chemical profile is built up across the star as shown by *Figure* 7.7. It is evident that the model with diffusion has a significantly smaller core compared to that computed of the model with fully mixed overshoot. On the other hand the higher mean free path adopted here makes the extension of the CNO processed region larger in the model with diffusion. To avoid confusion one should bear in mind that the two profiles shown in *Figure* 7.7 have a different origin. The one of the model with diffusion is determined both by partial mixing shrinkage of the core, while the profile of the model with fully mixed overshoot is generated only by the shrinkage of core as as the evolution proceeds. In summary the core of the model with diffusion burns about the same amount of fuel as that with full mixing, but engulfs it from a larger region (and at a smaller efficiency).

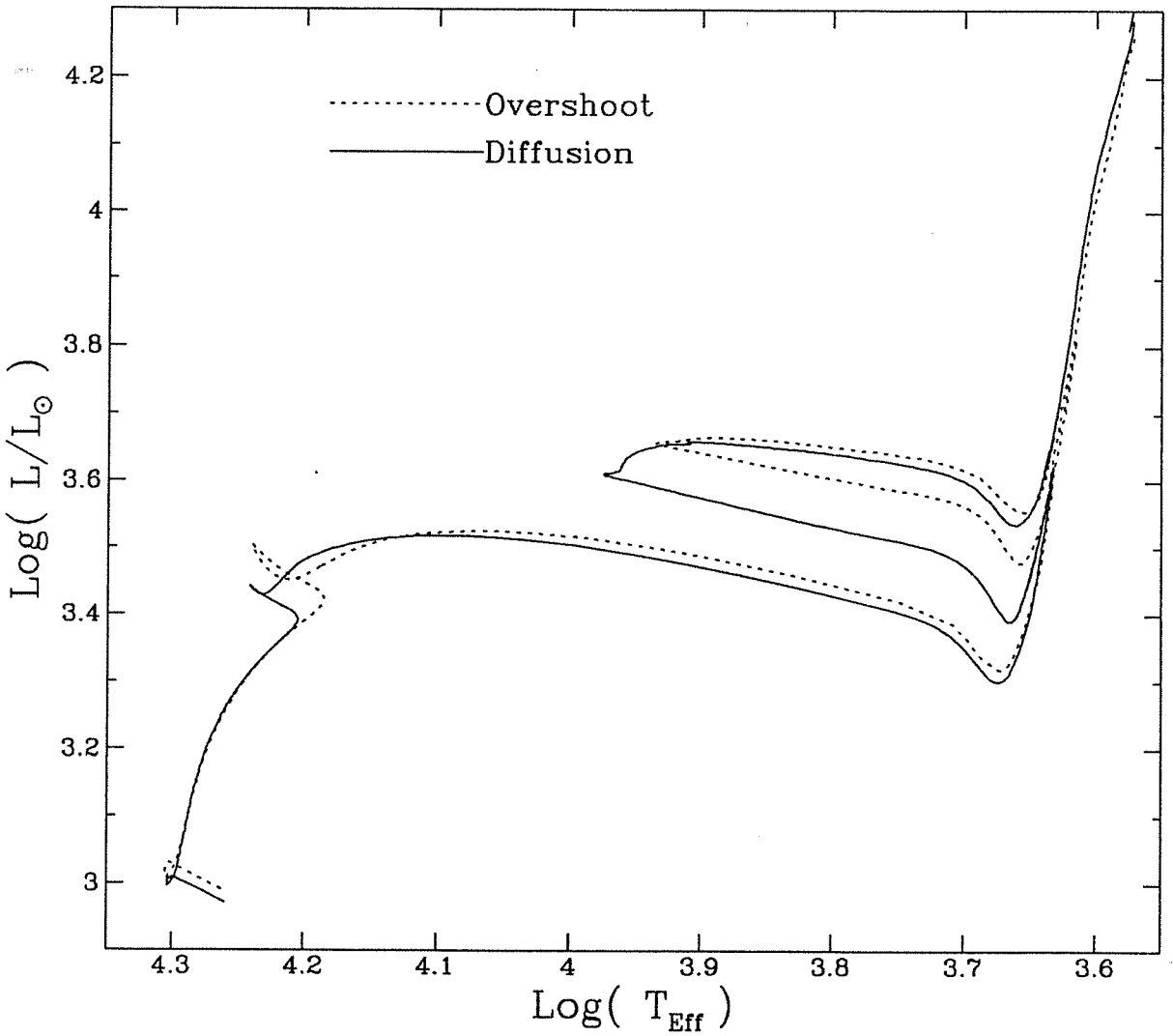

Figure 7.6: The HRD of a $6M_{\odot}$ star, evolved according to different mixing schemes. The solid line shows the models with diffusion, while the dashed line show the models with instantaneous overshoot from Bressan et al. (1993).

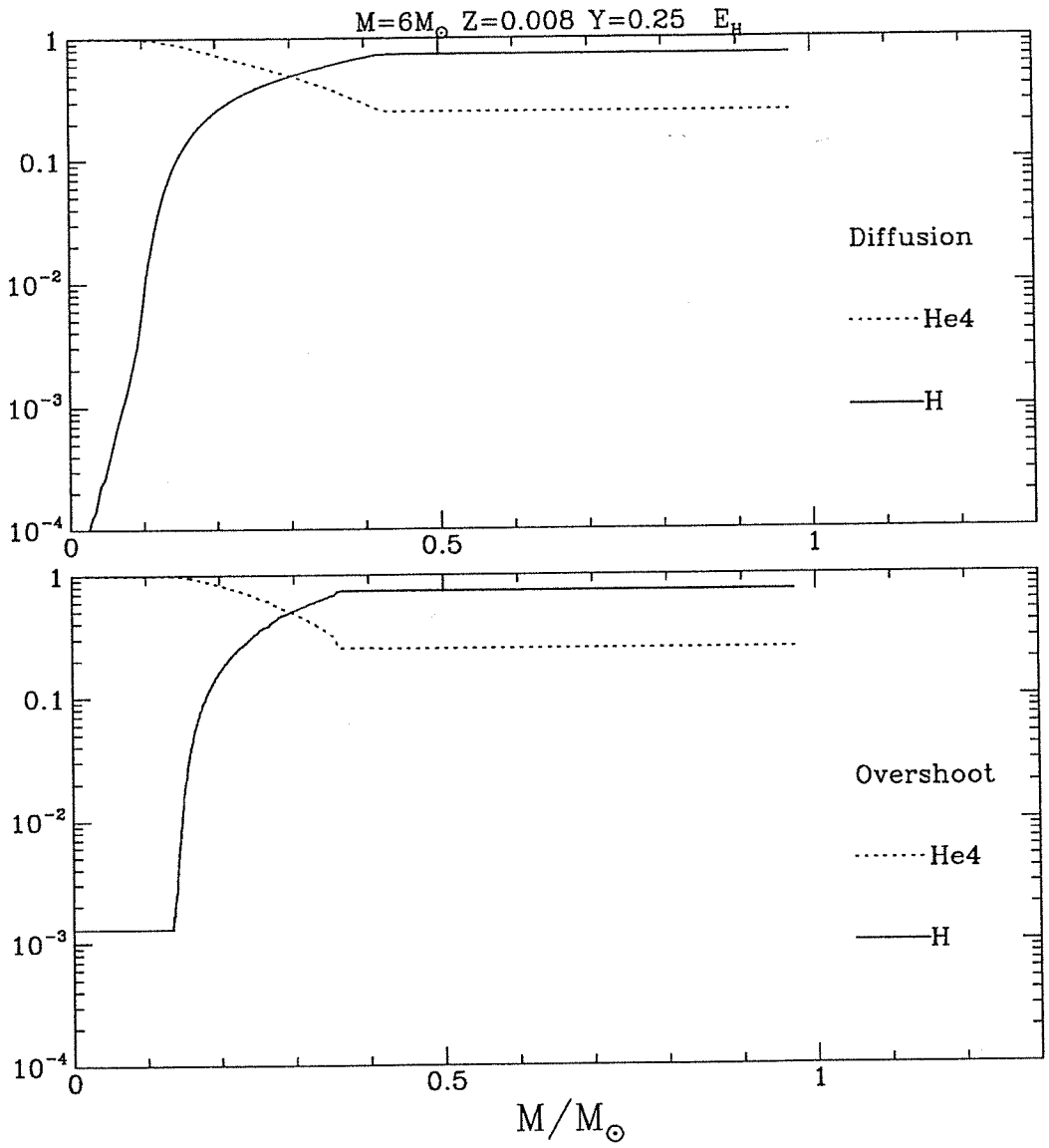

Figure 7.7: The hydrogen and helium profiles near the end of H-burning phase. The upper panel is for the diffusion models. It must be pointed out that the two plots do not refer to the same evolutionary stage of core H-burning. The one in the top panel is closer to central H-exhaustion than the one in the bottom panel as it is indicated by the different abundance of hydrogen in the core.

The core He-burning phase shows much larger differences between diffusion and overshoot models. As illustrated in *table* 7.5, in models with turbulent diffusion the core He-burning life time gets about 50% larger than in those with fully mixed overshoot, in that contrary to the H- burning life time which remains almost unchanged. This is a general property of the diffusion model. The reason for this is that the mixing efficiency gets higher at the conditions of core He-burning. Specifically, because the core size is smaller than in core H-burning and the characteristic velocity predicted by convection theory we are using is almost the same as before, the mixing speed is larger.

In addition to this, the longer He-burning life time of the model with diffusion is also a result of its lower luminosity during this phase. Because of the smaller core size resulted from the former core H-burning stage, a lower luminosity is maintained throughout the He-burning phase. The core size becomes larger as the evolution goes on, and eventually encompasses that of the overshoot model, as it can be seen from *Figure* 7.8 where we show the chemical profiles for the two cases near the end of He-burning.

Finally our model shows a more extended loop, by about Δ $\log(T_{Eff})0.5$ which could be explained by the lower mixing efficiency during the H-burning phase (Alongi et al 1992).

7.3 Models of Massive stars

The existing stellar models provide a good tool for understanding the physics that governs the evolution of massive stars. Of course for a meaningful discussion one has to address to the observations. These will be examined in detail in the chapter. In the following, I present a schematic overview of the current stellar models and different evolutionary scenarios resulting from the adoption of different schemes of mixing, namely convection and semiconvection, and compare the new models with the old ones.

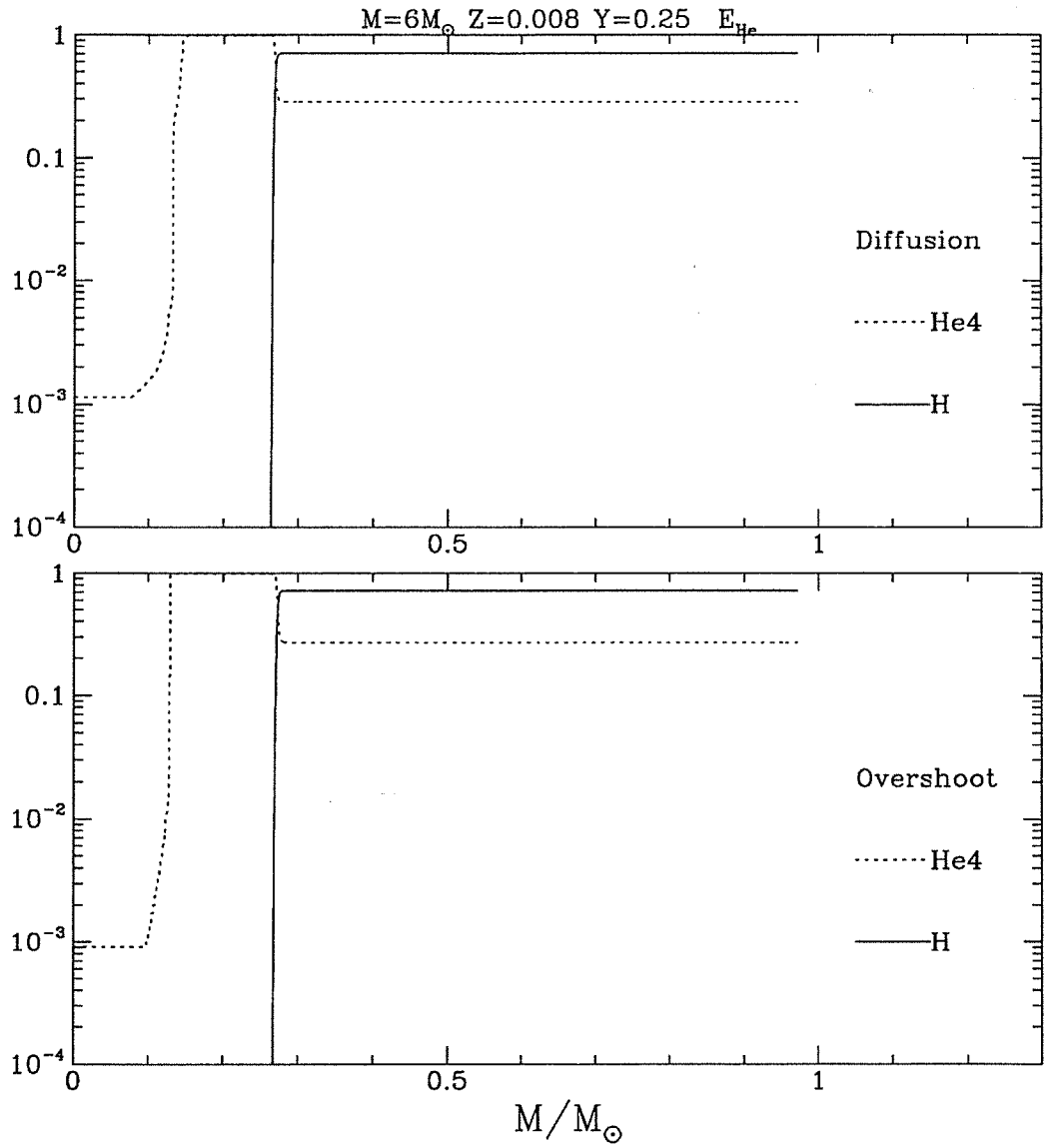

Figure 7.8: The same as in *Figure* 7.7, but for the phase near the end of He-burning. It must be pointed out the different He-profiles in the very central part of the star.

7.3.1 Evolutionary Scenarios

Limiting the discussion to models without rotation and magnetic fields (eg: Meader 1991, Sreenivasan 1993, Weiss 1989), existing models of massive stars can be grouped into three broad categories.

1. **The standard models** which assume the Schwarzschild criterion for convective instability, both for the convective and semiconvective region, and neglect overshoot or other extra mixing process;

2. **The standard models in which the Ledoux criterion** for convective and semiconvective instability is adopted.

3. **Models with overshoot** for whatever mechanism, such as those computed by the PADOVA group, which adopt the Schwarzschild criterion for convective instability, or those computed by Langer (1987) with overshoot and semiconvection;

In addition to this, we divide the models looking at the type of evolution in the HRD, as this is the basic tool to interpret the observations. As proposed by Fitzpatrick & Garmany (1990), and recently by Stothers (1993), the classification suggested by Chiosi & Summa (1970) in their pioneer study on the effects the instability criteria on massive stars can be taken as representative for the general evolution of stars in this mass range.

1. **Case A evolution:** the models move to the red side of HRD after finishing H-burning in the core within the Kelvin-Helmholtz time scale, spend a fraction of their He-burning phase near the Hayashi line, make a blue loop to the high temperature region of the HRD, and spend a fraction of the He-burning time near the tip of the loop. Finally, they return to the red before exhausting helium in the core, and remain there for the rest of their life. This evolution is often indicated by O-BSG-RSG-YSG-RSG, where O stands s for O type supergiant, BSG for the blue supergiant phase and RSG for the red supergiant phase.

2. **Case B evolution:** After the H-burning phase the models get thermal equilibrium while igniting helium in the core somewhere to the red of the main sequence band. These models evolve slowly toward the red side of the HRD on the time scale of central He-burning and terminate the core He-burning phase in the red. This kind of evolution is indicated by O-BSG-YSG-RSG.

3. **The Red-Blue evolution:** these models follow the case A evolution until the first arrival at Hayashi track. However, they never return to the high temperature region, and spend the whole He-burning life-time as red supergiants. This kind of evolution is named O-BSG-RSG because these models have no equilibrium configurations in the middle of HRD between the main sequence band and the Hayashi limit.

4. **The SN1987A progenitor evolution:** by this I mean all the models that match the observational data of the progenitor star, namely a blue supergiant before the supernova event with anomalous surface composition. They are similar to case A all the way to the end of He-burning, but these tracks show a final loop to the blue shortly before the explosion. Since we consider the anomaly of the surface abundance of He and N to be a signature of a previous RSG phase and because of other observational evidences, we do not include in this group the models presented for SN1987A that do not follow the case A for the He-burning phase.

In the following I summarize the main properties of these last groups.

7.3.2 The evolution following case A

In the original work of Chiosi & Summa (1970), case A is obtained adopting the Ledoux criterion for the neutrality condition in occurrence of semiconvection. A $20M_{\odot}$stellar sequence at constant mass was calculated. The resulting scenario accounts both for the blue supergiants, because of the extended loop and red supergiants, because these models spend a fraction of the stationary He-burning lifetime at low effective temperatures. Moreover, because this

scenario has a red phase before looping back to the blue, the surface abundances are altered by the deep penetration of the envelope convection mixing CNO processed material up to the surface. Therefore, this scenario also accounts for the observations of anomalous surface abundances among blue supergiants (Kudritzki 1990, Blaha & Fitzpatrick 1992). The physical assumptions underlying this scenario are still a matter of debate. The inclusion of mass loss, slightly modify the above scheme by affecting the extension of the loop. Among the models that adopt the most updated input physics, those computed with overshoot both in the convective core and the convective envelope strictly follow case A evolution (Bressan et al. 1993).

Our models also follow this scenario. They possess the following characteristics: the lifetime of core H-burning is very close to that of overshoot models with full efficiency for $\Lambda = 0.5$, while the core He-burning lifetime is 50% longer. Concerning the morphology in HRD, in general our models possess more extended blue loops than the overshoot models, but slightly narrower than predicted by classical mixing,

7.3.3 The evolution following case B

Evolutionary models following case B show in the HRD a stationary phase after leaving the MSB, somewhere in between this and the Hayashi limit. Therefore, they can account for the distribution of supergiant stars in the HRD, somewhat fail but to match the observations of surface abundances, because if they start core He-burning in the blue, and spend part of the lifetime of this phase at relatively high temperatures and part in the red, it is not possible for a single star to show variations of the surface abundances. The prototype of this kind of models are those computed with the Schwarzschild criterion, eg. the original Case B of Chiosi & Summa (1970), and the models by Schaller et al. (1992) for $M \geq 20 M_{\odot}$. With our diffusion models, this happens for low mixing efficiencies, i.e. small P_{dif}. In the upper panel of *Figure* 7.9, we show a track for the $20 M_{\odot}$star with $Z = 0.008$ computed with $P_{dif} = 0.01$. This track follows the classical scheme of case.

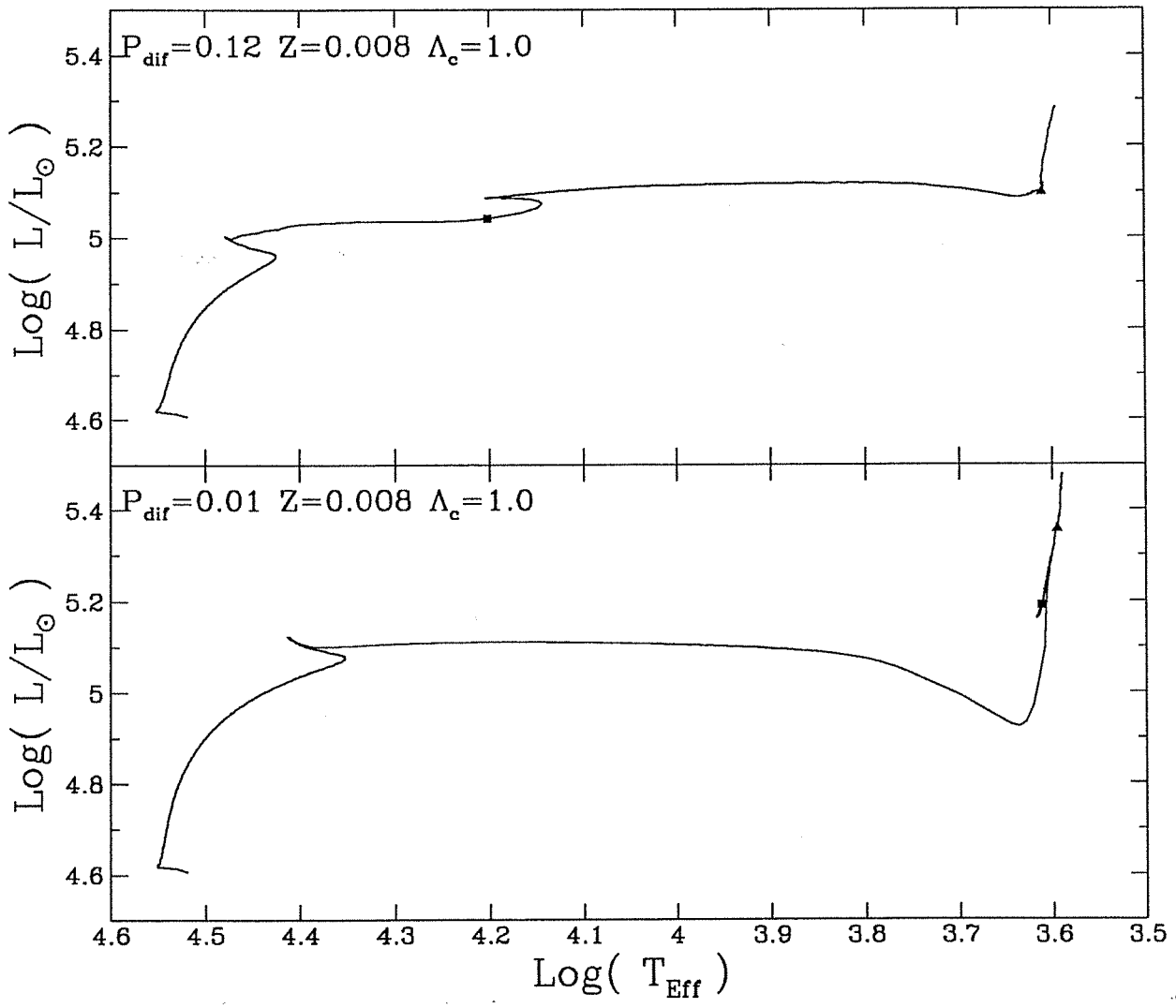

Figure 7.9: Evolutionary tracks for a $20M_{\odot}$star with $Z = 0.008$ and $P_{dif} = 0.0\,1$(upper panel), and $P_{dif} = 0.12$ (lower panel).

7.3.4 The Blue-Red evolution

This behaviour is characteristic of the models with overshoot only from the core (Maeder 1992). Langer (1991) found that a small amount of overshoot ($0.2H_p$) from the convective core inhibits the originally very extended loops. The tracks (cf. Langer's 1991 track # 13) follow the blue-red evolution. In our models, this always happens for a large diffusion coefficient. By adopting P_{dif}=0.12, which is 50% larger than for the sequence in *Figure* 7.1, the models start to burn helium in the red, and spend all the He-burning lifetime as a RSG. This is shown in the lower panel of *Figure* 7.9, where the whole He-burning lifetime is spent in the red near the Hayashi track.

7.4 Models of Very Massive Stars

We extended our two grids of models up to 120 $M_\odot$. For all masses greater than about 20 $M_\odot$mass loss plays the key role and strongly affects their evolution. We encountered numerical difficulties with models in the mass range 25-60 $M_\odot$during the central He-burning phase. Specifically, because of mass loss, the steep discontinuity in molecular weight caused by the intermediate convective zone reaches the surface, and the models of the RSG phase could not reach the equilibrium configuration located far away in the blue side of the HRD. For masses greater than about M>60 $M_\odot$this was less of a problem because mass loss is so efficient that the H-rich envelope is soon peeled off and the star never enters the RSG phase. The numerical difficulties encountered in the lower mass range do not appear.

When the surface hydrogen content of these models falls below the characteristic value of 0.3 (by mass) the star is supposed to begin the WR phase with consequent enhancement of the mass-loss rate. As already discussed by Maeder (1992), the stars move quickly to the blue side of the HRD, where they begin the central He-burning phase. Following Maeder (1992), we split the WR phase into the different sub-phases depending on the surface abundance. The star is considered to be a WNL object if enhanced nitrogen abundance is shown at the surface, but still some hydrogen is present. The star becomes a WNE object when the

surface hydrogen abundance falls to zero. When mass loss exposes the central core in which He-burning was active (no more Nitrogen exits in these regions) the star is considered to be a WC star, and finally when the ratio (by number) $(^{12}C+^{16}O/^{4}He) > 1$, the star is considered to be a WO object. The characteristic lifetimes spent by our models in those phases are listed in *table* (7.4).

7.5 Global Mixing and Evolution of Massive Stars

Before concluding this chapter I would like to discuss a particular scenario for the evolution of massive that I have obtained adopting a different mixing scheme.

Since the numerical code is independent from the particular formalism used for the diffusion coefficient, I computed some models with the mixing scheme suggested by Schatzman (1977) to account for the solar Lithium problem, with the purpose of investigating the effects of this mechanism on the structure and evolution of massive stars. Schatzman (1977) introduced the concept of "global diffusion" as defined by means of the critical Reynolds number at which the global mild turbulence sets in. Schatzman (1977) used $R_c = 166.$ which yields a diffusion coefficient outside the unstable region

$$\mathcal{D}_g = 166 * \nu \tag{7.1}$$

where ν is the radiative viscosity given by $\nu_r = \frac{4}{5}\frac{aT^4}{\kappa c \rho^2}$.

There is no theoretical prediction showing that this kind of mixing is related to convection. However, mild turbulence could be the result of the exponentially decaying convective overshoot according to Xiong's predictions, if the chemical self–correlation function overshoots in the same manner as the velocity field, i.e. slowly but over a very extend region.

Figure 7.10 shows the HRD for a set of stellar models computed with the "global mixing scheme". The chemical composition is Z = 0.008, Y = 0.250. For stars of initial mass higher than $12M_{\odot}$, the evolution with this mechanism is controlled by the interplay between the mixing rate and mass loss. The mixing extends all the way to the surface, however with

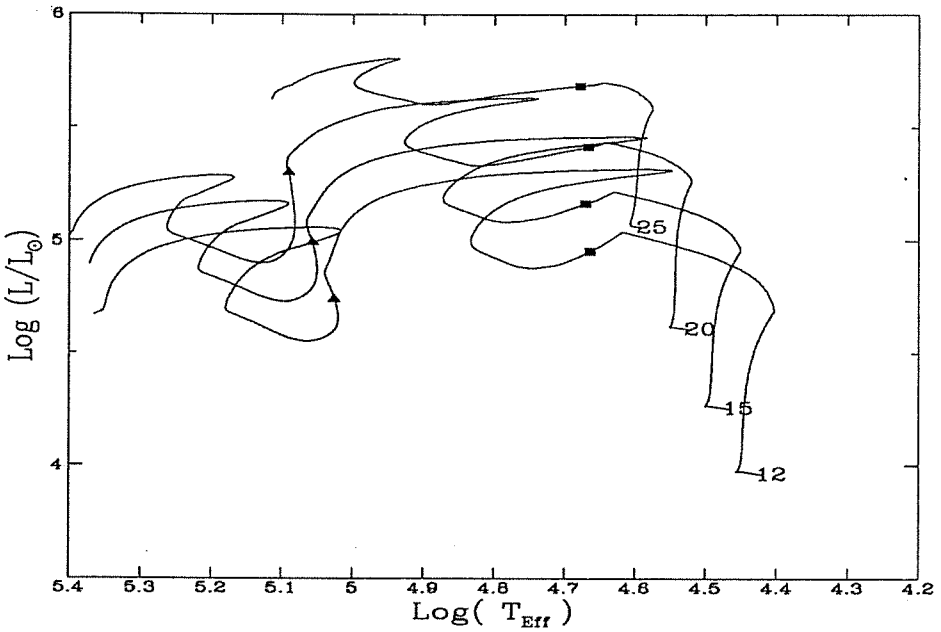

Figure 7.10: The HRD for the global diffusion scheme. The initial masses are indicated along the tracks. The physical quantities for relevant evolutionary stages of each sequence are given in *table* (7.6). The squares on the tracks indicate the start of WN phase, while the triangles show the initial positions of WC stage.

a slow rate and makes the core larger. A larger core in turn yields higher luminosity and therefore higher mass loss. Because of the mixing, some of the material processed in the core is brought to the surface, causing a higher luminosity, due to a higher mean molecular weight and consequently a higher mass loss rate. These tracks never go to the red side of the HRD, but after a small excursion to slightly cooler effective temperatures they evolve to the blue at the start of He-burning in the core. As the surface abundance of hydrogen falls below 0.3 the models enter the WNL phase where, according to empirical estimates, the mass loss is enhanced and dominates the remaining evolution. For purposes of illustration *Figure* 7.11 gives a plot of the variation of the hydrogen profile inside a model of $15M_{\odot}$ star with global diffusion at different evolutionary stages. It can be seen that this type of mixing produces a smooth profile from the core all the way up to the surface. The depletion of the surface hydrogen is caused both by mixing, very slow indeed, and mass loss.

These stars enter directly the WR stage without the need of a massive progenitor (M>60 $M_{\odot}$) as it occurs with all other mixing schemes and suitable mass-loss rate. As it will be

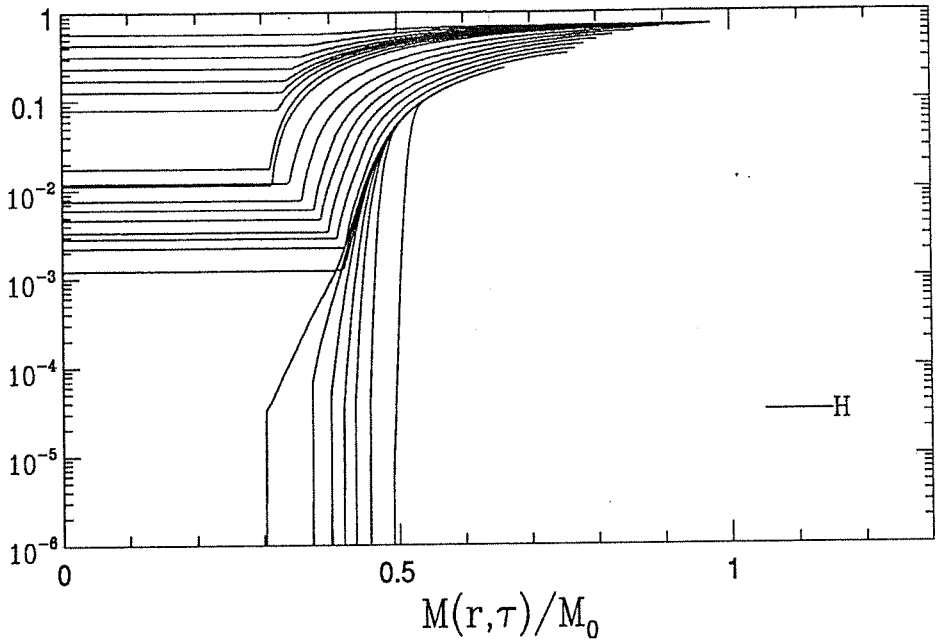

Figure 7.11: The hydrogen profile for every successive 20 models of the $15M_{\odot}$star of *Figure* 7.10. The abscissa is the ratio between the mass within the mesh point and the initial mass ($15M_{\odot}$).

further discussed in the next chapter, what makes these models appealing is the fact that their WR stage is located in the HR diagram exactly where these stars are observed (Hamann et al. 1993). This cannot be explained by all other current evolutionary models. If this kind of mixing really occurs in stars, perhaps as a cause of some peculiar situation (rotation), these models have the potential of understanding the WR objects found at lower luminosity in the HRD. *Figure* (7.12) gives a plot of changes of the surface abundance at the transition stage from normal supergiants to WR stars. The properties of these models are given in *table* (7.6)

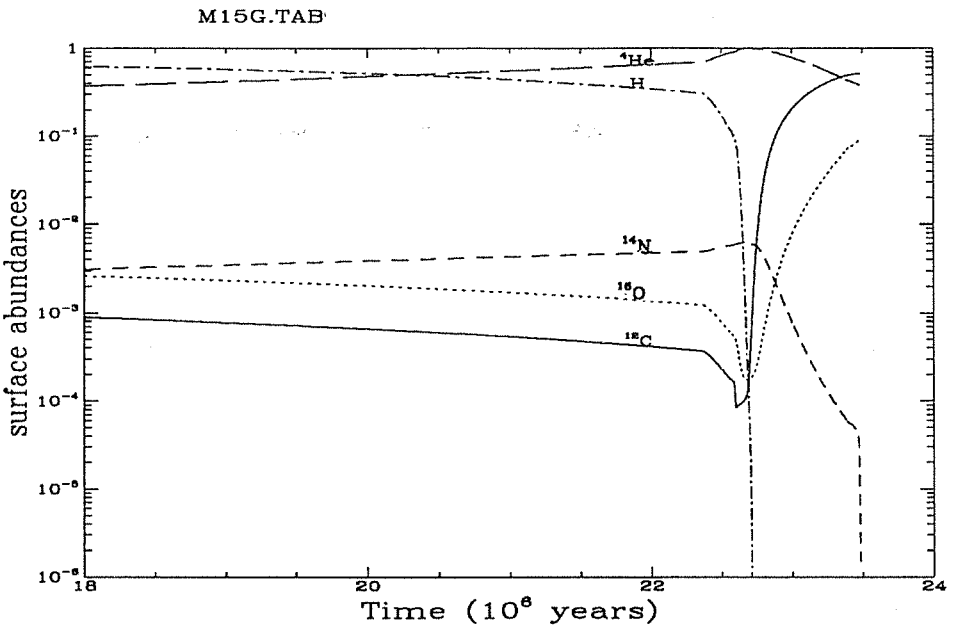

Figure 7.12: The surface abundance variations of a $15M_\odot$ with global turbulent diffusion. The initial composition for this sequence is $Z = 0.008, Y = 0.250$. As it is clearly indicated by the changing of the surface abundances, this track enters WR stages, to be compared with *Figure* 7.13.

Table 7.2: (Page 109-115) Evolutionary sequences for $Z = 0.020, Y = 0.280$. The layout is the same as in *table* 7.1. The tracks are shown in *Figure* (7.2), while the corresponding life-times and life-time ratios are listed in *table* (7.3)

Table 7.2 M = 20.00 $M_\odot$ Z=0.020 Y=0.280 Diffusion

		AGE	M	$L/L_\odot$	T_{eff}	G	T_c	ρ_c	COMP	XC	XO	CONV	Q_{disc}	L_H	$Q1_H$	L_{He}	$\dot{M}$	X_{sup}	Y_{sup}	XC_{sup}	XN_{sup}	XO_{sup}
H	1	0.00000E+00	20.00	4.654	4.536	4.177	7.546	0.643	0.683	1.31E-4	9.71E-3	0.5927	0.5869	4.653	0.000	0.000	-7.757	7.00E-1	2.80E-1	4.94E-3	1.24E-3	1.06E-2
		1.72007E+06	19.94	4.716	4.530	4.087	7.549	0.629	0.600	1.19E-4	4.58E-3	0.5761	0.5958	4.717	0.000	0.000	-7.535	7.00E-1	2.80E-1	4.94E-3	1.24E-3	1.06E-2
B		3.49364E+06	19.87	4.789	4.519	3.970	7.556	0.622	0.500	1.43E-4	2.41E-3	0.5509	0.5979	4.790	0.000	0.000	-7.295	7.00E-1	2.80E-1	4.94E-3	1.24E-3	1.06E-2
U		4.89222E+06	19.78	4.856	4.503	3.836	7.566	0.628	0.400	1.63E-4	1.43E-3	0.5227	0.6007	4.857	0.000	0.000	-7.068	7.00E-1	2.80E-1	4.94E-3	1.24E-3	1.06E-2
R		6.02093E+06	19.65	4.918	4.478	3.673	7.578	0.645	0.300	1.79E-4	9.20E-4	0.4924	0.6046	4.919	0.000	0.000	-6.848	7.00E-1	2.80E-1	4.94E-3	1.24E-3	1.06E-2
N		6.93617E+06	19.48	4.975	4.440	3.461	7.593	0.677	0.200	1.94E-4	6.57E-4	0.4576	0.6098	4.976	0.000	0.000	-6.635	7.00E-1	2.80E-1	4.94E-3	1.24E-3	1.06E-2
I		7.68660E+06	19.26	5.028	4.381	3.165	7.616	0.738	0.100	2.15E-4	5.08E-4	0.4248	0.6168	5.029	0.000	0.000	-6.427	7.00E-1	2.80E-1	4.94E-3	1.24E-3	1.06E-2
N		8.05683E+06	19.09	5.054	4.339	2.966	7.637	0.799	0.050	2.22E-4	4.56E-4	0.4077	0.6219	5.055	0.000	0.000	-6.330	7.00E-1	2.80E-1	4.94E-3	1.24E-3	1.06E-2
G	2	8.28911E+06	18.99	5.073	4.312	2.838	7.668	0.890	0.016	2.49E-4	4.27E-4	0.3954	0.6257	5.073	0.000	0.000	-6.268	7.00E-1	2.80E-1	4.94E-3	1.24E-3	1.06E-2
		8.33224E+06	18.96	5.078	4.311	2.831	7.681	0.929	0.010	2.66E-4	4.21E-4	0.3921	0.6265	5.077	0.000	0.000	-6.259	7.00E-1	2.80E-1	4.94E-3	1.24E-3	1.06E-2
		8.41616E+06	18.92	5.092	4.342	2.938	7.742	1.113	0.001	3.20E-4	4.10E-4	0.3778	0.6280	5.074	0.000	0.000	-6.259	7.00E-1	2.80E-1	4.94E-3	1.24E-3	1.06E-2
		8.42634E+06	18.91	5.103	4.364	3.015	7.786	1.249	0.000	3.52E-4	4.09E-4	0.3592	0.6282	5.056	0.000	0.000	-6.263	7.00E-1	2.80E-1	4.94E-3	1.24E-3	1.06E-2
	3	8.42634E+06	18.91	5.103	4.364	3.015	7.786	1.249	0.000	3.52E-4	4.09E-4	0.3592	0.6282	5.807	0.000	0.000	-6.263	7.00E-1	2.80E-1	4.94E-3	1.24E-3	1.06E-2
	4	8.43055E+06	18.91	5.127	4.383	3.065	7.895	1.621	0.000	3.86E-4	4.08E-4	0.1058	0.6283	4.880	0.248	0.000	-6.232	7.00E-1	2.80E-1	4.94E-3	1.24E-3	1.06E-2
		8.43577E+06	18.91	5.128	4.262	2.580	8.037	2.186	0.000	3.86E-4	4.08E-4	0.0000	0.6811	5.109	0.295	0.000	-6.135	7.00E-1	2.80E-1	4.94E-3	1.24E-3	1.06E-2
He	5	8.43681E+06	18.91	5.131	4.212	2.377	8.066	2.293	0.981	3.86E-4	4.08E-4	0.0000	0.6811	5.106	0.308	0.000	-6.113	7.00E-1	2.80E-1	4.94E-3	1.24E-3	1.06E-2
		8.43767E+06	18.91	5.131	4.161	2.175	8.091	2.380	0.981	3.86E-4	4.08E-4	0.0000	0.6811	5.102	0.314	0.000	-6.103	7.00E-1	2.80E-1	4.94E-3	1.24E-3	1.06E-2
B		8.43900E+06	18.90	5.130	4.057	1.761	8.130	2.515	0.981	3.89E-4	4.08E-4	0.0000	0.6812	5.089	0.325	1.732	-6.101	7.00E-1	2.80E-1	4.94E-3	1.24E-3	1.06E-2
U		8.43995E+06	18.90	5.126	3.951	1.340	8.159	2.608	0.980	4.13E-4	4.08E-4	0.0023	0.6812	5.080	0.329	2.850	-6.103	7.00E-1	2.80E-1	4.94E-3	1.24E-3	1.06E-2
R		8.44080E+06	18.90	5.116	3.840	0.904	8.185	2.684	0.980	4.71E-4	4.08E-4	0.0267	0.6812	5.064	0.336	3.768	-6.086	7.00E-1	2.80E-1	4.94E-3	1.24E-3	1.06E-2
N		8.44167E+06	18.90	5.080	3.736	0.525	8.207	2.737	0.980	5.52E-4	4.08E-4	0.0668	0.6812	5.023	0.342	4.473	-6.048	7.00E-1	2.80E-1	4.94E-3	1.24E-3	1.06E-2
I		8.44258E+06	18.90	5.010	3.630	0.171	8.218	2.756	0.979	7.28E-4	4.08E-4	0.1130	0.6813	4.953	0.346	4.782	-5.997	7.00E-1	2.80E-1	4.94E-3	1.24E-3	1.06E-2
N	6	8.44289E+06	18.90	5.006	3.613	0.106	8.220	2.758	0.979	7.97E-4	4.08E-4	0.1352	0.6813	4.930	0.348	4.823	-5.979	7.00E-1	2.80E-1	4.94E-3	1.24E-3	1.06E-2
G	7	8.44478E+06	18.90	5.228	3.575	-0.269	8.227	2.760	0.977	1.26E-3	4.08E-4	0.1825	0.4285	4.919	0.354	4.873	-5.548	6.12E-1	3.68E-1	3.05E-3	5.54E-3	8.00E-3
	8	8.44935E+06	18.88	5.212	3.576	-0.249	8.234	2.765	0.975	2.99E-3	4.10E-4	0.2112	0.4263	4.924	0.364	4.869	-5.563	6.12E-1	3.68E-1	3.04E-3	5.56E-3	7.98E-3
		8.47453E+06	18.83	5.136	3.586	-0.131	8.254	2.807	0.950	2.59E-2	5.07E-4	0.2322	0.4278	4.747	0.386	4.897	-5.721	6.12E-1	3.68E-1	3.04E-3	5.56E-3	7.98E-3
		8.52536E+06	18.74	5.107	3.604	-0.032	8.260	2.808	0.900	7.41E-2	1.11E-3	0.2833	0.4299	4.628	0.402	4.929	-5.811	6.12E-1	3.68E-1	3.04E-3	5.56E-3	7.98E-3
		8.59085E+06	18.65	5.191	3.713	0.315	8.268	2.818	0.803	1.67E-1	3.84E-3	0.2920	0.4401	4.759	0.414	4.957	-5.864	6.12E-1	3.68E-1	3.04E-3	5.56E-3	7.98E-3
		8.59259E+06	18.65	5.199	3.762	0.503	8.269	2.818	0.800	1.69E-1	3.95E-3	0.2920	0.4410	4.776	0.414	4.957	-5.898	6.12E-1	3.68E-1	3.04E-3	5.56E-3	7.98E-3
		8.59661E+06	18.64	5.199	3.873	0.949	8.269	2.820	0.794	1.75E-1	4.22E-3	0.2942	0.4420	4.802	0.415	4.958	-5.973	6.12E-1	3.68E-1	3.04E-3	5.56E-3	7.98E-3
		8.60716E+06	18.63	5.193	3.974	1.358	8.269	2.818	0.779	1.90E-1	4.95E-3	0.2943	0.4445	4.813	0.416	4.962	-5.998	6.12E-1	3.68E-1	3.04E-3	5.56E-3	7.98E-3
	9	8.61370E+06	18.62	5.193	3.979	1.379	8.270	2.820	0.769	1.98E-1	5.45E-3	0.2944	0.4461	4.812	0.417	4.964	-6.001	6.12E-1	3.68E-1	3.04E-3	5.56E-3	7.98E-3
		8.65734E+06	18.58	5.193	3.951	1.266	8.276	2.829	0.700	2.63E-1	9.89E-3	0.2972	0.4510	4.782	0.421	4.988	-5.998	6.12E-1	3.68E-1	3.04E-3	5.56E-3	7.98E-3
		8.72992E+06	18.51	5.195	3.929	1.174	8.285	2.846	0.600	3.52E-1	2.04E-2	0.3050	0.4596	4.743	0.427	5.012	-5.992	6.12E-1	3.68E-1	3.04E-3	5.56E-3	7.98E-3
		8.80379E+06	18.43	5.193	3.869	0.932	8.295	2.864	0.500	4.35E-1	3.71E-2	0.3141	0.4640	4.688	0.433	5.037	-5.979	6.12E-1	3.68E-1	3.04E-3	5.56E-3	7.98E-3
		8.85949E+06	18.37	5.187	3.769	0.537	8.307	2.890	0.405	5.08E-1	5.93E-2	0.3152	0.4675	4.603	0.437	5.063	-5.928	6.12E-1	3.68E-1	3.04E-3	5.56E-3	7.98E-3
		8.86228E+06	18.36	5.186	3.765	0.522	8.307	2.892	0.400	5.12E-1	6.07E-2	0.3152	0.4676	4.599	0.437	5.064	-5.925	6.12E-1	3.68E-1	3.04E-3	5.56E-3	7.98E-3
		8.89423E+06	18.32	5.152	3.658	0.126	8.308	2.890	0.365	5.33E-1	7.41E-2	0.3209	0.4687	4.467	0.439	5.067	-5.836	6.12E-1	3.68E-1	3.04E-3	5.56E-3	7.98E-3
		8.95472E+06	18.22	5.133	3.608	-0.054	8.322	2.924	0.300	5.67E-1	1.05E-1	0.3316	0.4722	4.163	0.443	5.089	-5.780	6.12E-1	3.68E-1	3.04E-3	5.56E-3	7.98E-3
		9.01877E+06	18.12	5.136	3.603	-0.082	8.341	2.974	0.200	6.04E-1	1.67E-1	0.3336	0.4750	3.961	0.447	5.110	-5.764	6.12E-1	3.68E-1	3.04E-3	5.56E-3	7.98E-3
		9.09370E+06	17.98	5.144	3.595	-0.123	8.370	3.053	0.100	5.84E-1	2.88E-1	0.3360	0.4780	3.726	0.451	5.130	-5.734	6.12E-1	3.68E-1	3.04E-3	5.56E-3	7.98E-3
		9.14188E+06	17.89	5.153	3.592	-0.148	8.394	3.126	0.050	5.22E-1	3.99E-1	0.3366	0.4805	3.616	0.454	5.141	-5.710	6.12E-1	3.68E-1	3.03E-3	5.56E-3	7.98E-3
		9.19030E+06	17.79	5.170	3.588	-0.182	8.440	3.262	0.010	4.29E-1	5.30E-1	0.3335	0.4829	3.651	0.457	5.142	-5.673	6.12E-1	3.68E-1	3.01E-3	5.57E-3	7.98E-3
		9.20142E+06	17.77	5.185	3.585	-0.213	8.490	3.414	0.001	4.05E-1	5.62E-1	0.3128	0.4835	3.821	0.458	5.032	-5.638	6.12E-1	3.68E-1	3.00E-3	5.57E-3	7.98E-3
		9.20401E+06	17.76	5.200	3.581	-0.240	8.534	3.550	0.000	4.03E-1	5.64E-1	0.2936	0.4836	3.930	0.458	4.915	-5.616	6.12E-1	3.68E-1	3.00E-3	5.58E-3	7.98E-3
	10	9.20467E+06	17.76	5.207	3.579	-0.254	8.546	3.588	0.000	4.02E-1	5.64E-1	0.2918	0.4836	3.952	0.458	4.891	-5.597	6.12E-1	3.68E-1	2.99E-3	5.58E-3	7.98E-3
	11	9.21381E+06	17.73	5.341	3.566	-0.444	8.776	4.434	0.000	4.02E-1	5.64E-1	0.0000	0.4691	1.341	0.459	5.227	-5.309	6.11E-1	3.69E-1	2.84E-3	5.77E-3	7.96E-3
		9.21390E+06	17.73	5.339	3.564	-0.449	8.778	4.446	0.000	4.02E-1	5.64E-1	0.0000	0.4688	1.339	0.459	5.246	-5.299	6.11E-1	3.69E-1	2.84E-3	5.77E-3	7.96E-3

Table 7.2 (continued) - M = 15.00 $M_\odot$ Z=0.020 Y=0.280 Diffusion

		AGE	M	$L/L_\odot$	T_{eff}	G	T_c	ρ_c	COMP	XC	XO	CONV	Q_{disc}	L_H	$Q1_H$	L_{He}	$\dot{M}$	X_{sup}	Y_{sup}	XC_{sup}	XN_{sup}	XO_{sup}
H	1	0.00000E+00	15.00	4.295	4.484	4.202	7.526	0.755	0.689	1.06E-4	1.01E-2	0.5444	0.5444	4.290	0.000	0.000	-8.740	7.00E-1	2.80E-1	4.94E-3	1.24E-3	1.06E-2
		2.69550E+06	14.99	4.361	4.477	4.108	7.529	0.736	0.600	1.08E-4	4.52E-3	0.5285	0.5484	4.362	0.000	0.000	-8.468	7.00E-1	2.80E-1	4.94E-3	1.24E-3	1.06E-2
B		5.35411E+06	14.98	4.436	4.468	3.996	7.536	0.728	0.500	1.34E-4	2.43E-3	0.5038	0.5488	4.437	0.000	0.000	-8.181	7.00E-1	2.80E-1	4.94E-3	1.24E-3	1.06E-2
U		7.31869E+06	14.96	4.504	4.455	3.874	7.546	0.732	0.400	1.53E-4	1.50E-3	0.4765	0.5495	4.505	0.000	0.000	-7.911	7.00E-1	2.80E-1	4.94E-3	1.24E-3	1.06E-2
R		8.87289E+06	14.93	4.568	4.435	3.732	7.558	0.748	0.300	1.68E-4	9.90E-4	0.4411	0.5505	4.569	0.000	0.000	-7.658	7.00E-1	2.80E-1	4.94E-3	1.24E-3	1.06E-2
N		1.00848E+07	14.90	4.625	4.408	3.565	7.573	0.779	0.200	1.83E-4	7.10E-4	0.4033	0.5518	4.626	0.000	0.000	-7.424	7.00E-1	2.80E-1	4.94E-3	1.24E-3	1.06E-2
I		1.10620E+07	14.85	4.676	4.371	3.363	7.596	0.838	0.100	2.03E-4	5.57E-4	0.3641	0.5535	4.678	0.000	0.000	-7.204	7.00E-1	2.80E-1	4.94E-3	1.24E-3	1.06E-2
N		1.15233E+07	14.82	4.701	4.350	3.254	7.617	0.897	0.050	2.11E-4	5.00E-4	0.3436	0.5548	4.702	0.000	0.000	-7.106	7.00E-1	2.80E-1	4.94E-3	1.24E-3	1.06E-2
G	2	1.17342E+07	14.80	4.714	4.343	3.212	7.635	0.950	0.026	2.27E-4	4.73E-4	0.3317	0.5554	4.715	0.000	0.000	-7.061	7.00E-1	2.80E-1	4.94E-3	1.24E-3	1.06E-2
		1.18610E+07	14.79	4.725	4.347	3.218	7.660	1.024	0.010	2.53E-4	4.60E-4	0.3213	0.5558	4.723	0.000	0.000	-7.042	7.00E-1	2.80E-1	4.94E-3	1.24E-3	1.06E-2
		1.19480E+07	14.78	4.744	4.378	3.323	7.720	1.204	0.001	3.08E-4	4.47E-4	0.2923	0.5561	4.714	0.000	0.000	-7.056	7.00E-1	2.80E-1	4.94E-3	1.24E-3	1.06E-2
	3	1.19568E+07	14.78	4.755	4.393	3.371	7.753	1.311	0.000	3.31E-4	4.45E-4	0.2649	0.5562	4.696	0.000	0.000	-7.061	7.00E-1	2.80E-1	4.94E-3	1.24E-3	1.06E-2
		1.19577E+07	14.78	4.758	4.395	3.377	7.759	1.333	0.000	3.37E-4	4.45E-4	0.2570	0.5562	4.685	0.000	0.000	-7.059	7.00E-1	2.80E-1	4.94E-3	1.24E-3	1.06E-2
	4	1.19611E+07	14.78	4.771	4.404	3.399	7.814	1.558	0.000	3.69E-4	4.45E-4	0.0305	0.5562	4.613	0.123	0.000	-7.037	7.00E-1	2.80E-1	4.94E-3	1.24E-3	1.06E-2
		1.19701E+07	14.78	4.767	4.287	2.935	7.943	2.234	0.000	3.69E-4	4.45E-4	0.0000	0.5710	4.817	0.199	0.000	-6.867	7.00E-1	2.80E-1	4.94E-3	1.24E-3	1.06E-2
	5	1.19741E+07	14.78	4.775	4.192	2.546	8.004	2.480	0.000	3.69E-4	4.45E-4	0.0000	0.5710	4.818	0.218	0.000	-6.754	7.00E-1	2.80E-1	4.94E-3	1.24E-3	1.06E-2
		1.19749E+07	14.78	4.775	4.168	2.450	8.018	2.530	0.000	3.69E-4	4.45E-4	0.0000	0.5710	4.817	0.218	0.000	-6.738	7.00E-1	2.80E-1	4.94E-3	1.24E-3	1.06E-2
He		1.19783E+07	14.78	4.762	4.039	1.949	8.075	2.729	0.981	3.69E-4	4.45E-4	0.0000	0.5710	4.805	0.233	0.000	-6.691	7.00E-1	2.80E-1	4.94E-3	1.24E-3	1.06E-2
		1.19800E+07	14.78	4.744	3.935	1.551	8.105	2.828	0.980	3.73E-4	4.45E-4	0.0000	0.5710	4.794	0.239	1.045	-6.671	7.00E-1	2.80E-1	4.94E-3	1.24E-3	1.06E-2
B		1.19817E+07	14.78	4.699	3.774	0.951	8.137	2.925	0.980	4.25E-4	4.45E-4	0.0000	0.5710	4.774	0.243	2.190	-6.609	7.00E-1	2.80E-1	4.94E-3	1.24E-3	1.06E-2
U		1.19826E+07	14.78	4.592	3.653	0.575	8.155	2.968	0.980	5.84E-4	4.45E-4	0.0023	0.5711	4.759	0.246	2.820	-6.523	7.00E-1	2.80E-1	4.94E-3	1.24E-3	1.06E-2
R	6	1.19830E+07	14.78	4.523	3.619	0.506	8.164	2.987	0.980	6.33E-4	4.45E-4	0.0058	0.5711	4.742	0.247	3.127	-6.420	7.00E-1	2.80E-1	4.94E-3	1.24E-3	1.06E-2
N		1.19857E+07	14.78	4.840	3.569	-0.009	8.200	3.029	0.979	1.19E-3	4.45E-4	0.0623	0.4183	4.709	0.255	4.257	-6.138	6.70E-1	3.10E-1	3.64E-3	3.49E-3	9.51E-3
I	7	1.19880E+07	14.77	4.893	3.566	-0.074	8.204	3.008	0.978	1.72E-3	4.45E-4	0.0974	0.3449	4.737	0.259	4.340	-6.035	6.39E-1	3.41E-1	3.26E-3	4.66E-3	8.69E-3
N	8	1.19885E+07	14.77	4.896	3.566	-0.079	8.205	3.004	0.977	1.86E-3	4.45E-4	0.1009	0.3425	4.743	0.259	4.335	-6.030	6.38E-1	3.42E-1	3.25E-3	4.69E-3	8.66E-3
G		1.20281E+07	14.74	4.827	3.575	0.026	8.226	3.005	0.950	2.64E-2	5.33E-4	0.1323	0.3313	4.642	0.286	4.354	-6.129	6.34E-1	3.46E-1	3.20E-3	4.85E-3	8.55E-3
		1.21065E+07	14.69	4.715	3.586	0.182	8.233	2.988	0.900	7.52E-2	1.12E-3	0.1817	0.3327	4.417	0.302	4.405	-6.292	6.34E-1	3.46E-1	3.20E-3	4.85E-3	8.55E-3
		1.22182E+07	14.64	4.704	3.597	0.235	8.242	2.992	0.800	1.71E-1	3.78E-3	0.1878	0.3339	4.354	0.313	4.451	-6.331	6.34E-1	3.46E-1	3.20E-3	4.85E-3	8.55E-3
		1.23303E+07	14.59	4.728	3.608	0.254	8.249	2.995	0.700	2.64E-1	9.41E-3	0.1949	0.3403	4.356	0.320	4.483	-6.331	6.34E-1	3.46E-1	3.20E-3	4.85E-3	8.55E-3
		1.23582E+07	14.57	4.859	3.744	0.665	8.251	3.000	0.674	2.88E-1	1.14E-2	0.1950	0.3419	4.500	0.321	4.488	-6.355	6.34E-1	3.46E-1	3.20E-3	4.85E-3	8.55E-3
		1.23613E+07	14.57	4.865	3.851	1.088	8.252	3.001	0.671	2.91E-1	1.16E-2	0.1950	0.3427	4.538	0.322	4.488	-6.462	6.34E-1	3.46E-1	3.20E-3	4.85E-3	8.55E-3
		1.23676E+07	14.57	4.863	3.982	1.613	8.252	3.002	0.665	2.97E-1	1.21E-2	0.1951	0.3440	4.580	0.322	4.489	-6.520	6.34E-1	3.46E-1	3.20E-3	4.85E-3	8.55E-3
		1.24012E+07	14.56	4.858	4.084	2.024	8.256	3.006	0.631	3.27E-1	1.52E-2	0.1952	0.3487	4.604	0.324	4.504	-6.552	6.34E-1	3.46E-1	3.20E-3	4.85E-3	8.55E-3
		1.24312E+07	14.55	4.861	4.096	2.071	8.259	3.010	0.600	3.55E-1	1.83E-2	0.1953	0.3529	4.602	0.326	4.516	-6.550	6.34E-1	3.46E-1	3.20E-3	4.85E-3	8.55E-3
	9	1.24449E+07	14.55	4.862	4.098	2.077	8.260	3.012	0.585	3.67E-1	2.00E-2	0.1954	0.3543	4.600	0.327	4.522	-6.549	6.34E-1	3.46E-1	3.20E-3	4.85E-3	8.55E-3
		1.25467E+07	14.52	4.864	4.074	1.980	8.268	3.019	0.500	4.39E-1	3.35E-2	0.2050	0.3614	4.580	0.333	4.551	-6.538	6.34E-1	3.46E-1	3.20E-3	4.85E-3	8.55E-3
		1.26483E+07	14.49	4.867	4.048	1.869	8.281	3.044	0.400	5.17E-1	5.53E-2	0.2054	0.3664	4.548	0.337	4.588	-6.527	6.34E-1	3.46E-1	3.20E-3	4.85E-3	8.55E-3
		1.27774E+07	14.45	4.869	4.012	1.722	8.295	3.069	0.300	5.78E-1	9.36E-2	0.2135	0.3725	4.509	0.343	4.626	-6.514	6.34E-1	3.46E-1	3.20E-3	4.85E-3	8.55E-3
		1.29292E+07	14.40	4.872	3.980	1.591	8.308	3.090	0.200	6.07E-1	1.65E-1	0.2232	0.3788	4.463	0.350	4.658	-6.501	6.34E-1	3.46E-1	3.20E-3	4.85E-3	8.55E-3
		1.29828E+07	14.39	4.863	3.878	1.191	8.327	3.142	0.154	6.13E-1	2.05E-1	0.2235	0.3793	4.406	0.352	4.682	-6.480	6.34E-1	3.46E-1	3.20E-3	4.85E-3	8.55E-3
		1.30358E+07	14.37	4.850	3.777	0.801	8.340	3.175	0.108	6.03E-1	2.61E-1	0.2239	0.3806	4.337	0.355	4.696	-6.428	6.34E-1	3.46E-1	3.20E-3	4.85E-3	8.55E-3
		1.30462E+07	14.36	4.837	3.732	0.634	8.345	3.188	0.100	5.99E-1	2.73E-1	0.2240	0.3807	4.307	0.355	4.699	-6.400	6.34E-1	3.46E-1	3.20E-3	4.85E-3	8.55E-3
		1.30537E+07	14.36	4.771	3.631	0.295	8.348	3.197	0.094	5.95E-1	2.83E-1	0.2240	0.3808	4.203	0.355	4.703	-6.284	6.34E-1	3.46E-1	3.20E-3	4.85E-3	8.55E-3
		1.32092E+07	14.27	4.784	3.584	0.089	8.373	3.264	0.050	4.87E-1	4.35E-1	0.2325	0.3828	3.865	0.360	4.728	-6.208	6.34E-1	3.46E-1	3.20E-3	4.85E-3	8.55E-3
		1.32767E+07	14.23	4.804	3.580	0.052	8.420	3.402	0.010	4.01E-1	5.59E-1	0.2307	0.3840	3.889	0.362	4.734	-6.177	6.34E-1	3.46E-1	3.20E-3	4.85E-3	8.55E-3
		1.32924E+07	14.22	4.826	3.577	0.021	8.470	3.555	0.001	3.76E-1	5.92E-1	0.2175	0.3843	3.979	0.363	4.617	-6.144	6.34E-1	3.46E-1	3.20E-3	4.85E-3	8.55E-3
		1.32948E+07	14.21	4.836	3.576	0.005	8.502	3.658	0.000	3.74E-1	5.95E-1	0.1815	0.3843	4.037	0.363	4.243	-6.129	6.34E-1	3.46E-1	3.20E-3	4.85E-3	8.55E-3
	10	1.32952E+07	14.21	4.840	3.576	0.000	8.511	3.686	0.000	3.74E-1	5.95E-1	0.1685	0.3843	4.043	0.363	4.177	-6.126	6.34E-1	3.46E-1	3.20E-3	4.85E-3	8.55E-3
	11	1.33240E+07	14.17	5.135	3.531	-0.474	8.883	4.971	0.000	3.74E-1	5.95E-1	0.1138	0.3683	0.000	0.364	4.918	-5.580	6.32E-1	3.48E-1	3.04E-3	5.07E-3	8.50E-3
		1.33438E+07	14.12	5.116	3.544	-0.405	8.887	4.943	0.000	3.74E-1	5.95E-1	0.1412	0.3308	0.000	0.331	4.894	-5.647	5.99E-1	3.82E-1	2.90E-3	5.63E-3	8.06E-3

Table 7.2 (continued) - M = 12.00 $M_\odot$ Z=0.020 Y=0.280 Diffusion

		AGE	M	$L/L_\odot$	T_{eff}	G	T_c	ρ_c	COMP	XC	XO	CONV	Q_{disc}	L_H	$Q1_H$	L_{He}	$\dot{M}$	X_{sup}	Y_{sup}	XC_{sup}	XN_{sup}	XO_{sup}
H	1	0.00000E+00	12.00	3.997	4.438	4.218	7.508	0.847	0.693	9.51E-5	1.02E-2	0.5066	0.5031	3.988	0.000	0.000	-9.692	7.00E-1	2.80E-1	4.94E-3	1.24E-3	1.06E-2
		4.13003E+06	12.00	4.065	4.431	4.123	7.511	0.827	0.600	1.03E-4	4.64E-3	0.4930	0.5066	4.066	0.000	0.000	-9.374	7.00E-1	2.80E-1	4.94E-3	1.24E-3	1.06E-2
B		7.88438E+06	12.00	4.143	4.423	4.012	7.519	0.818	0.500	1.26E-4	2.63E-3	0.4675	0.5067	4.143	0.000	0.000	-9.033	7.00E-1	2.80E-1	4.94E-3	1.24E-3	1.06E-2
U		1.07655E+07	11.99	4.215	4.411	3.892	7.529	0.821	0.400	1.45E-4	1.63E-3	0.4384	0.5069	4.216	0.000	0.000	-8.710	7.00E-1	2.80E-1	4.94E-3	1.24E-3	1.06E-2
R		1.29471E+07	11.99	4.281	4.393	3.755	7.542	0.835	0.300	1.58E-4	1.09E-3	0.4043	0.5072	4.282	0.000	0.000	-8.412	7.00E-1	2.80E-1	4.94E-3	1.24E-3	1.06E-2
N		1.46534E+07	11.98	4.341	4.369	3.597	7.557	0.864	0.200	1.73E-4	7.83E-4	0.3708	0.5075	4.342	0.000	0.000	-8.133	7.00E-1	2.80E-1	4.94E-3	1.24E-3	1.06E-2
I		1.59927E+07	11.96	4.396	4.336	3.409	7.580	0.921	0.100	1.93E-4	6.18E-4	0.3283	0.5081	4.398	0.000	0.000	-7.873	7.00E-1	2.80E-1	4.94E-3	1.24E-3	1.06E-2
N		1.66159E+07	11.95	4.423	4.318	3.312	7.601	0.979	0.050	2.01E-4	5.52E-4	0.3063	0.5085	4.424	0.000	0.000	-7.757	7.00E-1	2.80E-1	4.94E-3	1.24E-3	1.06E-2
G	2	1.68735E+07	11.95	4.436	4.314	3.281	7.617	1.026	0.028	2.14E-4	5.24E-4	0.2966	0.5087	4.437	0.000	0.000	-7.708	7.00E-1	2.80E-1	4.94E-3	1.24E-3	1.06E-2
		1.70590E+07	11.94	4.449	4.320	3.292	7.644	1.103	0.010	2.41E-4	5.03E-4	0.2863	0.5089	4.447	0.000	0.000	-7.686	7.00E-1	2.80E-1	4.94E-3	1.24E-3	1.06E-2
		1.71639E+07	11.94	4.471	4.350	3.392	7.702	1.281	0.001	2.95E-4	4.87E-4	0.2513	0.5090	4.437	0.000	0.000	-7.702	7.00E-1	2.80E-1	4.94E-3	1.24E-3	1.06E-2
	3	1.71743E+07	11.94	4.486	4.364	3.433	7.735	1.391	0.000	3.20E-4	4.86E-4	0.2175	0.5090	4.416	0.000	0.000	-7.704	7.00E-1	2.80E-1	4.94E-3	1.24E-3	1.06E-2
		1.71749E+07	11.94	4.487	4.365	3.435	7.739	1.407	0.000	3.24E-4	4.85E-4	0.2107	0.5090	4.407	0.000	0.000	-7.701	7.00E-1	2.80E-1	4.94E-3	1.24E-3	1.06E-2
	4	1.71782E+07	11.94	4.497	4.371	3.448	7.772	1.561	0.000	3.54E-4	4.85E-4	0.0029	0.5090	4.295	0.088	0.000	-7.680	7.00E-1	2.80E-1	4.94E-3	1.24E-3	1.06E-2
		1.71916E+07	11.94	4.498	4.259	2.999	7.872	2.273	0.000	3.54E-4	4.85E-4	0.0000	0.5090	4.564	0.153	0.000	-7.446	7.00E-1	2.80E-1	4.94E-3	1.24E-3	1.06E-2
	5	1.71978E+07	11.94	4.511	4.173	2.642	7.927	2.519	0.000	3.54E-4	4.85E-4	0.0000	0.5090	4.572	0.172	0.000	-7.279	7.00E-1	2.80E-1	4.94E-3	1.24E-3	1.06E-2
		1.71991E+07	11.94	4.511	4.151	2.555	7.940	2.569	0.000	3.54E-4	4.85E-4	0.0000	0.5090	4.572	0.176	0.000	-7.250	7.00E-1	2.80E-1	4.94E-3	1.24E-3	1.06E-2
		1.72043E+07	11.94	4.497	4.035	2.106	7.995	2.767	0.000	3.54E-4	4.85E-4	0.0000	0.5090	4.566	0.191	0.000	-7.148	7.00E-1	2.80E-1	4.94E-3	1.24E-3	1.06E-2
He		1.72083E+07	11.94	4.461	3.881	1.525	8.041	2.916	0.980	3.54E-4	4.85E-4	0.0000	0.5091	4.551	0.202	0.000	-7.047	7.00E-1	2.80E-1	4.94E-3	1.24E-3	1.06E-2
		1.72103E+07	11.94	4.409	3.750	1.053	8.065	2.991	0.980	3.55E-4	4.85E-4	0.0000	0.5091	4.536	0.205	0.000	-6.932	7.00E-1	2.80E-1	4.94E-3	1.24E-3	1.06E-2
B		1.72117E+07	11.94	4.286	3.636	0.719	8.082	3.041	0.980	3.57E-4	4.85E-4	0.0000	0.5091	4.519	0.207	0.286	-6.739	7.00E-1	2.80E-1	4.94E-3	1.24E-3	1.06E-2
U	6	1.72124E+07	11.94	4.243	3.617	0.687	8.090	3.065	0.980	3.60E-4	4.85E-4	0.0000	0.5091	4.501	0.209	0.544	-6.690	7.00E-1	2.80E-1	4.94E-3	1.24E-3	1.06E-2
R		1.72164E+07	11.94	4.600	3.571	0.146	8.144	3.197	0.980	7.58E-4	4.85E-4	0.0015	0.3679	4.522	0.218	2.535	-6.410	6.69E-1	3.11E-1	3.59E-3	3.55E-3	9.49E-3
N	7	1.72229E+07	11.94	4.681	3.563	0.032	8.189	3.198	0.977	2.56E-3	4.86E-4	0.0681	0.3122	4.578	0.227	3.966	-6.277	6.49E-1	3.31E-1	3.32E-3	4.35E-3	8.93E-3
I	8	1.72275E+07	11.93	4.692	3.561	0.013	8.191	3.169	0.975	3.63E-3	4.87E-4	0.0858	0.3071	4.598	0.230	3.946	-6.257	6.47E-1	3.33E-1	3.30E-3	4.42E-3	8.89E-3
N		1.72767E+07	11.91	4.652	3.569	0.083	8.207	3.150	0.950	2.65E-2	5.68E-4	0.1037	0.3027	4.543	0.254	3.977	-6.313	6.46E-1	3.34E-1	3.28E-3	4.48E-3	8.84E-3
G		1.73035E+07	11.86	4.488	3.584	0.305	8.215	3.114	0.900	7.55E-2	1.15E-3	0.1541	0.3040	4.279	0.275	4.064	-6.521	6.46E-1	3.34E-1	3.28E-3	4.48E-3	8.84E-3
		1.75591E+07	11.82	4.432	3.602	0.432	8.225	3.106	0.800	1.72E-1	3.78E-3	0.1633	0.3068	4.126	0.288	4.130	-6.616	6.46E-1	3.34E-1	3.28E-3	4.48E-3	8.84E-3
		1.76345E+07	11.80	4.592	3.733	0.798	8.228	3.108	0.753	2.17E-1	5.96E-3	0.1635	0.3124	4.284	0.292	4.147	-6.621	6.46E-1	3.34E-1	3.28E-3	4.48E-3	8.84E-3
		1.76392E+07	11.80	4.601	3.838	1.208	8.229	3.108	0.750	2.19E-1	6.12E-3	0.1635	0.3131	4.326	0.292	4.147	-6.823	6.46E-1	3.34E-1	3.28E-3	4.48E-3	8.84E-3
		1.76485E+07	11.80	4.601	3.953	1.666	8.229	3.109	0.744	2.25E-1	6.44E-3	0.1635	0.3148	4.371	0.293	4.150	-6.928	6.46E-1	3.34E-1	3.28E-3	4.48E-3	8.84E-3
	9	1.77074E+07	11.79	4.600	4.041	2.018	8.232	3.109	0.704	2.62E-1	8.82E-3	0.1664	0.3221	4.401	0.297	4.169	-6.975	6.46E-1	3.34E-1	3.28E-3	4.48E-3	8.84E-3
		1.77143E+07	11.79	4.601	4.041	2.019	8.233	3.109	0.700	2.66E-1	9.12E-3	0.1665	0.3228	4.401	0.297	4.170	-6.974	6.46E-1	3.34E-1	3.28E-3	4.48E-3	8.84E-3
		1.78712E+07	11.78	4.605	4.012	1.900	8.241	3.114	0.600	3.56E-1	1.81E-2	0.1719	0.3305	4.383	0.304	4.210	-6.947	6.46E-1	3.34E-1	3.28E-3	4.48E-3	8.84E-3
		1.80178E+07	11.76	4.610	3.996	1.828	8.252	3.128	0.500	4.41E-1	3.16E-2	0.1737	0.3360	4.364	0.309	4.252	-6.926	6.46E-1	3.34E-1	3.28E-3	4.48E-3	8.84E-3
		1.81640E+07	11.74	4.616	3.979	1.754	8.262	3.140	0.400	5.20E-1	5.29E-2	0.1789	0.3407	4.341	0.314	4.291	-6.906	6.46E-1	3.34E-1	3.28E-3	4.48E-3	8.84E-3
		1.83102E+07	11.72	4.618	3.943	1.607	8.279	3.171	0.300	5.87E-1	8.56E-2	0.1810	0.3447	4.307	0.319	4.330	-6.879	6.46E-1	3.34E-1	3.28E-3	4.48E-3	8.84E-3
		1.84884E+07	11.70	4.616	3.881	1.362	8.298	3.209	0.200	6.26E-1	1.46E-1	0.1875	0.3502	4.257	0.324	4.372	-6.835	6.46E-1	3.34E-1	3.28E-3	4.48E-3	8.84E-3
		1.86086E+07	11.68	4.603	3.778	0.962	8.318	3.257	0.127	6.30E-1	2.15E-1	0.1884	0.3529	4.186	0.328	4.400	-6.751	6.46E-1	3.34E-1	3.28E-3	4.48E-3	8.84E-3
		1.86440E+07	11.67	4.569	3.666	0.547	8.324	3.275	0.106	6.23E-1	2.43E-1	0.1885	0.3531	4.113	0.329	4.408	-6.621	6.46E-1	3.34E-1	3.28E-3	4.48E-3	8.84E-3
		1.86549E+07	11.67	4.494	3.612	0.406	8.327	3.281	0.100	6.21E-1	2.51E-1	0.1886	0.3532	3.961	0.329	4.411	-6.549	6.46E-1	3.34E-1	3.28E-3	4.48E-3	8.84E-3
		1.87508E+07	11.64	4.522	3.588	0.282	8.352	3.352	0.050	5.72E-1	3.49E-1	0.1891	0.3541	3.801	0.331	4.430	-6.498	6.46E-1	3.34E-1	3.28E-3	4.48E-3	8.84E-3
		1.88140E+07	11.62	4.604	3.695	0.628	8.301	3.191	0.171	4.79E-1	3.22E-1	0.1962	0.3553	4.110	0.333	4.413	-6.627	6.46E-1	3.34E-1	3.28E-3	4.48E-3	8.84E-3
		1.88650E+07	11.61	4.508	3.597	0.330	8.319	3.240	0.137	4.87E-1	3.48E-1	0.2006	0.3563	3.809	0.334	4.423	-6.537	6.46E-1	3.34E-1	3.28E-3	4.48E-3	8.84E-3
		1.90827E+07	11.54	4.561	3.581	0.212	8.407	3.495	0.010	3.73E-1	5.87E-1	0.2018	0.3585	3.758	0.339	4.470	-6.436	6.46E-1	3.34E-1	3.28E-3	4.48E-3	8.84E-3
		1.91033E+07	11.53	4.587	3.578	0.171	8.456	3.646	0.001	3.49E-1	6.20E-1	0.1884	0.3588	3.869	0.339	4.341	-6.408	6.46E-1	3.34E-1	3.28E-3	4.48E-3	8.84E-3
	10	1.91058E+07	11.53	4.598	3.577	0.157	8.481	3.728	0.000	3.46E-1	6.23E-1	0.1509	0.3588	3.918	0.339	3.926	-6.395	6.46E-1	3.34E-1	3.28E-3	4.48E-3	8.84E-3
		1.91060E+07	11.53	4.599	3.577	0.156	8.484	3.735	0.000	3.46E-1	6.23E-1	0.1444	0.3588	3.921	0.339	3.864	-6.394	6.46E-1	3.34E-1	3.28E-3	4.48E-3	8.84E-3
	11	1.91572E+07	11.48	4.978	3.523	-0.440	8.872	5.071	0.000	3.46E-1	6.23E-1	0.1204	0.3440	0.000	0.341	4.829	-5.804	6.43E-1	3.36E-1	3.14E-3	4.68E-3	8.78E-3
		1.91633E+07	11.47	4.983	3.522	-0.450	8.873	5.064	0.000	3.46E-1	6.23E-1	0.1244	0.3413	0.000	0.341	0.000	-5.790	6.41E-1	3.39E-1	3.13E-3	4.73E-3	8.75E-3

Table 7.2 (continued) - M = 9.00 $M_\odot$ Z = 0.020 Y = 0.280 Diffusion

		AGE	$L/L_\odot$	T_{eff}	G	T_c	ρ_c	COMP	XC	XO	CONV	Q_{disc}	L_H	$Q1_H$	$Q2_H$	L_{He}	$Q1_{He}$	$Q2_{He}$	L_C	$-L_\mu$	Q_{Tmax}
H	1	0.00000E+00	3.595	4.373	4.238	7.487	0.984	0.684	6.55E-5	9.21E-3	0.4693	0.4619	3.596	0.0000	0.3254	0.000	0.0000	0.0000	0.000	0.000	0.0000
		6.64421E+06	3.659	4.366	4.145	7.488	0.958	0.600	9.02E-5	4.81E-3	0.4513	0.4712	3.660	0.0000	0.2990	0.000	0.0000	0.0000	0.000	0.000	0.0000
B		1.21855E+07	3.726	4.358	4.034	7.495	0.947	0.500	1.13E-4	2.78E-3	0.4232	0.4712	3.726	0.0000	0.2833	0.000	0.0000	0.0000	0.000	0.000	0.0000
U		1.80720E+07	3.807	4.346	3.916	7.505	0.947	0.400	1.33E-4	1.78E-3	0.3950	0.4712	3.808	0.0000	0.2652	0.000	0.0000	0.0000	0.000	0.000	0.0000
R		2.17522E+07	3.873	4.330	3.784	7.518	0.960	0.300	1.46E-4	1.22E-3	0.3614	0.4712	3.874	0.0000	0.2439	0.000	0.0000	0.0000	0.000	0.000	0.0000
N		2.45601E+07	3.934	4.308	3.636	7.533	0.988	0.200	1.60E-4	8.88E-4	0.3254	0.4712	3.935	0.0000	0.2221	0.000	0.0000	0.0000	0.000	0.000	0.0000
I		2.67281E+07	3.988	4.279	3.468	7.556	1.043	0.100	1.78E-4	6.85E-4	0.2863	0.4712	3.989	0.0000	0.2005	0.000	0.0000	0.0000	0.000	0.000	0.0000
N		2.77236E+07	4.015	4.265	3.386	7.577	1.099	0.050	1.87E-4	6.17E-4	0.2642	0.4712	4.016	0.0000	0.1947	0.000	0.0000	0.0000	0.000	0.000	0.0000
G	2	2.80934E+07	4.027	4.262	3.363	7.591	1.141	0.029	1.98E-4	5.52E-4	0.2496	0.4712	4.027	0.0000	0.2057	0.000	0.0000	0.0000	0.000	0.000	0.0000
		2.83928E+07	4.042	4.270	3.379	7.619	1.221	0.010	2.24E-4	5.66E-4	0.2379	0.4712	4.039	0.0000	0.2359	0.000	0.0000	0.0000	0.000	0.000	0.0000
a		2.85378E+07	4.070	4.261	3.471	7.675	1.395	0.001	2.77E-4	5.48E-4	0.1995	0.4712	4.029	0.0000	0.3042	0.000	0.0000	0.0000	0.000	0.000	0.0000
n		2.85516E+07	4.086	4.312	3.501	7.705	1.515	0.000	3.04E-4	5.46E-4	0.1497	0.4712	4.006	0.0000	0.3454	0.000	0.0000	0.0000	0.000	0.000	0.0000
d	3	2.85551E+07	4.090	4.314	3.506	7.720	1.613	0.000	3.20E-4	5.46E-4	0.0709	0.4712	3.996	0.0000	0.3843	0.000	0.0000	0.0000	0.000	0.000	0.0000
		2.85747E+07	4.093	4.240	3.205	7.741	2.192	0.000	3.31E-4	5.46E-4	0.0000	0.4712	4.160	0.0855	0.3218	0.000	0.0000	0.0000	0.000	0.000	0.0000
R		2.85906E+07	4.122	4.167	2.885	7.786	2.484	0.000	3.31E-4	5.46E-4	0.0000	0.4712	4.177	0.1109	0.2863	0.000	0.0000	0.0000	0.000	0.000	0.0000
G	4	2.85966E+07	4.125	4.136	2.758	7.807	2.583	0.000	3.31E-4	5.46E-4	0.0000	0.4712	4.179	0.1206	0.2794	0.000	0.0000	0.0000	0.000	0.000	0.0000
B		2.86057E+07	4.121	4.078	2.529	7.843	2.732	0.000	3.31E-4	5.46E-4	0.0000	0.4712	4.179	0.1359	0.2655	0.000	0.0000	0.0000	0.000	0.000	0.0000
		2.86148E+07	4.103	3.994	2.213	7.886	2.882	0.000	3.31E-4	5.46E-4	0.0000	0.4712	4.174	0.1459	0.2522	0.000	0.0000	0.0000	0.000	0.000	0.0000
		2.86209E+07	4.079	3.912	1.910	7.917	2.983	0.000	3.31E-4	5.46E-4	0.0000	0.4712	4.165	0.1524	0.2417	0.000	0.0000	0.0000	0.000	0.000	0.0000
		2.86251E+07	4.056	3.834	1.624	7.940	3.052	0.000	3.31E-4	5.46E-4	0.0000	0.4712	4.156	0.1555	0.2354	0.000	0.0000	0.0000	0.000	0.000	0.0000
		2.86280E+07	4.018	3.764	1.376	7.957	3.102	0.000	3.31E-4	5.46E-4	0.0000	0.4712	4.149	0.1585	0.2333	0.000	0.0000	0.0000	0.000	0.000	0.0000
		2.86303E+07	3.967	3.689	1.128	7.970	3.141	0.000	3.31E-4	5.46E-4	0.0000	0.4712	4.140	0.1606	0.2292	0.000	0.0000	0.0000	0.000	0.000	0.0000
	5	2.86340E+07	3.865	3.631	0.998	7.993	3.204	0.000	3.31E-4	5.46E-4	0.0000	0.4712	4.113	0.1649	0.2250	0.000	0.0000	0.0000	0.000	0.000	0.0000
		2.86351E+07	3.886	3.619	0.928	7.999	3.223	0.000	3.31E-4	5.46E-4	0.0000	0.4712	4.104	0.1649	0.2230	0.000	0.0000	0.0000	0.000	0.000	0.0000
He	6	2.86961E+07	4.229	3.573	0.304	8.168	3.403	0.969	9.41E-3	5.57E-4	0.0945	0.2680	4.276	0.1997	0.2230	3.243	0.0000	0.0316	0.000	0.000	0.0000
		2.87996E+07	4.292	3.577	0.256	8.178	3.356	0.950	2.69E-2	6.34E-4	0.1072	0.2680	4.224	0.2187	0.2405	3.430	0.0000	0.0377	0.000	0.000	0.0000
B		2.89910E+07	4.153	3.599	0.548	8.189	3.318	0.900	7.57E-2	1.18E-3	0.1189	0.2680	4.027	0.2367	0.2569	3.545	0.0000	0.0453	0.000	0.000	0.0000
U		2.92047E+07	4.019	3.608	0.752	8.199	3.295	0.800	1.73E-1	3.80E-3	0.1298	0.2685	3.782	0.2496	0.2722	3.627	0.0000	0.0453	0.000	0.000	0.0000
R	7	2.94189E+07	4.013	3.615	0.788	8.202	3.292	0.763	2.07E-1	5.45E-3	0.1303	0.2696	3.753	0.2528	0.2763	3.660	0.0000	0.0453	0.000	0.000	0.0000
N		2.95858E+07	4.192	3.889	1.703	8.207	3.294	0.700	2.67E-1	8.99E-3	0.1303	0.2767	4.005	0.2570	0.2893	3.685	0.0000	0.0529	0.000	0.000	0.0000
I	8	2.96871E+07	4.206	3.900	1.972	8.210	3.292	0.661	3.03E-1	1.18E-2	0.1324	0.2827	4.042	0.2605	0.2931	3.706	0.0000	0.0529	0.000	0.000	0.0000
N		2.98662E+07	4.207	3.935	1.871	8.216	3.291	0.600	3.58E-1	1.77E-2	0.1359	0.2876	4.036	0.2649	0.2878	3.734	0.0000	0.0529	0.000	0.000	0.0000
G		3.01324E+07	4.217	3.926	1.827	8.226	3.298	0.500	4.44E-1	3.08E-2	0.1376	0.2923	4.019	0.2695	0.2931	3.783	0.0000	0.0529	0.000	0.000	0.0000
		3.03979E+07	4.226	3.916	1.777	8.238	3.308	0.400	5.22E-1	5.10E-2	0.1427	0.2982	4.006	0.2743	0.2982	3.828	0.0000	0.0609	0.000	0.000	0.0000
		3.06578E+07	4.231	3.892	1.675	8.253	3.330	0.300	5.91E-1	8.14E-2	0.1450	0.3018	3.982	0.2788	0.3033	3.875	0.0000	0.0609	0.000	0.000	0.0000
		3.09591E+07	4.232	3.848	1.500	8.272	3.362	0.200	6.34E-1	1.38E-1	0.1503	0.3065	3.942	0.2827	0.3065	3.924	0.0000	0.0684	0.000	0.000	0.0000
		3.12279E+07	4.177	3.655	0.782	8.302	3.434	0.100	6.46E-1	2.32E-1	0.1517	0.3091	3.798	0.2878	0.3075	3.969	0.0000	0.0771	0.000	0.000	0.0000
	9	3.15478E+07	4.115	3.616	0.690	8.304	3.416	0.102	5.37E-1	3.33E-1	0.1584	0.3111	3.572	0.2912	0.3091	4.003	0.0000	0.0771	0.000	0.000	0.0000
		3.16872E+07	4.133	3.602	0.615	8.332	3.495	0.050	5.07E-1	4.14E-1	0.1584	0.3116	3.481	0.2923	0.3080	4.021	0.0000	0.0855	0.000	0.000	0.0000
		3.18294E+07	4.162	3.594	0.552	8.379	3.631	0.010	4.31E-1	5.31E-1	0.1584	0.3116	3.541	0.2936	0.3070	4.028	0.0000	0.0945	0.000	0.000	0.0000
		3.18638E+07	4.199	3.589	0.495	8.427	3.782	0.001	4.05E-1	5.65E-1	0.1446	0.3116	3.655	0.2941	0.3052	3.895	0.0000	0.1790	0.000	0.000	0.0000
		3.18677E+07	4.212	3.587	0.474	8.450	3.863	0.000	4.03E-1	5.68E-1	0.1007	0.3113	3.702	0.2943	0.3049	3.362	0.0000	0.1928	0.000	0.000	0.0000
		3.18921E+07	4.315	3.578	0.334	8.567	4.500	0.000	4.03E-1	5.68E-1	0.0000	0.3112	1.270	0.2943	0.3021	4.292	0.0993	0.2120	0.000	2.592	0.0000
E		3.19024E+07	4.404	3.567	0.203	8.606	4.699	0.000	4.03E-1	5.68E-1	0.0000	0.3112	0.000	0.2943	0.2991	4.371	0.1142	0.2096	0.000	2.862	0.0000
A		3.19174E+07	4.491	3.555	0.067	8.667	5.007	0.000	4.03E-1	5.68E-1	0.0000	0.3075	0.000	0.2943	0.0000	4.454	0.1345	0.2072	0.000	3.333	0.0000
G		3.19338E+07	4.571	3.540	-0.072	8.761	5.547	0.000	4.03E-1	5.68E-1	0.0000	0.3010	0.000	0.2943	0.0000	4.527	0.1577	0.2001	2.867	4.155	0.0000
B		3.19605E+07	4.665	3.531	-0.204	8.841	5.299	0.000	4.03E-1	5.68E-1	0.0858	0.2974	0.000	0.2943	0.0000	4.582	0.1754	0.2067	4.702	4.632	0.0000
	10	3.20636E+07	4.737	3.521	-0.314	8.852	5.170	0.000	4.03E-1	5.68E-1	0.1161	0.2911	0.000	0.2911	0.0000	4.616	0.2165	0.2527	5.005	4.948	0.0000
		3.22123E+07	4.628	3.524	-0.165	8.861	5.085	0.000	4.03E-1	5.68E-1	0.1409	0.2931	4.297	0.2923	0.2932	3.748	0.2557	0.2827	5.262	5.217	0.0000

Table 7.2 (continued) - M = 7.00 $M_\odot$ Z = 0.020 Y = 0.280 Diffusion

		AGE	$L/L_\odot$	T_{eff}	G	T_c	ρ_c	COMP	XC	XO	CONV	Q_{disc}	L_H	$Q1_H$	$Q2_H$	L_{He}	$Q1_{He}$	$Q2_{He}$	L_C	$-L_\mu$	Q_{Tmax}
H	1	0.00000E+00	3.219	4.313	4.261	7.462	1.108	0.692	6.26E-5	1.00E-2	0.4391	0.3956	3.220	0.0000	0.4252	0.000	0.0000	0.0000	0.000	0.000	0.0000
		1.22826E+07	3.285	4.304	4.162	7.465	1.082	0.600	8.26E-5	5.03E-3	0.4191	0.4410	3.285	0.0000	0.2854	0.000	0.0000	0.0000	0.000	0.000	0.0000
B		2.33274E+07	3.358	4.295	4.052	7.472	1.069	0.500	1.05E-4	3.01E-3	0.3915	0.4410	3.359	0.0000	0.2656	0.000	0.0000	0.0000	0.000	0.000	0.0000
U		3.16409E+07	3.427	4.283	3.936	7.482	1.070	0.400	1.18E-4	1.97E-3	0.3584	0.4410	3.427	0.0000	0.2453	0.000	0.0000	0.0000	0.000	0.000	0.0000
R		3.78084E+07	3.489	4.267	3.809	7.495	1.082	0.300	1.35E-4	1.37E-3	0.3236	0.4487	3.490	0.0000	0.2236	0.000	0.0000	0.0000	0.000	0.000	0.0000
N		4.24070E+07	3.545	4.246	3.669	7.510	1.110	0.200	1.48E-4	1.01E-3	0.2861	0.4487	3.546	0.0000	0.2028	0.000	0.0000	0.0000	0.000	0.000	0.0000
I		4.59399E+07	3.593	4.220	3.517	7.533	1.164	0.100	1.65E-4	7.70E-4	0.2499	0.4487	3.595	0.0000	0.1827	0.000	0.0000	0.0000	0.000	0.000	0.0000
N		4.74807E+07	3.618	4.209	3.446	7.552	1.219	0.050	1.75E-4	6.88E-4	0.2252	0.4487	3.618	0.0000	0.1819	0.000	0.0000	0.0000	0.000	0.000	0.0000
G	2	4.80995E+07	3.630	4.208	3.431	7.569	1.265	0.027	1.88E-4	6.51E-4	0.2190	0.4487	3.630	0.0000	0.1905	0.000	0.0000	0.0000	0.000	0.000	0.0000
		4.84964E+07	3.645	4.217	3.451	7.594	1.338	0.010	2.09E-4	6.21E-4	0.2051	0.4487	3.640	0.0000	0.2165	0.000	0.0000	0.0000	0.000	0.000	0.0000
a		4.87020E+07	3.678	4.245	3.533	7.646	1.509	0.001	2.60E-4	6.02E-4	0.1560	0.4487	3.632	0.0000	0.2795	0.000	0.0000	0.0000	0.000	0.000	0.0000
n	3	4.87206E+07	3.692	4.254	3.553	7.668	1.626	0.000	2.86E-4	6.00E-4	0.0991	0.4487	3.627	0.0000	0.3199	0.000	0.0000	0.0000	0.000	0.000	0.0000
d		4.87873E+07	3.730	4.169	3.176	7.651	2.385	0.000	3.06E-4	5.99E-4	0.0000	0.4487	3.762	0.0567	0.2759	0.000	0.0000	0.0000	0.000	0.000	0.0000
	4	4.88389E+07	3.741	4.108	2.920	7.696	2.681	0.000	3.06E-4	5.99E-4	0.0000	0.4487	3.772	0.0871	0.2528	0.000	0.0000	0.0000	0.000	0.000	0.0000
R		4.88477E+07	3.741	4.095	2.869	7.708	2.731	0.000	3.06E-4	5.99E-4	0.0000	0.4487	3.773	0.0901	0.2453	0.000	0.0000	0.0000	0.000	0.000	0.0000
G		4.88899E+07	3.724	4.007	2.532	7.777	2.986	0.000	3.06E-4	5.99E-4	0.0000	0.4487	3.770	0.1123	0.2248	0.000	0.0000	0.0000	0.000	0.000	0.0000
B		4.89120E+07	3.693	3.920	2.218	7.828	3.140	0.000	3.06E-4	5.99E-4	0.0000	0.4487	3.759	0.1217	0.2129	0.000	0.0000	0.0000	0.000	0.000	0.0000
		4.89275E+07	3.653	3.833	1.908	7.864	3.242	0.000	3.06E-4	5.99E-4	0.0000	0.4487	3.741	0.1271	0.2031	0.000	0.0000	0.0000	0.000	0.000	0.0000
		4.89414E+07	3.563	3.687	1.415	7.903	3.344	0.000	3.06E-4	5.99E-4	0.0000	0.4487	3.704	0.1332	0.1947	0.000	0.0000	0.0000	0.000	0.000	0.0000
	5	4.89482E+07	3.474	3.648	1.347	7.922	3.395	0.000	3.06E-4	5.99E-4	0.0000	0.4487	3.665	0.1355	0.1905	0.000	0.0000	0.0000	0.000	0.000	0.0000
		4.89571E+07	3.601	3.617	1.098	7.948	3.462	0.000	3.06E-4	5.99E-4	0.0000	0.4410	3.655	0.1392	0.1863	0.000	0.0000	0.0000	0.000	0.000	0.0000
He	6	4.90846E+07	3.932	3.589	0.655	8.141	3.655	0.970	9.50E-3	6.12E-4	0.0791	0.2296	3.896	0.1700	0.1879	2.779	0.0000	0.0228	0.000	0.000	0.0000
		4.93011E+07	3.888	3.592	0.709	8.150	3.587	0.950	2.75E-2	6.93E-4	0.0866	0.2296	3.840	0.1880	0.2055	2.886	0.0000	0.0283	0.000	0.000	0.0000
B		4.97123E+07	3.690	3.611	0.984	8.162	3.533	0.900	7.58E-2	1.26E-3	0.0961	0.2296	3.580	0.2055	0.2217	3.030	0.0000	0.0312	0.000	0.000	0.0000
U	7	5.03336E+07	3.556	3.638	1.225	8.172	3.503	0.804	1.68E-1	3.81E-3	0.1050	0.2306	3.347	0.2163	0.2359	3.125	0.0000	0.0370	0.000	0.000	0.0000
R		5.03581E+07	3.558	3.639	1.227	8.172	3.503	0.800	1.73E-1	3.97E-3	0.1050	0.2311	3.347	0.2166	0.2365	3.128	0.0000	0.0370	0.000	0.000	0.0000
N	8	5.07581E+07	3.769	3.892	2.030	8.178	3.498	0.727	2.42E-1	7.52E-3	0.1063	0.2410	3.642	0.2227	0.2497	3.166	0.0000	0.0370	0.000	0.000	0.0000
I		5.09193E+07	3.763	3.875	1.965	8.180	3.494	0.700	2.67E-1	9.31E-3	0.1077	0.2429	3.634	0.2250	0.2429	3.181	0.0000	0.0370	0.000	0.000	0.0000
N		5.15072E+07	3.778	3.863	1.904	8.189	3.487	0.600	3.58E-1	1.83E-2	0.1123	0.2497	3.630	0.2307	0.2507	3.228	0.0000	0.0428	0.000	0.000	0.0000
G		5.20315E+07	3.792	3.860	1.878	8.199	3.486	0.500	4.44E-1	3.14E-2	0.1152	0.2552	3.629	0.2355	0.2560	3.292	0.0000	0.0428	0.000	0.000	0.0000
		5.25178E+07	3.804	3.852	1.835	8.211	3.493	0.400	5.24E-1	5.05E-2	0.1163	0.2601	3.620	0.2399	0.2611	3.345	0.0000	0.0449	0.000	0.000	0.0000
		5.29994E+07	3.813	3.839	1.772	8.225	3.506	0.300	5.94E-1	8.01E-2	0.1195	0.2647	3.606	0.2443	0.2647	3.396	0.0000	0.0486	0.000	0.000	0.0000
		5.35683E+07	3.814	3.799	1.613	8.244	3.533	0.200	6.40E-1	1.33E-1	0.1235	0.2694	3.570	0.2493	0.2694	3.452	0.0000	0.0567	0.000	0.000	0.0000
		5.40279E+07	3.767	3.674	1.157	8.274	3.599	0.100	6.56E-1	2.16E-1	0.1235	0.2722	3.445	0.2530	0.2708	3.500	0.0000	0.0631	0.000	0.000	0.0000
	9	5.45562E+07	3.703	3.630	1.046	8.290	3.620	0.071	5.94E-1	3.06E-1	0.1272	0.2747	3.204	0.2565	0.2722	3.541	0.0000	0.0652	0.000	0.000	0.0000
		5.46805E+07	3.704	3.626	1.028	8.302	3.653	0.050	5.75E-1	3.47E-1	0.1287	0.2747	3.183	0.2572	0.2722	3.549	0.0000	0.0715	0.000	0.000	0.0000
		5.49450E+07	3.735	3.615	0.955	8.347	3.785	0.010	5.00E-1	4.62E-1	0.1272	0.2747	3.233	0.2586	0.2714	3.556	0.0000	0.0791	0.000	0.000	0.0000
		5.50091E+07	3.779	3.607	0.878	8.384	3.933	0.001	4.75E-1	4.96E-1	0.1123	0.2747	3.353	0.2593	0.2698	3.415	0.0000	0.1446	0.000	0.000	0.0000
		5.50154E+07	3.795	3.605	0.854	8.414	4.008	0.000	4.72E-1	5.00E-1	0.0686	0.2747	3.400	0.2594	0.2692	2.851	0.0000	0.1600	0.000	0.000	0.0000
		5.50667E+07	3.898	3.594	0.708	8.489	4.634	0.000	4.72E-1	5.00E-1	0.0000	0.2745	0.743	0.2594	0.2669	3.894	0.0713	0.1732	0.000	1.832	0.0000
E		5.50928E+07	3.994	3.585	0.574	8.521	4.828	0.000	4.72E-1	5.00E-1	0.0000	0.2745	0.000	0.2594	0.2638	3.979	0.0828	0.1732	0.000	2.047	0.0000
A		5.51284E+07	4.086	3.578	0.454	8.567	5.078	0.000	4.72E-1	5.00E-1	0.0000	0.2744	0.000	0.2594	0.0000	4.066	0.1024	0.1732	0.000	2.398	0.0000
G		5.51667E+07	4.181	3.564	0.305	8.625	5.394	0.000	4.72E-1	5.00E-1	0.0000	0.2712	0.000	0.2594	0.0000	4.154	0.1235	0.1732	0.000	2.898	0.0000
B		5.51950E+07	4.273	3.551	0.162	8.678	5.777	0.000	4.72E-1	5.00E-1	0.0000	0.2662	0.000	0.2594	0.0000	4.238	0.1404	0.1716	0.751	3.495	0.0015
		5.52151E+07	4.359	3.539	0.029	8.819	5.668	0.000	4.72E-1	5.00E-1	0.0779	0.2354	0.000	0.2353	0.0000	4.240	0.1542	0.1716	4.420	4.096	0.0000
	10	5.52869E+07	4.366	3.540	0.025	8.819	5.492	0.000	4.72E-1	5.00E-1	0.0845	0.2240	0.000	0.2239	0.0000	4.306	0.1670	0.1926	4.273	4.210	0.0000
		5.53597E+07	4.275	3.554	0.172	8.825	5.406	0.000	4.72E-1	5.00E-1	0.0947	0.2240	0.000	0.2239	0.2243	4.179	0.1843	0.2106	4.404	4.341	0.0000
		5.53832E+07	4.181	3.567	0.316	8.827	5.384	0.000	4.72E-1	5.00E-1	0.0975	0.2242	2.723	0.2239	0.2248	4.030	0.1886	0.2146	4.429	4.377	0.0000
		5.54089E+07	4.266	3.555	0.184	8.828	5.365	0.000	4.72E-1	5.00E-1	0.1002	0.2247	2.966	0.2240	0.2247	3.735	0.1922	0.2165	4.467	4.408	0.0000
		5.54271E+07	4.303	3.549	0.122	8.828	5.356	0.000	4.72E-1	5.00E-1	0.1002	0.2251	4.108	0.2245	0.2251	3.556	0.1939	0.2175	4.477	4.421	0.0000

Table 7.2 (continued) - M = 6.00 $M_\odot$ Z = 0.020 Y = 0.280 Diffusion

		AGE	$L/L_\odot$	T_{eff}	G	T_c	ρ_c	COMP	XC	XO	CONV	Q_{disc}	L_H	$Q1_H$	$Q2_H$	L_{He}	$Q1_{He}$	$Q2_{He}$	L_C	$-L_\mu$	Q_{Tmax}
H	1	0.00000E+00	2.985	4.273	4.272	7.448	1.188	0.693	5.83E-5	1.02E-2	0.4165	0.3180	2.986	0.0000	0.4304	0.000	0.0000	0.0000	0.000	0.000	0.0000
		1.74816E+07	3.049	4.265	4.173	7.451	1.163	0.600	7.81E-5	5.16E-3	0.3994	0.4221	3.049	0.0000	0.2794	0.000	0.0000	0.0000	0.000	0.000	0.0000
B		3.28137E+07	3.119	4.255	4.063	7.458	1.151	0.500	9.69E-5	3.16E-3	0.3700	0.4331	3.120	0.0000	0.2581	0.000	0.0000	0.0000	0.000	0.000	0.0000
U		4.44993E+07	3.184	4.242	3.948	7.468	1.151	0.400	1.15E-4	2.10E-3	0.3416	0.4439	3.185	0.0000	0.2356	0.000	0.0000	0.0000	0.000	0.000	0.0000
R		5.31458E+07	3.243	4.226	3.823	7.479	1.162	0.300	1.28E-4	1.48E-3	0.3071	0.4519	3.244	0.0000	0.2136	0.000	0.0000	0.0000	0.000	0.000	0.0000
N		5.94835E+07	3.294	4.205	3.688	7.495	1.190	0.200	1.41E-4	1.09E-3	0.2688	0.4519	3.295	0.0000	0.1913	0.000	0.0000	0.0000	0.000	0.000	0.0000
I		6.42093E+07	3.338	4.180	3.546	7.517	1.245	0.100	1.57E-4	8.36E-4	0.2286	0.4519	3.339	0.0000	0.1719	0.000	0.0000	0.0000	0.000	0.000	0.0000
N		6.63815E+07	3.360	4.170	3.483	7.536	1.300	0.050	1.68E-4	7.46E-4	0.2063	0.4519	3.360	0.0000	0.1719	0.000	0.0000	0.0000	0.000	0.000	0.0000
G	2	6.70683E+07	3.369	4.169	3.472	7.549	1.335	0.031	1.76E-4	7.12E-4	0.1997	0.4519	3.369	0.0000	0.1771	0.000	0.0000	0.0000	0.000	0.000	0.0000
		6.77142E+07	3.387	4.179	3.493	7.577	1.418	0.010	2.00E-4	6.73E-4	0.1834	0.4519	3.382	0.0000	0.2056	0.000	0.0000	0.0000	0.000	0.000	0.0000
a		6.79738E+07	3.423	4.208	3.570	7.626	1.584	0.001	2.48E-4	6.52E-4	0.1360	0.4519	3.376	0.0000	0.2669	0.000	0.0000	0.0000	0.000	0.000	0.0000
n	3	6.79922E+07	3.432	4.213	3.582	7.639	1.661	0.000	2.62E-4	6.51E-4	0.0935	0.4519	3.378	0.0000	0.2906	0.000	0.0000	0.0000	0.000	0.000	0.0000
d		6.79979E+07	3.432	4.213	3.584	7.640	1.714	0.000	2.72E-4	6.50E-4	0.0570	0.4519	3.393	0.0000	0.3146	0.000	0.0000	0.0000	0.000	0.000	0.0000
		6.81368E+07	3.477	4.141	3.249	7.588	2.436	0.000	2.84E-4	6.49E-4	0.0000	0.4519	3.494	0.0415	0.2600	0.000	0.0000	0.0000	0.000	0.000	0.0000
R	4	6.82793E+07	3.486	4.079	2.993	7.643	2.789	0.000	2.84E-4	6.49E-4	0.0000	0.4519	3.507	0.0766	0.2323	0.000	0.0000	0.0000	0.000	0.000	0.0000
G		6.82981E+07	3.485	4.067	2.946	7.656	2.841	0.000	2.84E-4	6.49E-4	0.0000	0.4519	3.508	0.0796	0.2323	0.000	0.0000	0.0000	0.000	0.000	0.0000
B		6.83810E+07	3.464	3.985	2.640	7.733	3.102	0.000	2.84E-4	6.49E-4	0.0000	0.4519	3.503	0.0994	0.2088	0.000	0.0000	0.0000	0.000	0.000	0.0000
		6.84231E+07	3.430	3.907	2.360	7.787	3.258	0.000	2.84E-4	6.49E-4	0.0000	0.4519	3.488	0.1082	0.1935	0.000	0.0000	0.0000	0.000	0.000	0.0000
		6.84488E+07	3.387	3.829	2.091	7.826	3.361	0.000	2.84E-4	6.49E-4	0.0000	0.4519	3.467	0.1157	0.1866	0.000	0.0000	0.0000	0.000	0.000	0.0000
		6.84728E+07	3.306	3.709	1.693	7.865	3.463	0.000	2.84E-4	6.49E-4	0.0000	0.4519	3.430	0.1198	0.1787	0.000	0.0000	0.0000	0.000	0.000	0.0000
	5	6.84957E+07	3.217	3.649	1.544	7.906	3.565	0.000	2.84E-4	6.49E-4	0.0000	0.4519	3.362	0.1265	0.1719	0.000	0.0000	0.0000	0.000	0.000	0.0000
		6.85013E+07	3.263	3.640	1.460	7.916	3.590	0.000	2.84E-4	6.49E-4	0.0000	0.4519	3.362	0.1265	0.1701	0.000	0.0000	0.0000	0.000	0.000	0.0000
He	6	6.86833E+07	3.663	3.602	0.907	8.123	3.833	0.971	8.73E-3	6.60E-4	0.0491	0.2101	3.632	0.1533	0.1684	2.426	0.0000	0.0194	0.000	0.000	0.0000
		6.90827E+07	3.614	3.604	0.964	8.132	3.736	0.950	2.82E-2	7.55E-4	0.0766	0.2101	3.574	0.1731	0.1880	2.539	0.0000	0.0245	0.000	0.000	0.0000
B		6.97729E+07	3.386	3.628	1.289	8.144	3.672	0.900	7.59E-2	1.36E-3	0.0876	0.2101	3.284	0.1895	0.2039	2.694	0.0000	0.0271	0.000	0.000	0.0000
U	7	7.06254E+07	3.260	3.652	1.511	8.153	3.643	0.821	1.52E-1	3.44E-3	0.0943	0.2109	3.076	0.1980	0.2157	2.781	0.0000	0.0321	0.000	0.000	0.0000
R		7.08449E+07	3.286	3.661	1.520	8.155	3.639	0.800	1.72E-1	4.26E-3	0.0957	0.2126	3.098	0.1998	0.2184	2.796	0.0000	0.0321	0.000	0.000	0.0000
N	8	7.13066E+07	3.463	3.830	2.021	8.159	3.634	0.750	2.20E-1	6.67E-3	0.0961	0.2199	3.349	0.2040	0.2282	2.825	0.0000	0.0321	0.000	0.000	0.0000
I		7.17373E+07	3.456	3.804	1.924	8.163	3.630	0.700	2.67E-1	9.75E-3	0.0961	0.2236	3.332	0.2074	0.2236	2.855	0.0000	0.0321	0.000	0.000	0.0000
N		7.27354E+07	3.479	3.805	1.904	8.172	3.617	0.600	3.57E-1	1.94E-2	0.1022	0.2296	3.340	0.2127	0.2300	2.918	0.0000	0.0390	0.000	0.000	0.0000
G		7.35565E+07	3.496	3.804	1.884	8.182	3.613	0.500	4.43E-1	3.26E-2	0.1038	0.2353	3.341	0.2172	0.2353	2.976	0.0000	0.0390	0.000	0.000	0.0000
		7.44251E+07	3.511	3.797	1.840	8.194	3.614	0.400	5.22E-1	5.32E-2	0.1078	0.2398	3.335	0.2219	0.2408	3.035	0.0000	0.0390	0.000	0.000	0.0000
		7.51567E+07	3.520	3.787	1.789	8.208	3.624	0.300	5.92E-1	8.21E-2	0.1095	0.2440	3.322	0.2258	0.2445	3.088	0.0000	0.0443	0.000	0.000	0.0000
		7.60272E+07	3.519	3.747	1.631	8.227	3.647	0.200	6.40E-1	1.33E-1	0.1136	0.2482	3.282	0.2304	0.2482	3.147	0.0000	0.0511	0.000	0.000	0.0000
		7.67265E+07	3.463	3.671	1.385	8.256	3.708	0.100	6.60E-1	2.12E-1	0.1136	0.2510	3.139	0.2337	0.2500	3.197	0.0000	0.0576	0.000	0.000	0.0000
	9	7.76193E+07	3.420	3.644	1.318	8.274	3.734	0.063	5.95E-1	3.14E-1	0.1177	0.2532	2.952	0.2373	0.2516	3.239	0.0000	0.0594	0.000	0.000	0.0000
		7.77386E+07	3.418	3.640	1.307	8.284	3.760	0.050	5.83E-1	3.39E-1	0.1177	0.2532	2.938	0.2376	0.2516	3.244	0.0000	0.0594	0.000	0.000	0.0000
		7.81598E+07	3.449	3.630	1.234	8.329	3.890	0.010	5.10E-1	4.51E-1	0.1177	0.2535	2.988	0.2391	0.2505	3.252	0.0000	0.0659	0.000	0.000	0.0000
		7.82597E+07	3.500	3.621	1.147	8.374	4.038	0.001	4.85E-1	4.86E-1	0.0993	0.2535	3.118	0.2397	0.2494	3.113	0.0000	0.0678	0.000	0.000	0.0000
		7.82687E+07	3.517	3.618	1.120	8.393	4.110	0.000	4.82E-1	4.89E-1	0.0588	0.2535	3.167	0.2398	0.2488	2.528	0.0000	0.1396	0.000	0.000	0.0000
	10	7.82696E+07	3.519	3.618	1.116	8.396	4.123	0.000	4.82E-1	4.89E-1	0.0250	0.2535	3.174	0.2398	0.2488	2.321	0.0000	0.1435	0.000	0.000	0.0000

Table 7.2 (continued) - M = 5.00 $M_\odot$ Z = 0.020 Y = 0.280 Diffusion

		AGE	$L/L_\odot$	T_{eff}	G	T_c	ρ_c	COMP	XC	XO	CONV	Q_{disc}	L_H	$Q1_H$	$Q2_H$	L_{He}	$Q1_{He}$	$Q2_{He}$	L_C	$-L_\mu$	Q_{Tmax}
H	1	0.00000E+00	2.705	4.225	4.279	7.430	1.285	0.688	5.34E-5	9.65E-3	0.3993	0.3281	2.707	0.0000	0.4337	0.000	0.0000	0.0000	0.000	0.000	0.0000
		2.48101E+07	2.762	4.216	4.186	7.433	1.263	0.600	7.12E-5	5.38E-3	0.3794	0.4202	2.763	0.0000	0.2797	0.000	0.0000	0.0000	0.000	0.000	0.0000
B		4.90500E+07	2.829	4.206	4.077	7.440	1.252	0.500	8.83E-5	3.31E-3	0.3502	0.4469	2.830	0.0000	0.2519	0.000	0.0000	0.0000	0.000	0.000	0.0000
U		6.64162E+07	2.889	4.192	3.964	7.449	1.253	0.400	1.06E-4	2.23E-3	0.3172	0.4598	2.890	0.0000	0.2262	0.000	0.0000	0.0000	0.000	0.000	0.0000
R		7.92910E+07	2.941	4.176	3.845	7.461	1.267	0.300	1.14E-4	1.59E-3	0.2850	0.4598	2.942	0.0000	0.2041	0.000	0.0000	0.0000	0.000	0.000	0.0000
N		8.88289E+07	2.985	4.155	3.718	7.476	1.293	0.200	1.32E-4	1.18E-3	0.2512	0.4598	2.986	0.0000	0.1793	0.000	0.0000	0.0000	0.000	0.000	0.0000
I		9.59511E+07	3.021	4.131	3.588	7.497	1.349	0.100	1.47E-4	9.11E-4	0.2112	0.4598	3.022	0.0000	0.1608	0.000	0.0000	0.0000	0.000	0.000	0.0000
N		9.89677E+07	3.039	4.123	3.535	7.516	1.403	0.050	1.59E-4	8.14E-4	0.1927	0.4598	3.040	0.0000	0.1608	0.000	0.0000	0.0000	0.000	0.000	0.0000
G	2	9.91941E+07	3.042	4.122	3.532	7.519	1.410	0.046	1.60E-4	8.06E-4	0.1878	0.4598	3.042	0.0000	0.1624	0.000	0.0000	0.0000	0.000	0.000	0.0000
		1.00862E+08	3.068	4.134	3.550	7.556	1.521	0.010	1.88E-4	7.36E-4	0.1643	0.4598	3.062	0.0000	0.1887	0.000	0.0000	0.0000	0.000	0.000	0.0000
a		1.01237E+08	3.107	4.161	3.620	7.602	1.684	0.001	2.34E-4	7.15E-4	0.1089	0.4598	3.059	0.0000	0.2504	0.000	0.0000	0.0000	0.000	0.000	0.0000
n	3	1.01270E+08	3.110	4.163	3.625	7.603	1.828	0.000	2.53E-4	7.12E-4	0.0268	0.4598	3.098	0.0000	0.3197	0.000	0.0000	0.0000	0.000	0.000	0.0000
d		1.01271E+08	3.110	4.163	3.625	7.602	1.835	0.000	2.54E-4	7.12E-4	0.0233	0.4598	3.101	0.0000	0.3197	0.000	0.0000	0.0000	0.000	0.000	0.0000
		1.01799E+08	3.163	4.093	3.291	7.537	2.604	0.000	2.51E-4	7.12E-4	0.0000	0.4598	3.171	0.0445	0.2402	0.000	0.0000	0.0000	0.000	0.000	0.0000
R	4	1.02030E+08	3.167	4.061	3.161	7.572	2.817	0.000	2.51E-4	7.12E-4	0.0000	0.4598	3.179	0.0646	0.2258	0.000	0.0000	0.0000	0.000	0.000	0.0000
G		1.02206E+08	3.161	4.017	2.992	7.626	3.031	0.000	2.51E-4	7.12E-4	0.0000	0.4598	3.181	0.0769	0.2112	0.000	0.0000	0.0000	0.000	0.000	0.0000
B		1.02372E+08	3.126	3.932	2.685	7.712	3.296	0.000	2.51E-4	7.12E-4	0.0000	0.4598	3.165	0.0932	0.1878	0.000	0.0000	0.0000	0.000	0.000	0.0000
		1.02452E+08	3.073	3.848	2.403	7.770	3.452	0.000	2.51E-4	7.12E-4	0.0000	0.4598	3.137	0.1013	0.1751	0.000	0.0000	0.0000	0.000	0.000	0.0000
		1.02500E+08	3.009	3.761	2.120	7.810	3.556	0.000	2.51E-4	7.12E-4	0.0000	0.4598	3.103	0.1080	0.1667	0.000	0.0000	0.0000	0.000	0.000	0.0000
		1.02545E+08	2.895	3.692	1.958	7.851	3.658	0.000	2.51E-4	7.12E-4	0.0000	0.4598	3.043	0.1116	0.1591	0.000	0.0000	0.0000	0.000	0.000	0.0000
	5	1.02567E+08	2.857	3.671	1.912	7.872	3.709	0.000	2.51E-4	7.12E-4	0.0000	0.4598	3.008	0.1152	0.1558	0.000	0.0000	0.0000	0.000	0.000	0.0000
		1.02659E+08	3.075	3.638	1.559	7.952	3.914	0.000	2.51E-4	7.12E-4	0.0000	0.3529	3.060	0.1234	0.1498	0.000	0.0000	0.0000	0.000	0.000	0.0000
He	6	1.02901E+08	3.322	3.615	1.220	8.103	4.037	0.974	6.82E-3	7.20E-4	0.0445	0.1883	3.298	0.1394	0.1514	2.041	0.0000	0.0163	0.000	0.000	0.0000
		1.03734E+08	3.252	3.622	1.318	8.112	3.914	0.950	2.90E-2	8.39E-4	0.0691	0.1883	3.218	0.1586	0.1707	2.109	0.0000	0.0210	0.000	0.000	0.0000
B		1.05070E+08	2.980	3.650	1.704	8.123	3.845	0.900	7.64E-2	1.54E-3	0.0785	0.1884	2.881	0.1725	0.1846	2.272	0.0000	0.0239	0.000	0.000	0.0000
U	7	1.06221E+08	2.890	3.668	1.865	8.129	3.823	0.847	1.27E-1	2.93E-3	0.0815	0.1892	2.737	0.1781	0.1931	2.340	0.0000	0.0239	0.000	0.000	0.0000
R		1.07120E+08	3.014	3.711	1.913	8.133	3.814	0.800	1.72E-1	4.75E-3	0.0827	0.1939	2.877	0.1818	0.2005	2.375	0.0000	0.0284	0.000	0.000	0.0000
N	8	1.07438E+08	3.051	3.740	1.992	8.134	3.811	0.784	1.87E-1	5.56E-3	0.0838	0.1962	2.943	0.1834	0.2023	2.385	0.0000	0.0284	0.000	0.000	0.0000
I		1.09004E+08	3.052	3.726	1.935	8.141	3.797	0.700	2.65E-1	1.10E-2	0.0869	0.2015	2.929	0.1882	0.2020	2.443	0.0000	0.0284	0.000	0.000	0.0000
N		1.10902E+08	3.078	3.727	1.913	8.150	3.781	0.600	3.55E-1	2.15E-2	0.0925	0.2069	2.942	0.1930	0.2074	2.511	0.0000	0.0284	0.000	0.000	0.0000
G		1.12581E+08	3.101	3.727	1.892	8.161	3.772	0.500	4.39E-1	3.64E-2	0.0955	0.2120	2.948	0.1973	0.2127	2.576	0.0000	0.0341	0.000	0.000	0.0000
		1.14136E+08	3.117	3.724	1.863	8.172	3.770	0.400	5.18E-1	5.73E-2	0.0985	0.2171	2.943	0.2013	0.2171	2.638	0.0000	0.0341	0.000	0.000	0.0000
		1.15856E+08	3.128	3.716	1.820	8.187	3.771	0.300	5.84E-1	9.12E-2	0.1030	0.2219	2.925	0.2057	0.2219	2.703	0.0000	0.0393	0.000	0.000	0.0000
		1.17245E+08	3.122	3.702	1.769	8.205	3.793	0.200	6.36E-1	1.38E-1	0.1046	0.2249	2.879	0.2092	0.2249	2.760	0.0000	0.0393	0.000	0.000	0.0000
		1.18926E+08	3.069	3.672	1.702	8.233	3.842	0.100	6.43E-1	2.30E-1	0.1080	0.2278	2.716	0.2129	0.2268	2.821	0.0000	0.0445	0.000	0.000	0.0000
	9	1.19349E+08	3.054	3.664	1.685	8.246	3.872	0.071	6.34E-1	2.67E-1	0.1080	0.2278	2.658	0.2137	0.2268	2.835	0.0000	0.0512	0.000	0.000	0.0000
		1.21012E+08	3.060	3.657	1.652	8.262	3.889	0.050	5.53E-1	3.70E-1	0.1007	0.2302	2.608	0.2165	0.2288	2.871	0.0000	0.0531	0.000	0.000	0.0000
		1.21720E+08	3.095	3.647	1.576	8.306	4.020	0.010	4.84E-1	4.78E-1	0.1007	0.2302	2.670	0.2178	0.2283	2.877	0.0000	0.0586	0.000	0.000	0.0000
		1.21894E+08	3.154	3.638	1.480	8.351	4.167	0.001	4.59E-1	5.12E-1	0.0894	0.2302	2.817	0.2183	0.2268	2.733	0.0000	0.0604	0.000	0.000	0.0000
		1.21909E+08	3.173	3.636	1.455	8.368	4.236	0.000	4.56E-1	5.15E-1	0.0416	0.2302	2.867	0.2185	0.2263	2.150	0.0000	0.1208	0.000	0.000	0.0000
		1.21938E+08	3.272	3.625	1.311	8.405	4.495	0.000	4.56E-1	5.16E-1	0.0000	0.2302	2.986	0.2185	0.2254	2.307	0.0306	0.1449	0.000	1.050	0.0000
E		1.22135E+08	3.381	3.613	1.154	8.431	5.032	0.000	4.56E-1	5.16E-1	0.0000	0.2302	-0.619	0.2191	0.2235	3.376	0.0708	0.1514	0.000	1.321	0.0000
A		1.22250E+08	3.499	3.603	0.996	8.452	5.226	0.000	4.56E-1	5.16E-1	0.0000	0.2304	0.000	0.2191	0.0000	3.490	0.0865	0.1526	0.000	1.556	0.0000
G		1.22336E+08	3.595	3.594	0.866	8.476	5.384	0.000	4.56E-1	5.16E-1	0.0000	0.2304	0.000	0.2191	0.0000	3.582	0.1000	0.1548	0.000	1.774	0.0000
B		1.22416E+08	3.701	3.585	0.722	8.502	5.553	0.000	4.56E-1	5.16E-1	0.0000	0.2296	0.000	0.2191	0.0000	3.684	0.1116	0.1577	0.000	2.048	0.0000
		1.22471E+08	3.792	3.576	0.596	8.523	5.700	0.000	4.56E-1	5.16E-1	0.0000	0.2258	0.000	0.2191	0.0000	3.768	0.1219	0.1605	0.000	2.297	0.0000
		1.22520E+08	3.886	3.562	0.447	8.539	5.863	0.000	4.56E-1	5.16E-1	0.0000	0.2239	0.000	0.2191	0.0000	3.858	0.1345	0.1637	0.000	2.559	0.0028
		1.22559E+08	3.980	3.548	0.294	8.542	6.038	0.000	4.56E-1	5.16E-1	0.0000	0.2219	0.000	0.2191	0.0000	3.946	0.1455	0.1669	0.000	2.824	0.0121
		1.22592E+08	4.072	3.536	0.154	8.526	6.230	0.000	4.56E-1	5.16E-1	0.0000	0.2166	0.000	0.2165	0.0000	4.032	0.1556	0.1711	0.000	3.097	0.0445
		1.22620E+08	4.163	3.527	0.030	8.473	6.439	0.000	4.56E-1	5.16E-1	0.0000	0.1935	0.000	0.1935	0.0000	4.112	0.1645	0.1752	0.000	3.343	0.0708
		1.22639E+08	4.253	3.516	-0.103	8.400	6.613	0.000	4.56E-1	5.16E-1	0.0000	0.1894	0.000	0.1894	0.0000	4.192	0.1717	0.1790	0.253	3.511	0.0938
	10	1.22649E+08	4.304	3.506	-0.195	8.352	6.715	0.000	4.56E-1	5.16E-1	0.0000	0.1884	0.000	0.1884	0.0000	4.237	0.1759	0.1816	0.605	3.590	0.1076
		1.22651E+08	4.313	3.505	-0.210	8.342	6.737	0.000	4.56E-1	5.16E-1	0.0000	0.1883	0.000	0.1883	0.0000	4.246	0.1767	0.1823	0.614	3.606	0.1099

Table 7.3 Life-times and Life-time Ratios (I)

$M/M_\odot$	τ_H	τ_{He}	τ_{He}/τ_H	He/He_i	C/C_i	N/N_i	O/O_i
			Z=0.008,	Y=0.250			
4	169.258	35.698	0.2109	1.104	0.742	2.763	0.903
5	105.827	14.664	0.1386	1.120	0.718	2.946	0.889
6	71.640	8.8328	0.1232	1.132	0.707	3.129	0.875
7	51.559	5.8100	0.1126	1.148	0.677	3.405	0.858
8	39.655	4.4407	0.1120	1.156	0.662	3.546	0.847
9	31.521	3.1156	0.0988	1.164	0.652	3.673	0.837
12	18.093	1.9330	0.1068	1.224	0.616	4.104	0.801
15	12.650	1.4727	0.1164	1.284	0.606	4.392	0.771
20	9.141	0.8290	0.0907	1.360	0.611	4.712	0.726
30	6.379						
40	5.056						
60	3.996						
80	3.742						
			Z=0.020	Y=0.280			
5	101.27	19.21	0.1897	1.105	0.7510	2.588	0.9147
6	67.992	9.586	0.1410	1.190	0.7340	2.734	0.9029
7	48.721	6.103	0.1253	1.130	0.7113	2.965	0.8914
9	28.555	3.233	0.1132	1.143	0.6872	3.209	0.8735
12	17.174	1.8894	0.1100	1.193	0.664	3.613	0.834
15	11.957	1.3169	0.1099	1.236	0.648	3.911	0.807
20	8.426	0.7640	0.0907	1.314	0.615	4.484	0.753
30	6.056						
40	4.874						
60	4.060						

Table 7.3: Life times (in 10^6 years) of the main stages of evolution (see text) for all the models listed in *table* (7.1), and *table* (7.2). Surface enrichment of ^{4}He, ^{12}C, ^{14}N, ^{16}O are given in the last 4 columns respectively

Table 7.4 Life-times and Life-time Ratios (II)

$M_i/M_\odot$	τ_H	τ_{He}	τ_{He}/τ_H	τ_{WN}	τ_{WC}	τ_{WR}/τ_t	$M_f/M_\odot$
			Z=0.008, Y=0.250				
100	2.484	0.390	0.157	0.592	0.270	0.300	12.5
120	2.599	0.410	0.158	0.398	0.243	0.213	12.1
			Z=0.020, Y=0.280				
80	3.577	0.484	0.135	0.405	0.558	0.237	5.7
100	3.357	0.602	0.179	0.644	0.591	0.312	5.6

Table 7.4: The models of very massive stars for the two compositions. The life times are all in units of 10^6 years. The last column gives the final mass of the sequences

Table 7.5 Life-times and Life-time ratios (III)

	Overshoot			Classical Mixing			Comparison Ratios			
$M/M_\odot$	τ_H	τ_{He}	τ_{He}/τ_H	τ_H	τ_{He}	τ_{He}/τ_H	${}^H R_{ov}$	${}^{He}R_{ov}$	${}^H R_{se}$	${}^{He}R_{se}$
				Z=0.008	**Y=0.250**					
4	169.75	23.745	0.140	129.10	42.557	0.330	0.997	1.503	1.311	0.838
5	104.75	10.197	0.097	81.206	18.930	0.233	1.010	1.438	1.303	0.775
6	71.536	5.6120	0.078	57.051	10.171	0.178	1.001	1.574	1.256	0.868
7	52.336	3.5966	0.069	42.559	6.1211	0.144	0.985	1.615	1.211	0.949
9	32.387	1.9975	0.062	26.877	3.0546	0.114	0.973	1.560	1.173	1.020
12	19.830	1.1906	0.060	16.722	1.6371	0.098	0.912	1.624	1.082	1.181
15	14.015	0.8776	0.063	11.970	1.1234	0.094	0.903	1.678	1.057	1.311
20	0.9430	0.6451	0.068	8.3121	0.7766	0.093	0.969	1.285	1.100	1.067
				Z=0.020	**Y=0.280**					
5	103.81	10.94	0.105	81.580	19.41	0.239	0.976	1.756	1.241	0.990
6	68.924	5.566	0.081	–	–	–	0.986	1.722	–	–
7	49.595	3.523	0.071	40.415	5.881	0.146	0.982	1.732	1.205	1.038
9	29.861	1.884	0.063	24.925	2.772	0.111	0.956	1.716	1.145	1.166
12	17.765	1.104	0.062	12.205	1.507	0.087	0.967	1.711	1.407	1.254
15	12.501	0.811	0.065	10.904	1.016	0.093	0.956	1.624	1.097	1.296
20	8.545	0.605	0.071	7.550	0.711	0.094	0.986	1.263	1.121	1.075

Table 7.5: The lifetimes and lifetime ratios of overshoot (instantaneous) and classical models by Fagotto et al. (1993), and lifetime ratios between the present models and those of Fagotto et al. (1993): ${}^H R_{ov}$ is $(\tau_H)_{dif}/(\tau_H)ov$, ${}^{He}R_{ov}$ is $(\tau_{He})_{dif}/(\tau_{He})_{ov}$, ${}^H R_{se}$ is $(\tau_H)_{dif}/(\tau_H)se$, and ${}^{He}R_{se}$ is $(\tau_{He})_{dif}/(\tau_{He})_{se}$.

Table 7.6 Life times and life-time ratios (IV)

Mass/$M_\odot$	τ_H	τ_{He}	τ_{He}/τ_H	τ_{WN}	τ_{WC}	τ_{WR}/τ_t
20	13.956	0.699	0.05	0.3043	0.5987	0.0588
15	21.782	0.829	0.04	0.3302	0.6521	0.0420
12	32.441	1.008	0.03	0.3968	0.7307	0.0328

Table 7.6: Lifetimes and lifetime ratios for the global mixing scheme. The lifetimes are all in 10^6 years. The definition of the WR stages are according to Meader (1992), see also *Section* (4.2). τ_{WR} gives the total WR lifetime. $\tau_t = \tau_H + \tau_{He}$.

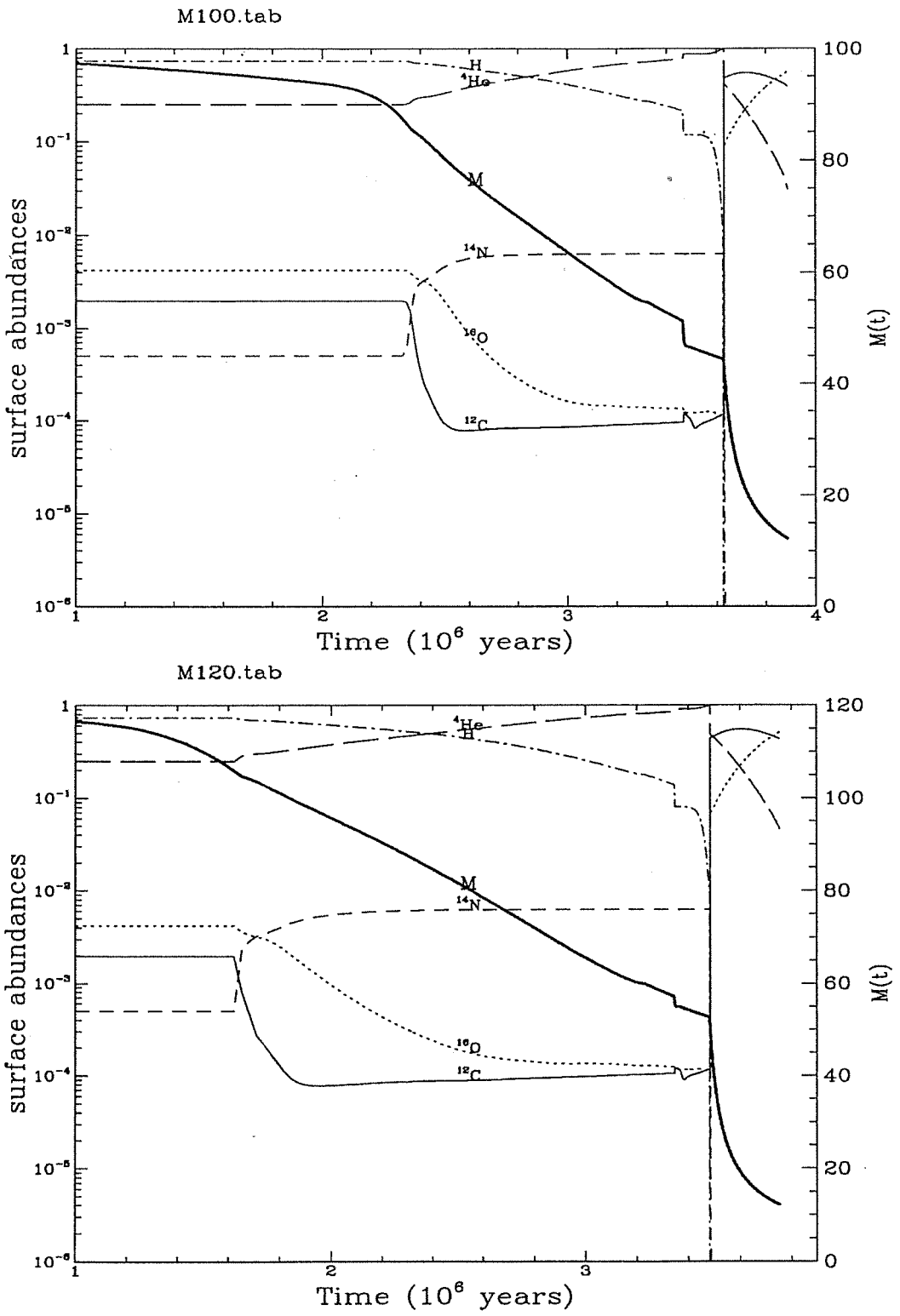

Figure 7.13: The surface abundance changes for the WR models for $Z = 0.008$, the initial masses are $100M_\odot$(the upper one) and $120M_\odot$(lower) the lifetimes and the lifetime ratios are all presented in *table* (7.3)

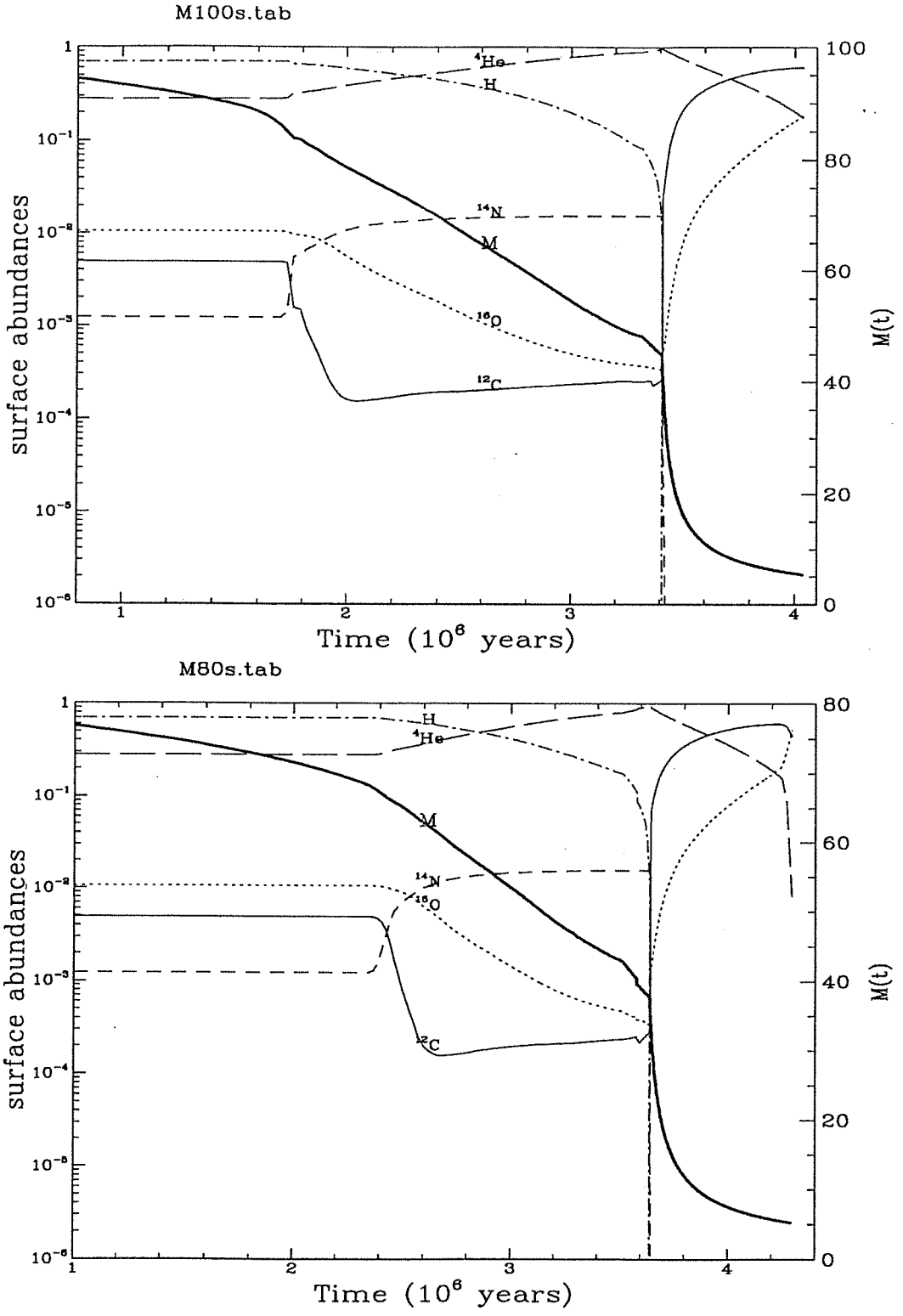

Figure 7.14: The same as *Figure* 7.13 but for $Z = 0.020$, with initial masses of $100M_\odot$(upper),and $80M_\odot$.(lower)

8 New Interpretation of the HRD of Massive Stars

The HRD is the traditional tool to understand the structure and the evolution of stars. Statistically, the ratio of the lifetime spent in different evolutionary phases is directly reflected by the number of stars we count in the different areas of the HRD. This is one of the most important constraints that the theory of stellar evolution must obey. In this chapter, I discuss the HRD of supergiant stars, the observational counterpart of massive stars, in the light of our new models.

8.1 The theoretical HRD

The HRDs for the two compositions have been shown in *Figure* 7.2 & *Figure* 7.1 in *Chapter* 7. The general features noticed in these theoretical HRDS are the wider MSB compared with that for the classical models (see *Figure* 7.5). The width of the MSB is similar to that of models with standard overshoot and $\Lambda_c = 0.5$ (*Figure* 7.3, 7.4). In the luminosity range appropriate to the HRDs of Galactic and LMC supergiants (-7$\leq M_{bol} \leq$-9), our models with solar composition possess blue loops that are somewhat more extended than those obtained by means of the full overshoot scheme, but narrower than those of the classical mixing scheme. In the case of the lower metal content, the models show loops as extended as those of classical mixing scheme by Fagotto et al. (1993). As far as the ratio between the number of post main sequence (PMS) to main sequence stars (MS) is concerned, we already have shown in the previous chapter that the new models generally show a higher He- to H- burning life-time ratio. These general properties are basic to the interpretation of the distribution of star

counts across the observational HRDs.

8.2 PMS/MS & BSG/RSG ratios

From the observational data of supergiant stars one may easily derive the ratio of the number of PMS to MS stars and the ratio of the number of blue-supergiants (BSG) to that of red-supergiants (RSG). The theoretical predictions for star counts derived from evolutionary sequences up $20M_{\odot}$ are presented in *table* 8.1, namely the theoretical PMS/MS ratios in column (2), the BSG/RSG ratio in column (3), the location in HRD of the tip of the blue loop in columns (4) & (5), the location of the TAMS in the HRD in column (6) & (7). Comparing those data with the corresponding ones contained in *table* 7.3, we see that the remaining lifetime spent beyond the main burning phases is negligible.

PMS/MS: The observational values for this ratio have been published by Blaha & Humphreys (1989) for the sample of galactic and LMC supergiants (see also *Chapter* 4). For stars in the magnitude interval -7< M_{bol} <-9, Blaha & Humphreys (1989) report that about 40% of these are observed beyond the MSB. This latter is defined by means of the tracks of Maeder & Meynet (1987), whose TAMS lies around $\log T_{eff}$=4.4 at M_{bol}=-8, i.e. for stars of about 20-25$M_{\odot}$. This corresponds to a PMS/MS ratio of the oder of 2/3.

Since the evolution of massive stars proceeds at almost constant luminosity after the MS, no matter whether or not they perform blue loops (Chiosi & Maeder 1986), the number of stars found beyond the MSB has to be accounted by progenitors populating the same luminosity range on the MS. The contribution to the RSG populations from stars of lower mass, such as intermediate mass stars evolving along the AGB phase, is expected to be negligible (Chiosi et al. 1992). In brief, the theoretical analog of the ratio PMS/MS is τ_{He}/τ_{H} (with a very little correction to τ_{He} to account for the additional time of PMS star counts for phases later than core He-burning). The ratios expected from classical models differ from the observed values by a factor of about 2 to 3 for stars more massive than about $12M_{\odot}$.

Indeed this difference is highly embarrassing because the lifetimes are known to depend

Table. 8.1 Lifetime & lifetime ratios (V)

$M/M_\odot$	PMS/MS	BSG/RSG	Loop-tip		TAMS	
			$\log L/L_\odot$	$\log T_{ff}$	$\log L/L_\odot$	$\log T_{ff}$
Z=0.008						
4	0.261	3.637	2.7811	3.8030	2.6968	4.1045
5	0.161	2.092	3.2847	3.8910	3.0978	4.1589
6	0.138	1.939	3.6100	3.9740	3.3910	4.2050
7	0.127	2.076	3.8636	4.0325	3.6321	4.2413
8	0.122	2.243	4.0729	4.0729	3.8442	4.2694
9	0.109	1.671	4.2454	4.1040	4.0178	4.2938
12	0.117	4.060	4.5899	4.2002	4.4018	4.3478
15	0.127	8.640	4.8432	4.2617	4.6839	4.3798
20	0.097	6.676	5.1765	4.2847	5.0475	4.3784
Z=0.020						
5	0.222	1.152	3.0496	3.7394	3.0417	4.1225
6	0.151	1.683	3.4623	3.8301	3.3636	4.1693
7	0.135	1.263	3.7668	3.8916	3.6231	4.2073
9	0.148	1.528	4.2056	3.9597	4.0243	4.2629
12	0.109	1.037	4.6001	4.0413	4.4382	4.3140
15	0.100	1.214	4.8618	4.0969	4.7160	4.3430
20	0.094	0.650	5.1957	3.9624	5.0749	4.3114

Table 8.1: The PMS/MS, BSG/RSG ratios and the maximum extension of the blue loop and TAMS for all the models described in *Chapter* 6.

on the amount of nuclear fuel available to each burning stage, and current understanding of the stellar evolution cannot alter the lifetimes as much as suggested by the observational PMS/MS ratio. The key point is obviously the location of the red boundary of the MSB, because the observations give only the number distribution of stars in the HRD. As suggested by several authors a much wider MSB is a way out (Bressan et al. 1981, Bertelli et al. 1984). Wider MSBs can be obtained in several ways. Convective overshoot was invoked by Bressan et al. (1981) and Maeder & Mermiliod (1982) because the extension of the MSB increases with the overshoot distance (up to a certain limit). Bertelli et al. (1984) also suggested a modification of the radiative opacities in the CNO ionization region. It was found that enhancing the radiative opacity there (bump-like structure) could extend the MSB all the way across the HRD. However, such modification of the opacity, although present in recent opacity calculations (Rogers et al. 1992) occurs too far out in the star to affect the extension of the outermost region. The problem is still under debate.

BSG/RSG ratio: This ratio reflects the different lifetime spent by the stars as blue and red supergiants. Presenting the data of *table* 8.1 we have assumed $\log T_{Eff}$=3.7 as the divide between the blue and red parts of the loop. The exact value is less of a problem, because both the observed HRDs for Galactic and LMC supergiants and the theoretical HRD possess a clear gap at about this effective temperature. The term 'blue' should not be mistaken: we have included all the He-burning lifetime spent at temperatures higher than $\log T_{eff} = 3.7$. Once more, the star counts by Blaha & Humphreys (1989) show that this ratio is about 10, in agreement with the data of massive star of *table* 8.1 for the metallicity Z=0.008, but not with the data for the metallicity Z=0.02. It is worth noticing however that the theoretical lifetime depends also on details of stellar physics, such as the $^{12}C(\alpha,\gamma)^{16}O$ reaction rate and the efficiency of envelope overshoot.

8.2.1 The blue loop

The blue loop is a common feature to all diffusive models in the mass range suitable for the HRDs of supergiant stars. The loop are generally more extended for the lower metallicity in agreement with the general understanding of morphology of the loops at varying metallicity (Stothers & Chin 1991). Our models with $Z = 0.020$ predict loops whose extension is narrower that required by the HRD of Blaha & Humphreys (1989). In the case of the lower metallicity, our models of 12-20$M_{\odot}$stars have loops which extend beyond $\log T_{eff}$=4.2. At increasing mass the loops get more luminous and hotter. They define a diagonal region in the HRD whose red limit well matches the so-called 'ledge' observed by Fitzpatrick & Garmany (1990) in the HRD of LMC supergiant stars.

8.2.2 Surface abundances

We have already reported upon the variations in surface abundance occurring in our models after the first dredge-up along the Hayashi track (*table* 7.3). The amplitude of this variation is determined by the depth of the convective envelope. With the adopted amount of overshoot from the bottom of convective envelope, the abundances are slightly increased and in agreement with the observations by Fitzpatrick & Bohannan (1992) for blue supergiants (stars in the loop in our scheme). These authors reported a surface enhancement of about 3 for ^{14}N 1.1 for H, and a depletion to about 0.9 and 0.66 of the original value for the ^{16}O and the ^{12}C respectively. These values must be compared with the abundances listed in *table* 7.3.

8.3 Numerical simulation: synthetic HRDs

Having discussed the main properties of the evolutionary tracks we try to understand the global morphological properties of the HRD by means of synthetic simulations obtained with the new models and the Monte Carlo technique.

The simulations are first performed at fixed composition and then with a spread in the

	M_{bol}	MS	PMS	$R_{PMS}(\%)$
	-7– -8	155	133	46.18
Z=0.008	-8– -9	182	69	27.49
	-7– -9	337	202	37.47
	-7– -8	222	112	33.53
Z=0.020	-8– -9	166	61	26.87
	-7– -9	388	173	30.84
	-7– -8	189	123	39.39
ALL	-8– -9	174	65	27.20
	-7– -9	363	188	34.09

Table 8.2: PMS/MS ratios in various luminosity intervals. MS is the number of stars counted for temperature higher than $\log T_{eff} = 4.3$, while PMS is number of stars cooler than this limit. The first column indicates the HRD on which the counts have been performed.

initial composition mimicking inhomogeneities of the interstellar medium. Finally we tested the effects of possible observational errors, especially in the conversion of the color into effective temperature (see Chiosi et al. 1992).

The numerical simulations are made according to the following prescription. About 1500 stars are randomly distributed HRD assuming continuous star formation in the age range 10^8 yr to 10^5 yr, the Salpeter initial mass function (with slope -2.35 by number), and a cutoff at the absolute visual magnitude M_V=-4.5. This magnitude corresponds to the completeness limit quoted by Fitzpatrick & Garmany (1990). The synthetic HRDs contain roughly as many stars above the completeness limit (RSG excluded) as those counted by Fitzpatrick & Garmany (*Figure* 4.2, page 36) in the observational HRD for the LMC supergiants.

The simulated HRD for $Z = 0.008 and Y = 0.250$ is shown in *Figure* 8.1, while that for $Z = 0.020 and Y = 0.280$ is presented in *Figure* 8.2. *Figure* 8.3 is a superposition of the previous HRDs, with equal wight assigned to the two compositions, no observational errors, and the total number of 1500 stars. The heavy solid lines in all the simulated HRDs correspond to the Fitzpatrick & Garmany (1990) incompleteness limit of M_v=-6.

table 8.3 gives the star counts from our synthetic HRDs. The boundary separating MS from PMS stars is set at $\log T_{eff} = 4.3$. The numbers of stars in the MS and PMS phase

are listed together with the percentages of PMS stars in the luminosity intervals of (-7– -9), (-7– -8) and (-8– -9) in M_{bol}. While these number ratios fairly agree with the star counts for PMS/MS stars given by Blaha & Humphreys (1989) for the solar vicinity. However, considering that the simulation are meant to reproduce the HRD of the LMC and that they are obtained by assuming a significant incompleteness in the main sequence stars (indeed the cutoff at M_V=-4.5 almost excludes half of the main sequence lifetime of a model of $20M_\odot$), the true PMS/MS ratio one has to look at is the ratio τ_{He}/τ_H reported in *table* 7.3, for the luminosity level at $M_{bol} = -8.5$. This comparison suggests that if the models are correct, about half of MS stars are still missing from the sample.

8.4 The blue gap

The blue gap arises from the theoretical inability of predicting any stationary phase in the region just to the right side of main sequence. Actually no scenario is able to produce such high number density of stars as that seen in the HRD of LMC and, to a lesser extent, in the HRD of the solar vicinity shown in *Chapter* 4. The theoretical calculations performed to investigate this problem are made at a given composition, but this condition if true for a very strictly coeval group of stars such as those of a single cluster, may not be applicable to samples of stars such those of our HRDs. As a matter of facts, the HRDs on consideration, in particular the one for the the LMC, are from a large sample of stars which most likely do not have the same chemical composition. All existing models (Meader & Maynet 1989, 1990; Schaller et al. 1992; Bressan et al. 1993; Fagotto et al. 1993) show that the evolutionary patterns vary considerably at changing the initial chemical composition. In brief, stellar models with high metal abundance reach lower effective temperatures during the central H-burning phase, and produce narrower loops. The opposite is true for low metal abundances.

In our computations the high metallicity models stretch their MSB up to $\log T_{eff}$=4.37 on the main sequence, whereas the low metallicity models extend their loops up to $\log T_{eff}$=4.3. As indicated by the error bar in *Figure* 4.2, the uncertainty in this region is around 0.1

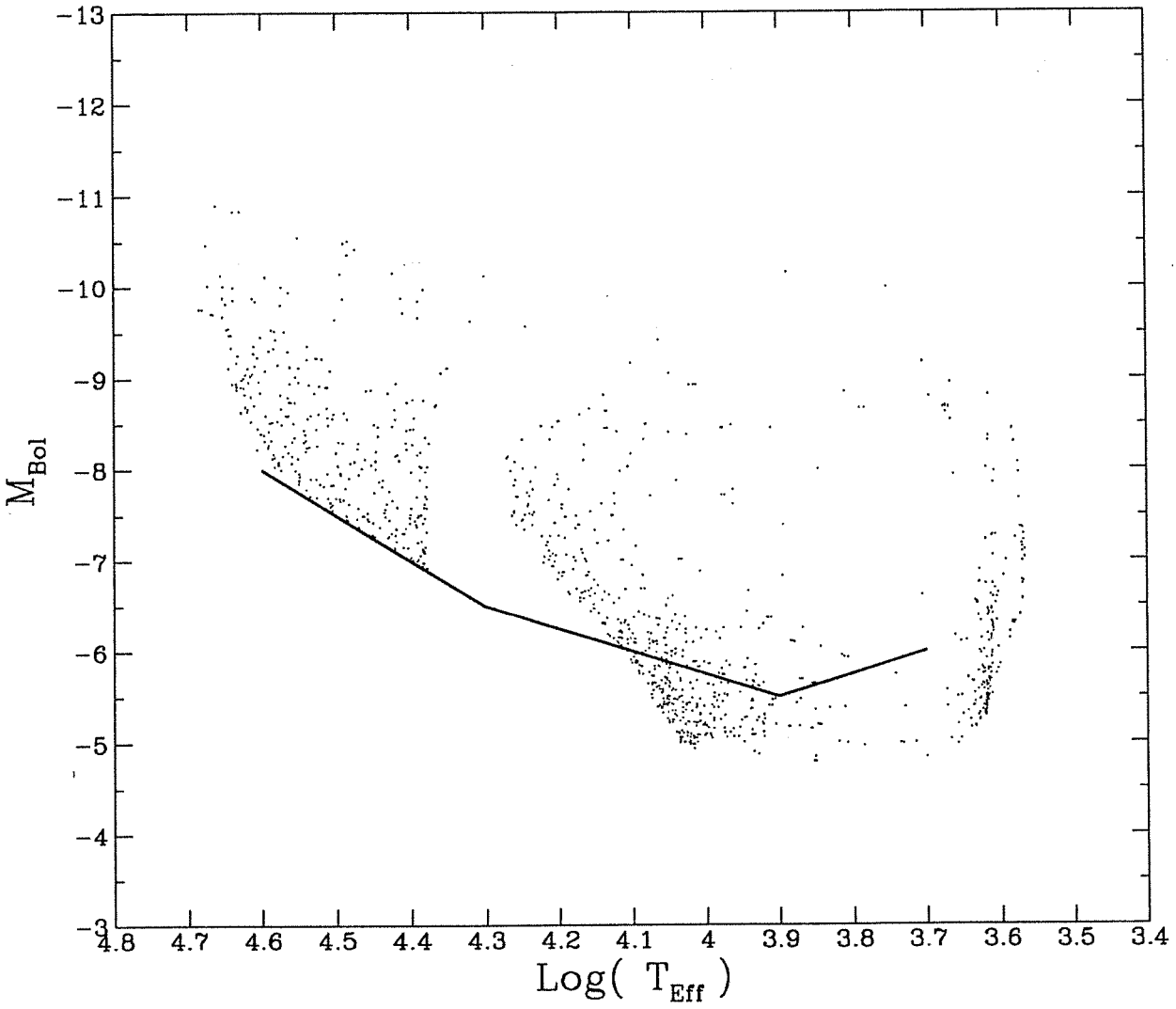

Figure 8.1: The synthetic HRD for $Z = 0.008$. The theoretical sequences in used are those of the set shown in *Figure* 7.1. This simulation is obtained with the Monte Carlo Method technique. 1500 stars of random age and mass are injected above the completeness limit (solid line) by Fitzpatrick & Garmany 1990), assuming continuous star formation and the Salpeter (1955) initial mass function.

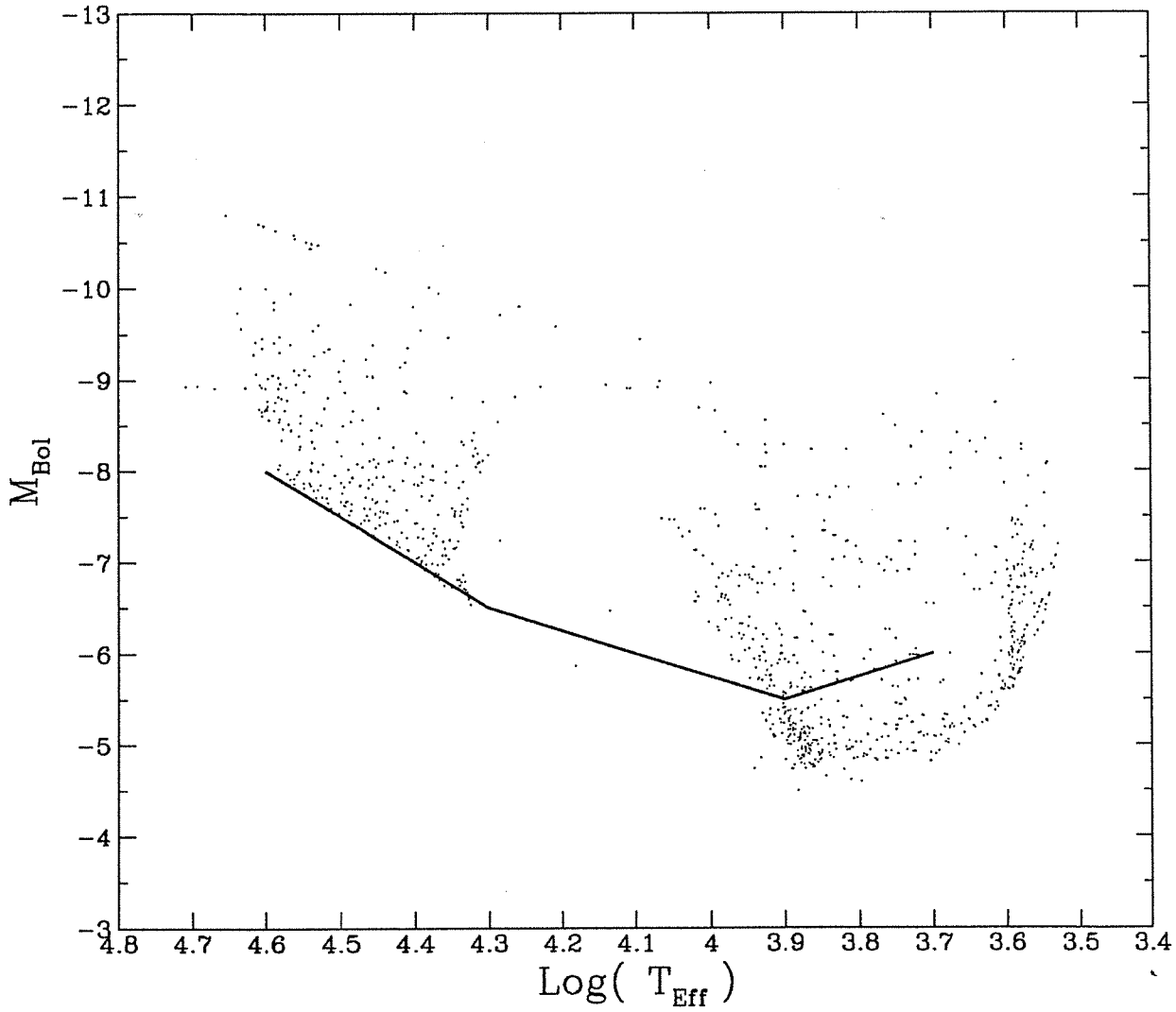

Figure 8.2: The same as *Figure* 8.1, but for $Z = 0.020$

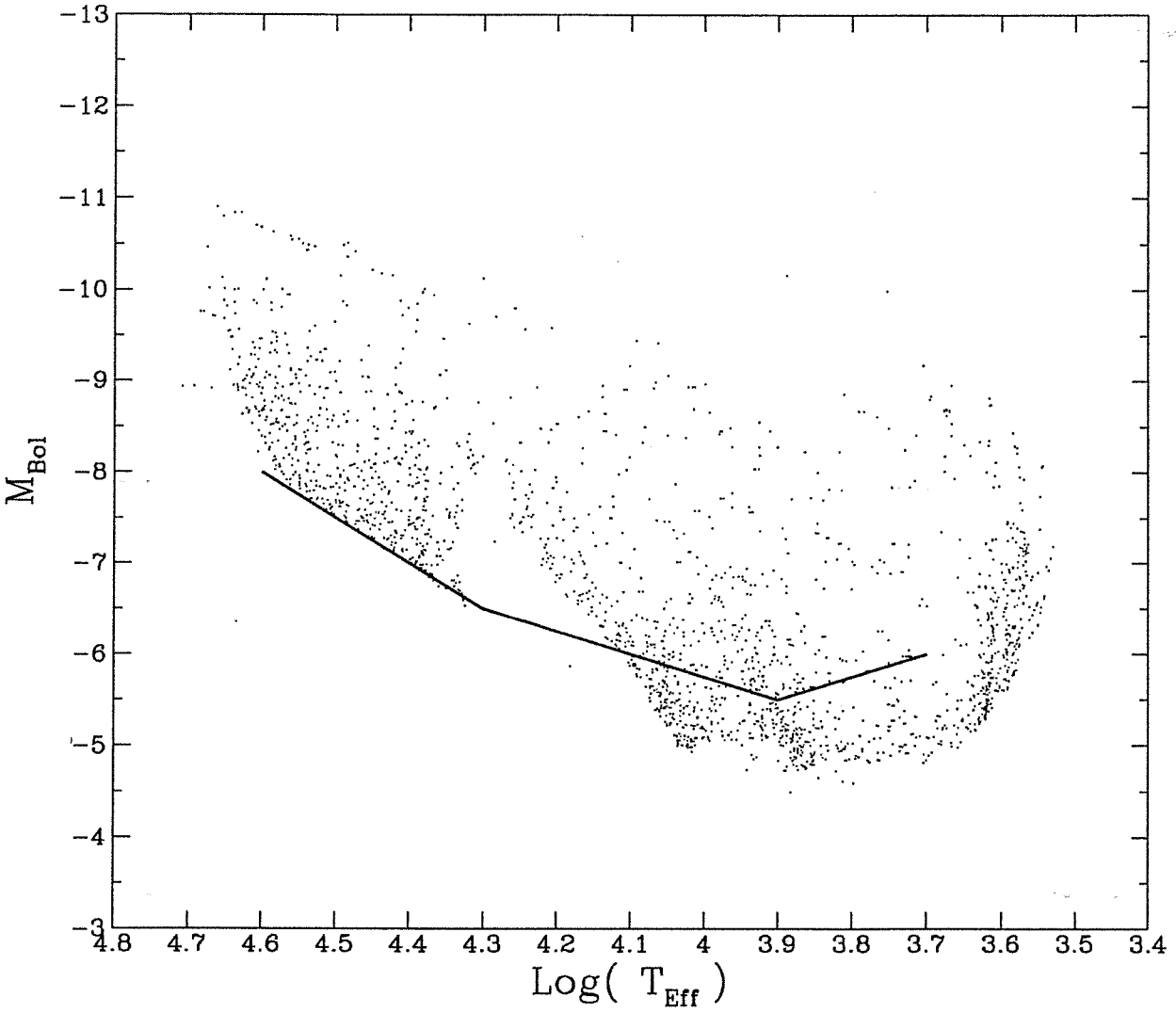

Figure 8.3: A synthetic HRD for LMC Supergiants. This is obtained by superposing the synthetic HRDs for the two metallicities. The blue gap is significantly reduced.

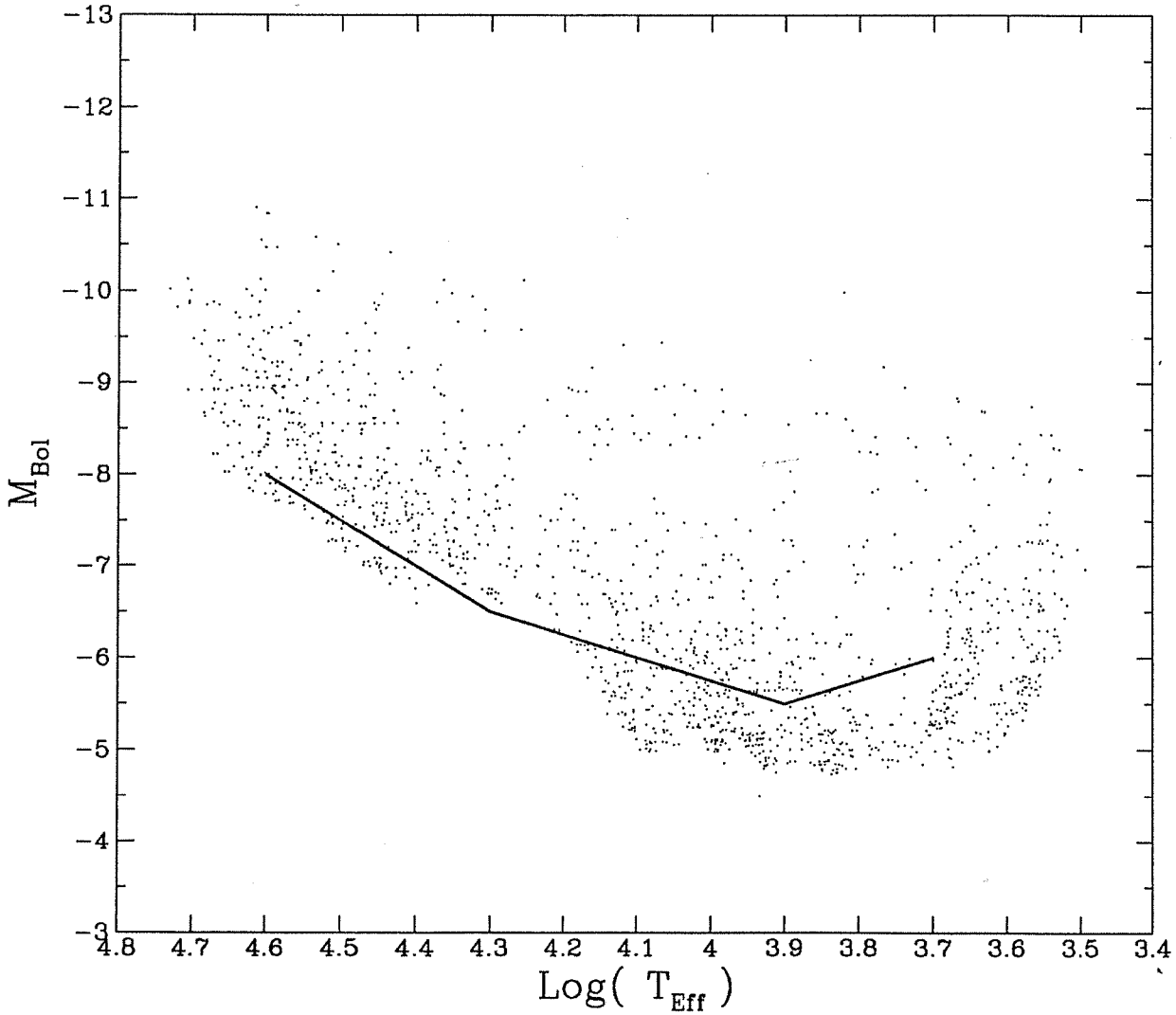

Figure 8.4: The same as *Figure* 8.3, but with assuming an error in $\log T_{eff}$ of 0.04.

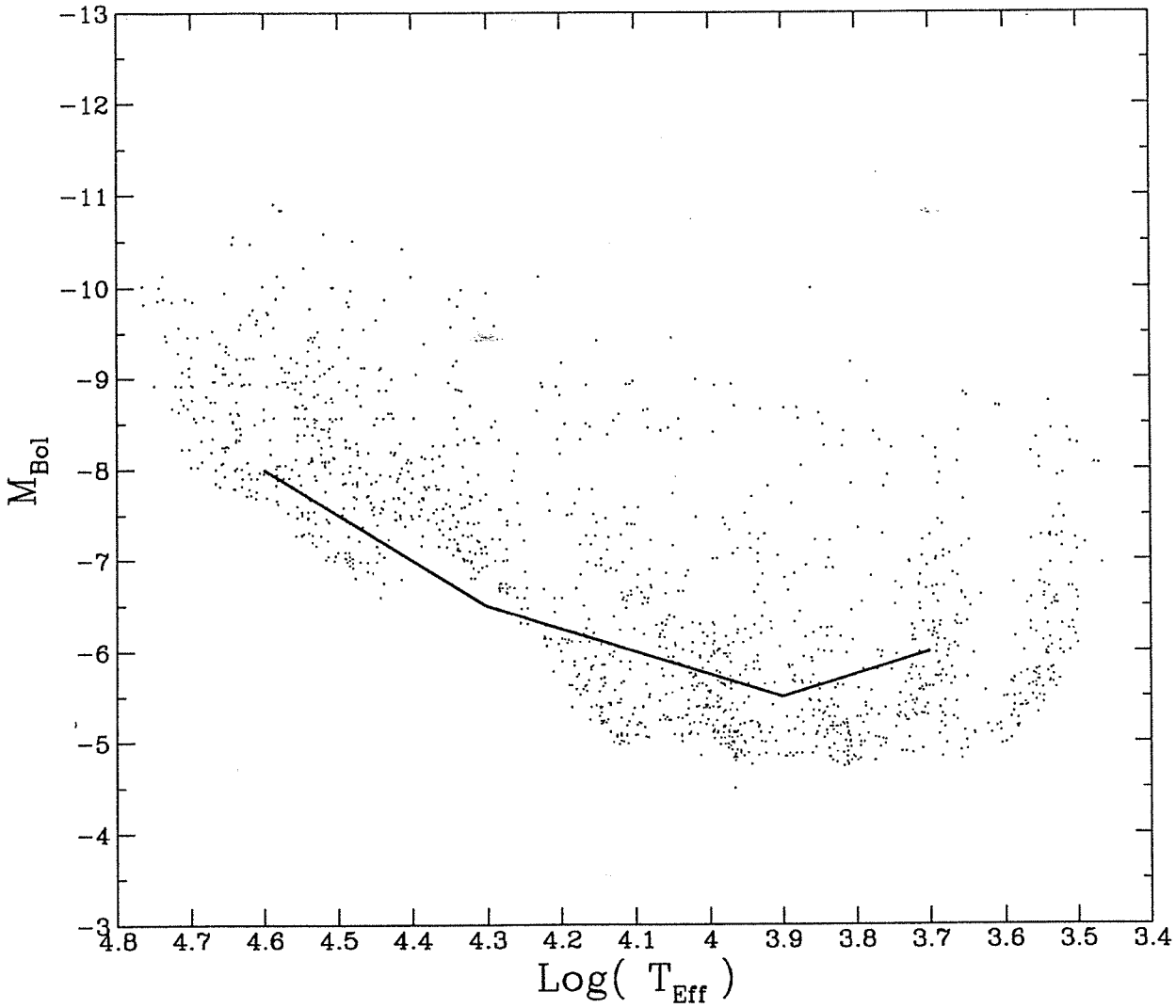

Figure 8.5: The same as *Figure* 8.4, but with an error in $\log T_{Eff}$ of 0.08.

in $\log T_{eff}$. Therefore, if any spread in the metallicity is present in the observed sample, the gap could be masked by the quoted observational errors (see also Chiosi et al. 1991). As a preliminary attempt to evaluate the above effect, we plot in *Figure* 8.6 the lifetime distribution from our $20M_{\odot}$sequences with the two compositions. The distribution of the lifetimes is binned in intervals of $\Delta \log T_{eff} = 0.05$. As we can see, not only the gap has disappeared but also the luminosity function of the ledge of blue stars in Fitzpatrick & Garmany (1990) is well modeled.

This interpretation of the absence of the gap is supported by the observational data of the blue supergiant abundances presented by Fitzpatrick & Blaha (1992). Specifically, the high metal content stars (with original surface abundances), which contribute to the blue side of gap due their cooler TAMS, are exactly in the same proportions as expected from considering the belonging to the metal poor population.

To extend the comparison further, we assigned the data of 8.3 a random error of $\Delta \log T_{eff}$=0.05 and $\Delta \log T_{eff}$=0.08, to account for the observational errors which are known to affect the original data (see *Chapter* 4). The results are shown in *figures* 8.4 and 8.4 respectively. The most remarkable feature is that the distribution of stars, especially the in the blue gap, becomes continuous from the zero age main sequence to the blue edge of the red Hertzsprung gas. Furthermore, the larger the error, the more invisible the blue gap (see *Section* 4.1.2 and compare with *Figure* 4.2). The larger error is compatible with the estimate given by Fitzpatrick & Garmany (1990). These simulations show that our models fit well the morphology of the observed HRD for the LMC supergiants.

It is worth emphasizing that the new models can reproduce the the morphology of HRD much better than previous models. Indeed Langer (1989) did the same fitting with his semiconvective diffusion models, and to simulate the HRD he used a much larger error on the effective temperature but the blue gap is still clearly visible in his HRD. The obvious implications is that Langer's models that were specifically designed to explain the blue progenitor of SN1987A, cannot explain at the same time the distribution on the HRD of the

bulk population of supergiant stars.

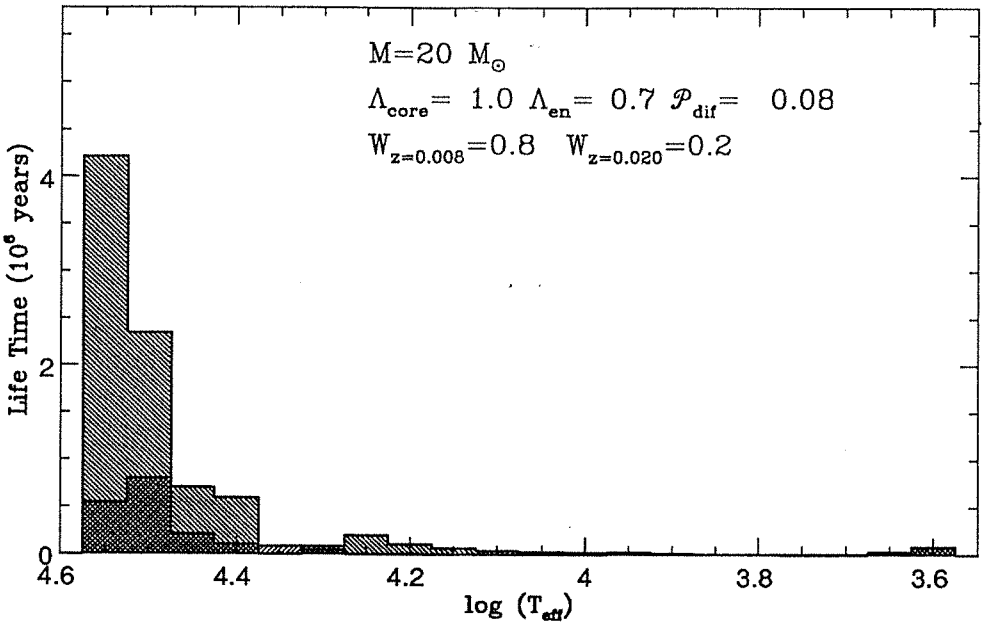

Figure 8.6: Lifetime distributions of the $20M_{\odot}$star models with two metallicities. The distribution is binned in $\log T_{Eff} = 0.05$ (which approximately corresponds to the uncertainties in $\log T_{eff}$ of the observational data. The transversally drawn lines from upper left to the lower right show the low metallicity models, the other lines show the high metallicity ones. Each model is assigned a relative weight of 0.8 and 0.2 as indicated in order to account for the spread in the metallicity in the LMC stars. The gap has disappeared, and lifetime distribution well reproduce the luminosity function at the the ledge (see the text for more details).

8.5 The nature of the WR stars

In the current evolutionary scenarios, WR stars are considered as bare He cores left over by massive stars, which have lost their H-rich envelope by heavy mass loss (see the review by Maeder 1992). From a theoretical point of view, the initial mass of these stars able to reach this configuration, cannot be smaller than about 30-40$M_{\odot}$(Schaller et al. 1992). The variations of surface abundances in the course of can explain the observed pattern of abundances. Despite this, there are many obscure aspects that do not allow us to get full understanding of this class of stars. Whether the lack (little evidence) of C in WN stars and of N in WC and WO stars reflects real underabundances of these elements, or instead is the result of unusual excitation conditions in their atmospheres, is still controversial, even if

the evolutionary interpretation is presently favored (Willis 1982). Detailed analyses done by Nugis (1975, 1982) and Smith (1973) support the chemical anomaly hypothesis.

Furthermore, the current evolutionary models cannot explain the low luminosities and rather low effective temperatures assigned to most of these stars. Indeed with the initial masses that able to generate bare He-cores the evolutionary tracks usually possess too high luminosity, and are the too blue to fit the observational data. *Figure* 8.7 present the current observational status of the galactic WN stars (Hamann et al. 1993).

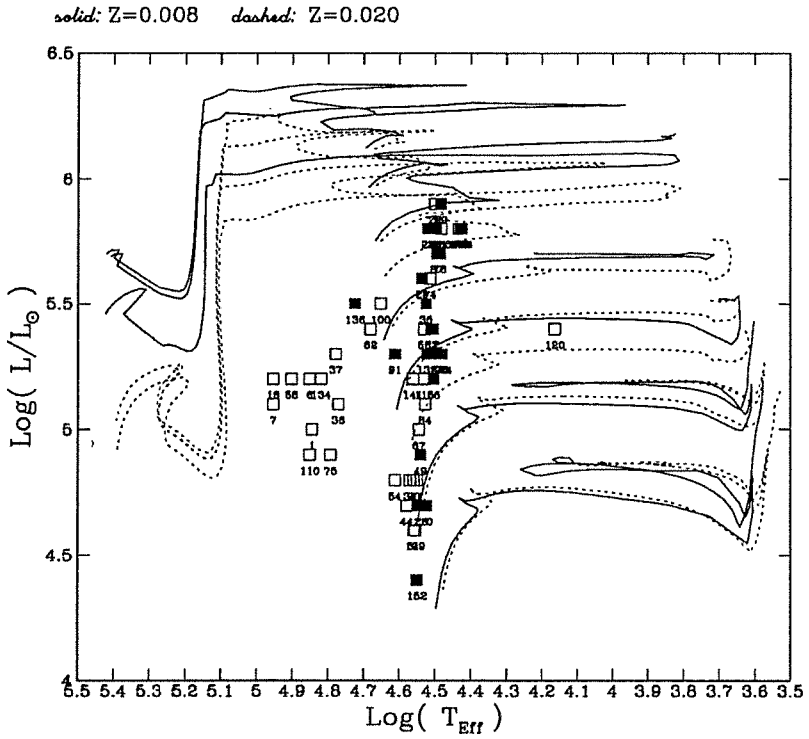

Figure 8.7: The population of the galactic WN stars. Open symbols are stars without any evidence of hydrogen in the atmospheres, while the solid symbols are stars with hydrogen detection. The data are reproduced from Hamann et al. (1993) (for the present purpose of qualitative comparison, the other details about the classification of their objects are not shown). Superposed are the models with diffusive mixing and the metallicities Z=0.008 (solid lines) and Z=0.02 (dotted lines).

Our models of massive stars with both compositions and diffusive mixing evolve to the stages where the chemical signatures of the WR stars appear, but their location in the HRD is systematically too bright and too blue. Similar discrepancy was noticed Hamann et al. (1993) comparing their data with the models by Schaller et al. (1992) with standard overshoot.

The discrepancy in the luminosity is particularly difficult to eliminate, while that in the effective temperature can be cured by by applying the well known correction to the model effective temperature in order to take into account the effects induced by the departure from hydrostatic equilibrium in the real atmospheres of WR stars. Indeed the photosphere of an expanding envelope could be different from that of an hydrostatic model, namely at larger radii and hence cooler effective temperatures (Bertelli et al. 1984; Maeder 1987, 1993; Hamann et al. 1993)). However, it is worth recalling that extended atmospheres are found only in WNE stars with strong emission lines. The most serious difficulty is with the luminosity, because the current models of massive stars cannot evolve into the region where the majority of the WR stars are found (*Figure* 8.7). Furthermore, limit of initial mass around $40M_{\odot}$that its required to get the desired surface abundances in the bare core scheme, cannot is in conflict with the luminosity of the vast majority of WR stars if generated by single, losing mass objects.

The situation is much better using models with global diffusion (see the discussion in *Chapter* 6. As a matter of facts, the evolutionary behaviour of models with lower mass is very promising. *Figure* 8.8. shows the HRD for the global diffusion models for of 12, 15, and $20M_{\odot}$ stars on which the data for WN stars by Hamann et al. (1993) are superposed. The dotted line indicates the start of the WNL phase, while the dashed line indicates the start of WC phase of the models.

This comparison is only avery preliminary one, because our global mixing models are computed with metallicity Z=0.008 which is not suited the Galactic WR stars.

Without correcting the effective temperature, the WN phase is very close to the positions of WN stars. Even more important is the luminosity of these models. The 12 $M_{\odot}$track starts the WNL phase at a luminosity as low as $\log L/L_{\odot}$=5, which is the lowest luminosity for the WNL stars in the sample. As pointed out by Chiosi & Maeder (1986), the mixing process is one of the most important mechanisms for WR formation. The models with global diffusion could be the extreme case, which if occurring in nature, could produce WR stars even for

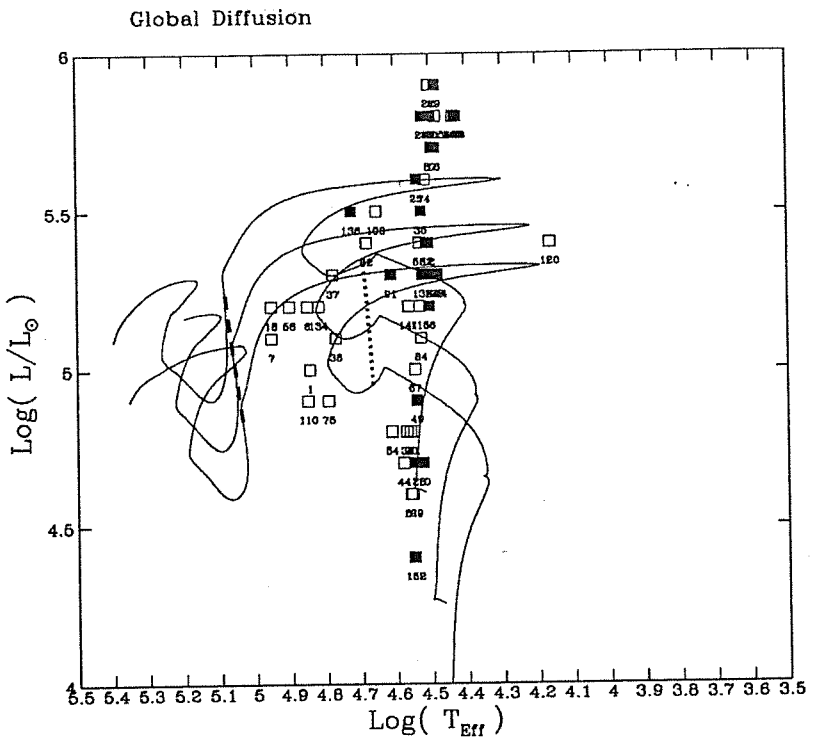

Figure 8.8: The global diffusion models compared to the Galactic WN stars from Hamann et al. (1993). The dotted line shows the start of WNL phase, while the dashed shows the beginning of the WC phase.

initial masses much lower than those of the standard scenario. This problem and the global mixing hypothesis deserve further investigation.

8.6 The progenitor of the supernova SN1987A

As far as this problem is concerned, even our models with diffusive mixing cannot provide the desired blue progenitor, as all they do not have the required effective temperature at the stage of CO core contraction. The reason for which a blue progenitor can be formed are not easy to understand.

The failure of the present models to account for the blue progenitor of SN1987A can be attributed to computational details adopted in this study. More precisely, after core He-burning, diffusive mixing has been switched off to save computing time and the models calculated with instantaneous mixing. The possibility remains that a more accurate treatment of the shell and envelope convection in all stages beyond central He-exhaustion yield the

desired model, namely a star ending its evolutionary history as a blue supergiants. More work is required to elucidate the point.

9 Summary and Conclusions

In this study we have presented a new treatment of mixing in convective regions going from central cores, external envelopes, and intermediate shells. Key points of our analysis are the diffusion description, the new formulation of the diffusion coefficient, and the mixing time scale. We find that in a convective regions two regimes can be identified. Taking the convective core as an example we distinguish the central region, in which both the high diffusion coefficient and the physical properties of convection secure full mixing, and the surrounding region of overhsoot in which according to the value of the diffusion coefficient we go from the case of virtually no mixing (like to a radiative structure) to full mixing (like in standard treatments of overshoot. The same considerations apply to the convective envelope and the intermediate convective shell if present The size of the overshoot region from the core and the envelope is obtained from the formalism of Bressan et al. (1981) and Alongi et al. (1992), respectively, adopting $\Lambda_c = 1.0$ for the former and $\Lambda_{env} = 0.7$ for the latter.

With aid our the above scheme we have computed two sets of stellar models for intermediate and high mass stars with chemical compositions of Z=0.008 Y=0.250 and Z=0.020 Y=0.280.

We find that adopting a mild efficiency of the mixing process for the region of overshoot ($P_{dif} = 0.04$ in our formalism) the models possess at the same evolutionary characteristics that were separately typical of model calculated with different schemes. In other words, the new models share the same properties of models with standard overshoot, namely a wider main sequence band, higher luminosity, and longer lifetimes, but at same time they also possess extended loops that are the main signature of the classical (semiconvective)

description of convection at the border of the core.

These models have been applied to understand the properties of the HRD of Galactic and LMC supergiant reaching unprecedented level of agreement. In particular, we call the attention on the explanation of the many stars falling in the so-called blue gap of the HRD. In addition to this we addressed the problem of the location in the HRD of WR stars, and with the aid of a new class of stellar models based on the global diffusion mechanism we got satisfactory good agreement with the observational data.

9.1 Concluding Remarks on the Diffusive Models

We conclude this study with short comments on the results obtained and how the compare with those from different mixing schemes.

1. The lifetime of the core H-burning phase is the same in models with full efficient overshoot. Recalling that $\Lambda_c^{dif}/\Lambda_c^{ov}$=2 this means that with the adopted P_{dif} the mixing rate is about is about 50% for the standard models (see *table* 7.5, on page 117).

2. With the same value of P_{dif}, the mixing rate during the core He-burning phase is higher. This fact combined with a lower luminosity for the whole phase imply a longer lifetime compared to the models with standard overshoot: $\tau_{He}^{dif}/\tau_{He}^{ov}$ is about 1.5.

3. As a result of item 1) and 2), the lifetime ratios for our models turn out to be 20-50% higher than in the case of full overshoot with $\Lambda_c = 0.5$. Our lifetime ratios of the two main burning phases lie in between those of full overshoot and classical models. This ratio is in close agreement with the value inferred from from observations of the young populous star clusters of the LMC.

4. The loops are in general more extended than those of the standard overshoot models. With the solar metallicity they are slightly narrower than those of the classical semi-convective models, while for the lower metallicity the loops are as extended as those

of the semiconvective models. Our models rule out a point of embarrassment of the standard overshoot models, namely their narrow blue loops.

5. The MSB is slightly narrower (*table* 8.1, on page 123) compared to that with standard overshoot even if the core H-burning lifetime is the same. In any case, the MSB is much larger that that of the semiconvective models.

6. Since our calculations were performed for initial masses down to 4 $M_{\odot}$, it is interesting to have look

   The critical mass M_{up} separating massive from intermediate mass stars which distinguish intermediate and massive stars is the same as that of models computed with full efficient overshoot and same Λ_c. The value of M_{up} is about $5M_{\odot}$. This confirms the conclusion of point 5).

9.2 Perspectives of Future work

The mixing scheme presented in this study ought to be considered as still preliminary and subject to many future implementations. Nevertheless, the present study brings into evidence the main feature of stellar models undergoing incomplete turbulent mixing. The crucial assumptions of our scheme are the dimensions of the the turbulent region expressed as function of the pressure scale hight and the use of P_{dif} as a parameter. Therefore also these models require an accurate comparison with the observational data to fix the dimensional scale of mixing and the diffusion efficiency.

It would be desirable to devise a scheme in which the diffusive efficiency alone determines both the spatial and the temporal behaviour of the mixing process. Considering that a fully satisfactory theory of stellar convection is not yet available, possible lines to tackle the problem are

- Treat mixing together with thermodynamics, and look for a parameter accounting both for overshoot and mixing efficiency consistently.

- Get rid of overshoot distance and find another type of diffusion coefficient. A limit to overshoot outside the classical border of the convective region can be defined automatically when mixing gets negligible.

Concerning the first point, we plan to derive an expression for the diffusion coefficient from the detailed thermodynamic treatment of the field of convection, and to solve the problem of mixing of chemicals separately from the physical structure. In such a case, the complications brought about by the chemical elements (as discussed in *Section* 3.3) can be removed. There should be some suitable relation between the diffusion coefficient and the internal structure of the stars allowing us to get rid of the parameter P_{dif} used in this study. Hopefully, such a dependence of the diffusion coefficient on the thermodynamical structure of the turbulence could be derived from the sophisticated theories of turbulent convection by Gough & Weiss (1976), Xiong (1985), Canuto Mazzitelli (1991), and Canuto (1992, 1993). At the same time, it should keep an affordable level of complicacy to be applied to stellar model calculations.

The second point is more easy to solve. With our assumptions for the mixing process, i.e. that mixing of chemicals is carried out down to the smallest scales, while the bulk of the thermal energy is dominantly carried away the large scales in the convective field, we can try to separate mixing from energy transfer. There are already suggestions about the possible transfer coefficient for the slower mixing process. Maeder (1992) suggested a diffusion coefficient with a linear dependence on the radiative diffusion coefficient. But he limited himself to considering the diffusion coefficient for the semiconvective case with particular attention to the problem of the blue precursor of the SN1987A. As we have discussed in *Section* 7.5, the radiative diffusion coefficient grows from center to the surface which, by itself, cannot help to set a natural boundary.

However from the inspection of our numerical results we notice that the difference between the radiative and the adiabatic gradient could be used to infer the overshoot distance from the star structure itself. This difference is shown in *Figure* 9.1, where we see that difference from its value at the classical core boundary keeps almost constant as the star evolves. The

difference between the two gradients is a measure of the buoyancy force when the molecular weight gradient ignored (Bressan et al. 1981). Taking this quantity as a measure of the overshoot distance would allow us to define the boundary of the overshoot distance having the desired dependence on the stellar mass. As proposed long ago by Massevitch & Popova (1979), a fixed value along the contour map yields a relative amount of mass in the region of overshoot that decreases with the stars mass. In such a case, the divergence of the mixed region at decreasing stars mass, a problem encountered by Aparicio et al. (1990), Maeder et al. (1992) and Bressan et al. (1993) and solved modify the overshoot parameter for masses below about 1.6 $M_{\odot}$, should by automatically ruled out.

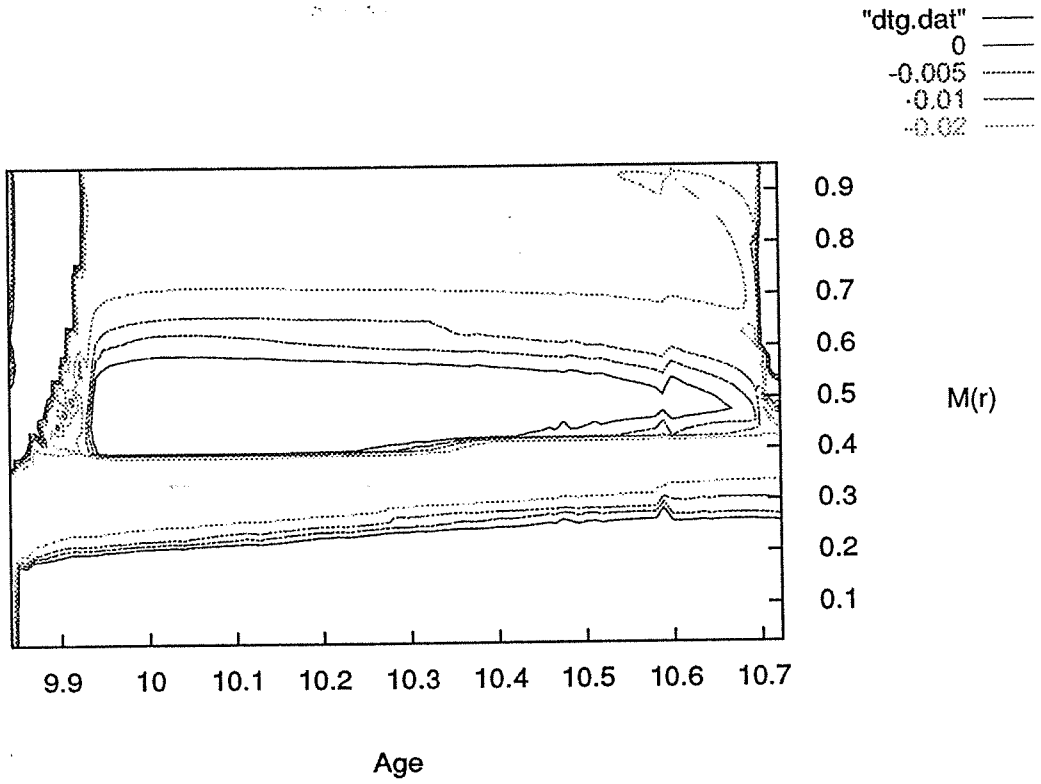

Figure 9.1: The contour plot of $(\nabla_r - \nabla_{ad})$ for the $20M_\odot$star with $Z = 0.008$ $Y = 0.250$ during the core He-burning phase. The abscissa is the age in units of 10^6 yr. The value associated to each contour line are indicated at the top of the plot.

References

Alexander, D. R., 1975, Ap. J. Suppl. **29**, 363.

Alexander, D. R.,et al, 1983, Ap. J., **273**, 773.

Anders, E., Grevesse, N., 1989, Geochim. Cosmochim. Acta **53**, 197

Alongi, M., Bertelli, G., Bressan, A., Chiosi, C., 1991a, A. Ap. **244** 95.

Alongi, M. Bertelli, G. Bressan, A., Chiosi, C., Greggio, L. 1991b

Arnett D. 1991, Ap.J. **383**, 295.

Bessel, M. S., Brett, J. M., Scholz, M., Wood, P. R., 1989, A.Ap.Suppl. **77**, 1.

Bessel, M. S., Brett, J. M., Scholz, M., Wood, P. R., 1991, A.Ap.Suppl. Erratum.

Bohannan, B., Abbott, D. D., Voels, A. A., Hummer, D. G., 1986, Ap.J. **308**, 728

Brunish, W. M., Truran, J. W., 1982a, Ap.J. **256**, 247

Brunish, W. M., Truran, J. W., 1982b, Ap.J.Suppl. **49**, 447

Brunish W. M., Gallagher, J.S. Truran, J. W. 1986 A.J. **91**, 598.

Backer, N.H., Kuhuβ, R., 1987, A. Ap., **185**, 117.

Bertelli, G., Bressan, A., Chiosi, C., 1984, **130**, 279.

Bessell, M.S. et al, 1989, AAS **77**, 1.

Biermann, L., 1976, Proceedings of IAU Colloquium No. 38, 4.

Blaha C., Humphreys R.M. 1989, A.J. **98**, 1598.

Böhm, 1976, Proceedings of IAU Colloquium No. 38.

Böhm-Vitense, 1958, Z. Astrophys., **46**, 108.

Bressan, A., 1984, Unpublished SISSA Thesis.

Bressan, A, 1989, Italian National School for Astronomy, proceedings, 1990

Bressan, A., Bertelli, G., Chiosi, C., 1981, A. Ap., **102**, 25.

Bressan, A. Fagotto, G. Bertelli G. and Chiosi, C 1993 A. Ap. Suppl. **100**, 647.

Castor, J.I., Abbot, D.C., Klein, R.I., 1975, Ap.J., **195**, 157.

Caloi, V. and Mazzitelli 1990 A. Ap., **240**, 305.

Canuto V. M. 1992 Ap.J. 392, 218

Canuto V. M. 1993 Ap.J. 416, 331

Canuto V. M. and Mazzitelli, I. 1991 Ap.J.

Castellani, V., Gianone, P., Renzini, A. *a,b* Ap.Sp.Sci **10**, 340, 355.

Caughlan, G. R., Fowler, W. A., Harris, M., Zimmermann, B. 1985, Atomic Data Nuc. Data Tables **32**, 197.

Chaboyer, B. Zhan J.P. 1992 A. Ap. **253** 173.

Chandrasekhar, S. 1939 *An introduction too the study of stellar structure* Univ. of Chicago Press, Chicago

Chang, J. S., Cooper, G, 1970, J. Comp. Physics, **6**, 1.

Chiosi C. In *Wolf-Rayet stars: Observations, physics, Evolution*, ed. C. de Loore, A.J. Willis, pp.323. Dordrecht: Reidel.

Chiosi, C., Bertelli, G., Bressan, A., 1991, Ap. J.,In *Instabilities in evolved super and hyper-giants*, ed. C. de Jager & H. Nieuwenhuijzen.

Chiosi, C., Bertelli, G., Bressan, A., 1992 Ann. Rev. A. Ap., **30**, 305.

Chiosi, C., Maeder, A. 1986, Ann. Rev. A. Ap., **26**, 329.

Chiosi. C., Nasi, E., 1974, Astro. Space Sci., **56**, 431.

Chiosi, C., Nasi,E., Sreenivasan, S. R., 1978, AA. **63**, 103.

Chiosi, C., Wood, P. R., Bertelli, G., Bressan, A., Mateo, M.,1991, Ap. J., (in press).

Chiosi, C., Summa, C., 1970, Astr. Space Sci., **8**, 478.

Chiosi, C. 1986 In *The nucleosynthesis and stellar evolution*, 16th Saas-Fee course, Eds B. Hauck, A. Maeder & Meynet

Charbonnel, C. and Vauclair, S. 1992 A. Ap. **265** 55.

Cloutman, L. D., Eoll, J. D., 1976, Ap. J., **206**, 548.

Cloutman, L. D., Whitaker, R. W., 1980, Ap. J., **237**, 900.

Conti P.S., Garmany C.D. de Loore C. Vanbeveren D, 1983 Ap.J., **274**, 302.

Cox, J.P., Giuli, R. T., 1968, *Stellar Structure.*

Cox, A. N., Stewart, J. N., 1970, Ap. J., **19** 243.

Cranck, J., 1986, *The Mathematics of Diffusion*, Clarendon Press.

de Jager, C. Nieuwenhuijijzen, H. van der Hucht K.A. 1988 A. Ap. Suppl. **72**, 259

Demmarque P. Mengel J.C. 1972 Ap.J. **171**, 583

Eggleton, P.P., 1971, M. N. R. A. S., **151**, 351.

Eggleton, P.P., 1972, M. N. R. A. S., **156**, 316.

Fagotto, F. Bressan, A. Bertelli, G. Chiosi A. Ap. Suppl. in press.

Fagotto, F. Bressan, A., Bertelli, G. Chiosi, C. 1993b *Preprint.*

Feast, M.W. 1992a, In *Instabilities in Evolved super and Hypergiants*, ed. C. de Jager, H. Nieuwenhuijzen. Amsterdam: North Holland, pp. 18

Fernando, H. J. S. 1991 Annu. Rev. Fluid Mech. **23**, 455.

Fitzpatrick E.L., Garmany C.D. 1990, Ap.J. **363**, 119

Garmany C.D., Conti P.S. Chiosi C. 1982 Ap.J. **263**, 777

Grevesse, N., 1991, A.Ap. **242**, 488

Hannaford, P., Lowe, R. M., Grevesse, M., Noels, A., 1992, A.Ap., in press

Hillebrandt, P, Hoflich 1987, Nature **327**, 597.

Iglesias, C. A., Rogers, F. J., 1991a Ap.J. **371**, 408.

Iglesias, C. A., Rogers, F. J., 1991b Ap.J. **371**, L73.

Iglesias, C. A., Rogers, F. J., Wilson, B. G., 1987, Ap.J. **322**, L45.

Iglesias, C. A., Rogers, F. J., Wilson, B. G., 1990, Ap.J. **360**, 221.

Iglesias, C. A., Rogers, F. J., Wilson, B. G., 1992, Ap.J. submitted.

Maeder, A., 1981a, In *the most massive stars*, ed. S.D'Odorico, D. Baade, K. Kjar,pp.173. Garching:ESO.

Maeder, A., 1981b, A. Ap. **99**, 97.

Saio H. Kato M. Nomoto K. 1988 Ap.J. **331**, 388.

Smith L.J., Willis, A.J. 1982 M.N.R.A.S. **201**, 451

Wood P.R., Faulkner D.J. 1987 Proc.astr.Soc.Austr. **7** 75.

Langer N. 1991, A. Ap. **253** , 669.

Maeder, A., 1992, In *New aspects of Magellanic Cloud research*, ed. B. Baschek, G. Klare, J. Lequeux, pp.284. Heidelberg

Schaller G., Schaerer D., Meynet G., Maeder A. 1992 A. Ap. Suppl. in press

Schmutz, W., Hamann., W.R., Wesselowski, U. 1989 A.ap. **210**, 236

Fowler, W. A., et al, 1975, Annu. Rev. Astron. Astrophys. **13** 69.

Gough, D. O., 1969, J. Atmos. Sci., **26**, 448.

Graboske, H. C., de Witt, H. E., Grossman, A. S., Cooper, M. S., 1973, A.J. **181**, 547.

Graboske, H. C., de Witt, H. E., Grossman, A. S., Cooper, M. S., 1973,

Greggio, L. 1984, *In Observational Tests of the Stellar Evolution Theory*, ed. A. Maeder, A. Renzini, p. 329.

Hamann W.R. Koesterke L. Wessolowski U. 1993, A. Ap. **274**, 397

Huebner W.F., Merts, A.L., Magee, N.H. Argo M.F. 1977 *Los Alamos Scientific Laboratory Report* LA-6760-M.

Humphreys, R. 1993 Preprent.

Humphreys, R. and Davison, K. 1979 Ap.J **232**, 243.

Jost, W., 1960, *Diffusion in Solids, Liquids, Gases.*

Kato, S., 1966, Publ. Astron. Soc. Japan, **18**, 374.

Kettner, K. U. et al., 1982, Phys. A-Atoms and Nuclei **308**, 73

Kettner, K. U. et al 1982, Z. Phys. A-Atoms and Nuclei **308**, 73.

Kippenhahn, R., Wiegert, A., 1991, *Stellar Structure and Evolution*, Springer-Verlag, Berlin.

Kippenhahn,R., Weigert, A., Hofmeister, E., 1967, Meth. Com. Phys., **7**, 129.

Kudritzski, R. P., Pauldrach, A., Puls, J., Abbot, D. C., 1989, A. Ap. **219**, 205

Landau and Lifshitz, 1987, *Fluid Mechanics*, Pergamon Press.

Langer, N., 1989a, AA **210**, 93.

Langer, N., 1989b, AA **220**, 135.

Langer,N., El Eid, M.F., Fricke, K.J., 1985, A. Ap., **145**, 179.

Langer,N., Sugimoto,D., Fricke,K.J., 1983, A. Ap.,**126**, 207.

Langanke, K., Koonin, S. E., 1982, Nuclear Physics **A410**, 334

Lattanzio, J.C. 1986 Ap.J. **311**, 708

Lattanzio, J.C. 1987b Ap.J. **313**, L15

Ledoux,P., 1947, Ap.J., **105**, 205.

Maeder, A., 1975, A. Ap. **164**, 45.

Maeder, A., 1983, A. Ap. **120**, 113.

Maeder, A. 1990 A. Ap. Suppl. **84**, 139

Maeder, A., Meynet, G., 1989, A. Ap., **210**, 155.

Maeder, A. 1993 *STScI Workshop*, Baltimore, ed. Leithever, C. et al Cambridge Univ. Press

Malagoli A., Cataneo F., and Brummell N.H. 1990, Ap.J. **361**, L33.

Mermoiloid, J.C., Maeder, A., 1982, A. Ap., **189**, 34.

Meylan, G., Maeder, A., 1982, A. Ap., **108**, 148.

Munakata, H., Kohyama, Y., Itoh, N., 1985, Ap.J. **296**, 197

Paczynski, B. 1971 Acta Astron. **21**, 417

Parildrach, A., Puls, J., Kudrizki, R.P., 1986, A. Ap., **164**, 86.

Renzini,A., 1987, A. Ap., **188**, 49.

Renzini,A., Fusi-Pesci, F. 1988 Ann. Rev. A. Ap. **26**, 199.

Rogers, F. J., Iglesias, C. A., 1992, Ap.J. in press.

Rogers, F. J., Iglesias, C. A., 1992, Ap.J.Suppl. 79, 507.

Roxboug, I., 1965, M.N.R.A.S., **130**, 223.

Roxburg, I., 1989, A. Ap. **221**, 316.

Sakashita,S., Hayashi,C., 1961 Prog. Theor. Phys. Kyoto, **26**, 942.

Saslow, W.C., Schwarzschild, M., 1965, Ap.J., **142**, 1468.

Schatzman, E. 1977, **56**, 211.

Schwarzschild, M., Härm, R., 1958, Ap.J., **128**, 348.

Shariv, G., Salpeter, E.E., 1973, Ap.J., **184**, 191.

Simpson, E.E., 1971, Ap.J., **188**, 166.

Spiegel, E.A., 1960, Ap.J., **132**, 716.

Spiegel, E.A., Veronis, 1960, Ap.J., **131**, 442.

Spiegel, E.A. 1971,1972 *Ann. Rev. A. Ap.*

Seecnivansan, S.R., Wilson, W.J.F., 1978, Astro. Space Sci. **53**, 193.

Stothers, R., 1970, M.N.R.A.S., **151**, 65.

Stothers, R. Chin C.W. 1981 Ap.J **247**,1063

Stothers, R. Chin C.W. 1990 Ap.J **348**, L21

Sweigart, A., Demarque, P. 1972 A. Ap. **20**, 445

Sweigart, A., Gross, P.G., 1976 Ap.J. Suppl. **36**, 405

Ulrich, R.K., 1970, Astro. Space Sci., **7**, 183.

Unno, W., 1967, Publ. Astron. Soc. Japan, **18**, 40.

Vitense, E., 1953, Z. Astrophys., **46**, 108.

Weaver, T.A.,Woosley, G.B., 1978, Ap.J. **225**, 1021.

Weiss, A., 1989, Ap. J., **339** 365.

Wood, D.O.S., Churchwell, E. 1989, Ap.J. **340**, 265

Woosley, S. E., 1988, Ap. J.,**330**, 218.

Xiong, D., 1985, A. Ap., **150** 133.

Xiong, D., 1986, A. Ap., **167**, 239.

Xiong, D., 1990, A. Ap., **232**, 31.

Zahn, J. P. 1991 A. Ap., **252**, 179.

Acknowledgement

I would like to thank Cesare Chiosi and Dennis Sciama for making possible my stay at SISSA, and continuous encouragement during all the time in which this research project has been developed.

In particular I would like to express all my gratitude to the friends met in Padova from whom I have got many scientific advices and unvaluable help.

Special thanks are due to Alessandro Bressan, one of supervisors. Without his dedicated assistance, continuous help, friendly relationship, accomplishing this project would have been much more difficult, if not impossible.

Finally, I like to acknowledge all the friends I have met in Tieste: thanks to them my stay has been a real pleasure.